Condition Monitoring and Performance Optimisation of Pulverised Fuel Vertical Spindle Type Mills

Hamresin Archary
EPPEI Specialisation Centre in Combustion Engineering
University of the Witwatersrand, Johannesburg

A dissertation submitted to the Faculty of Engineering and the Built Environment, University of the Witwatersrand, Johannesburg, in fulfilment of the requirements for the degree of Master of Science in Engineering.

Johannesburg, 2015

Declaration

I declare that this dissertation is my own unaided work. It is being submitted to the degree of Master of Science in Engineering to the University of the Witwatersrand, Johannesburg. It has not been submitted before for any degree or examination to any other University.

……

(Signature of Candidate)

…… day of …… year ……

Abstract

In order to alleviate the current bottleneck caused by the milling plant, two problems were identified. Monitoring of the key performance indicators of the milling plant (throughput and particle fineness) required improvement, and the average throughput must be increased without sacrificing the product quality. Monitoring of the coal mass flow was achieved by means of an on-line Mill Energy Balance. The Particle Size Analyser evaluation identified five key test parameters which caused inaccuracies in results. Relationships were established enabling one to commission this instrument to achieve precise and accurate measurement for continued condition monitoring.

Extensive testing was performed on a pilot scale mill where the operational control parameters were related to the key mill performance indicators. Characterisation of the relationships between the throughput, classifier setting, air/fuel ratio and particle fineness were successfully established. An operating regime was then developed which increased the maximum sustainable throughput while maintaining optimal particle fineness.

Dedication

I dedicate this dissertation to my father

Sundramurthi Archary

Acknowledgements

I would like to acknowledge the following people:

- Thank you to Prof. Louis Jestin for industrial mentorship and training leading up to and during the course of this research
- Thank you to Prof. Walter Schmitz for continued guidance and support for the course of this research
- Thank you to Chris Du Toit from Camden Power Station for his support during testing as well as for his industrial support and mentorship
- Thank you to Bonny Nyangwa for the use of the pilot scale mill and for the support provided during testing
- Thank you to The Eskom Power Plant Engineering Institute (EPPEI)

Contents

List of Figures

List of Tables

List of Acronyms

PF	Pulverised Fuel
DCS	Distributed Control System
PSA	Particle Size Analyser
DAQ	Data Acquisition system
DP	Differential Pressure
OEM	Original Equipment Manufacturers
MCR	Maximum Continuous Rating
MEB	Mill Energy Balance
NO_x	Oxides of Nitrogen
HGI	Hardgrove Grindability Index
AI	Abrasive Index
SFV	Spatial Filtering Velocimetry
FSS	Fibre-optic Spot Scanning
R,T&D	Eskom Research Testing and Development
CFBC	Circulating Fluidised Bed Combustion

Nomenclature

Symbol	Description	
DP_x	Differential pressure	[Pa]
ρ_{pf}	Apparent density	[kg/m^3]
g	Gravity	[m^2/s]
h	Height between the pressure taps	[m]
V_f	Velocity of air	[m/s]
M_f	Mass flow of air	[kg/s]
S	Section area	[m^2]
V_p	Velocity of particle	[m/s]
V_{slip}	Velocity slip factor	[%]
M_p	Mass flow in suspension	[kg/s]
$\dot{m}_{PA}$	Mass flow of primary air	[kg/s]
$h_{PA_{in}}$	Enthalpy of primary air, into the mill	[kJ/kg]
$h_{PA_{H_2O\_in}}$	Enthalpy of H_2O in primary air, into the mill	[kJ/kg]
$h_{PA_{out}}$	Enthalpy of primary air, out of the mill	[kJ/kg]
$h_{PA_{H_2O\_out}}$	Enthalpy of H_2O in primary air, out of the mill	[kJ/kg]
f_{PA}	Moisture fraction of primary air	[%]
$\dot{m}_{SA}$	Mass flow of seal air	[kg/s]
$h_{SA_{in}}$	Enthalpy of seal air, into the mill	[kJ/kg]
$h_{SA_{H_2O\_in}}$	Enthalpy of H_2O in seal air, into the mill	[kJ/kg]
$h_{SA_{out}}$	Enthalpy of seal air, out of the mill	[kJ/kg]
$h_{SA_{H_2O\_out}}$	Enthalpy of H_2O in seal air, out of the mill	[kJ/kg]
f_{SA}	Moisture fraction of seal air	[%]
$\dot{m}_C$	Mass flow of coal	[kg/s]
$h_{C_{in}}$	Enthalpy of coal, into the mill	[kJ/kg]
$h_{C_{H_2O\_in}}$	Enthalpy of H_2O in coal, into the mill	[kJ/kg]
$h_{C_{out}}$	Enthalpy of coal, out of the mill	[kJ/kg]
$h_{C_{H_2O\_out}}$	Enthalpy of H_2O in coal, out of the mill	[kJ/kg]
$h_{VAP_{H_2O\_90deg}}$	Heat of vaporisation of H_2O @ 90˚C	[kJ/kg]
f_C	Moisture fraction of coal	[%]
$M_{Power_{in}}$	Mill motor power, into the mill	[kW]
q_{out}	Convective heat loss through the mill body	[kW]

Chapter 1: Introduction

In the South African power generation industry, the parastatal Eskom supplies approximately 95% of the country's total electricity requirements and approximately 45% of the electricity used in the whole of Africa (Eskom, n.d.). The Eskom fleet consists of 13 coal fired power stations amongst the 1 nuclear, 1 wind farm, 2 hydroelectric, 2 pumped storage and 4 open cycle gas turbine plants. The 13 coal fired power stations all have between 6 and 10 generating units each. South Africa's future reliance on coal as a source of energy is evident as Eskom is currently in the process of building two supercritical steam boiler power stations (Medupi and Kusile) of 6 generating units each. Both of these are amongst the largest coal fired power stations in the world. The high reliance on coal fired technology is largely due to the abundance of coal reserves available in the northern regions of the country. This abundance of coal reserves has meant that coal has been very cheap in relation to the price of coal in European countries (Kohler, 2013).

However, fast growing coal fired power generation in countries such as China and India have led to the increase in financial gain of exporting high-quality coal to these countries. Increased exports have led to the increase in the price of coal in South Africa. Due to this rise in coal price locally, Eskom has made the strategic decision to burn lower quality coal in order to keep the price of electricity down for local consumption. Lower quality coal in general terms has a lower calorific value, lower volatile matter and higher ash contents. Due to these factors it is required that more coal is fed to the boilers in order to achieve the same energy input and thus maintain the full load of the plant. It is also vital that the product from the mill is of the correct particle size distribution in order to ensure de-volatilisation and complete combustion of the pulverised fuel in the furnace region. These are further exacerbated by the introduction of the Low NO_x burner, and the stringent particle size distribution requirements in order to

reduce the increased unburnt carbon effect associated with the technology (Kitto & Stultz, 2005). This means that the milling plant has to grind raw coal to the optimal particle size while increasing the throughput of coal flow to meet the boiler energy requirements.

The average age of coal fired power stations owned by Eskom is approximately 30 years old, with the oldest being 53 years old. Due to the energy supply crisis facing the country three mothballed power stations were returned to service contributing substantially to the high average age of the fleet. These power stations are further faced with the problem of availability of design specification coal as the current coal seam quality has deteriorated over these years.

The compounding problem of both ageing plant as well as deteriorating coal quality has led to the situation that many of the older power stations are finding a bottleneck in terms of coal flow through the milling plant. This bottleneck is a contributing factor to the power stations not being able to achieve the Maximum Continuous Rating (MCR) that they were originally designed for. Load losses incurred as a result of poor milling performance are in some cases as high as 35 MW per unit. This capacity loss is critical as the country currently operates with very little excess capacity even while running the expensive peaking plants well beyond their duty cycle.

The first unit of Medupi Power Station, which is one of the two new power stations in the current build programme, is due to come online in 2014. However, even after completion of the new power station the power grid in South Africa will continue to operate at critical margins. In order to alleviate the pressure on the power grid in the short term and beyond, some progress has to be made in order to reduce or completely eradicate these load losses.

1.1. Background

Coal fired power stations, even with the recent drive towards cleaner fuels, remain the most widely used and cost effective solution in power generation worldwide. This is largely due to the favourable cost per kilojoule ratio of coal fuels. Coal as a fuel, however, has many process related challenges that engineers have to contend with. These include the pre-processing (grinding and drying) and post-processing (de-dusting and ash removal) of the fuel. The coal milling plant is responsible for the pre-processing and thus serves two major roles, to prepare fuel and feed it to the furnace for combustion.

The preparation process entails the grinding and drying of raw coal into Pulverised Fuel (PF) of the correct specification in order to ensure both stable and complete combustion in the furnace. The effects of a poorly maintained or poorly controlled mill on combustion, is evident all the way through the air and flue-gas circuit. Coal that is ground too fine will cause slagging in the furnace region. This can grow so severe that it completely seals a burner opening, thus disrupting the air/fuel ratio and mass flow to the rest of the burners. Besides the effect on combustion efficiency, without accurate control of air and coal flow to each burner, technologies such as low NO_x burners become ineffective. Coal that is too coarse has a longer burnout time and therefore raises the height of the fire ball in the furnace. Larger coal particles still burn at the superheater levels and begin to stick to the tubes forming clinkers. This reduces the heat pick up through the tubes and leads to flue gas exhaust temperatures that are so high in some cases that the Fabric Filter Plant (FFP) bags begin to burn.

The second role of the mill is to feed the required mass flow of coal to the furnace. This is determined by the energy requirements of the boiler as well as the specific energy of the fuel. As discussed, one of the problems facing South African power stations is the deteriorating Calorific Value (CV) of coals burned for local consumption. This means that mills must operate close to the maximum designed throughput capacity in order to

achieve the required increased mass flow of coal. Operating mills at such increased throughput requires the mill to be in good mechanical condition in order to achieve the correct particle fineness at higher average mill load.

This emphasises the importance of maintaining proper control and good health of the milling plant. Milling plant maintenance and monitoring however, is currently performed on a time and failure based system. With the advent of on-line monitoring systems in the power station environment it has recently become possible to shift towards condition based maintenance of the milling plant. There are however, three prerequisites which must be met. In order to implement a condition based maintenance plan, one must first understand clearly, the dynamics of the system that govern the operation of a milling plant. Then the mill must be instrumented with performance monitoring equipment for both 'current status' monitoring as well as historical data acquisition. The interpretation of this data, in conjunction with tools such as mass and energy balances, will then allow the determination of the health of the mill or specific components of the mill. By understanding the milling system, monitoring its key performance parameters and interpreting the resulting data, a mill condition monitoring system can be developed thereby paving the way for a condition based maintenance strategy to be implemented. Condition based maintenance begins with both good understanding and good condition monitoring of the system.

1.2. Plant Description

1.2.1. Coal Milling Overview

Early power stations used a coal firing system called a chain grate. Large chunks of coal were fed into a furnace on a chain grate conveyor system to be burned while air was supplied through the chain grate from below. This technology had serious disadvantages at the time. A large excess air coefficient was fundamentally required due to the large particle size of coal

burnt. There was also high un-burnt carbon in ash resulting from uneven thermal distribution and low temperatures at the inlet where the drying rate of coal may be low (Liu et al., 2008). Combustion efficiency was improved slightly by the late nineteenth century by which stage travelling chain grate combustors were widely used in power generation, but the fundamentals of combustion efficiency remain a function of the combustion temperature and the surface area of the fuel. Large leaps in combustion efficiency were made when pulverised fuel (PF) combustion by suspension firing was introduced in 1890 (Williams et al, 2000). The technology was so popular that it attracted extensive research and has grown technologically since. Pulverised fuel burner combustion is the technology of choice in today's large high efficiency power generation units. And thus, the coal pulverising plant (or milling plant) is now an integral part of the modern power station. Unlike PF combustion as a technology, academic research in the field of coal milling has been slow to progress. This is in part due to the high level of secrecy amongst competing Original Equipment Manufacturers (OEM's) and also due to the highly abrasive nature of the process and the technical difficulties associated with analysing the flow in such an environment.

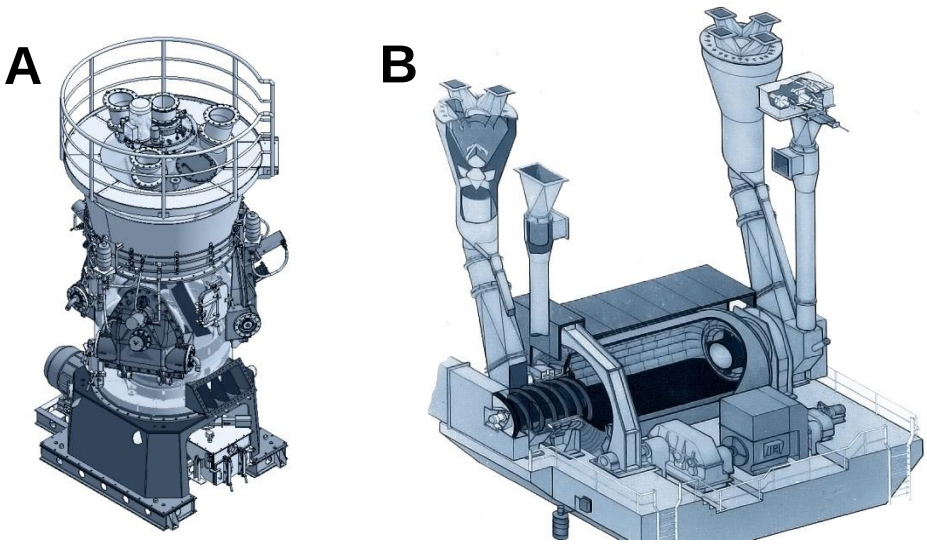

Figure 1.1: Vertical Spindle Mill (A) and Tube Mill (B) (Alstom, n.d.)

The vertical spindle mill is the most widely used type of coal mill in PF fired boilers. Tube mills are also very popular and have some advantages and

disadvantages over vertical spindle mills. Broadly speaking the high capital cost of tube mills and high auxiliary power consumption is offset against the high maintenance cost of vertical spindle mills. Tube mills are also more robust in terms of changes to the quality of coal that is being crushed and also respond better to load changes and part load operation. Whereas vertical spindle mills are very sensitive to coal quality changes and foreign objects such as tramp iron. In the Eskom fleet of 13 coal fired power stations, 6 plants utilise vertical spindle mills, 5 plants utilise tube mills and 2 plants have a mixture of both vertical spindle and tube type mills (Muller et al., 2014). Camden Power Station in Mpumalanga South Africa is made up of 8 units of 200MWe each. Each unit has 5 Lopulco LM14/3P vertical spindle mills (capable of full load with 4 mills in operation), each feeding a row of 4 front wall fired PF burners. This power station will be used as an example in order to explain more about the functions of a mill.

The performance of pulverised fuel mills are defined by the requirements of the modern PF boiler. The milling plant serves three main functions:

1. To dry the coal in order to assist the de-volatilisation and combustion in the furnace
2. To crush the coal thereby increasing the surface area to aid efficient combustion
3. To feed the required amount of coal necessary to meet the energy demands of the boiler

Coal is dried inside the mill by means of the hot primary air that flows through it. Primary air (PA) is heated by post combustion hot flue gases via a heat exchanger, referred to as the air heater, and is blown through the mill by the primary air fan. The mill outlet temperature is controlled at 90˚C by controlling the inlet air temperature. This is maintained by mixing the hot air from the air heater with cold air that enters the stream via a cold air damper upstream of the PA fan.

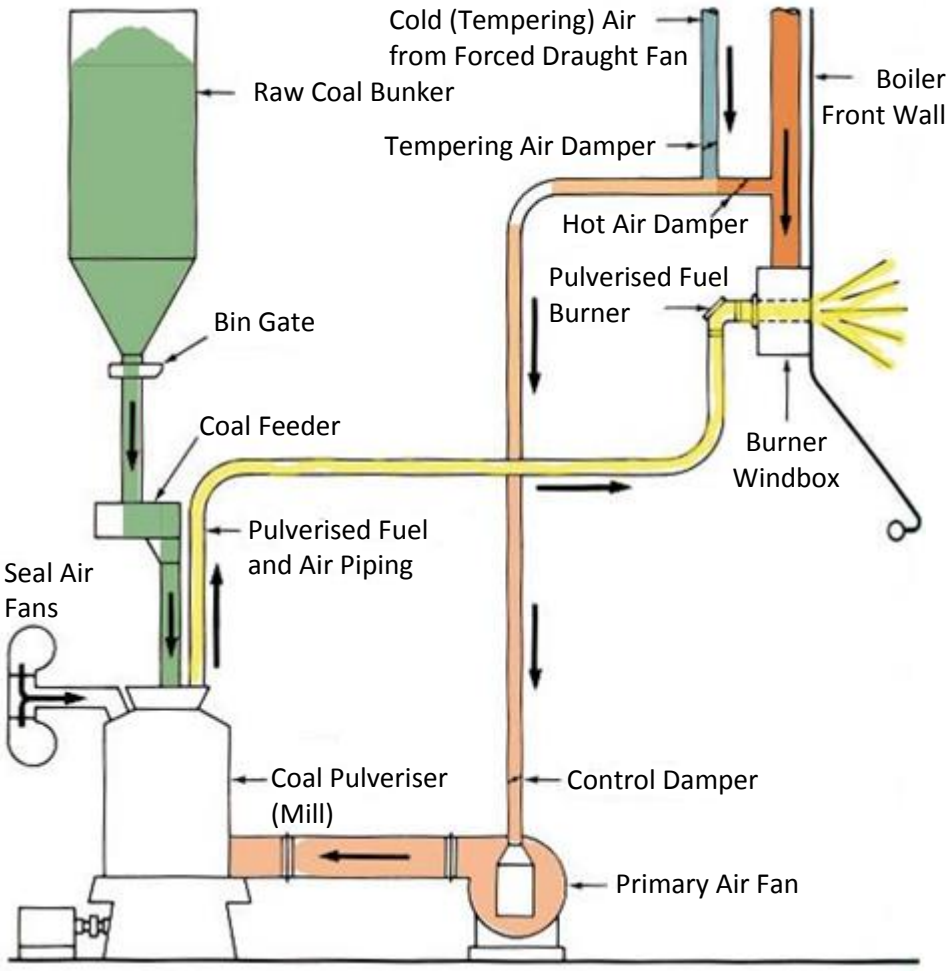

Figure 1.2: Mill and Firing System Circuit

Primary air is usually in the region of 250˚C before entering the mill and is dependent on the amount of moisture that has to be evaporated from the coal. A mill outlet temperature is maintained to dry the coal with the minimum primary air heat energy input. Camden Power Station resides at altitude with the ambient pressure of 83 kPa allowing the lower mill outlet temperature of 90˚C to be sufficiently close to the vaporisation temperature. At sea level the required mill outlet temperature would be closer to 100˚C in order to dry the coal.

The grinding of coal occurs in the mill as the coal is passed by centrifugal force between the table and roller grinding elements. The PF boiler requires that a well-defined range of particle fineness is maintained for optimal combustion. Fine particle slagging around the burner mouth can

grow to such an extent that it completely shuts off a burner causing severe fuel mal-distribution between burners of the same row. On the other hand, coarse particles grow clinkers on superheater tubes thus reducing the overall heat transfer coefficient as well as causing localised thermal stresses and fractures which are expensive to repair or replace. Table 1.1 shows the range of particles that should pass through the four vital sieve sizes for optimal pulverised fuel combustion.

Table 1.1: Range of optimal PF particle fineness

	Minimum	Ideal	Maximum
%< 75µm	65%	70%	75%
%< 106µm	76%	81.25%	86.5%
%< 150µm	89%	91.75%	94.5%
%< 300µm	99%	99.4%	99.8%

The percentage passage of the 75µm sieve size is most quoted in the power generation industry as an indication of a mills grinding performance. In the ideal scenario a mill should grind coal to a particle size distribution where 70% of the product is less than 75µm.

Coal flow through the mill is controlled by the steam flow and boiler energy requirements. The operator has an influence of the coal flow through each mill by adding or removing mills from service and thus sharing the total coal mass flow load. The fact that the coal mass flow is determined by the boiler energy demand is an important factor to consider. This means that the energy contained in the coal, quantified in MJ/kg by the Calorific Value (CV), has a direct influence on the mill throughput. As the CV of coal decreases, as is the case in many power stations in South Africa, the mass flow of coal has to increase in order to meet the same energy input into the boiler. The problem with increasing the mass flow of coal through the mill is that it has, as will be demonstrated later, some influence on the grinding capability of the mill.

1.2.2. Mechanical Description of the Milling Plant

The vertical spindle mill crushes coal by feeding it between a grinding roller and either a bowl, table or ring at the bottom. The grinding roller can be of a tyre (Figure 1.3) or ball type. While variations of these types of mills do exist, most are simply modifications to the shape of the grinding elements and thus the principle of operation remains almost identical. The nomenclature in Figure 1.3 below will be used in this description.

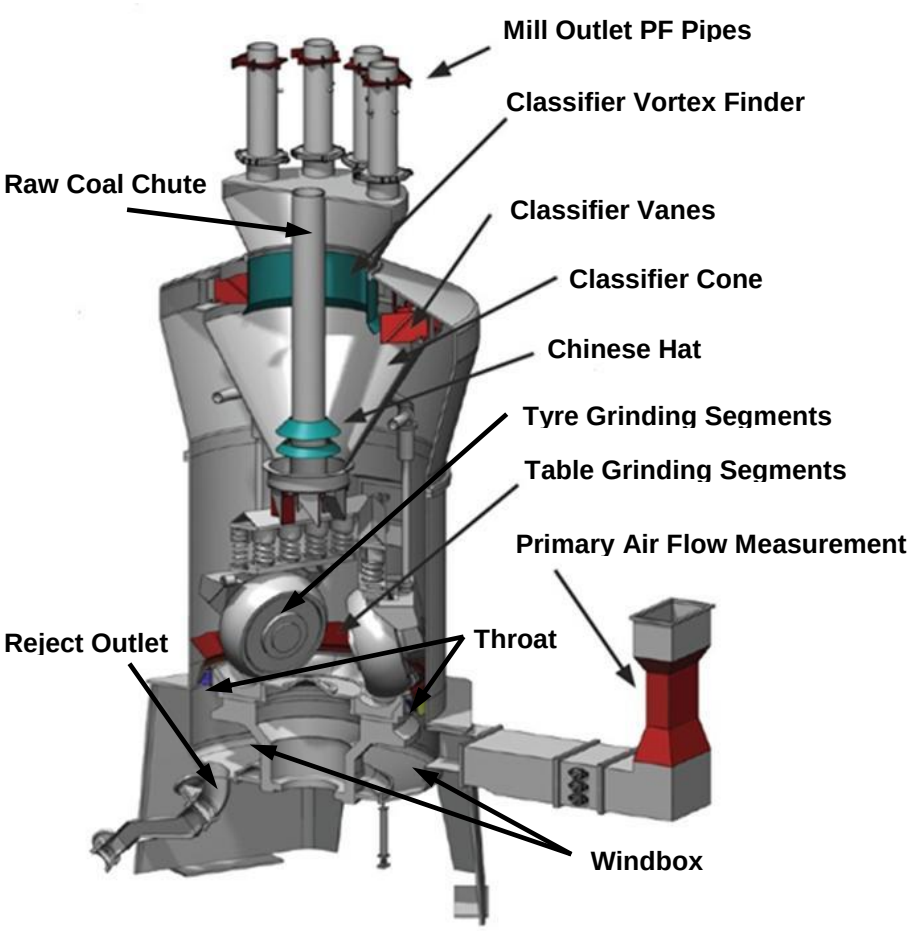

Figure 1.3: B&W roll wheel pulveriser (Powermag, 2011)

The table grinding segments form part of the table assembly and rotates about its vertical axis at a constant speed. The throat is made up of angled vanes that are fixed to the outer part of the table and therefore rotates at the same speed as the table. The roll wheel assembly and roll wheels are suspended by the spring frame above it where a ram force is exerted

downward by springs. A small gap is maintained at all times between the roll wheel and table grinding elements.

Raw coal with an average diameter of 30mm is fed into the mill through the raw coal chute at the top. This task is usually performed by a volumetric screw feeder but modern power stations employ gravimetric feeders for improved accuracy of coal mass flow. The raw coal falls by gravity onto the centre of the table and by the centrifugal force of the rotating table is fed outwards toward the grinding elements.

The coal undergoes comminution as it is passed through the small gap between the tyre and table grinding elements. Once the coal is crushed it reaches the edge of the table where the throat is located.

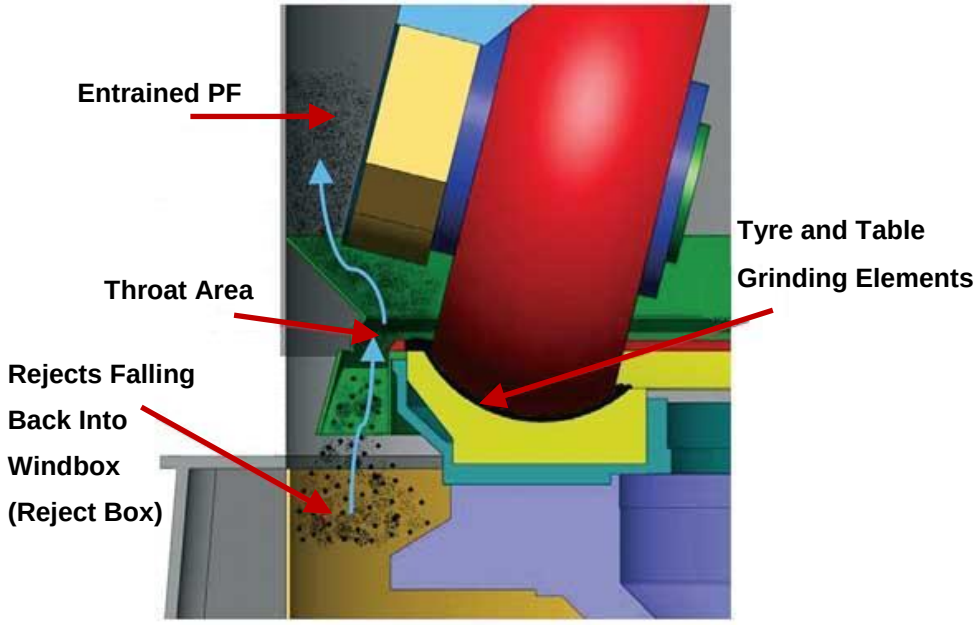

Figure 1.4: Grinding element and throat area (Powermag, 2011)

Hot air from the Primary Air (PA) fan enters the mill from the side and into the windbox which is the area below the throat. As the air is accelerated through the small throat area, it entrains the crushed coal in what resembles a fluidised bed, and carries it up to the primary classification zone. Here the increase in area causes the air to lose velocity and the fallout of large particles occurs. These particles are eventually returned to

the table to be reground. Lighter particles are carried all the way up to the classifier where vanes generate swirl in the flow. The classifier is essentially a cyclone separator inside the classifier cone and around the raw coal chute. Coarse particles are forced to the outside where the kinetic energy is dissipated by contact with the wall of the classifier cone. The coarse particles then build up a bed at the bottom of the classifier and around the Chinese hat in order to seal the classifier from reverse flow. These particles are eventually returned to the table for regrinding.

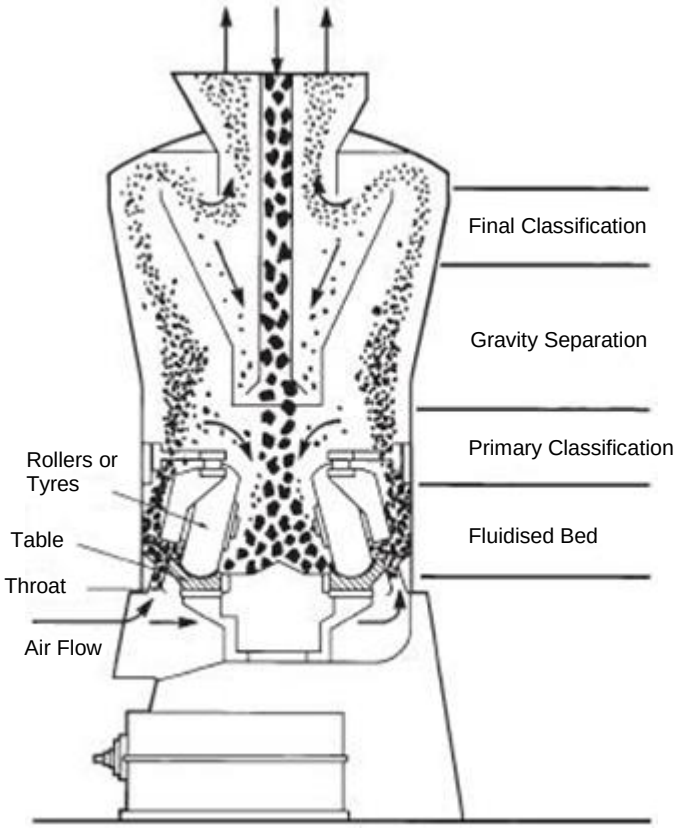

Figure 1.5: B&W mill internal recirculation (**Kitto & Stultz, 2005)**

The vortex finder, at the centre of the classifier and around the raw coal chute, allows the fine particles to escape the classifier and enter the discharge turret. The pulverised fuel is then transported via the PF pipes to the burners for combustion. The angle of the classifier vanes determine the amount of swirl that is generated in the classifier cone. This in turn determines the size of particle that is allowed to leave the classifier

through the vortex finder and what size of particle is returned to the table for regrinding.

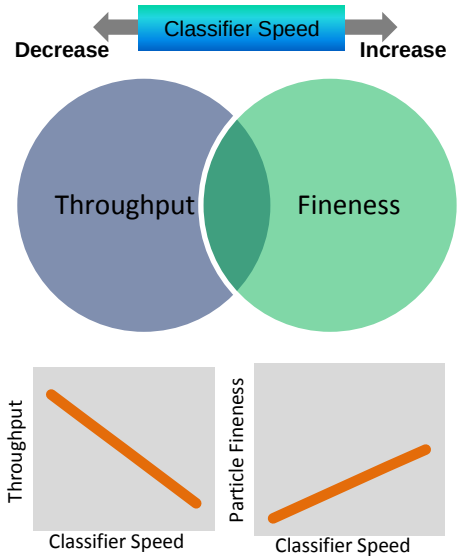

Figure 1.6: Relationships governing mill operation

Generating a lot of swirl in the classifier disturbs the flow and increases the total mill differential pressure. This also increases the mill internal coal recirculation which increases the mill differential pressure even further. This limits the throughput of a mill as the control system will trip the mill if the total mill differential pressure reaches 4.5kPa. This is to prevent the mill from choking and creating the possibility of a mill fire.

1.2.3. Control Description of the Milling Plant

The mill outlet temperature is controlled to a set point of 90˚C in order to dry the coal for transportation through the PF pipes and combustion in the furnace. The control parameter is the attemperating damper (cold air damper) position on the primary air fan inlet. The primary air fan draws hot air from the air heater and feeds it through the mill. In order to control the mill inlet temperature the primary air fan has two dampers. The hot air damper, which is open fully under normal operation, and the cold air damper which draws air from atmosphere on the PA fan inlet duct. The

ratio of hot to cold air, and thus the mill inlet air temperature, is controlled by the position of the attemperating damper. This is in turn adjusted to maintain the mill outlet temperature set point.

The set point of the mills in terms of load is derived from the total unit set point and the combustion controller. The actual coal flow for each mill is calculated from the feeder speed. Individual mills receive their set points from the combustion control as a mass flow in kg/s. The mill feeder controller tracks an operator defined value when the loop is in manual and tracks the combustion controller defined set point when in automatic operation. The set point of the feeder follows the mill load line as depicted in Figure 1.7. An upper limitation to the feeder fuel flow is defined by the mill differential pressure trip point of 4.5kPa. The load line is operated dynamically with a load line correction factor which is the actual feeder coal flow divided by the combustion controller required set point.

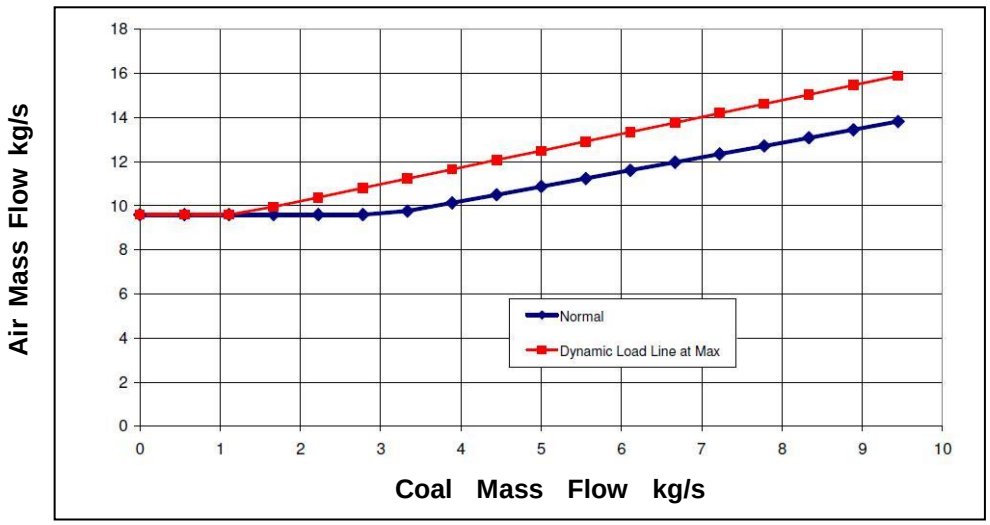

Figure 1.7: Mill load line for Camden Power Station (CMP, 2010)

Primary air mass flow is measured by means of a venturi or orifice plate at the mill inlet. The PA fan is a constant speed variable vane fan. Flow control is varied by fan vane positions. The PA fan vane position is controlled according to the mill load line and will follow the coal flow which is determined by the combustion controller. The primary air mass flow does have an overriding minimum set point. This is to ensure that a

minimum transportation velocity is maintained in the PF pipes in order to avoid particle settling as well as flash back from the furnace.

1.2.4. Performance Testing and Maintenance of the Milling Plant

PA Flow Calibration

A Pitot tube traverse is performed on the PA duct before the PA fan. On Camden power station five sampling points are available on the inlet duct to the PA fan for this purpose. For 25%, 50%, 75% and 100% radial vane openings, differential pressure is recorded for a full duct traverse with the calibrated Pitot tube (according to British Measurement Standard BS 893, now absorbed by BS ISO 13909). The calculated velocity from the Pitot traverse can then be mathematically converted to a mass flow after also measuring static pressure and air temperature at the traverse point.

Coal Drop Test

In order to calibrate the feeders for volumetric discharge, a drop test is conducted on the screw feeder. The drop test is conducted into 1m³ bags. The bags are weighed in order to determine the mass. Discharge from the feeder is achieved by removing the pipe leading to the raw coal chute situated directly above the classifier. A flexible chute is installed and this is fed into the sampling bag.

The test is conducted at multiple load points across the range of the feeder. Raw coal samples are taken from each bag in order to determine raw coal relative bulk density and moisture content. This information would then be used to verify the theoretical volumetric discharge of the feeder.

The raw coal moisture content is determined using the following formula:

$$\%\,\boldsymbol{Total\ Raw\ Coal\ Moisture} = \frac{(\boldsymbol{M_w}-\boldsymbol{M_d})-(\boldsymbol{M_d}-\boldsymbol{M_p})}{\boldsymbol{M_w}-\boldsymbol{M_p}} \times \frac{\mathbf{100}}{\mathbf{1}} \qquad \textbf{(1.1)}$$

Where:

M_w = Mass of the wet sample and pan (g)

M_d = Mass of the dried sample and pan (g)

M_p = Mass of the pan (g)

Relative bulk density is determined according to American National Standard ASTM D291 (similar to the BS ISO Standard 23499) where coal is dropped into a measuring box from a predetermined height through a cone. The actual volume of the measuring box is determined by filling it with water. The raw coal sample is first placed in the cone above, before being allowed to drop into the measuring box through the opening in the shutter. The coal is then levelled in the measuring box before being weighed. The following formula is used:

$$\boldsymbol{Relative\ Bulk\ Density\ of\ Raw\ Coal\ Sample}\ \left(\frac{\boldsymbol{kg}}{\boldsymbol{m^3}}\right) = \frac{(\boldsymbol{M_s - M_b})}{\boldsymbol{V_b}} \qquad \textbf{(1.2)}$$

Where:

M_s = Mass of the sample and box (kg)

M_b = Mass of the empty box (kg)

V_b = Volume of the box (m^3)

Clean Air Curve

The clean air curve gives an indication of the condition of the mill internals and especially the throat. During mill operation the harsh abrasive environment acts to wear away the unprotected components inside the mill. The most vulnerable being the blades of the throat where the flow is accelerated through the small throat area. This increases the throat area as the blades wear away between outages. Since the throat is not replaced at every outage, a clean air curve is required in order to determine how much of the throat needs to be blocked in order to reduce the area again and restore the velocity required. The primary air mass flow is determined as a function of the required PF pipe velocity and is embedded into the control system as a function of the coal mass flow rate.

Therefore it is better to restore the throat area back to good health than to increase the primary air to compensate for throat wear. The high velocity in the throat area is required to maintain the fluidised bed, primary classification and still carry finer particles up to the classifier. A larger throat area will collapse the bed and cause coal to enter the reject box.

To determine the mill's clean air curve, the PA radial vane control is opened through its range and primary air differential and mill differentials pressures plotted against each other.

It is important to note that the mill differential pressure is a function of all the restrictions inside the mill. Thus to achieve repeatability the mill settings such as classifier vane angle should not be changed. It is also important to note that the inlet and outlet temperatures are equal. In addition the classifier vanes, reject chamber, windbox, seal air fan filters and discharge turret must be clean of settled PF.

Control of Pulverised Fuel Fineness

Fineness control in the mill is achieved by adjusting the classifier vanes. The slew ring adjustment hand wheel is used for the adjustment of the vanes. An increase in vane angle results in a reduction in PF particle size. Adjustments of between 37.5˚ and 57.5˚ are possible. An improvement in PF fineness does however result in a reduction of the maximum mill throughput as well as an increase in mill differential pressure as more coal is re-circulated inside the mill.

PF particle fineness is measured by extracting a sample of PF from the PF pipes while the mill is in operation. The iso-kinetic sampler is used to perform this task. PF is extracted from the PF pipe at the same velocity that it is passing through the pipe in order to achieve a representative sample. This is achieved by controlling the suction flow of the probe in order to balance the static pressure in the probe to that of the PF pipe. PF is extracted from 32 points inside the pipe according to the British

Standard BS 893 for round ducts. This standard is based on the equal area principle, i.e. the cross sectional area is divided into equal area rings and samples are extracted from the centre of each area to make up 8 sampling points along an axis, and 4 axes of entry.

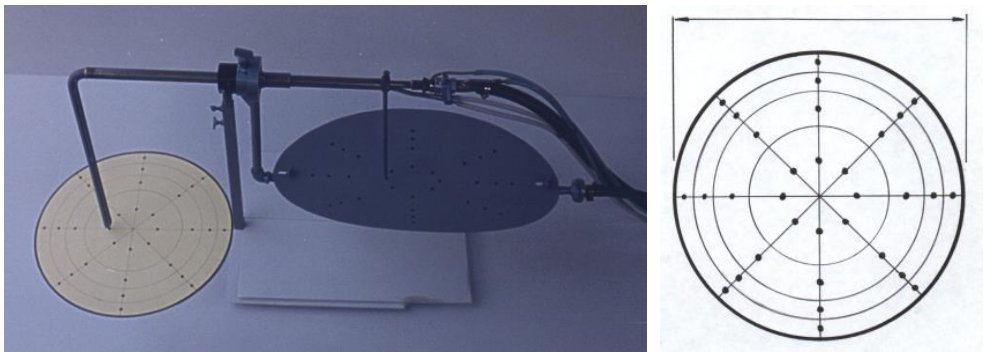

Figure 1.8: PF sampling probe and sampling points

Once the sample is extracted, it is taken to a lab for particle size grading. The total mass of the sample is recorded and the sample is then vibrated through a series of sieves of varying mesh sizes. The mass retained above each sieve is then recorded in Table 1.2 and a particle size distribution is determined.

Table 1.2: Typical particle size distribution results

Total Mass	67g	
Sieve Size	**Mass (retained above sieve)**	**% Particles (less than sieve size)**
300 µm	0.05g	98.89
150 µm	3.26g	94.03
106 µm	8g	82.09
75 µm	10g	67.16
Bottom Dish	45g	

Figure 1.9: Sieve stack and shaker

The percentage less than (also referred to as %passage) values are plotted on a Rosin Rammler graph in order to quickly be able to analyse the grinding performance of the mill with respect to the upper and lower limits as define in Table 1.1. The Rosin Rammler graph is a log-log plot that analyses the % (y-axis) of a sample that passes a certain sieve size with respect to that sieve size (x-axis).

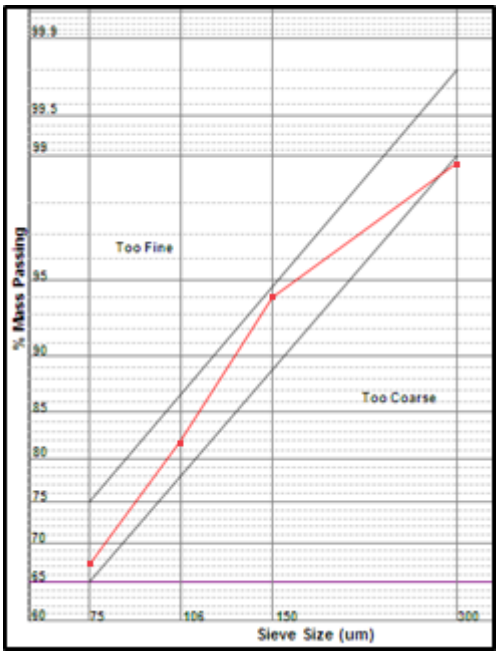

Figure 1.10: Rosin Rammler plot of the data in Table 1.2

The result of the Rosin Rammler graph gives an indication of which way and by how much the classifier blades need to be adjusted in order to shift the particle fineness to fit within the window of optimal grinding performance.

Setting the Mill Rollers

The rollers are set such that an average gap of 3 to 6mm is maintained between the faces of the grinding wheels and grinding ring segments. Weekly and/or monthly wear rates are established by monitoring the wear at mill outages. The rollers are thereafter checked and adjusted periodically to maintain efficient grinding.

1.3. Coal

1.3.1. Southern Hemisphere Coal Development

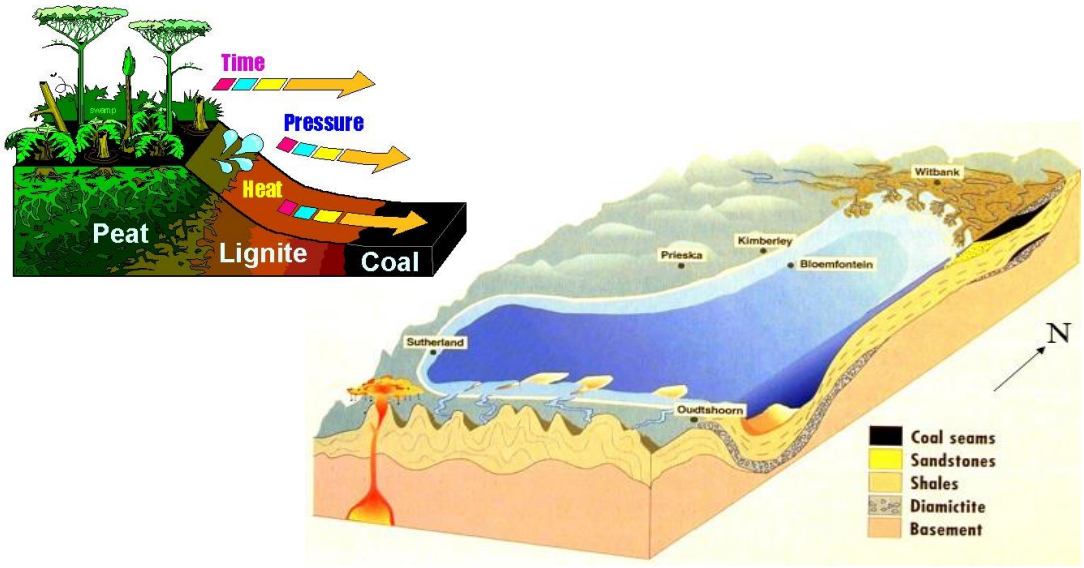

Figure 1.11: Coal formation and the ancient Karoo Sea (van Wyk, 2003)

Coal in South Africa and particularly the Witbank basin was formed by a chemical and geological process that spanned over millions of years. Coal began formation in this region approximately 285 million years ago when South Africa was a part of the prehistoric Gondwanaland super continent. Coals are formed by the progression of three main parameters. That being time, pressure and heat. The extent to which these parameters are applied determined the type or rank of coal. The specific coal properties and characteristics within a rank of coal are determined by the geological setting and the chain of events that led to the formation of coal in the area. Some 250 million years ago the Witbank basin was a swamp land at the shore of the Karoo Sea.

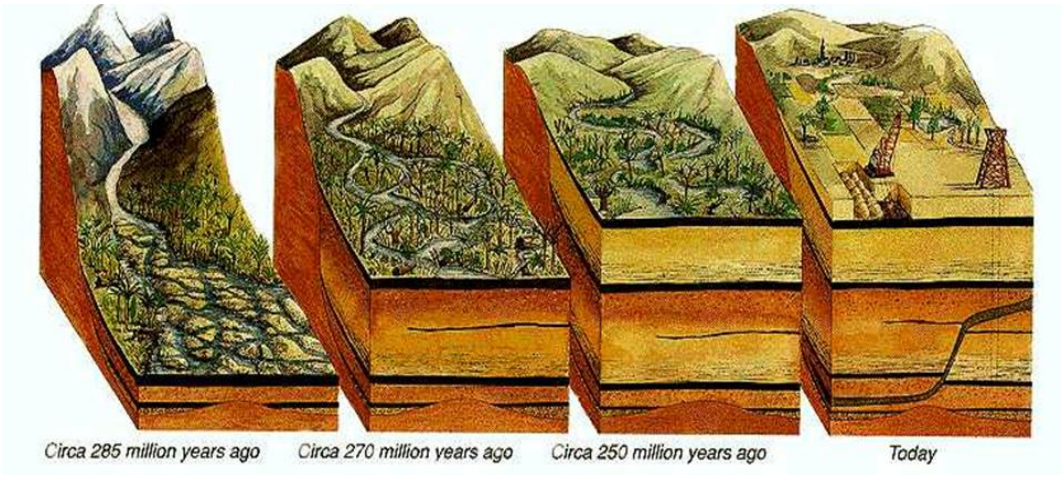

Figure 1.12: Development of coal in the Witbank Basin (van Wyk, 2003)

Millions of years passing through droughts and ice ages have generated layers of dead vegetation that through the application of pressure and heat have become the coal seams that we mine today.

1.3.2. Properties Affecting Coal Milling

The properties of coal that are most relevant to milling are the Calorific Value (CV), ash content, moisture content, Hardgrove Grindability Index (HGI) and the Abrasive Index (AI). Each of these parameters has a large impact on the performance of a mill both in terms of throughput as well as product fineness achievable.

The following table compares the current performance of a typical South African power station to its design conditions.

Table 1.3: Camden Combustion Reliability Investigation (CRI Report, 2011)

Parameter	Units	Camden (Design)	Camden (Current)
Date	-	1972	2010
Manufacturer	-	ICAL	ICAL
Type	-	2-Pass	2-Pass
Circulation	-	Natural	Natural
Burner configuration	-	20 – Front fired	20 – Front fired
Load (Gross)	MWe	200	~195
Ground level to drum level	m	48.15	48.15
Furnace width	m	13.70	13.70
Furnace depth	m	9.54	9.54
Burner belt height	m	13.50	13.50
Burner belt to superheater	m	11.78	11.78
Gross calorific value (HHV)	MJ/kg	24.7	20.5
Inherent moisture	%	5.0	-
Volatile matter	%	24.5	20.7
Fixed carbon content	%	52.5	47.9
Ash content	%	18.0	31.4
Total	%	100.0	100
Sulphur content	%	1.9	-
Net calorific value (LHV)	%	-	18.55
Ash content	%	-	29.33
Volatile content	%	-	19.34
Fixed carbon content	%	-	42.74
Total moisture	%	-	8.59
Total	%	-	100
Deformation temperature	C	-	1305
Softening temperature	C	1190	1340
Hemisphere temperature	C	-	1360
Flow/melting temperature	C	1290	1380
Superheat steam pressure	MPa	11.03	10.65
Superheat steam temperature	C	543	534.22
Superheat steam flow	C	206.6	201.09
Atmospheric pressure	kPa	83.5	83.5
Coal flow	Kg/s	24.63	27.39
Combustion air (Calculated)	Kg/s	226.92	207.5
Excess air	%	25.6	17.95
Burner rating (Calculated)	MW	37.3	37.3
Furnace residence time (Calc.)	s	1.27	1.34
Furnace gas outlet temp.	C	1166	1263.95
Economiser gas outlet temp.	C	323	345
Gas flow air heater inlet (Calc.)	Kg/s	254.51	22.9
Unit efficiency	%	29	-

*Dash (-) indicates information not available

Calorific Value

The CV of a coal is a measure of the chemical potential energy contained in the fuel per unit of mass. It relates the potential energy to the mass of the coal. This is an important parameter as it can tell us two vital things. The mass flow of coal required to achieve the specified total energy input to the boiler, and conversely, the total energy input to the boiler for a certain mass flow of coal. The first will help us in determining the total mass flow of coal required from the mills collectively, while the second will assist in determining the individual energy input that each mill can provide.

The most notable parameter change in the above table is the drop in calorific value of the coal from 24.7 to 20.5MJ/kg. This drop in CV relates to the increase in coal flow rate from 24.63 to 29.39kg/s as is required to achieve the same energy input into the boiler. As Camden is designed to operate with 4 mills in service at MCR (Maximum Continuous Rating), each mill should throughput 6.15 kg/s of coal at full load. While it is possible to operate the unit with all 5 mills in service at very low individual mill throughput, the operating and maintenance philosophy is such that MCR is sustainable with 4 mills in service allowing one mill to undergo maintenance at any given time. Due to the lower CV of the coal, the mills are required to throughput closer to 7.35kg/s of coal instead. However the current coal flow is only 27.39kg/s meaning that the mills are only capable of achieving less than 7kg/s in throughput. This is one performance aspect that contributes to the 5MW shortfall on the MCR of each of the 8 units at Camden power station.

Ash

Coal deposits are usually found intimately associated with inorganic material broadly referred to as ash. Ash in coal is made up of inorganic minerals such as sandstone, siltstone, shale and pyrites. These substances are so microscopically interlinked with the organic material that completely removing it would be a near impossible task. It is therefore inevitable that some level of ash has to be fed into the furnace for

combustion. The ash, of course, is inert and takes no part in the combustion process. It does however generate problems that must be dealt with.

The ash acts to dilute the specific heat content of the coal by adding mass without adding any potential chemical energy of its own. An inverse linear correlation between the ash content and the calorific value of coal in the Witbank basin has been established. The slope and constant of the linear trend is -0.402849 and 33.66 respectively. The trend also shows that as the ash tends to zero, the CV tends to 33.66MJ/kg which is close to the calorific value of pure carbon.

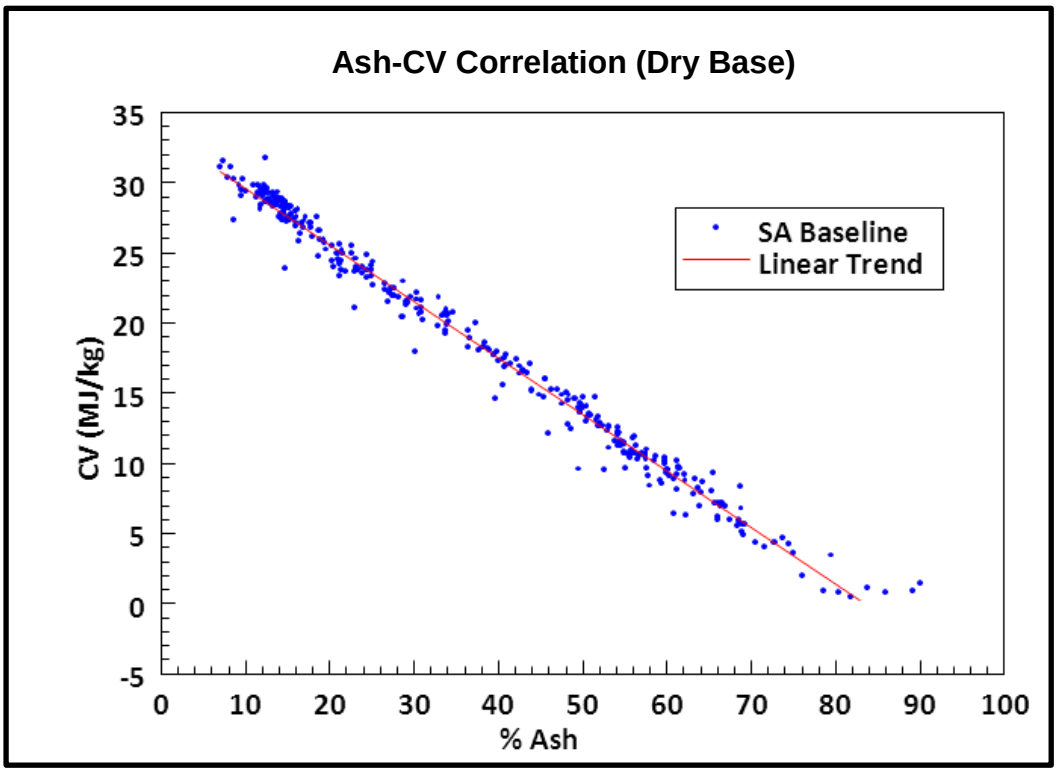

Figure 1.13: Ash-CV correlation for the Witbank basin (van Alphen, 2010)

In Table 1.3 above the ash content of current coal has risen substantially since the power stations design conditions. Ash content has risen from 18% ash in 1972 to 31.4% ash in 2010. This leads to an increase in volume of particulate matter that the induced draught fans have to extract after combustion as well as an increase in volume that the de-dusting and

ashing plants have to contend with. These are two more reasons accounting for the shortfall in MCR.

Hardgrove Grindability Index

The Hardgrove Grindability Index (HGI) is a measure of how susceptible a coal is to breakage. A coal with a high HGI value will be much easier to crush in the mill than a coal with a low HGI. As a result the mill power consumption will be lower, and so will the mill differential pressure due to the lower internal recirculation flow of coal in the mill. With a lower differential pressure the mill will be able to reach a higher maximum throughput of coal flow. A coal with a HGI value of 50 to 55 is normal. A HGI of less than 50 will result in increased energy consumption and higher internal recirculation in the mill. As a result the mill differential pressure will be increased and the PA fan will run out of surplus capacity. This results in the decrease of the maximum achievable mill throughput.

Abrasive Index

The abrasive index is the property of coal that is indicative of its ability to wear out components that it comes into contact with. Bunkers, chutes, metal liners, mills, burners, classifiers and pipe components are all subjected to wear during transporting and milling operations. In the mill, the grinding element life is most affected by this factor, and so are the throat and classifier components due to the accelerated velocities at these locations. A higher abrasive index leads to reduced life of these components and possible failure before the mill is due for outage. Due to the harsh abrasive nature of the flow inside the mill, these components are checked and often repaired at every mill outage (1500 hours of operation).

Moisture Content

The coal moisture content can be broken down into two constituents. The inherent moisture is that which exists as a quality of the coal seam in its natural state of deposition. The surface moisture is that which the coal has been exposed to during transportation, storage and other post mining processes. The milling process is controlled to maintain an outlet

temperature sufficient to remove the moisture content from the coal. And thus coals with high moisture content will result in increased mill inlet temperature in order to dry the coal. If the mill outlet temperature drops too low due to extremely wet coal, the mill will have to reduce load in order to avoid a mill trip. High moisture in coal also has other consequences such as coal hang ups in the bunker and feeder chute. This causes the screw feeder to inaccurately record the coal mass flow into the mill as it is a volumetric based feeding device.

1.4. Problem Statement

Power stations in South Africa are facing the reliability problems associated with an ageing generating fleet. The need for additional generating capacity does not allow for the decommissioning of older plants and has even forced the return to service of 3 previously mothballed power stations. Power stations are further forced to burn lower quality coal due to two main reasons. The coal that older power stations were designed for has become much more difficult to acquire as coal seams have depleted through the years and power stations are operated further beyond their design life. And secondly, the worldwide economic climate makes high quality coal much more profitable as an export commodity to fast growing emerging power sectors in China and India.

This deteriorating coal quality has since put additional strain on the milling plant by requiring a higher mean mass flow rate of fuel in order to maintain the (MCR) of the unit. Coal mills are required to increase throughput at a stage where late-life maintenance and reliability is both high and poor. The urgent need for generating capacity does not afford the luxury of accepting the current load losses as a result of the inability of mills to meet the coal throughput requirements.

1.5. Aim

In order to improve the reliability of the milling plant one must monitor the condition of the plant and be able to evaluate its current state of performance. A Mill Health Monitoring System (MHMS) has been proposed in order to meet this need. Such a system would require the implementation of real-time monitoring and tracking of all mill parameters in order to establish the health status of a mill. These may further be used to predict the cause of poor health in a real-time manner should it occur. Before a MHMS can be implemented however, it was found that two key performance evaluation parameters of the mill are currently inaccurately measured and not measured in an on-line, real-time manner. These are the coal throughput of the mill and the particle fineness produced by the mill, respectively. In the context of this study, the mill will therefore be evaluated in terms of quantity and quality, of the product it produces. As a step towards a condition monitoring system, real time methods of measuring both parameters must first be developed and evaluated.

Furthermore, it is hypothesised that the mill internal recirculating load may be inferred by means of differential pressure measurements at various heights of the mill body. This currently un-measureable parameter will contribute to the MHMS by providing further insight into the health of internal components such as the mill throat.

Increasing the throughput of an ageing mill requires that the dynamics of the milling plant system first be understood. Once the relationships between the control parameters and the performance evaluation parameters are well established, a control philosophy can be developed in order to maximise the mill performance of the system as a whole.

The aim of the research herein is to:

1. Develop a mill energy balance model that can be used to monitor the coal mass flow of the mill.

2. Assess and evaluate the applicability of an instrument adopted from the pharmaceutical industry, to measure the coal particle size distribution produced by the mill in real time.

3. Test a method of determining the mill internal recirculation load by means of measuring the differential pressures across various heights of the mill body.

4. Establish and understand the relationships between the control parameters, and the key performance indicators of the mill and use this information to optimise the mill for increased throughput.

By achieving the above four goals a step may be taken towards alleviating the problems of inaccurate coal flow and particle size measurements for condition monitoring, as well as to reduce power station load losses as a result of inadequate mill throughput capacity. By monitoring the performance of the mill in real time corrective action and maintenance can be taken as soon as problem is detected, avoiding a failure and thus improving overall milling plant reliability. Furthermore a control philosophy can be recommended to maximise the coal mass flow of the mill and reduce the current power station load losses due to lack of throughput capacity.

Chapter 2: Literature Review

2.1. Milling Plant Performance Modelling

In the field of milling plant condition monitoring, (Makokha et al. 2009) had shown that the mill outlet temperature and the pressure drop of a tube mill can be predicted by means of an energy balance model. The aim was to eventually incorporate the steady state model into the overall mill control scheme as an auxiliary monitoring tool for early detection of parameter drifts or malfunctions specific to tube mills. This is achieved by performing the calculation of the energy balance model, and comparing the expected values to those measured on the plant.

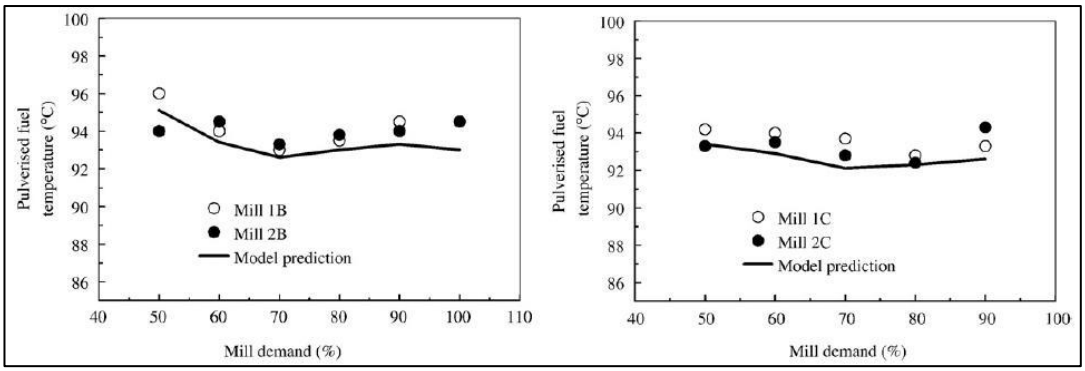

Figure 2.1: Prediction of mill outlet temperature (Makokha et al. 2009)

From Figure 2.1 the model predicts the mill outlet temperature fairly well below mill loads of 80%. At loads higher than 80% the model tends to under-predict the temperature but only by as much as 5%. It must be noted that this model was developed specifically for a tube type mill which is significantly different to the operation of a vertical spindle mill. The success of the model in predicting the mill outlet temperature and the mill differential pressure is promising in light of the task set out herein, i.e. to predict the mass flow of coal using an energy balance model.

The model of Makokha et al. (2009) was implemented in such a way that it shadows alongside the control system and purely provides advisory information to the operator. This concept was developed a step further

when Fan & Rees (1997) implemented their own model in such a way that it not only monitors the process and provides advice to the operator, but is also able to intervene in the control system. This model performs on-line parameter estimation and performance prediction and uses experience based knowledge to perform fault diagnosis and prognosis and even proposed the optimal corrective action. The second function of what they term the Knowledge Based mill Operator Support/control System (KBOSS) allows it to perform mill and fuel supervision and control. This monitors the unit fuel demand and controls the mill load sharing coefficients thereby varying the loads between mills based on grinding element wear, in order to maintain the overall unit power output.

Niemczyk et al. (2012) derived a mathematical coal mill model for control with the aim of providing better load following capabilities of pulverised fuel mills and thus of pulverised fuel fired power stations. The need for better load following capabilities has stemmed from the shift towards reduced power station emissions and new build projects based on renewal energy sources. This poses the problem of fluctuating load on the grid which base load coal fired power stations are forced to compensate for. An important bottleneck in the operation of coal fired power stations is the coal pulverisation process which gives rise to slow take up rates and frequent plant shut downs (Rees & Fan 2003). The paper explains though, that model based control of the milling plant has seen slow development due to the fact that the pulverised fuel leaving the mill had not been measureable in any real time manner due to the harsh and abrasive nature of pulverised fuel flow.

An observer based fault detection and moisture estimation system was presented by Odgaard & Mataji (2007) by means of a simple mill energy balance. The term “fault” refers to what is commonly known as a coal hang up. A very simple energy balance model is used to determine the coal moisture and detect a fault as soon as it occurs. While Odgaard et al. (2007) have developed an energy balance that can predict the steady

state operational moisture content of coal, they go on to refer to the prediction as a “noisy measurement”. Despite this the prediction followed measurement data very well as shown in Figure 2.2 below.

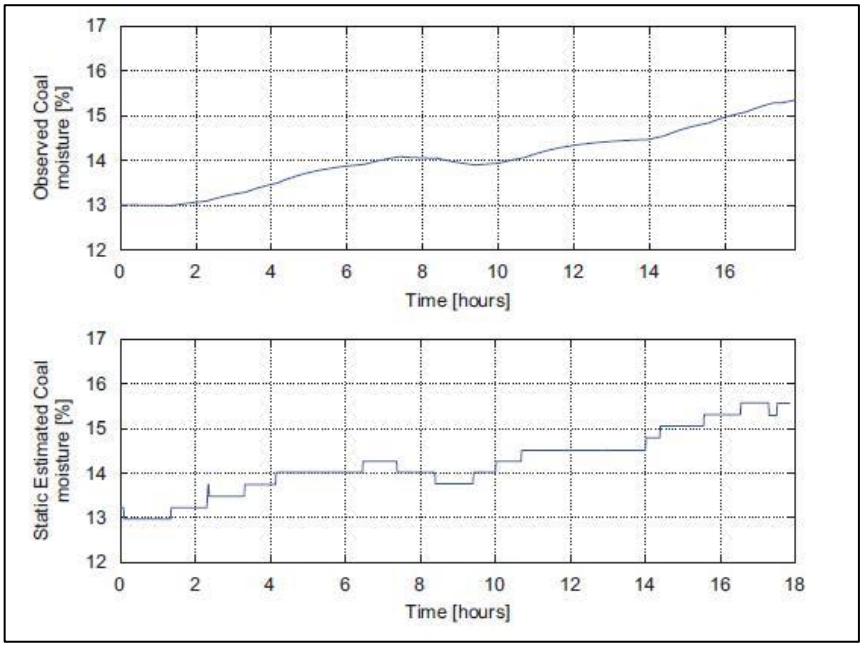

Figure 2.2: Moisture estimation compared to measured values (Odgaard et al. 2007)

The paper further emphasises, as was mentioned by Niemczyk et al. (2012) that the mass flow rate of coal out of the mill is an important variable that at the time was not possible to measure. This is important, as the focus of the energy balance that will be developed in this dissertation is to predict the coal mass flow through the mill.

Mill energy balance models and observer based mill monitoring systems have to date lacked vital measurement parameters as model inputs, thus limiting their use in true condition based monitoring and maintenance systems. The Knowledge Based mill Operator Support/control System (KBOSS) in the paper of Fan & Rees (1997), had come the closest to achieving a true mill condition monitoring system. However, the technology available to them did not allow accurate and on-line measurement of pulverised fuel mass flow leaving the mill.

Extensive work to build a multi-segment model of the milling plant was performed by Wei et al. (2007). The model consists of six segments that apply to different operating regimes of the mill. These are made up of start-up, standard milling, shut down, and transition periods in between. The model uses internal variables that reveal the characteristics of some un-measurable intermediate variables. These include the mass of coal in the mill, the mass of pulverised coal in the mill and the mass flow of pulverised coal out of the mill. It is noted that in this model the heat loss through the walls of the mill is assumed to be zero. This is similar to the assumption made in other models in literature but has been included in the mill energy balance derived in 0.

2.2. Particle Size Analyser

The most significant change in particle size analysis technology has been attributed to the shift of measurement techniques towards methods that are based on the interaction of particles with light. These methods may be divided into two categories, namely field scanning and stream scanning methods.

The laser diffraction method is widely known as the most commonly used field scanning technique. The theory states that when a spherical particle is illuminated by a parallel beam of mono-chromatic, coherent light, a diffraction pattern is formed (Wanogho et al., 1987). If, as per Figure 2.3, a lens is placed in the light path after the particle and a photo-electric sensor is positioned at the focal plane of that lens, then un-diffracted light is focused to a point. Any diffracted light will then form a pattern of rings around the central point. The movement of particles through the beam of light has no resultant effect on the diffraction pattern. Light diffracted at a certain angle will always have the same displacement in the focal plane, irrespective of the instantaneous position of that particle.

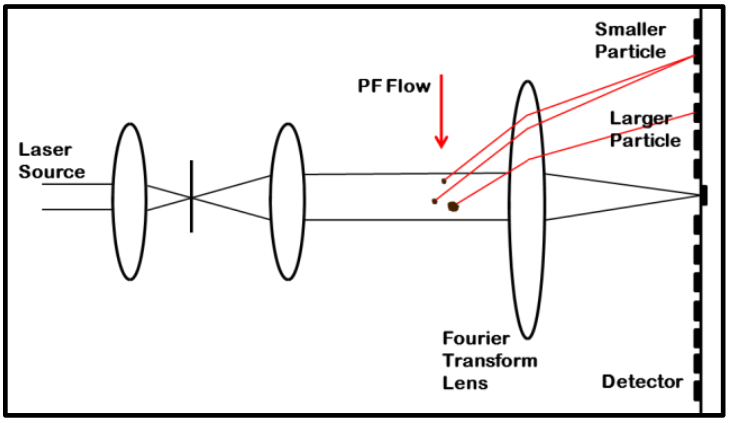

Figure 2.3: Optical layout and measurement principle (Wanogho et al. 1987)

The diameter of the diffraction pattern is inversely proportional to the diameter of the particle that passes through it. The particle size distribution may then be inferred by analysing the energy of light contained in any ring in the focal plane as indicated in Figure 2.4 below. A microprocessor analyses diffraction patterns that are summed for several measurements to obtain an integral measurement. This integral diffraction pattern is then used to determine a particle size distribution.

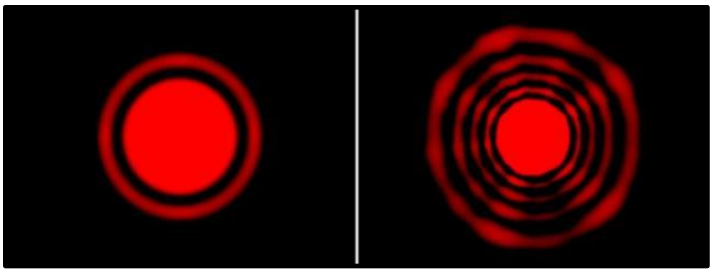

Figure 2.4: Diffraction patterns of small and large particles

Examples of stream scanning techniques comprise of focused beam reflectance measurement, shadow Doppler velocimetry, light scattering analysis, the phase Doppler method, Charge-Coupled Device (CCD) camera imaging techniques, and the spatial filtering technique. Petrak (2002) developed a method of using fibre-optic Spatial Filtering Velocimetry (SFV), modified by Fibre-optical Spot Scanning (FSS), in order to determine the particle size.

Spatial filtering velocimetry is a method of determining the velocity of an object by observing it through a spatial filter in front of a receiver. The details of which have been explained in the paper by Aizu & Asakura (1987). The modified spatial filtering technique as described by Petrak (2002) employs Fibre-optical Spot Scanning (FSS) as an addition to the SFV. Fibre-optical spot scanning observes the projected shadow of a particle as it moves across an optical fibre. As the shadow image is passed across the single fibre, an impulse is generated as illustrated in Figure 2.5. The width of the shadow is dependent on the particle size, the particle velocity, and the random spatial location of the particle and fibre. The shadow image of the particle is said to have the same size as the particle, under the circumstances that the light diffraction by the particle and the influence of a divergent angle of the illumination beam, may be neglected. (Petrak 2002)

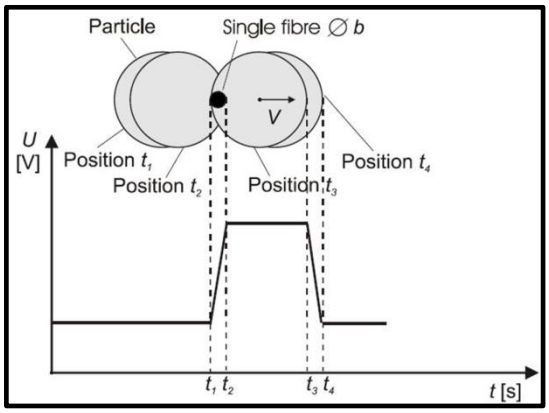

Figure 2.5: Impulse generated by fibre-optic spot scanning (Petrak 2002)

In this way the chord length of the projected surface of an individual particle is measured.

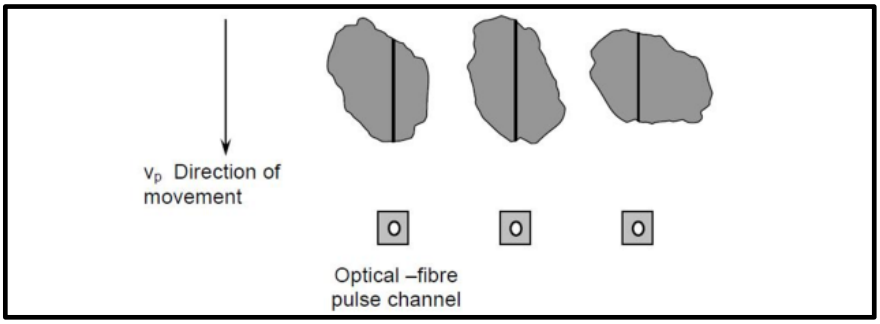

Figure 2.6: Chord lengths of projected face (Parsum, 2011a)

The chord length is the link between two points on the perimeter of the projected face of the measured particle (Figure 2.6). It describes particle size as a statistical value and is largely dependent on orientation as well as the trajectory of the particle.

The statistical evaluation of a specified quantity of individual particles is required in order to achieve a representative particle-size analysis.

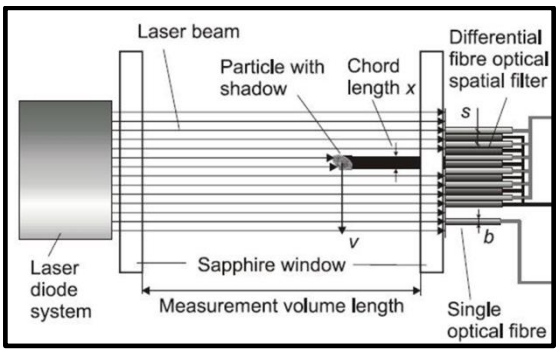

Figure 2.7: Chord length measurement using FSS and SFV (Petrak 2002)

Figure 2.7 illustrates the schematic arrangement of the measurement components as a coal particle passes through it.

In a paper by Dodds et al. (2004) an overview is given on the evolution of particle sizing technology by comparing the content of the Particle Size Analysis Conference of 1977 to that of the Particulate Systems Conference held in 2003. One of the major differences found was that the systems studied in 1977 were all dilute phase while modern technologies allowed the study of concentrated systems as well. Modern technologies

have also been instrumental in the shift toward on-line measurement systems. The paper goes on to emphasise the importance of in-line or in-situ measurement of particle size for process control. This is reiterated in the works of Hancke et al. (1996) where it is stated: “to put this parameter to its most effective use, it is necessary to measure it on-line” (Hancke et al. 1996).

The emphasis on the importance of maintaining a good particle size distribution is further outlined when Abbas et al. (1994) show the effect that particle size distribution has on NO_x formation and emission. Measurements taken on a pilot scale combustor showed that the NO_x emissions from ultrafine coal particles, in the region of 12µm, was approximately 30% higher than that of pulverised fuel of standard grind. This shows one of the drawbacks associated with PF that is ground too fine.

Furthermore, the effectiveness of NO_x reduction technologies is largely dependent on how well the process upstream of combustion is controlled. The most popular NO_x reduction technology is that of the Low NO_x Burner. Its operation is such that the burner holds the de-volatilization zone of pulverised fuel (PF) very close to the burner mouth while starving the de-volatilization process of oxygen, and thus preventing the formation of NO_x (Abbas et al. 1994). Secondary and tertiary air are well controlled and precisely staged in order to allow just enough oxygen to promote combustion in their respective zones thus forming CO_2 and N_2. In order for the burner to operate correctly and achieve NO_x reduction, the coal mass flow, air mass flow and coal particle size must be controlled accurately. In order to control those parameters accurately they must first be measured accurately.

On-line particle sizing has been achieved by the implementation of various technologies in recent times. The most popular are the laser diffraction, spatial filtering and image analysis techniques. A CCD camera based optical image analysis system for on-line measurement of the particle size

distribution was developed by Carter et al. (2007). This system incorporated a laser sheet generator to illuminate a plane through the field of suspended particles. The particle size distribution was generated by analysing the resulting images using processing algorithms. The results showed good comparison with offline methods of particle size determination, namely physical sieve analysis and the laser diffraction based Malvern Particle Size Analyser. This method was later incorporated into a mass flow measurement system by integrating it with an electrostatic particle velocity measurement as well as an additional image processing algorithm that determines the density of particles in the pipe (Carter et al. 2005). This work was taken even further when Chinnayya et al. (2009) used this technique to validate a numerical simulation (using Large Eddy Simulation) of the pulverised fuel pipe of a 4MW coal fired combustion test facility in France.

The image processing technique developed by Carter et al. (2005) showed good correlation to accepted laser diffraction results when Shao et al. (2011) had tested the system in a full scale power station. The laser diffraction device used was, once again, the Malvern Particle Size Analyser. The full scale results of this paper did not make comparison to the results of a physical sieve analysis. A comparison between the laser diffraction technique and manual methods of particle size determination was made by Pieri et al. (2006), however this research was based on the particle size measurement of various soils and the traditional technique compared was that of sedimentation. Although the laser diffraction results did tend to ‘underestimate’ the particle size distribution it was finally concluded that the benefits of the instrument outweighed the small difference to classical sedimentation results. These advantages were listed as, wide range of size classes, independence to particle density and the sheer speed of testing and result reporting.

The advantages of wide class sizes and fast testing are shared with the technique of fibre optic spatial filtering for particle size determination, as

are the advantages of on-line measurement and real-time reporting of results. This is the technique employed by the instrument tested in Chapter 5:. Although the method of laser diffraction can produce more classes of results at the smaller particle size diameters, the instruments that use this technique usually measure particles in a slurry and are commonly used in a lab environment away from the plant process. The Particle Size Analyser (PSA) that was chosen for testing on the power station uses the spatial filtering technique and can measure the particle size distribution of air swept particle flows directly in the process line. The same instrument was lab analysed in the paper by Petrak et al. (2002), where there were some discrepancies to the two lab prepared samples of spheres and narrow glass beads. These differences were said to be caused by the random cut effect and by the influence of laser diffraction on the cord length which is the primary measured parameter. The paper also mentions briefly that the probe is inserted into the pipe to take a reading and that ideally the entire process flow should be measured as opposed to a single point of measurement. From the lab analysis, Petrak et al. (2010) then tested this instrument in various industrial and technical processes. These were, fluid-bed granulation, high shear wet granulation, Wurster coating, mixing, spray drying, crystallization and milling. Similar conclusions were finally made to that of the lab experiments but little was looked into the physical measurement techniques of each application.

2.3. Mill Internal Flow Dynamics

The nature of the two phase flow inside a vertical spindle mill and its associated theory is explained in the book Thermal Power Plant Simulation and Control (Rees & Fan 2003:63-99). Focussing attention to the interaction of the coal with air, the coal output from the grinding media moves toward the throat of the mill where it mixes with the high-speed hot primary air. Heavier coal particles are immediately returned back to the bowl for further grinding whilst the lighter particles are entrained in the air

flow and carried to the separator section. The separator section refers to the expansion area above the mill throat and before the classifier. This area contains a large amount of coal particles in suspension by the powerful air flow. Here some of the heavier (larger) particles entrained in the primary air-coal mix fall out of suspension after the air reduces in velocity. These particles then fall back to the mill table for further grinding. Some of the lighter (smaller) particles also leave this suspended bed and remain entrained in the air flow which enters the classifier. Rees & Fan (2003) noted that the ability to measure the differential pressure between the top part of the mill and the under bowl is very useful in helping to understand the mill recirculating load.

Finally the classifier induces a swirl in the classifier cone area, similar to that of a cyclone separator, in order to separate the finer particles to be sent to the burners from the coarser particles to be returned to the grinding table. The similarities between the flow paths of a circulating fluidised bed and a vertical spindle mill can be seen in the side by side comparison in Figure 2.8 below.

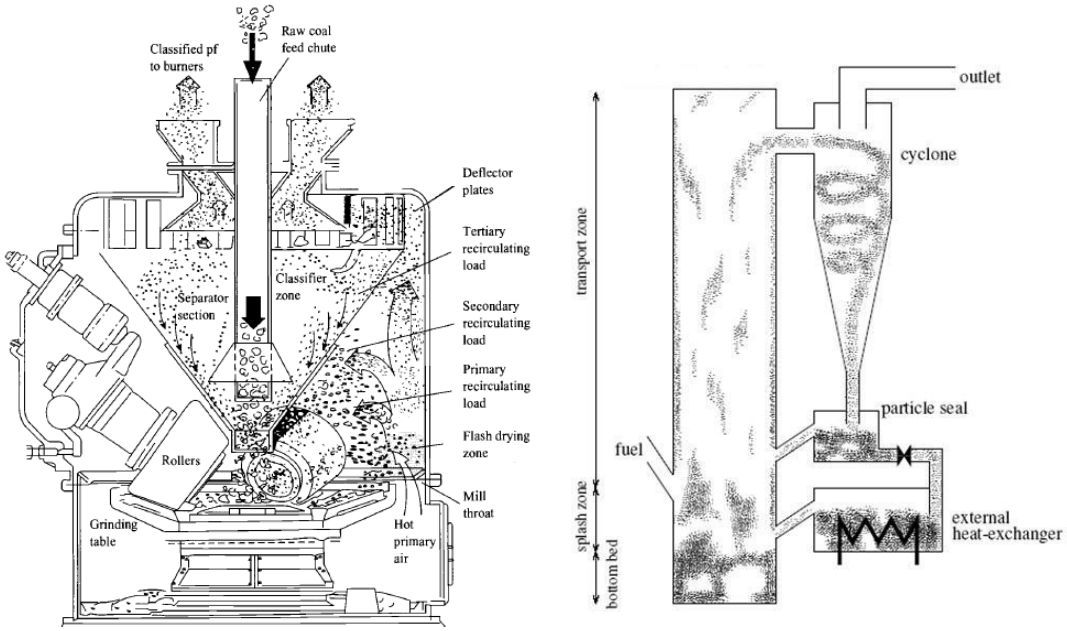

Figure 2.8: Vertical spindle mill and circulating fluidised bed (Kitto & Stultz, 2005)

The mill is effectively a circulating fluidised bed with the cyclone separator located inside the mill body. The method of particle size reduction in a circulating fluidised bed boiler is combustion whereas in a mill the method of size reduction is crushing. It is hypothesised then that the principles of calculating the bed height and the suspended mass of particles of a fluidised bed boiler can be applied to calculate the suspended mass of particles in a section of the mill.

At the fluidisation velocity the bed is said to be fully supported by the flow of gas and the pressure drop through the bed per unit of height is equal to the bed weight, ie. $\frac{\Delta P}{L} = \left(\left(1-\varepsilon_{mf}\right)\left(\rho_p-\rho_f\right)\right) \times g$ (Yang, 2003). The expression $\left(1-\varepsilon_{mf}\right)\left(\rho_p-\rho_f\right)$ is known as the apparent density $\left(\rho_{pf}\right)$ of the particle/air mixture. Therefore by measuring the differential pressure across a particular height, one may determine the apparent density of the mixture. Then furthermore, by understanding the geometry of the mill, the air velocity and applying a particle-air slip factor, one may calculate the mass flow of particles in suspension.

Clark et al. (1991) further used the method of dual static pressure probes (differential pressure) in the mid bed region to infer the presence of bubbles or slugs in fluidised beds. By studying the pressure signals produced by the dual static pressure probes, a database of pressure traces has been developed from a slugging bed. By analysing this data the slugging frequency and the slug rise velocity was determined. Saxena & Rao (1990) designed and fabricated a pressure transducer probe that is installed at the wall of the fluidised bed and is monitored by an automatic recording system of a predetermined sampling frequency. Pressure fluctuations were recorded and used as a diagnostic tool to establish the quality of fluidisation. The method was also used to detect voids and void renewal frequency in the bed.

The papers of Clark et al. (1991) and Saxena & Rao (1990) advance the basic principles of pressure measurement in fluidised beds by using static

pressures to monitor the quality of the fluidisation process and even detect common phenomena in the bed. Both agree that monitoring the static pressure (and static differential pressure) in fluidised beds can provide valuable information about the nature of the flow and the control of the fluidisation process.

Studies of the two-phase flow inside of a mill have been performed to various degrees worldwide in attempts to better understand the nature of the flow and how it relates to and influences the mill performance in terms of mill throughput and particle fineness. The bulk of these studies were based in the field of computational fluid dynamics in attempts to model mill behaviour.

Bhambare et al. (2010) developed a CFD model of a vertical spindle mill using a coupled discrete phase model in Fluent that considers coal moisture evaporation as well as particle velocities, trajectories and particle-air interaction. The analysis showed that the mal-distribution of primary air at the mill throat level (mill windbox) has a negative effect on both primary air distribution and pulverised fuel distribution between the different mill outlet (Pulverised Fuel) pipes. The paper states that an improvement in both primary air and coal particle distribution was achieved by homogenising the flow of air at the throat inlet. This change is stated to improve from 3.8% to 0.3% standard deviation for air and 3.5% to 2.8% standard deviation for coal.

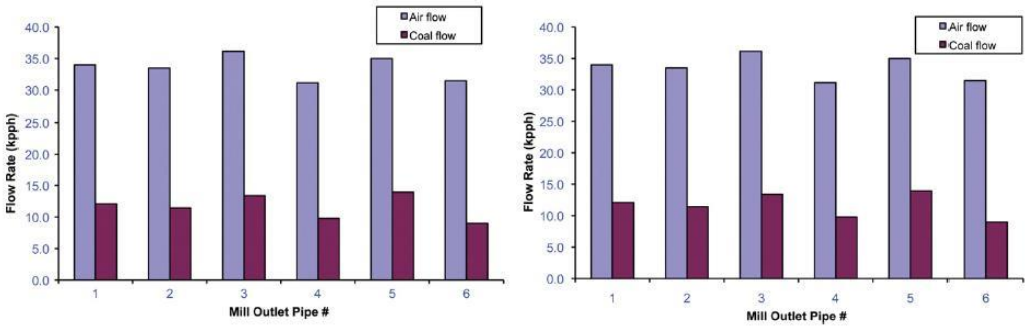

Figure 2.9: PF pipe distribution in kilo-pound per second (Bhambare et al. 2010)

The PF pipe distribution graphs (Figure 2.9) however showed very little change from mal-distributed flow at the throat on the left, to well distributed flow at the throat on the right. Figure 2.10 below shows typical test results of PF pipe distribution of a mill at Camden power station. Deviations of up to 8% from the mean are not uncommon and still considered to be within specification.

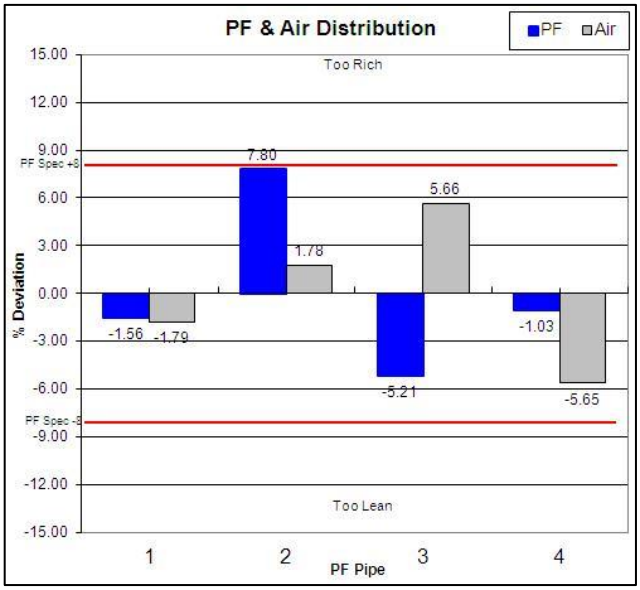

Figure 2.10: Camden PF and air distribution

It was also found by Bhambare et al. (2010) that the coarse particle mass fraction per pipe had improved with uniform air velocity at the throat, thereby producing a finer product overall. Correcting the distribution of air and coal between PF pipes as well as the improving the overall particle fineness is important for the operation of modern Low NO_x burners (van der Merwe et al., 2012).

Vuthaluru et al. (2009) performed a multiphase CFD analysis of a simplified pulveriser using a granular Eulerian-Eulerian approach in the Fluent CFD code. Areas of exceptionally high air velocity were found close to the walls, indicating a strong probability of the carryover of larger particles. The study showed that 100µm particles tended to follow the air path lines closely whereas the velocity vectors of the particles larger than 500µm had deviated significantly from those of the airflow. This is

indicative of the primary classification (large particle fallout and recirculation) that occurs around the grinding element section of the mill.

A dilute phase two phase Eulerian-Lagrangian model was used by Shah et al. (2009) to evaluate the effects of the classifier vane angle on various other operational parameters such as the mass flow rate of coal through the mill (or mill throughput/load), the classifier efficiency, and the size of particles allowed to leave the classifier. In this paper the classifier efficiency was defined as the ratio of coal particles that exit the classifier into the PF pipes as divided by the total coal particles that enter the classifier, i.e. the classifier throughput ratio. The CFD analysis, performed using Fluent, finally produced results that differed by 3-7% in terms of the particle fineness produced by the mill. The model was further used to optimise the classifier vane settings. An ideal classifier vane angle of 65% open was determined for the mill modelled in order to achieve the three main factors that were defined for determining mill performance. Those being:

- As close as possible uniformity of mass flow between the PF pipes
- A high as possible classifier efficiency, as well as
- Meeting the specified particle size output of 70% below 75um

Shah et al. (2009) give reference to the classifier blade angle. This refers to a static classifier (Figure 6.11) and closing of the vane angle is the equivalent exercise to decreasing the classifier speed in a rotating/dynamic type classifier (Figure 6.12) that will be encountered in later chapters. The three critical performance evaluation factors stipulated above are focussed mainly on the mill outlet, and specifically the classifier performance. The dissertation herein will however only focus on the mill performance as a vital pre-processor and integrated system to the rest of the generating unit. Thus the emphasis placed on the mill throughput as well as particle fineness.

Parham & Easson (2003) built a one third scale model of a vertical spindle mill classifier and used three-dimensional Laser Doppler Anemometry to characterise the aerodynamics of the classifier at different vane angles. The object was to compare the aerodynamic characteristics of a vertical spindle mill to those of and industrial cyclone separator. It was demonstrated that the flow within the classifier was characterised by two distinct regions.

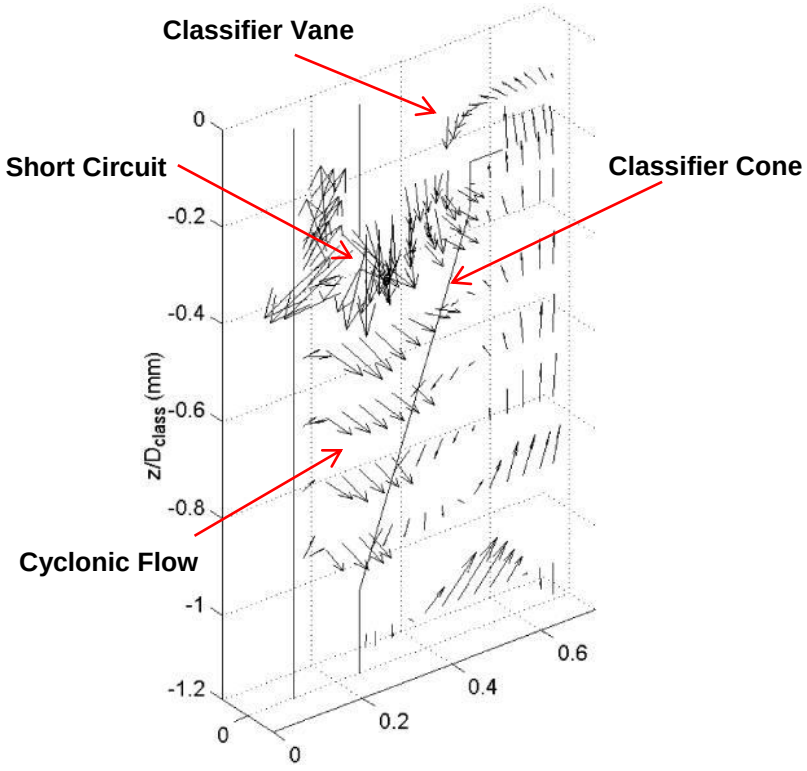

Figure 2.11: Short circuiting of the classifier (Parham et al. 2003)

The lower section of the cyclone showed close resemblance to the characteristics of a flow found inside a cyclone. However, in the upper section of the classifier there was strong evidence of classifier short circuiting where the flow leaves the vortex finder directly from the classifier vanes without undergoing any swirl. Cyclone separator models were therefore found not to be applicable in this area of the classifier.

2.4. Conclusion

Literature agrees that in order to best control the performance of the milling plant a combination of milling plant monitoring in conjunction with some form of mill modelling is required. The basic energy balance is most preferred and popular choice of such a modelling solution. Energy balance models have been used as a tool to monitor unmeasured and poorly measured parameters, to monitor mill components for calibration errors and incorrect parameter reporting, to monitor and alarm of process faults and even to intervene in the control of the milling plant. 0 will aim to develop a mill energy balance that can be used to accurately monitor the coal flow through the mill feeder and will form the first step towards a complete mill health monitoring system.

The second step towards such a system is to be able to accurately monitor the particle fineness produced by the mill. Literature shows multiple technologies that can be used for this purpose. The change to laser and optic based measurement techniques has been a major advancement in the measurement of this parameter, and the availability of modern powerful and portable processing has allowed the shift from lab based measurement to direct in-line process measurement. Such a direct method particle size measurement will be tested in the power station environment for use as an on-line measurement device.

The mill internal process shows great similarity to that of a circulating fluidised bed type boiler. The nature of the flow in the lower part of the mill has even further similarities to that of a fluidised bed in general. The basic principles of calculating the suspended bed mass is by using differential pressure measurements and many have taken this method a step further by using it to monitor and characterise the fluidisation process. It is expected that the same basic principles would apply to the fluidisation region of the mill.

Using CFD tools to model the flow through a mill has provided much insight into the nature of the flow in various areas of the mill, as well as some of the effects that process changes have on the output product. The harsh abrasive environment makes it difficult to take physical measurements on the internals of an operating mill. While there are a handful of researchers actively pursuing the CFD study of coal pulverisers, most research is focussed on vertical spindle mills with static classifiers similar to the mills found on Camden power station and in this study. However few studies are focussed on dynamic (rotating) classifiers of the type where swirl is generated in the mill body itself (like that of the pilot scale mill tested herein).

Chapter 3: Method of Research

3.1. Coal Mass Flow Rate

The coal feeder itself can be used to measure the flow through it but it is fundamentally a volumetric type screw feeder (on Camden power station) with no compensation for raw coal density or moisture changes. It therefore cannot be used as an accurate mass flow measurement tool. A Mill Energy Balance (MEB) has been identified as a tool that can be used to determine the coal mass flow rate through the feeder under steady state conditions. The mass and energy balance would also be used to detect feeder calibration errors and feeder drift.

An energy balance of the milling plant was developed from first principles based on a simplified mill layout. The input and output parameters of the MEB were measured on a full scale mill in operation at Camden Power Station and verified against the calculated values of the MEB. In order for the system to function as an on-line monitoring tool, only the signals currently monitored by the DCS were used as inputs to the MEB. This ensures easy rollout to all 40 mills on Camden Power Station and simplifies expansion to other power stations which already monitor the standard set of mill parameters.

3.2. Pulverised Fuel Particle Size Determination

The Particle Size Analyser (PSA) is an instrument that has been adopted from the pharmaceutical industry where it is used to measure the particle size distribution of fine powders. The coal fired power generation industry is a much harsher environment while measuring a substance that is substantially different to those of the pharmaceutical industry. The instrument was experimentally evaluated in terms of measurement accuracy and the results were compared to the proven iso-kinetic

sampling and sieving process. Research took the form of experimental testing and analysis.

The particle size analyser was used to measure the particle size distribution of the PF as it flows through the PF pipe at the mill outlet. This was performed on a full scale operational mill at Camden Power Station.

All tests were performed while the mill was operated in manual mode so as to eliminate the load fluctuations from the automatic control system. The tests were made up of five types of tests that study the effects of five different parameter changes. The purge air of the probe was suspected to have an effect on the nature of the flow for coal, through the laser eye. The effect on the particle fineness reported by the instrument, by changing the purge pressure, purge flow and purging time were studied individually. Furthermore the rotation of the probe in the sampling port as well as the measurement depth into the PF pipe was studied by monitoring the effect these parameters have on the results.

Once the probe has been characterised, the most accurate measurement settings can be selected for the specific plant layout and operating conditions under which the instrument will be used.

The same experimental procedure was followed on the pilot scale mill, and once the PSA was calibrated for that system, the instrument was be used to monitor in real time the changes in particle fineness due to the mill operational changes.

3.3. Mill Recirculating Load

3.3.1. Overview

An attempt was made to measure the recirculating mass of coal inside the mill at different stages of the mill internal processes. Differential pressure measurements coupled to a simple mathematical model was used for this purpose. A pilot scale mill was instrumented with eight static pressure taps

and differential pressure transducers at various heights along the mill body. During testing the mill operational parameters were changed in order to detect the change in suspended mass of coal by means of the installed instrumentation.

3.3.2. Instrumentation

Differential pressures across the throat, tyre area, classifier area and mill outlet were measured as shown in Figure 3.1 below.

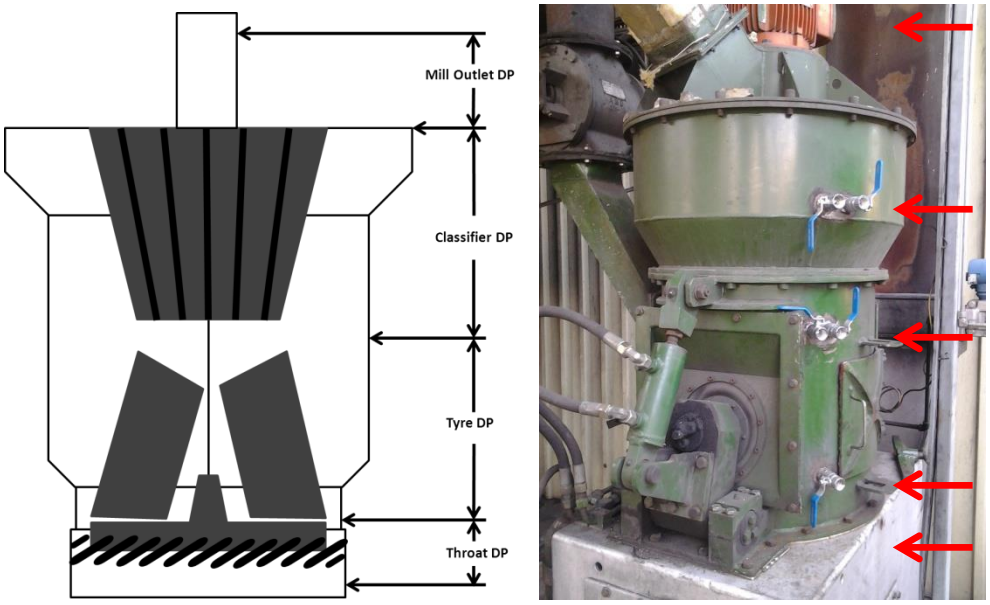

Figure 3.1: Pilot Scale Mill Pressure Taps Installed

The differential pressure measurements were performed with Siemens pressure transducers (Figure 3.2) linked to a dedicated laptop via a National Instruments data acquisition system.

Figure 3.2: Pressure transducers

3.3.3. Calculations

Calculating the mass of particles in suspension is achieved in CFBC (Circulating Fluidised Bed Combustion) boilers and is an important factor in determining the level of fluidised material in the furnace. This is done using a differential pressure measurement between two specified heights in the bed region. The characteristics of a fluidised bed are very similar in nature to the internals of a mill. In this way the differential pressure of the mill across a given height will be measured and the suspended mass of particles can be calculated using the following equations.

$$\boldsymbol{DP_1 = \rho_{pf} \times g \times h} \quad \textbf{(3.1)}$$

Rearranging this to solve for the apparent density, we have,

$$\boldsymbol{\rho_{pf} = \frac{DP_1}{g \times h}} \quad \textbf{(3.2)}$$

Next the primary air velocity is required,

$$\boldsymbol{V_f = \frac{M_f}{(\rho_f \times S)}} \quad \textbf{(3.3)}$$

The particle velocity is a function of the air velocity and a slip factor between the particle and air,

$$\boldsymbol{V_p = V_f - (V_f \times V_{slip})} \quad \textbf{(3.4)}$$

With the velocity of the particles in the section known, one may then calculate the mass flow of particles in suspension,

$$\boldsymbol{M_p = \rho_{pf} \times V_p \times S} \qquad \textbf{(3.5)}$$

Using the this method the mass in suspension is calculated for the tyre section (DP1) as well as the classifier section (DP2) and the difference is considered to have fallen out of suspension and returned to the grinding table.

3.3.4. Test Procedure

In order to test this principle on a pilot scale mill, various parameters were varied while measuring the differential pressures in an attempt to link the changes in differential pressure to changes in the suspended mass of PF.

The tests involved changing the mill load, air/fuel ratio and classifier speed while measuring the differential pressures depicted in Figure 3.1 above. The aim of which was to establish whether the change in suspended mass of coal is measureable using the technique of differential pressure measurement. The test cases were established as per Table 3.1 below. The notation “CL10 3:1” refers to a classifier speed of 10% and an air/fuel ratio of 3 to 1. For each fixed classifier speed and fixed air/fuel ratio, the mill was increased in load (coal mass flow) from the minimum to the maximum stable coal throughput.

Table 3.1: Recirculating load test cases

	Air/Fuel Ratio			
% Classifier	**3:1**	**4:1**	**5:1**	**6:1**
10	CL10 3:1	CL10 4:1	CL10 5:1	CL10 6:1
12	CL12 3:1	CL12 4:1	CL12 5:1	CL12 6:1
14	CL14 3:1	CL14 4:1	CL14 5:1	CL14 6:1
16	CL16 3:1	CL16 4:1	CL16 5:1	CL16 6:1

The expected outcomes were to see an increased suspended mass at the tyre section with increasing air/fuel ratio and therefore increasing throat

velocity. The effect of increasing the classifier speed should result in a decreased mill outlet DP and possibly an increased tyre DP.

3.4. Mill Characterisation and Optimisation

3.4.1. Overview

The mill characterisation and optimisation process followed a set of observational experiments, performed on a pilot scale mill, where the particle fineness was monitored as the key performance indicator for comparative analysis. It was expected to establish and quantify the relationships between the mill differential pressure, classifier speed and air/fuel ratio while studying their effects on the particle fineness and achievable throughput. This was done while changing the main mill operational variables, those being mill throughput (load), and classifier speed, from the minimum to the maximum allowable points. Further experiments looked at the changes in the air/fuel ratio and its effects on the particle fineness and mill differential pressure, and thus the mill throughput.

The particle fineness was measured using the particle size analyser after the instrument has been calibrated for the pilot scale plant. Manual sampling also took place for every test. The manual samples were lab sieved in order to verify the particle size distribution of each test performed. All other mill parameters were measured using the mill DCS (Distributed Control System) to log and timestamp the data.

The results of each test then contained a full set of operation variables (such as temperatures/differential pressure), the fixed operating condition for that test (such as the classifier speed and air/fuel ratio), the varied parameter (such as the mill load), and finally the particle size distribution form the PSA as well as the lab sieve analysis results. These results for the different test scenarios was analysed to determine the effect that each variable has on the mill load and the particle fineness. The relationships that are derived from this analysis were used to optimise the operation of

the pilot scale mill in terms of increasing the mill throughput and maintaining the particle fineness.

3.4.2. Instrumentation

The milling plant has various measurements and input parameters installed that serve specific functions. The “% coal feeder” and “% fan damper position” serve as input parameters in the DCS. These are to be defined by the operator and the plant will respond directly to this input. The same applies to the classifier speed which, incidentally, is also defined as a percentage of its maximum speed. Some parameters are used for automatic control such as the mill outlet temperature and the mill differential pressure. Other parameters are controlled by the DCS according to these. The temperature of the electric air heater, and thus the mill inlet temperature, is controlled in order to maintain a mill outlet temperature of 100˚C. This is different from the mill control system of Camden power station which is operated at 90˚C. All of these parameters are continuously logged in the DCS and time-stamped accordingly.

Additional measurements were installed for the purposes of the testing. These included the Particle Size Analyser (PSA) as was tested on Camden power station (Chapter 5: Particle Size Analysis Tool Evaluation) as well as four mill internal differential pressures in order to achieve the goals set out in Chapter 6: Monitoring Mill Recirculating Load.

3.4.3. Test Procedure

Testing took the form of two parts, preliminary testing and final testing. Preliminary testing consists of all the tests necessary to check equipment and prepare the plant for final testing. This includes the development of a load line in order to operate the mill during testing, the determination of the allowable maximum and minimum load points based on the mill DP, testing the data logging systems of the DCS and PSA and finally checking the results of the particle size distribution of the coal samples in the lab using physical sieves as well as the Mastersizer particle size analysis tool (see 7.3.4 Mastersizer).

In order to develop the load line the mass flow of air and coal has to be known. As the mill system is operated on a percentage of maximum capable flow of both air and fuel, the controlled percentage value has to first be related to the mass flow for that control value. This is referred to as the characterisation of the primary air fan and coal feeder respectively.

The air system is further complicated by the fact that the classifier speed affects the system pressure drop and therefore the mass flow of air for a given damper position. The primary air fan was ramped up from its minimum to its maximum fan damper position for three different classifier speeds. Recordings of the air temperature and mass flow was taken at 10 diameters away from a bend on a straight section of the mill outlet pipe using a type K thermocouple and a Pitot tube. Once the fan curves were developed it was used to relate the % damper position to the mass flow of air for a given classifier speed.

The coal feeder was characterised in a similar way. The coal feeder was operated from its minimum to its maximum capable speed while feeding into a collection vessel. Timed samples were weighed in a lab where the relative bulk density was also determined. A mass flow of coal was then established for each % feeder speed (load) setting.

Once the relationships between the mass flow and the % damper position and % feeder speed were established, the load lines were developed on a mass flow basis according to different air/fuel ratios, and finally converted back to percentage values for use in the mill control system.

The recording of data using the DCS and PSA systems were checked by performing tests using both systems and checking the recorded data for resolution and consistent recording of time-stamps. The PSA results were further checked and calibrated against the sieved particle size distribution.

The Malvern particle size analyser was used to establish the expected shape of the particle size distribution curve especially at smaller sieve sizes where physical sieves are unavailable.

The final testing consisted of various test scenarios. Test scenarios were made up of variations of the mill load, classifier speed and air/fuel ratio. Each of these three parameters was varied individually while the other two were fixed per test. The particle size distribution was then determined by means of the PSA as well as the lab sieved results. The results were studied by relating the varied a parameter to the particle size distribution of the pulverised fuel produced once stable operation is achieved.

Once the graphs of mill load, classifier speed and air/fuel ratio vs. particle fineness are established, these relationships were used to optimise the mill operation in order to maximise the throughput of the mill while minimising the effect of high load on particle fineness.

Chapter 4: Mill Energy Balance

4.1. Introduction

The milling plant consists of multiple key components. The mill body itself, which will form the boundary of the energy balance, is fed by the following auxiliary components at various points. Hot primary air blows upward through the mill from the PA fan. Raw coal is fed into the mill from the coal feeder above it. The mill motor supplies energy to the mill by rotating the mill table and thus crushing the raw coal between the grinding elements. Furthermore there is a seal air fan which supplies sealing air to the bearings and labyrinth seals at various points across the mill body.

The primary air fan extracts air, from the secondary air duct, which has been heated via the air heater. A cold air damper regulates the primary air temperature which is measured after the PA fan near the mill inlet. The coal flow is regulated in the control system by measuring the rotational speed of the screw feeder and applying a feed factor that is derived when calibrating the feeder. The measurement is volumetrically based and does not respond to changes in coal moisture or density. The energy balance will solve for the coal flow and be compared to the calibrated feeder value for verification. The seal air fan provides a constant flow of air to various points such as bearings and labyrinth seals via a ring main. The fan draws 1.25kg/s of air from atmosphere at ambient conditions through a porous paper filter. The moisture contained in the air and coal has a large effect on the energy transfer inside the mill. The mill is controlled to evaporate the moisture contained in the coal and, as it is a sealed system, adds it to the gas stream at the mill outlet. The mill outlet is therefore made up of a mixture of pulverised fuel, primary air, seal air, and water vapour.

4.2. Assumptions

In order to simplify the model and overcome parameters that are difficult to measure in a real time manner, certain assumptions had to be made. The mill is said to be in steady state. While it is not true that the mill inlet and outlet flows are always the same, for as long as the mill is not undergoing a load change, this assumption is fair. It is also assumed that heat loss through the walls of the mill is purely due to convective heat transfer. As the mills are exposed to a constant air flow at ground level, the effects of radiation and conduction heat transfer mechanisms are considered negligible in comparison. It is further assumed that the surface moisture contained in the coal is evaporated inside the mill. At an altitude of 1668m above sea level the atmospheric pressure is approximately 83kPa. This means that the mill outlet temperature set point of 90˚C is close enough to the vaporisation temperature of water at that pressure. Seal air is provided by a seal air fan which extracts air form atmosphere and feeds it to shafts and bearings in order to both stop any PF from escaping from the mill and prevent the PF from damaging sensitive components. It is assumed that all seal air at sealing points enter the mill and contribute to the outlet flow. This is not a critical parameter since the total seal air mass flow is small in comparison to the total primary air flow. The flow that is fed into the mill is considered to be entirely made of coal and it is assumed that no stone or tramp iron enters the mill. As a result the mill reject flow is taken to be zero. Finally the power that the mill motor draws is assumed to go directly into the grinding process as the mill table is rotated. There is a slight loss of energy through the mill gearbox which has an efficiency of 94%.

4.3. The Energy Balance

The Mill Energy Balance (MEB) was performed using a simplified model of a vertical spindle mill. The diagram represented by Figure 4.1 below shows the boundary and energy transfers across it.

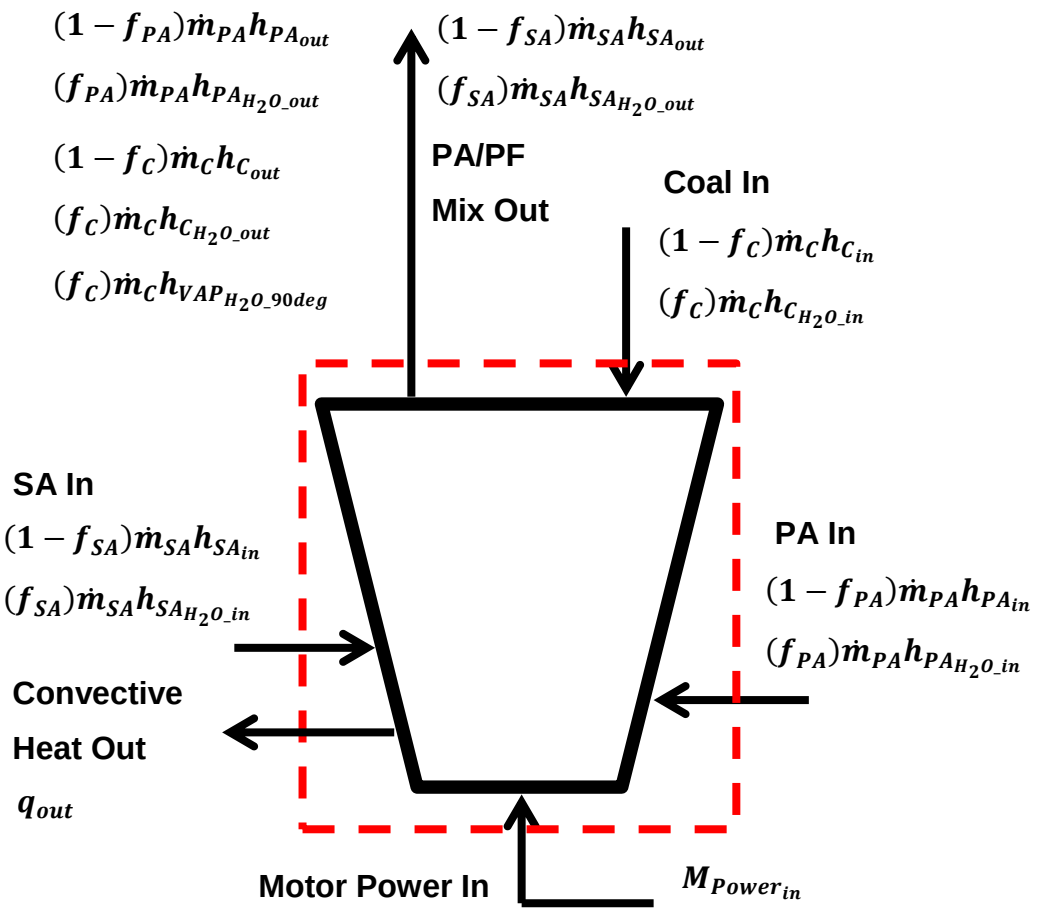

Figure 4.1: Mill Energy Balance Boundary

Mill motor power refers to the energy consumed in order to rotate the mill table and thus crush the coal. The flows into the mill include the coal, primary air (PA), seal air (SA) and their associated moisture contents. The flow out of the mill is a mixture of the PA, SA, coal and water vapour. The terminology used in the energy balance equation can be found in the Nomenclature.

Primary air in:

The primary air energy input to the mill is made up of the energy of air as well as the energy of the moisture in air. This is accounted for in the following terms:

$$(\mathbf{1} - \boldsymbol{f_{PA}})\dot{\boldsymbol{m}}_{\boldsymbol{PA}}\boldsymbol{h}_{\boldsymbol{PA}_{\boldsymbol{in}}}$$

$$(\boldsymbol{f_{PA}})\dot{\boldsymbol{m}}_{\boldsymbol{PA}}\boldsymbol{h}_{\boldsymbol{PA}_{\boldsymbol{H_2O\_in}}}$$

Similarly, the seal air energy and coal flow energy into the mill is accounted for in the following terms:

Seal air in:

$$(\mathbf{1} - \boldsymbol{f_{SA}})\dot{\boldsymbol{m}}_{\boldsymbol{SA}}\boldsymbol{h}_{\boldsymbol{SA}_{\boldsymbol{in}}}$$

$$(\boldsymbol{f_{SA}})\dot{\boldsymbol{m}}_{\boldsymbol{SA}}\boldsymbol{h}_{\boldsymbol{SA}_{\boldsymbol{H_2O\_in}}}$$

Coal flow in:

$$(\mathbf{1} - \boldsymbol{f_{C}})\dot{\boldsymbol{m}}_{\boldsymbol{C}}\boldsymbol{h}_{\boldsymbol{C}_{\boldsymbol{in}}}$$

$$(\boldsymbol{f_{C}})\dot{\boldsymbol{m}}_{\boldsymbol{C}}\boldsymbol{h}_{\boldsymbol{C}_{\boldsymbol{H_2O\_in}}}$$

Primary air out:

$$(\mathbf{1} - \boldsymbol{f_{PA}})\dot{\boldsymbol{m}}_{\boldsymbol{PA}}\boldsymbol{h}_{\boldsymbol{PA}_{\boldsymbol{out}}}$$

$$(\boldsymbol{f_{PA}})\dot{\boldsymbol{m}}_{\boldsymbol{PA}}\boldsymbol{h}_{\boldsymbol{PA}_{\boldsymbol{H_2O\_out}}}$$

Seal air out:

$$(\mathbf{1} - \boldsymbol{f_{SA}})\dot{\boldsymbol{m}}_{\boldsymbol{SA}}\boldsymbol{h}_{\boldsymbol{SA}_{\boldsymbol{out}}}$$

$$(\boldsymbol{f_{SA}})\dot{\boldsymbol{m}}_{\boldsymbol{SA}}\boldsymbol{h}_{\boldsymbol{SA}_{\boldsymbol{H_2O\_out}}}$$

Coal flow out:

$$(\mathbf{1} - \boldsymbol{f_{C}})\dot{\boldsymbol{m}}_{\boldsymbol{C}}\boldsymbol{h}_{\boldsymbol{C}_{\boldsymbol{out}}}$$

$$(\boldsymbol{f_{C}})\dot{\boldsymbol{m}}_{\boldsymbol{C}}\boldsymbol{h}_{\boldsymbol{C}_{\boldsymbol{H_2O\_out}}}$$

The change in internal energy of the system (E_{sys}) is equal to the difference in energy in and out, plus the energy generated internally.

$$\Delta \boldsymbol{E_{sys}} = \boldsymbol{E_{in}} - \boldsymbol{E_{out}} + \boldsymbol{E_{gen}} \quad \textbf{(4.1)}$$

Expressing this function as a rate we have:

$$\frac{\boldsymbol{dE_{sys}}}{\boldsymbol{dt}} = \boldsymbol{\dot{E}_{in}} - \boldsymbol{\dot{E}_{out}} + \boldsymbol{\dot{E}_{gen}} \quad \textbf{(4.2)}$$

For a steady state system the change in internal energy is zero. The mill is also considered to have no energy generation within the system. Therefore:

$$\boldsymbol{\dot{E}_{out}} = \boldsymbol{\dot{E}_{in}} \quad \textbf{(4.3)}$$

$$\boldsymbol{\dot{E}_{in}} = (\boldsymbol{Primary\ air\ in}) + (\boldsymbol{Seal\ air\ in}) + (\boldsymbol{Coal\ energy\ in}) + (\boldsymbol{Motor\ power\ in})$$

$$\boldsymbol{\dot{E}_{in}} = \left[(\mathbf{1} - \boldsymbol{f_{PA}})\dot{\boldsymbol{m}}_{\boldsymbol{PA}}\boldsymbol{h}_{\boldsymbol{PA_{in}}} + (\boldsymbol{f_{PA}})\dot{\boldsymbol{m}}_{\boldsymbol{PA}}\boldsymbol{h}_{\boldsymbol{PA_{H_2O_{in}}}}\right] + \left[(\mathbf{1} - \boldsymbol{f_{SA}})\dot{\boldsymbol{m}}_{\boldsymbol{SA}}\boldsymbol{h}_{\boldsymbol{SA_{in}}} + (\boldsymbol{f_{SA}})\dot{\boldsymbol{m}}_{\boldsymbol{SA}}\boldsymbol{h}_{\boldsymbol{SA_{H_2O_{in}}}}\right] + \left[(\mathbf{1} - \boldsymbol{f_C})\dot{\boldsymbol{m}}_{\boldsymbol{C}}\boldsymbol{h}_{\boldsymbol{C_{in}}} + (\boldsymbol{f_C})\dot{\boldsymbol{m}}_{\boldsymbol{C}}\boldsymbol{h}_{\boldsymbol{C_{H_2O_{in}}}}\right] + \left[\boldsymbol{M_{Power_{in}}}\right]$$

$$\boldsymbol{\dot{E}_{out}} = (\boldsymbol{Primary\ air\ out}) + (\boldsymbol{Seal\ air\ out}) + (\boldsymbol{Coal\ energy\ out}) + (\boldsymbol{Latent\ heat\ of\ vaporisation\ for\ H_2O\ in\ coal}) + (\boldsymbol{Convective\ heat\ loss})$$

$$\boldsymbol{\dot{E}_{out}} = \left[(\mathbf{1} - \boldsymbol{f_{PA}})\dot{\boldsymbol{m}}_{\boldsymbol{PA}}\boldsymbol{h}_{\boldsymbol{PA_{out}}} + (\boldsymbol{f_{PA}})\dot{\boldsymbol{m}}_{\boldsymbol{PA}}\boldsymbol{h}_{\boldsymbol{PA_{H_2O_{out}}}}\right] + \left[(\mathbf{1} - \boldsymbol{f_{SA}})\dot{\boldsymbol{m}}_{\boldsymbol{SA}}\boldsymbol{h}_{\boldsymbol{SA_{out}}} + (\boldsymbol{f_{SA}})\dot{\boldsymbol{m}}_{\boldsymbol{SA}}\boldsymbol{h}_{\boldsymbol{SA_{H_2O_{out}}}}\right] + \left[(\mathbf{1} - \boldsymbol{f_C})\dot{\boldsymbol{m}}_{\boldsymbol{C}}\boldsymbol{h}_{\boldsymbol{C_{out}}} + (\boldsymbol{f_C})\dot{\boldsymbol{m}}_{\boldsymbol{C}}\boldsymbol{h}_{\boldsymbol{C_{H_2O_{out}}}}\right] + \left[(\boldsymbol{f_C})\dot{\boldsymbol{m}}_{\boldsymbol{C}}\boldsymbol{h}_{\boldsymbol{VAP_{H_2O_{90deg}}}}\right] + [\boldsymbol{q_{out}}]$$

The energy balance equation is as follows:

$$(\mathbf{1}-\boldsymbol{f_{PA}})\dot{\boldsymbol{m}}_{\boldsymbol{PA}}\boldsymbol{h}_{\boldsymbol{PA}_{\boldsymbol{in}}}+(\boldsymbol{f_{PA}})\dot{\boldsymbol{m}}_{\boldsymbol{PA}}\boldsymbol{h}_{\boldsymbol{PA}_{\boldsymbol{H_2O\_in}}}+(\mathbf{1}-\boldsymbol{f_{SA}})\dot{\boldsymbol{m}}_{\boldsymbol{SA}}\boldsymbol{h}_{\boldsymbol{SA}_{\boldsymbol{in}}}+$$
$$(\boldsymbol{f_{SA}})\dot{\boldsymbol{m}}_{\boldsymbol{SA}}\boldsymbol{h}_{\boldsymbol{SA}_{\boldsymbol{H_2O\_in}}}+(\mathbf{1}-\boldsymbol{f_C})\dot{\boldsymbol{m}}_{\boldsymbol{C}}\boldsymbol{h}_{\boldsymbol{C}_{\boldsymbol{in}}}+(\boldsymbol{f_C})\dot{\boldsymbol{m}}_{\boldsymbol{C}}\boldsymbol{h}_{\boldsymbol{C}_{\boldsymbol{H_2O\_in}}}+\boldsymbol{M}_{\boldsymbol{Power}_{\boldsymbol{in}}}=$$
$$(\mathbf{1}-\boldsymbol{f_{PA}})\dot{\boldsymbol{m}}_{\boldsymbol{PA}}\boldsymbol{h}_{\boldsymbol{PA}_{\boldsymbol{out}}}+(\boldsymbol{f_{PA}})\dot{\boldsymbol{m}}_{\boldsymbol{PA}}\boldsymbol{h}_{\boldsymbol{PA}_{\boldsymbol{H_2O\_out}}}+(\mathbf{1}-\boldsymbol{f_{SA}})\dot{\boldsymbol{m}}_{\boldsymbol{SA}}\boldsymbol{h}_{\boldsymbol{SA}_{\boldsymbol{out}}}+$$
$$(\boldsymbol{f_{SA}})\dot{\boldsymbol{m}}_{\boldsymbol{SA}}\boldsymbol{h}_{\boldsymbol{SA}_{\boldsymbol{H_2O\_out}}}+(\mathbf{1}-\boldsymbol{f_C})\dot{\boldsymbol{m}}_{\boldsymbol{C}}\boldsymbol{h}_{\boldsymbol{C}_{\boldsymbol{out}}}+(\boldsymbol{f_C})\dot{\boldsymbol{m}}_{\boldsymbol{C}}\boldsymbol{h}_{\boldsymbol{C}_{\boldsymbol{H_2O\_out}}}+$$
$$(\boldsymbol{f_C})\dot{\boldsymbol{m}}_{\boldsymbol{C}}\boldsymbol{h}_{\boldsymbol{VAP}_{\boldsymbol{H_2O\_90deg}}}+\boldsymbol{q_{out}} \qquad \textbf{(4.4)}$$

Rearranging to solve for the coal mass flow:

$$\dot{\boldsymbol{m}}_{\boldsymbol{C}}=\frac{(1-f_{PA})\dot{m}_{PA}\left(h_{PA_{in}}-h_{PA_{out}}\right)+(f_{PA})\dot{m}_{PA_{H_2O}}\left(h_{PA_{H_2O\_in}}-h_{PA_{H_2O\_out}}\right)+(1-f_{SA})\dot{m}_{SA}\left(h_{SA_{in}}-h_{SA_{out}}\right)+(f_{SA})\dot{m}_{SA_{H_2O}}\left(h_{SA_{H_2O\_in}}-h_{SA_{H_2O\_out}}\right)+M_{Power_{in}}-q_{out}}{(1-f_C)\left(h_{C_{out}}-h_{C_{in}}\right)+(f_C)\left(h_{C_{H_2O\_out}}-h_{C_{H_2O\_in}}\right)+(f_C)h_{VAP_{H_2O\_90deg}}} \qquad \textbf{(4.5)}$$

The total mill differential pressure at Camden power station fluctuates in the region of 4kPa. The bulk of the pressure drop occurs across the throat and across the classifier while the bulk of the enthalpy change occurs in the mill body between these two elements. It is therefore assumed that the pressure remains constant for the region of heat transfer from the hot primary air to the coal and seal air.

Calculating the enthalpy change of coal:

$$\boldsymbol{Enthalpy\ change\ of\ coal}=\boldsymbol{C_{pCOAL}}(\boldsymbol{T_{out}}-\boldsymbol{T_{in}}) \qquad \textbf{(4.6)}$$

Where the C_{pCOAL} for coal is 1.26 (Sonntag et al., 1998)

Calculating the enthalpy change of air:

$$\boldsymbol{Enthalpy\ change\ of\ air}=\boldsymbol{C_{pAIR}}(\boldsymbol{T_{in}}-\boldsymbol{T_{out}}) \qquad \textbf{(4.7)}$$

Where the C_{pAIR} for dry air is 1.008 at 90˚C (Incropera et al., 2007)

Calculating the enthalpy change of moisture in air (vapour):

$$\boldsymbol{Enthalpy\ change\ of\ PA\ H_2O}=\boldsymbol{C_p}(\boldsymbol{T_{in}}-\boldsymbol{T_{out}}) \qquad \textbf{(4.8)}$$

Where the C_{pH2O} for vapour in air is 1.993 at 90˚C (Incropera et al., 2007)

The heating and vaporisation of the moisture in coal is handled as per Figure 4.2 below.

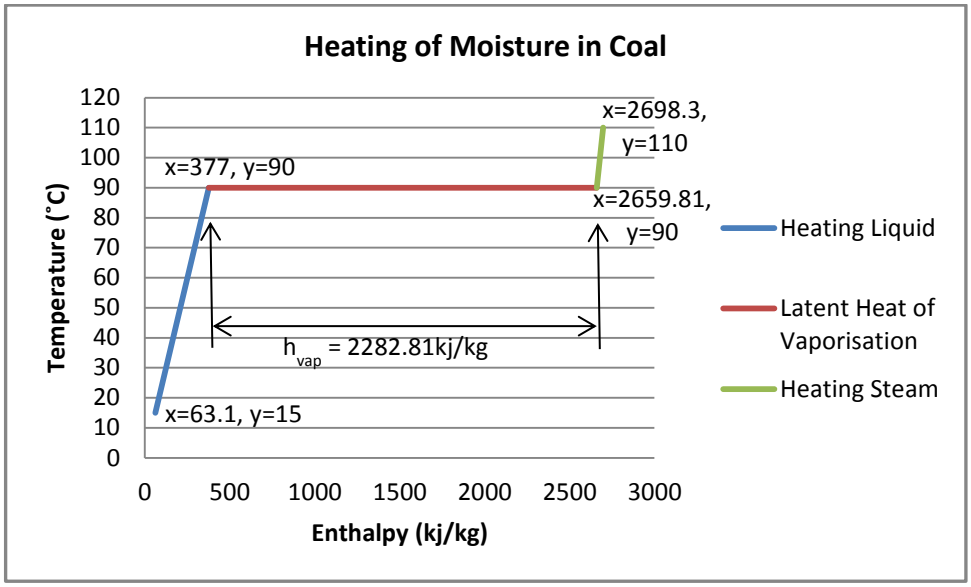

Figure 4.2: Heating of Moisture in coal

In the liquid heating region the enthalpy is raised from 63.1 to 377kJ/kg until it reaches the saturation temperature. The heat of vaporisation of water at 90˚C raises the enthalpy by a further 2282.81kJ/kg. No further heating of the vapour phase is expected to happen as the mill outlet conditions are just below the vaporisation temperature of 94.5˚C. While the control system does allow the outlet temperature to fluctuate to a certain extent, this fluctuation is fairly small as will be discussed in the verification section to follow. Thus the change in energy added to the vapour as a result of this fluctuation may be neglected.

Fixed inputs to the model include the raw coal temperature, seal air mass flow, primary air moisture, seal air moisture and convective heat loss. The raw coal temperature was measured at 15˚C as it is fed through the concrete bunker into the feeder.

The seal air mass flow was determined using the rated volume flow of the fan and the air density at ambient pressure and temperature.

Volume flow = 1.271kg/m^3 (rated)

$$\boldsymbol{Seal\ air\ mass\ flow} = (\boldsymbol{Volume\ flow})\frac{\mathbf{83000}}{(\mathbf{287.06}\times(\mathbf{273.15}+\mathbf{20}))} = \mathbf{1.25}\boldsymbol{kg/s} \quad \textbf{(4.9)}$$

The primary air and seal air moisture was determined by taking the average ambient relative humidity and calculating the specific humidity.

$$\boldsymbol{Specific\ humidity} = (\mathbf{0.622})\frac{\boldsymbol{Relative\ humidity}\times\boldsymbol{\rho_{ws}}}{(\boldsymbol{\rho_{air}}-\boldsymbol{\rho_{ws}})} \quad \textbf{(4.10)}$$

$\rho_{ws} = density\ of\ moisture\ in\ air = 0.4959kg/m^3\ from\ steam\ tables$

$$\boldsymbol{\rho_{air}} = \frac{\mathbf{83000}}{(\mathbf{287.05}\times(\mathbf{273.15}+\mathbf{20}))} = \mathbf{0.986}\boldsymbol{kg/m^3} \quad \textbf{(4.11)}$$

$Relative\ humidity = 80\%$

$Specific\ humidity = (0.622)\frac{0.8\times0.4959}{(0.986-0.4959)} = 0.5kg_{H_2O}/kg_{air}$

The mill motor input power is calculated based on the 21Amp 3-phase current draw at the rated 6.6kV motor voltage.

$$\boldsymbol{Mill\ motor\ power} = \sqrt{\mathbf{3}}\times\boldsymbol{V}\times\boldsymbol{I}\times\boldsymbol{P_f} \quad \textbf{(4.12)}$$

$$Mill\ motor\ power = \sqrt{3}\times 6600\times 21\times 0.91 = 218.46kW$$

The mill gearbox has an efficiency of 94%. Therefore the power into the mill is reduced to:

$$Mill\ motor\ power\ in = 0.94\times 218.46kW = 205kW$$

The convective heat loss through the mill body is as a result of the location of the mills. On the ground floor of Camden power station there is an access roadway through the power station building that generates a fairly strong breeze past the mills. This has been measured to be 5m/s using a vane anemometer. The average surface temperature of the mill body is 34˚C and the surface area has been approximated to be a uniform cylinder with a diameter of 3m and a height of 5m.

$T_\infty = 20℃$

Therefore: (Incropera et al., 2007)

$Pr = 0.709$

$\nu = 15.28 \times 10^{-6}$

$k = 25.75 \times 10^{-3}$

$$\boldsymbol{Re = \frac{(u_\infty D)}{\nu} = \frac{(5\times3)}{15.28\times10^{-6}} = 981033} \quad \textbf{(4.13)}$$

For Re < 10^6 and Pr > 0.7 the Zukauskas correlation applies.

$Pr_s = 0.706$ (surface Prandtl number)

$$\boldsymbol{\overline{Nu_D} = 0.076 Re_D^{0.7} Pr^{0.37} \left(\frac{Pr}{Pr_s}\right)^{1/4} = 1047.59} \quad \textbf{(4.14)}$$

$$\boldsymbol{\bar{h} = \overline{Nu_D} \times \frac{k}{D} = 1047.59 \times \frac{25.75\times10^{-6}}{15.28\times10^{-3}} = 8.99\ W/m^2 \cdot K} \quad \textbf{(4.15)}$$

$$\boldsymbol{q = \bar{h}A(T_s - T_\infty) = 8.99 \times 47.12 \times (33 - 20) = 5932\ W} \quad \textbf{(4.16)}$$

The above calculated values are fixed in the energy balance solver as they are parameters that are not measured on-line. These may be recalculated using updated test data such as mill surface temperatures or updated weather data such as seasonal changes in temperature and relative humidity.

4.4. Verification

The verification test parameters were derived from the DCS of 5 running mills, of Camden Power Station. The verification measurements and DCS values were taken after a feeder drop test and calibration was performed in order to be able to compare the mass flow rate of the feeder to the calculated value of the MEB.

Table 4.1: Mill A - MEB verification results

Unit 2 – Mill C	Unit	Value
Input Parameters		
Coal temperature	˚C	15
Coal moisture (by mass)	%	7
PA moisture (by mass)	%	0.5
PA mass flow	kg/s	11.2
PA temperature in	˚C	231
PA/PF temperature out	˚C	92.91
Seal air moisture	%	0.5
Seal air flow	kg/s	1.25
Seal air temperature	˚C	20
Mill motor power	kW	205
Convective heat loss	kW	5.932
Calculated Parameters		
Enthalpy change – Seal air	kJ/kg	-73.49
Enthalpy change – Seal air H_2O	kJ/kg	-145.31
Enthalpy change – Primary air	kJ/kg	140.06
Enthalpy change – Primary air H_2O	kJ/kg	276.93
Enthalpy change – Coal H_2O	kJ/kg	327.77
Output Parameter		
Mass flow of coal (from MEB)	kg/s	6.24
Mass flow of coal (from Feeder)	kg/s	6.11
% difference	%	2.13

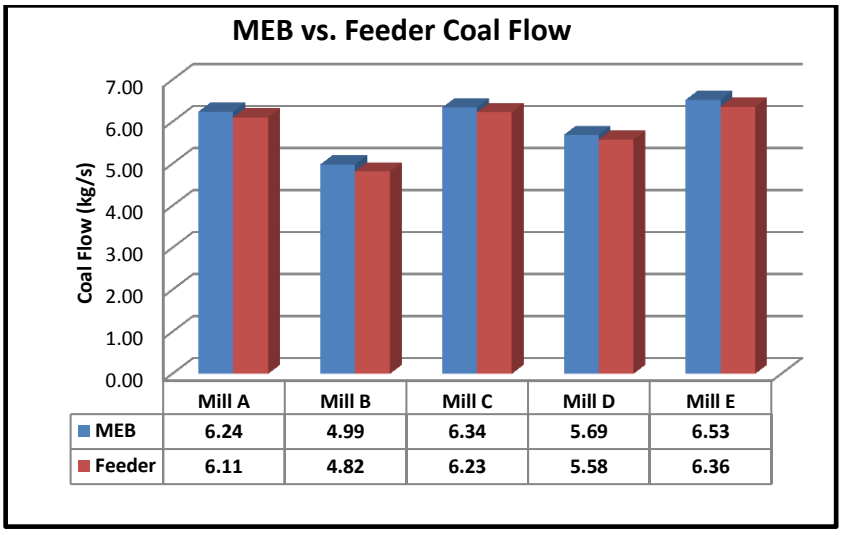

Figure 4.3: MEB verification tests

Table 4.1 above shows the results for Unit 2 - mill A. Input parameters were measured and recorded from the DCS. Calculated parameters are those calculated in the MEB. The output parameter is the mass flow of coal of 6.24kg/s. This compares very well to the feeder flow rate of 6.11kg/s which was recorded soon after a calibration was performed. This particular test showed a 2.13% difference between the calculated MEB coal flow and the reported feeder coal flow. Four other mills were also tested (Mills B, C, D and E), and the average percentage difference was 2.33% (Figure 4.3). The results of all mills can be found in Appendix A: MEB Verification Results.

4.5. Sensitivity Analysis

A sensitivity analysis was performed to evaluate the effect of changes to the input parameters in the model. Each parameter was varied by ±10% to norm and the resulting change in coal flow was recorded in Table 4.2 below.

Table 4.2: Sensitivity analysis

Input Variable	Actual value	New Coal Flow (+10%)	New Coal Flow (-10%)	Average % Diff
Raw coal temp (^{o}C)	15.00	6.29	6.19	0.78
Coal H_2O (%)	7.00	5.86	6.68	6.56
Humidity in air (%)	0.50	6.25	6.24	0.04
PA Flow (kg/s)	11.21	6.83	5.66	9.37
PA inlet temp (^{o}C)	231.86	7.22	5.27	15.63
Mill motor power (kW)	205.00	6.32	6.17	1.22
Conv. Heat loss (kW)	5.93	6.24	6.25	0.04
Mill outlet temp (^{o}C)	92.91	5.54	7.02	11.85
Actual coal flow (kg/s)	6.24			

From this table the average percentage difference for a 10% change in the respective input variables is given in the last column. The raw coal temperature, the humidity in air, the mill motor power and the convective heat loss show the lowest sensitivity in terms of its effect on the coal flow

calculated. Figure 4.4 below gives a clearer comparison of the high sensitivity variables.

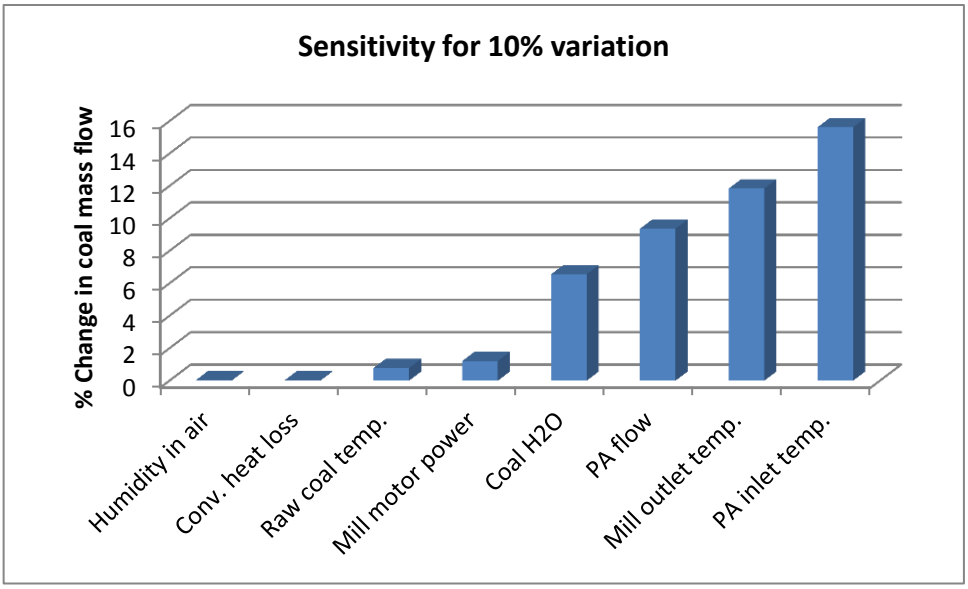

Figure 4.4: Bar graph of the sensitivity analysis in Table 4.2

The primary air temperature and mass flow as well as the mill outlet temperature show the largest effect on the calculation. These values are however well known as they are both accurately measured on line and recorded in the DCS. Of concern is the sensitivity of variations in the coal moisture on the coal flow calculation as this is a manual periodic measurement. A 10% change in coal moisture results in a 6.56% error on the coal flow prediction. A coal moisture variation of 10% of its last measured value within a day is a likely possibility in a power station environment. Therefore it is advised to increase the reliability of the coal flow prediction model by measuring the coal moisture using an on line coal moisture analyser and pass this value into the model in a real-time manner.

Alternatively the coal mass flow can be measured at the mill inlet by means of a gravimetric coal feeder or at the mill outlet by means of a microwave coal mass flow measurement in the PF pipes. The accurately measured coal flow can then be used as an input to the MEB and the model can be used to predict the coal moisture on-line. The sensitivity of

coal moisture content to changes in the coal mass flow can be seen in Table 4.3 below.

Table 4.3: Sensitivity of coal moisture to changes in coal mass flow

Input Variable	Actual value	New Coal H_2O (+10%)	New Coal H_2O (-10%)	Average % Diff
Coal flow (kg/s)	6.24	5.92	8.38	17.54
Actual coal H_2O (%)	7			

From the table above it can be seen that a 10% change in coal mass flow results in a 17.54% change in coal moisture which makes it more than twice as sensitive as changes in the coal moisture was. A measurement error on the coal mass flow will result in a larger MEB prediction error of the coal moisture. And a measurement error on the coal moisture will result in a relatively smaller error in the MEB prediction of the coal mass flow. The model is therefore more accurate in determining the coal mass flow, using coal moisture as an input than it is at calculating the coal moisture, using the coal mass flow as an input. Figure 4.5 below shows the sensitivity of moisture in coal to changes in the coal mass flow and vice versa.

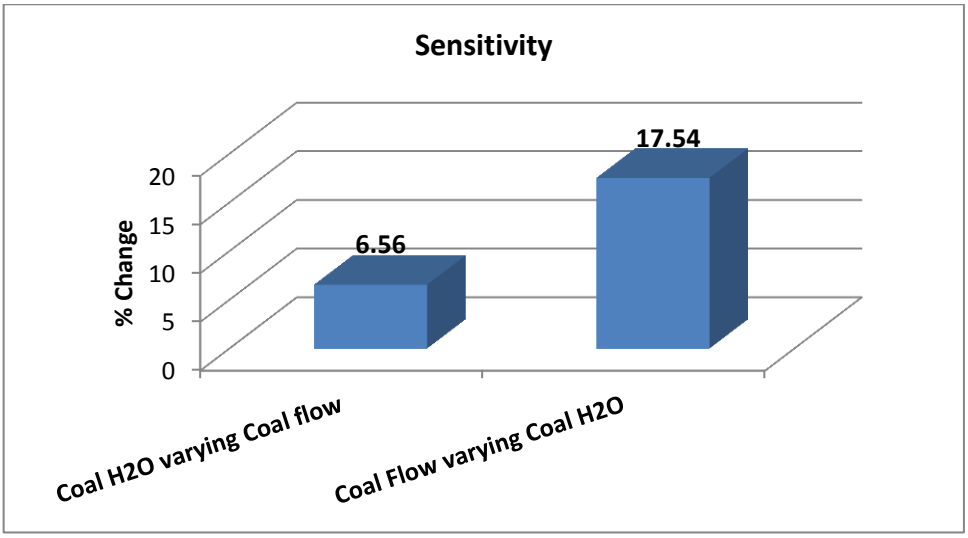

Figure 4.5: Sensitivity of coal moisture and coal flow

The sensitivity as a result of the uncertainty of measurement is shown in Table 4.4 below. The highest uncertainty of measurement is that of the raw coal. This is due to the measurement taken using a thermocouple lowered into the raw coal bunker where the surface temperature of the coal in the bunker is taken. The temperature of the raw coal is expected to fluctuate before it reaches the mill due to conduction to the bunker walls as well as evaporation and, to a greater extent, absorption of moisture from the air. One can, at best, assume that the temperature at the bunker inlet is within 5˚C of the mill inlet temperature of coal. The determination of the coal moisture content also has uncertainties related to the preservation of the moisture in the sample during transport, the splitting of the sample (using the cone and quarter technique) as well as the moisture absorption phenomena during the surface moisture determination (exposing the sample to atmosphere under sunny conditions). Primary air mass flow is measured on Camden power station using an electrostatic mass flow measurement device with an uncertainty of 1%. Temperatures at the mill inlet and outlet are measured and reported to the DCS using type K thermocouples with an overall uncertainty of 1˚C. Finally, the mill motor power is a function of the current draw of the mill motor, which is also measured and reported to the DCS.

Table 4.4: Sensitivity as a result of measurement uncertainty

Input Variable	**Actual value**	**New Coal Flow (+)**	**New Coal Flow (-)**	**Average % Diff**
Raw coal temp (±5^{o}C)	15.00	6.41	6.08	2.62
Coal H_2O (±3%)	7.00	6.12	6.37	1.96
Moisture in air (±10%)	0.50	6.25	6.24	0.04
PA Flow (±1%)	11.21	6.30	6.19	0.92
PA inlet temp (±1^{o}C)	231.86	6.29	6.20	0.67
Motor power (±0.2%)	205.00	6.25	6.24	0.02
Mill out temp (±1^{o}C)	92.91	6.16	6.32	1.27
Actual coal flow (kg/s)	6.24			

The raw coal temperature has the largest effect on reported coal flow. This is largely due to the high uncertainty of the measurement which can be

reduced by measuring closer to the mill inlet and by measuring in a chute with a smaller cross sectional area. In order to make this possible however, some modification to the chute would have to be performed in order to allow such access. The moisture content is the second highest contributor and varies the coal flow calculation by 1.96% due to the measurement uncertainty. This uncertainty can also be reduced by means of alternate moisture analysis technologies.

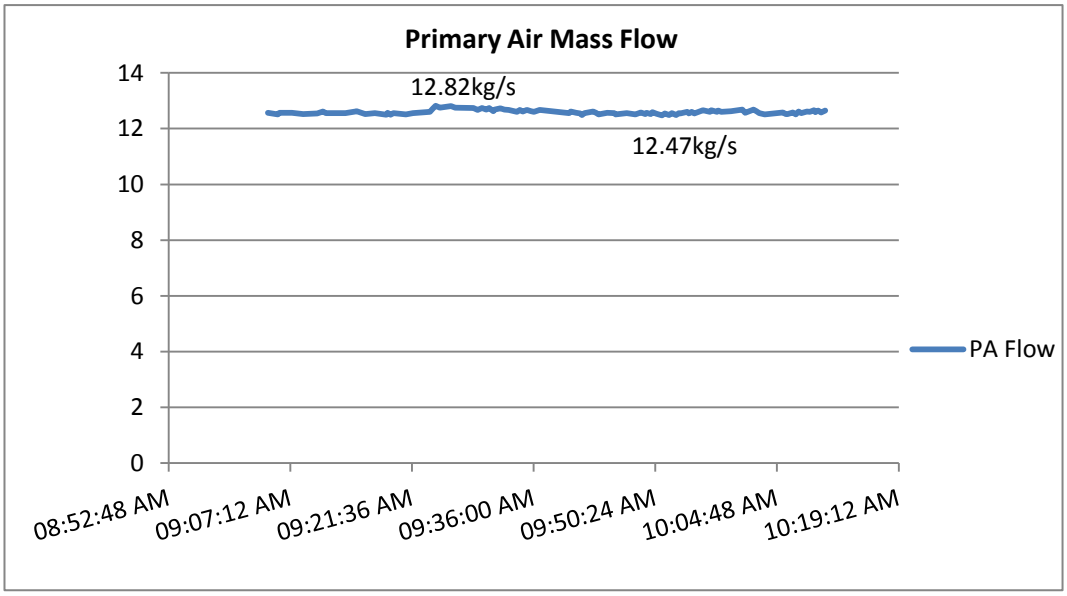

Figure 4.6: Primary air mass flow fluctuations

The error due to uncertainty in the primary mass flow measurement of 0.92% may be neglected as the measurement uncertainty of 1% is smaller than the fluctuations in measurement. Figure 4.6 above shows the primary air mass flow recorded over a one hour period of stable operation. The peak value was 12.82kg/s and the lowest value was 12.47kg/s. The resulting fluctuation is approximately 2.7% of the highest reading (12.82kg/s) in this dataset. The same can be said for the primary air inlet and mill outlet temperatures. The fluctuations in measurement, as per Figure 4.7 below, are 2.8˚C and 4.58˚C for the primary air inlet and mill outlet temperatures respectively.

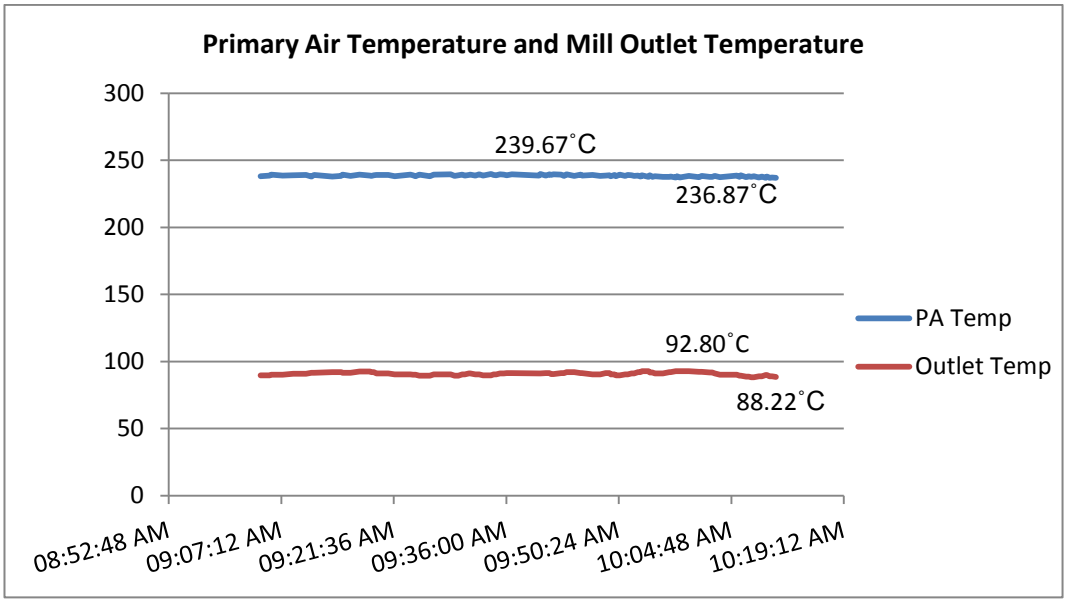

Figure 4.7: Primary air and mill outlet temperature fluctuations

Chapter 5: Particle Size Analysis Tool Evaluation

5.1. Introduction

Emission control in coal fired power generation, as with most other industries, have become an increasingly important topic of discussion in recent years. This is leading to large investments in new technologies in order to remove pollutants such as SO_2, SO_3, NO_2 and NO_3 (commonly referred to as SO_x and NO_x). While SO_x may be removed from flue gas via post combustion processing, the most economically viable way to reduce the amount of NO_x produced by a utility is to refine the combustion process itself. This is performed by the modern Low NO_x burner. In order for low NO_x burner technology to operate correctly it is vital that the PF particle size, PF mass flow and air mass flow to the different stages of the burner are controlled accurately.

In order to maintain the correct particle fineness it is important that the milling plant is well maintained, well monitored and performing optimally. The common method of PF size measurement is known as the iso-kinetic sampling and sieving process. In this process PF is iso-kinetically extracted from the PF pipes and vibrated through a series of sieves in order to determine the particle size distribution. This is usually a two day process performed twice a year per mill. These measurements provide valuable knowledge in mill condition monitoring and maintenance but the measurement frequency, due to manual and time consuming nature of the process, is far too low. The focus of this study aims to evaluate the use of the particle size analyser (PSA) for reliable and accurate use in mill condition monitoring and eventual integration into a Mill Health Monitoring System (MHMS).

5.2. Background

Particle characterisation technology has evolved vastly over the last four decades. A summary of the evolution of particle size analysis technologies was made by Dodds et al. (2004). It was noted that while the means of characterizing a particle has not differed from the basic principles of particle size and particle size distribution, new technologies employed have since transformed the industry away from laboratory analysis involving off-line measurements made using direct methods (e.g. counters, microscopy) or field classification methods (e.g. sedimentation, sieving). Instead, secondary methods of measurement and analysis (e.g. laser diffraction, spatial filtering, ultrasound attenuation) have taken precedence thereby moving the particle size analysis from the laboratory to the process plant using on-line technologies and modern computing for real time analysis.

The iso-kinetic sampling and sieving process has for decades been established as the standard method of determining the particle size distribution of PF in the power generation industry. The term “iso-kinetic” implies that the PF is extracted at the same velocity that it would have otherwise been travelling through the PF pipe had the probe not been present.

This is said to be achieved by adjusting the vacuum generated inside the probe used for the extraction of PF. The static pressure inside the PF pipe (P2) is monitored, as is the static pressure inside the extraction probe (P1). For as long as these two pressures (P1 and P2 in Figure 5.1) are maintained as equal, the sampling is considered to be iso-kinetic. The PF is separated from the air by two cyclone separators in series and stored in the glass collection jars. The sample is then taken to the lab to be weighed and sieved before a particle size distribution is available for analysis.

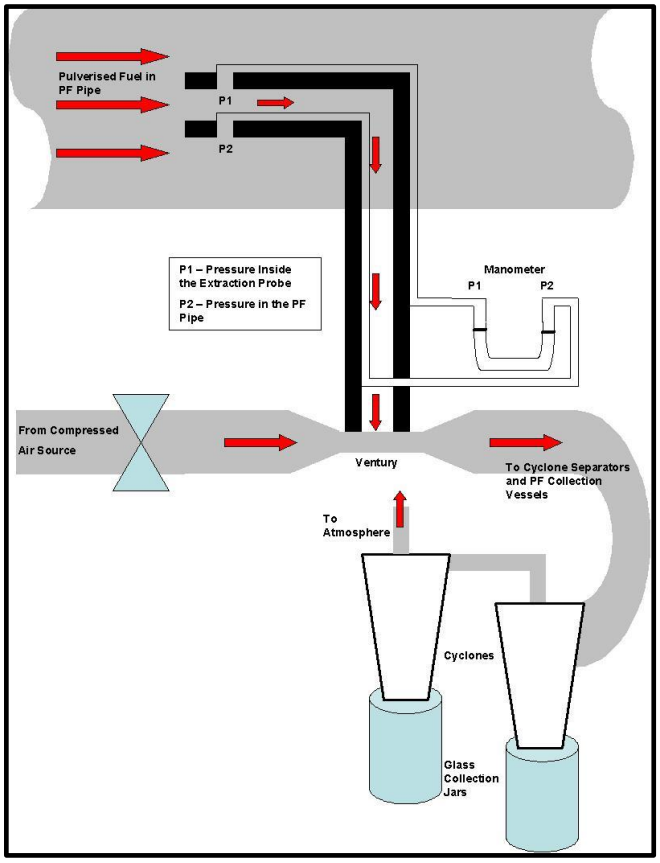

Figure 5.1: Iso-kinetic sampler - principle of extraction

This is a lengthy and labour intensive process that is performed bi-annually per mill, or upon suspicion of a problem. Such results are impossible to use in a performance or condition monitoring role as the measurements are infrequent. The results are also influenced by a large possibility of human error during the testing process. The pressure in the PF pipe (P2) is constantly fluctuating and therefore one has to constantly adjust the pressure inside the probe (P1) accordingly in order for them to match. If there is a pressure differential between these two values for any discernible period of time then one begins to under-sample or over-sample depending on which pressure is higher as illustrated in Figure 5.2.

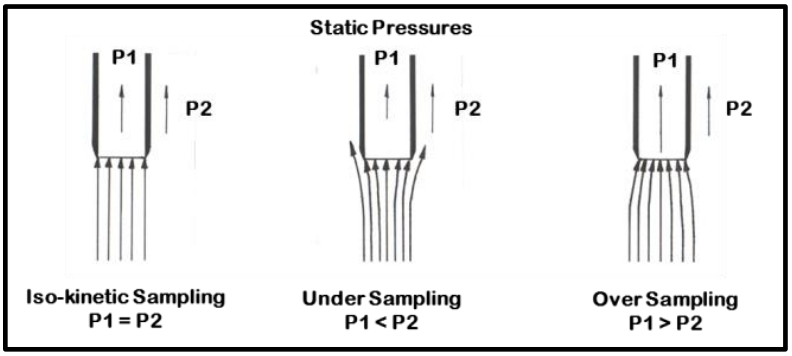

Figure 5.2: Under-sampling and Over-sampling

Under-sampling produces results that are too coarse, while over-sampling produces results that are too fine as compared to a correct, representative sample.

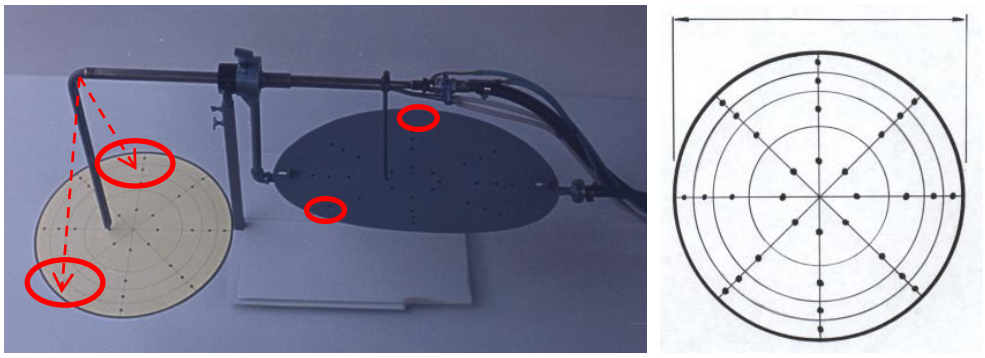

Figure 5.3: Incorrect iso-kinetic sampling (single port)

There are other points of contention as well. Most power stations only have single port access for iso-kinetic sampling. In order for the probe tip to extract PF from every point of the PF pipe cross section illustrated in Figure 5.3, the probe must be rotated in the sampling port so that the tip can reach the side walls for points that lie off its axis of insertion. However, with the probe now at an angle to the flow, it is incorrect to assume that the pressures should still be equalized in order to extract a sample iso-kinetically. The extraction process is also fundamentally an intrusive one meaning that the physical presence of the probe does have some effect on the flow characteristics inside the PF pipe.

All of these points considered, the iso-kinetic sampling and sieving process has still been accepted world-wide as the standard method of particle size distribution measurement in power generation.

The particle size analyser (PSA) that has been acquired by Eskom utilises the method of spatial filtering velocimetry and fibre-optic spot scanning to determine a particle size distribution of pulverised fuel from the mill. As discussed in the literature review, this method used an optical laser measurement technique that, when inserted into a pulverised fuel pipe, measures the particle size distribution of PF on-line as it flows in the pipe.

The probe itself consists of a long cylindrical shaft with a groove cut perpendicular to its length and near the tip. The laser eye fires longitudinally and across this groove to measure the size of pulverised fuel particles as they pass through the groove. This is shown in Figure 5.4.

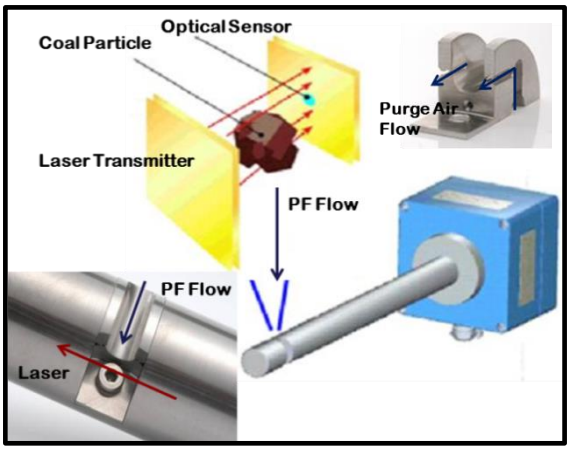

Figure 5.4: PSA principle of operation (Parsum, 2011a)

The probe also feeds purge air to the laser eye in order to maintain the cleanliness of the lens and the optical sensor on the other side. This purge air is fed from both the laser transmitter and optical sensor end and is done so in the direction of the flow of PF through the groove. The pressure and mass flow rate of the purge air can be controlled independently via a purge controller (Figure 5.5) which can also control the purging time of periodic purges.

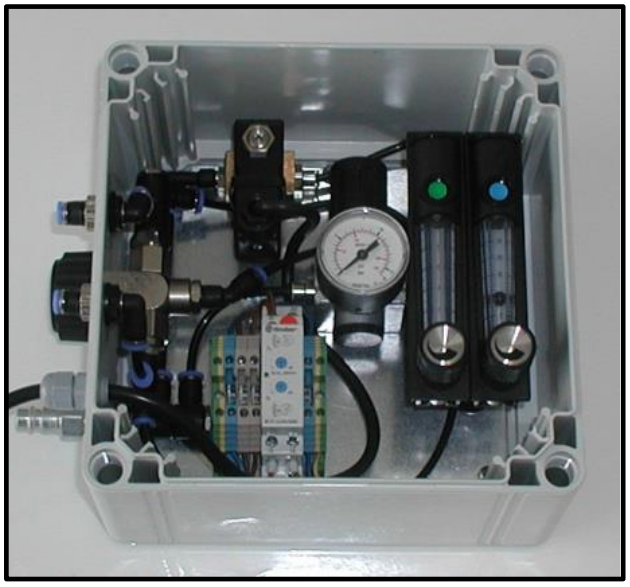

Figure 5.5: Purge air controller (Parsum, 2011a)

The probe is inserted into the PF pipe as per Figure 5.6 and is fed with compressed air via the purge air controller. The signal cable passes the signal through an analogue to digital converter to a PC for reporting and storage of the results.

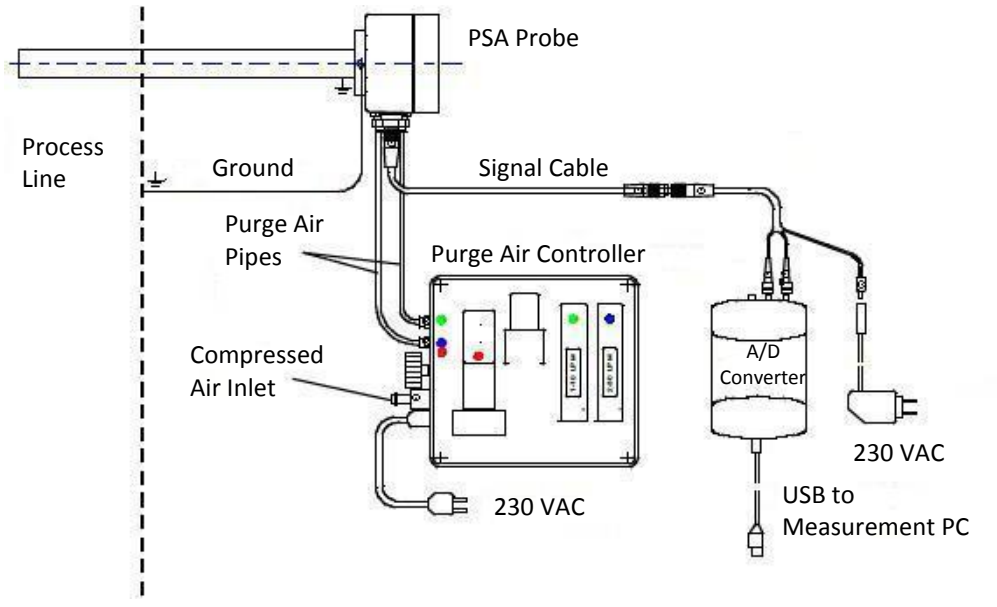

Figure 5.6: PSA general arrangement and connections (Parsum, 2011a)

Testing of the particle size analyser was focussed on vertical flow pipes in order to eliminate the effects of density gradients and particle settling on

the particle fineness results. As per below, the PF pipe layout for Camden power station is such that only mill A, which feeds the bottom most row of burners, has measurement points on the horizontal pipe section. Mills B, C, D and E all have measurement points on the vertical pipe sections.

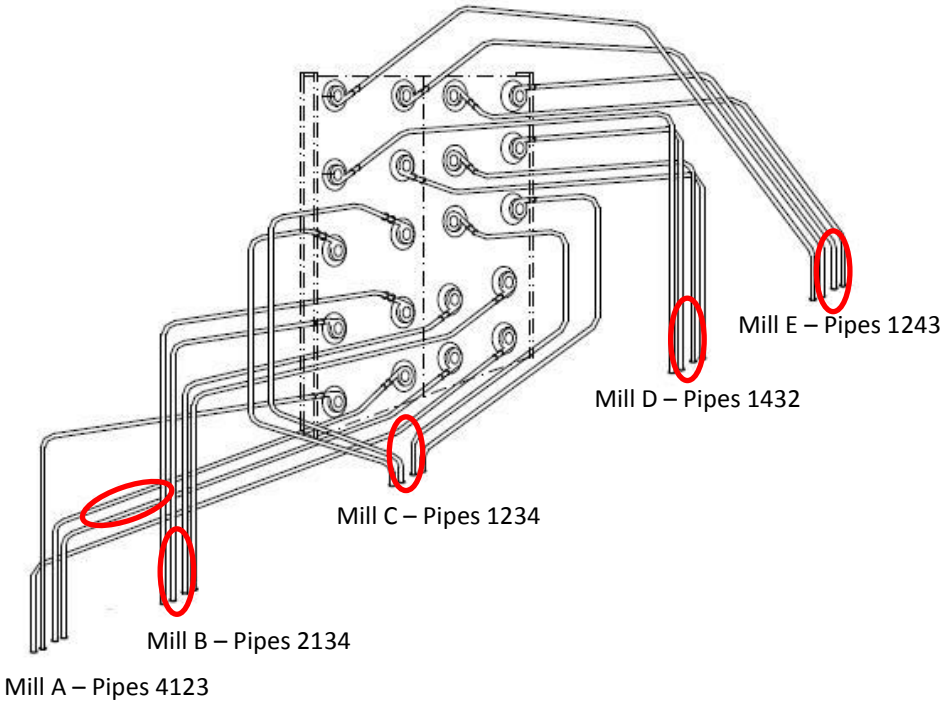

Figure 5.7: Camden PF pipe layout and measurement locations (CMP, 2010)

The PF pipes in Figure 5.7 are cut off at the floor level and actually continue straight down to the mill outlet located on the ground floor below. This allows a distance of at least 10 times the pipe diameter from the last bend.

5.3. Problem and Objective

Initial tests were performed on the Power Station as per the manufacturers test procedure. This was performed to compare between the results of simultaneous PSA and Iso-kinetic sampling and sieving. Typical results of which can be seen in Figure 5.9. The mills were operated in manual mode for the period of testing to prevent mill load changes due to the control

system responses to the boiler energy requirements. A single pipe was first tested using iso kinetic sampling and then tested using the particle size analyser for a period of 15 minutes. Each pair of tests was performed 4 times to show repeatability.

The PSA has also shown consistency and repeatability during these tests. The largest differences in repeated PSA tests were noticeable at 75µm and 150µm (2.24 and 2.17 percentage points respectively). This can be seen in Table 5.1 below. The table shows the percentage passage at the 4 main particle sizes for the 4 tests performed. The last two columns show the maximum difference between the highest and lowest figures and then compares that difference as a percentage of the optimal fineness window (Table 1.1, and in the Rosin Rammler Figure 5.8 below) at that particular sieve size. Although the percentage difference in the optimal fineness window at the 300µm particle size level is the highest, overall the difference is 0.19% of the mass of particles less than 300µm. This is much less than the instruments measurement uncertainty of 1% (Petrak et al., 2011).

Table 5.1: PSA repeatability test results

	Test 1	Test 2	Test 3	Test 4	Max % point diff	% of Window
%<300µm	99.56	99.61	99.43	99.62	0.19	23.75
%<150µm	93.41	93.51	93.24	93.91	0.67	12.18
%<106µm	82.34	84.32	83.12	84.50	2.17	20.61
%<75µm	65.46	67.69	66.59	66.43	2.24	22.35

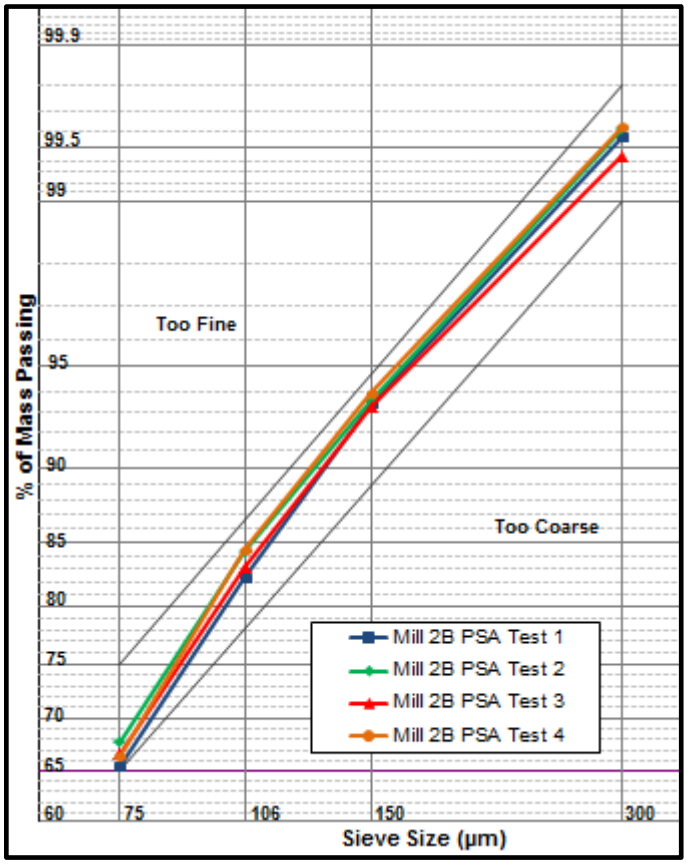

Figure 5.8: PSA repeatability test results

Comparing the PSA results to those of the iso-kinetic sampling it was found that the PSA was consistent in trend, to that of the iso-kinetic sampling results but differed in the absolute value of reported results of fineness for the mills of the same unit and load conditions. On mill 2B the difference was as high as 4.98 percentage points at 106µm. To put that in perspective it equates to 47.7% of the optimal fineness window. The PSA results of mill 2B at the 300µm particle size deviates from the iso-kinetic sampling results by 0.98 percentage points, or 123% of the optimal fineness window at 300µm. Focussing on the green and blue lines of mill 2B in Figure 5.9 the iso-kinetic results indicate that the mill is grinding optimally whereas the PSA results indicate the mill is grinding too coarse and the mill would need adjustment.

Table 5.2: Iso-kinetic sampling vs. PSA results

	2B Iso	2B PSA	2D Iso	2D PSA	Max % point diff	% of Window
%<300µm	98.63	99.61	99.73	99.01	Mill 2B 0.98	123.13
%<150µm	90.03	93.51	95.74	92.10	Mill 2D 3.64	66.18
%<106µm	79.34	84.32	89.00	84.52	Mill 2B 4.98	47.47
%<75µm	64.46	67.69	76.59	71.89	Mill 2D 4.70	46.95

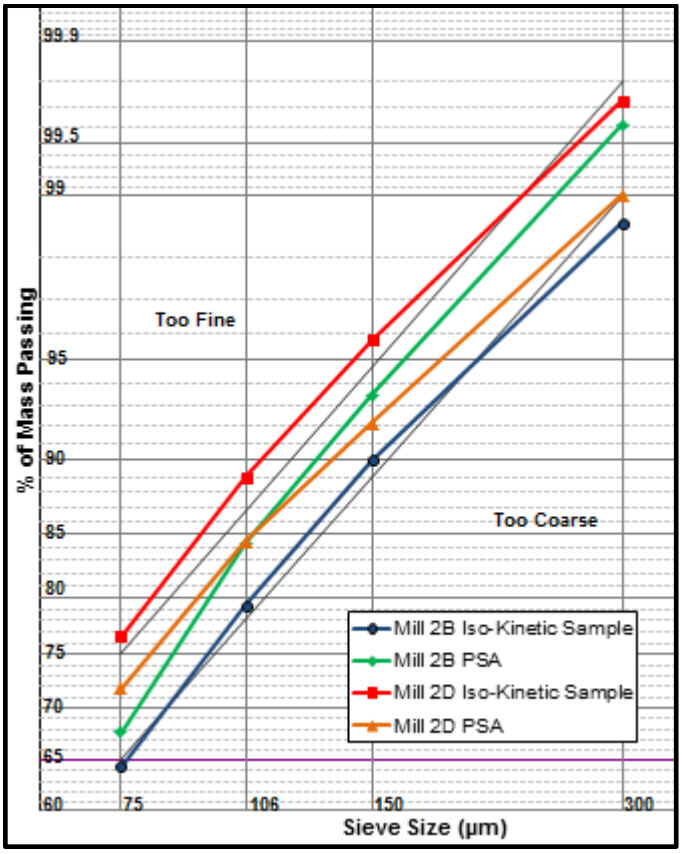

Figure 5.9: Iso-kinetic sampling vs. PSA results

This type of instrument behaviour is indicative of low accuracy performance (Figure 5.9) and high precision (Figure 5.8), as generally accepted by the Joint Committee for Guides in Metrology (JCGM, 2012).

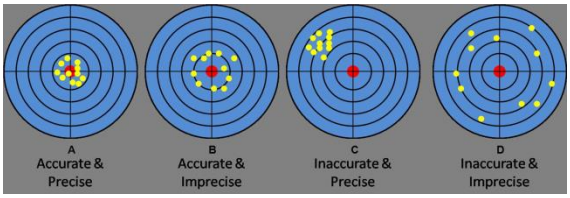

Figure 5.10: Accuracy vs. Precision

The behaviour indicated in Figure 5.9, is under normal circumstances, attributed to an instrument that requires a calibration to be performed in order to improve the accuracy, and thus produce results that are both repeatable (precise) and correct (accurate). However in the case of the PSA, the probe does not require a measurement calibration as it measures directly the chord lengths of every particle that passes through the laser. Instead the probe had been lab verified by the manufacturer after being challenged by these initial test results. Still the results showed differences when compared to the iso-kinetic sampler even after being proven accurate in a lab environment. This prompted an investigation to determine what other parameters are affecting the results of the PSA in power station conditions. The objectives were to understand how the test procedures and test parameters around the PSA affect the reported results. Once this has been understood one may be able to commission the equipment for accurate repeatable results.

5.4. Investigation Findings

5.4.1. Probe Angle Effect

The first thing to note is the effect that the orientation of the probe plays on the perceived results. This is due to the shape and orientation of the groove that the PF must pass through in order to pass the laser eye.

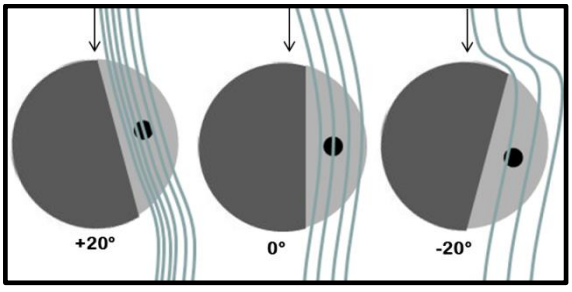

Figure 5.11: Flow Patterns for Different PSA Orientations

Figure 5.11 illustrates the flow pattern that the laser eye should see. However, when one considers the poly-dispersed two phase nature of the

flow, some questions may be raised as to the paths and deflections of the different sized particles either away or into the measurement path. The test conducted was aimed to study the effects of the probe orientation on the reported PF fineness. Measurements of PF fineness were taken for orientations of 0°, 10° and 20° in each direction. The two different cases shown in

Table 5.3 represent the results as the laser eye is rotated to face into the flow (towards +20°) and then away from the flow (towards -20°) as per Figure 5.11. The 0° orientation represents the correct orientation with respect to the pipe flow. The results at the various sieve sizes are consistent in their behaviour. From 0° rotating counter-clockwise to +10° the particle fineness sharply increases, and the results fail to show at 20° due to the PF building up to cover the laser eye. At that stage the angle is too large to allow a flow of PF through its desired path.

Table 5.3: Percentage passing for different PSA orientations

	+20°	**+10°**	**0°**	**-10°**	**-20°**
%<75µm	0%	72%	62%	51%	71%
Standard Deviation		0.7822	2.1752	0.7874	3.9837
%<106µm	0%	89%	82%	70%	86%
Standard Deviation		0.6647	1.3950	0.8291	5.9755
%<150µm	0%	97%	94%	86%	93%
Standard Deviation		0.2738	0.6416	0.7949	3.0743
%<300µm	0%	99.9%	99.6%	98.7%	99.8%
Standard Deviation		0.0707	0.1410	0.2449	0.0866

When rotating the probe clockwise from 0° to -10°, the particle fineness sharply drops indicating that finer particles are being deflected away from the path of the laser eye, or more of the larger particles are flying towards the eye. This is counter intuitive as it is expected that smaller particles would follow the fluid path closer. Rotating the probe further on, the results pass an inflection point and the particle fineness drastically increases once again. This indicates that at this higher angle, the coarser particles are more easily deflected away from the desired path and more fines are being measured. Either way, the effect of changing the angle of the probe

as inserted into the PF pipe has an adverse and drastic effect on the reported results. Within ±10° the results appear finer when the laser eye is angled towards the flow and coarser when angled away from the flow.

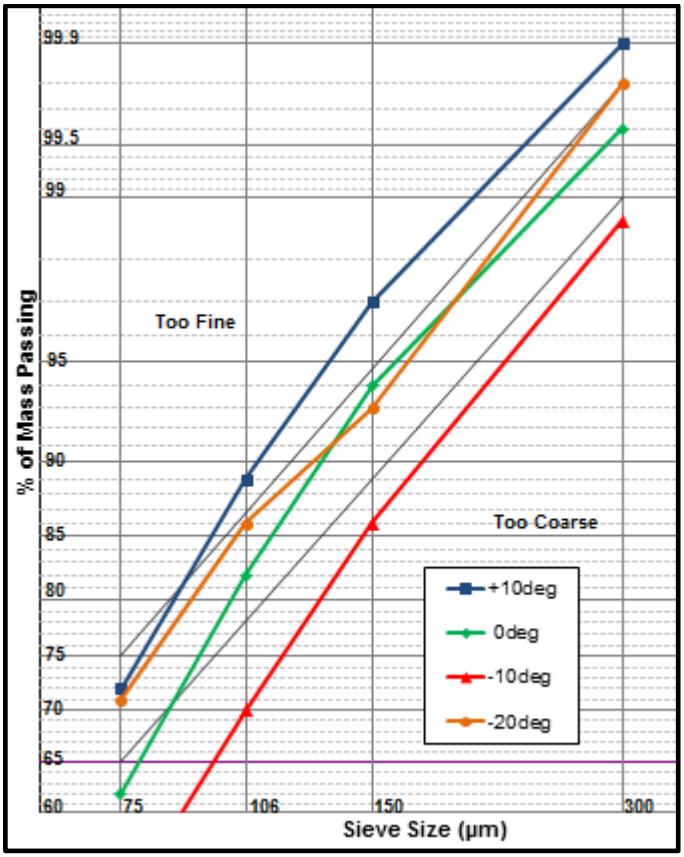

Figure 5.12: Rosin Rammler for different PSA orientations

Figure 5.13 below shows the same results on a bar graph with the standard deviations of measurement present. It can again be seen that within ±10˚ the effect of rotating the probe is such that particle fineness increases towards +10˚ and decreases towards -10˚. However as it approaches -20˚ the result is unpredictable and the deviation increases drastically.

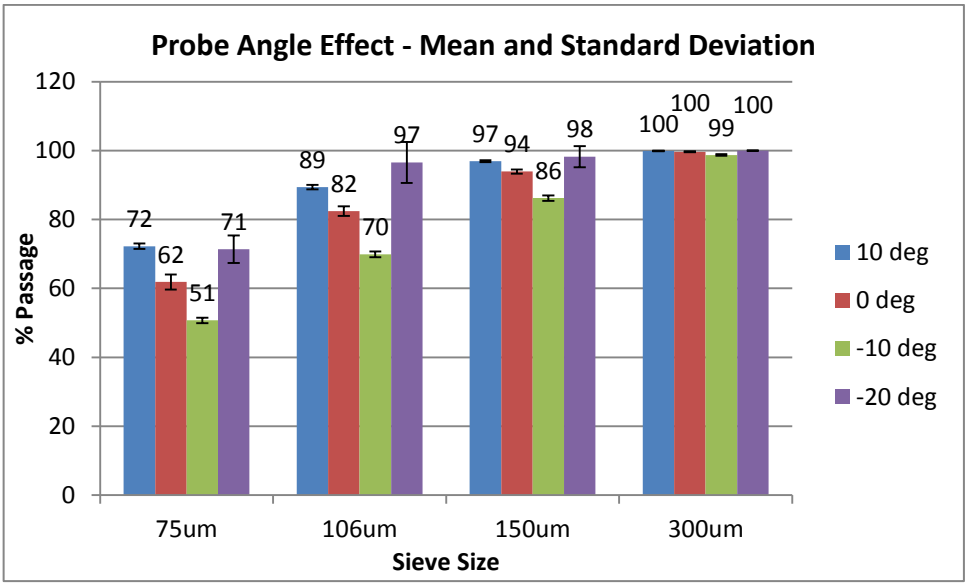

Figure 5.13: Probe angle effect results

5.4.2. Purge Air Pressure and Mass Flow Effect

The second area of investigation was based around the effect of the mass flow rate and pressure of the purge air supplied to the laser eye. It is envisaged that the purge air may be instrumental in deflecting the fine or coarse particles away from the laser eye and measurement path as illustrated in Figure 5.14. (Hayden et al., 2003)

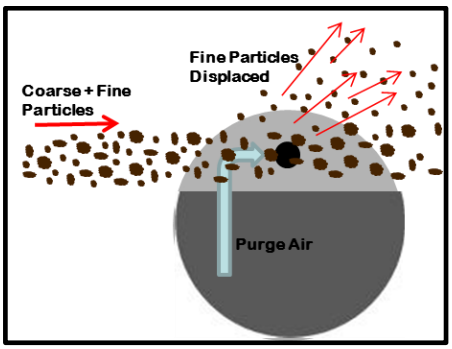

Figure 5.14: Purge air affecting the upstream flow

An increase in purge air pressure from 2 bar to 4 bar had indicated a drop in reported particle fineness of approximately 1 percentage point at the smaller particle sizes and 0.21% at the 300µm particle size. However the 0.21 percentage point fineness drop at the 300µm particle size equates to

26.25% of the optimal window which may lead an engineer to unnecessarily modify the mill operation.

Table 5.4: Purge air pressure results

	2 bar	3 bar	4 bar	Max % point diff	% of Window
%<300µm	99.73	99.58	99.52	0.21	26.25
Standard Deviation	0.1097	0.1950	0.2349		
%<150µm	96.08	95.93	95.16	0.92	16.72
Standard Deviation	0.4793	0.6548	0.8149		
%<106µm	86.99	86.98	85.97	1.02	9.71
Standard Deviation	0.5775	0.6084	0.8545		
%<75µm	67.46	67.49	66.65	0.84	8.40
Standard Deviation	0.6137	0.6317	0.9699		

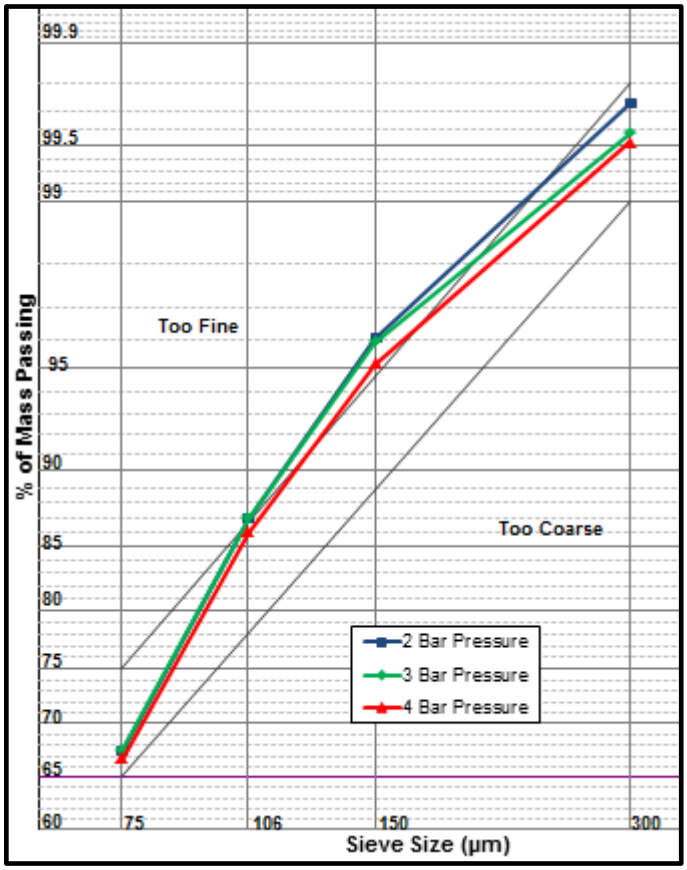

Figure 5.15: Rosin Rammler graph for varying purge air pressure

The trend in Figure 5.15 clearly shows that the increased pressure displaces finer (lower momentum) particles from the natural path creating a bias towards the larger particles. Looking at Figure 5.16 however it is noticed that the standard deviation overlaps between the 2 bar, 3 bar and

4 bar particle fineness results. Although the effect was found to be consistent amongst repeatability tests, the difference may be considered insignificant if looked at in isolation.

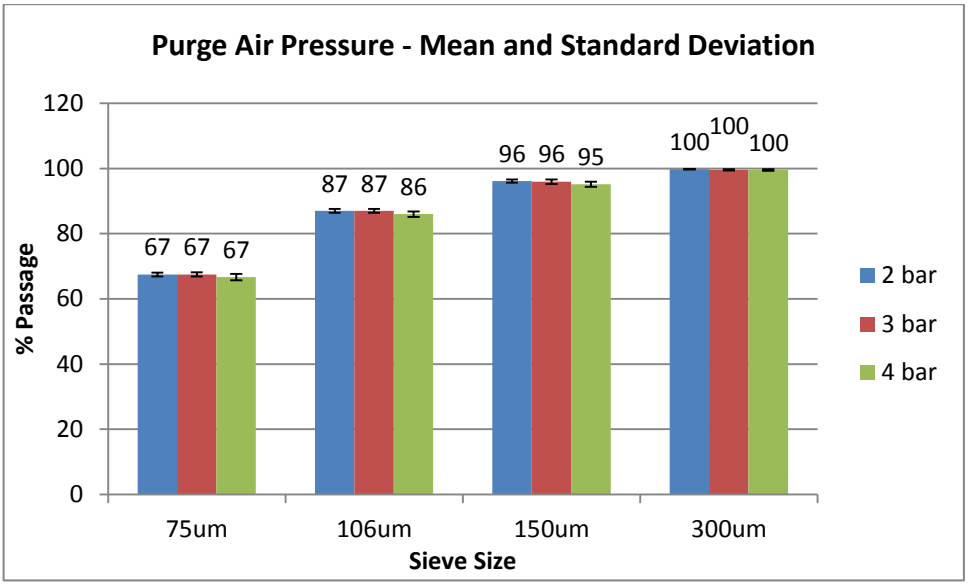

Figure 5.16: Purge air pressure results

An increase in mass flow of purge air, on the other hand, acts to produce a finer result as per the Rosin Rammler graph in Figure 5.17. As the purge air mass flow is increased, so does the reported results of PF fineness, thus showing that the purge air mass flow has an influence on the measurement results.

Table 5.5: Purge air mass flow results

	5 L/m	10 L/m	Max % point diff	% of Window
%<300µm	99.31	99.72	0.41	51.25
Standard Deviation	0.3505	0.1326		
%<150µm	94.31	95.38	1.07	19.45
Standard Deviation	0.6609	0.5546		
%<106µm	85.17	86.81	1.64	15.61
Standard Deviation	0.5900	0.7529		
%<75µm	67.25	69.17	1.92	19.2
Standard Deviation	0.5766	0.7798		

The difference is as high as 1.92 percentage points at the 75µm particle size, while the 300µm particle size group can change by 51.25% of the optimal fineness window.

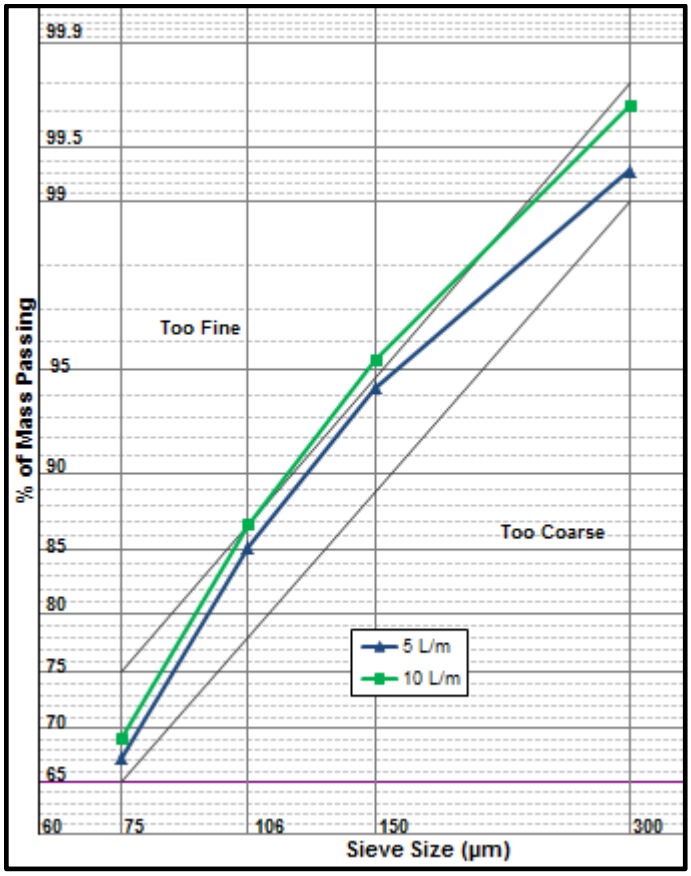

Figure 5.17: Rosin Rammler graph for varying purge air mass flow

In Figure 5.18 this effect is clear at the 75µm and 106µm sieve sizes where the particle size differences as a result of changing the purge air mass flow are larger than the standard deviation of measurement. However at the 150µm and 300µm sieve sizes the standard deviation of test results begin to overlap. It must be noted though that the window particle size requirements is an order of magnitude smaller at the 300µm sieve size that it is at the 75µm sieve size.

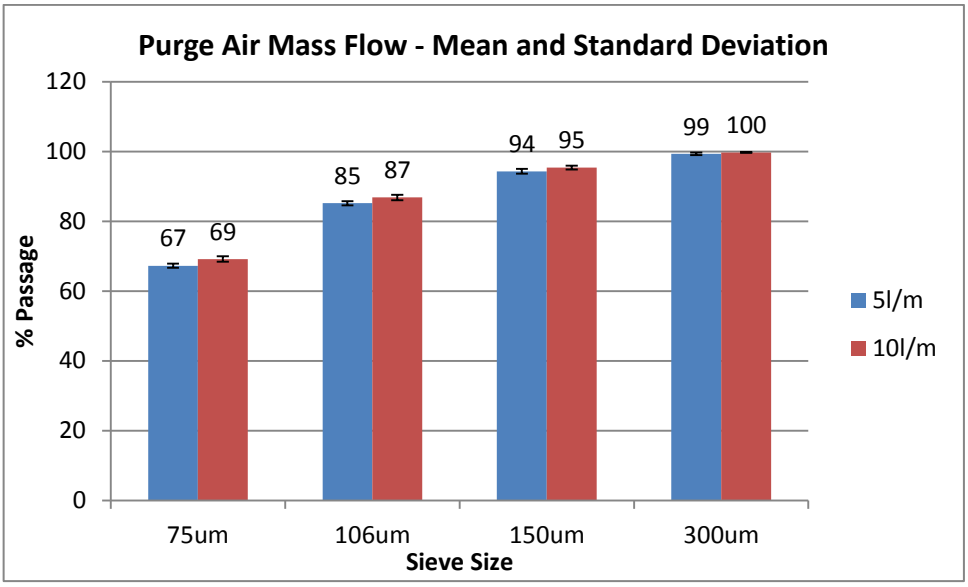

Figure 5.18: Purge air mass flow results

5.4.3. Purge Air Time Effect

The final purge air parameter to evaluate is the period of each purge. The purge settings allow for a burst of purge air to blow for either 2 or 4 seconds, with a 30 second interval between purges. Purging for longer than 4 seconds at a time caused the probe to read a zero result for a short period of time and therefore produced an incorrect average result. Figure 5.19 shows the effect of increasing the purge time, on the particle fineness.

Table 5.6: Purge air time results

	2 s	4 s	Max % point diff	% of Window
%<300µm	99.72	99.51	0.21	26.25
Standard Deviation	0.1264	0.5067		
%<150µm	95.38	94.97	0.41	7.45
Standard Deviation	0.5288	1.0046		
%<106µm	86.81	86.22	0.59	5.61
Standard Deviation	0.7178	1.2011		
%<75µm	69.17	68.43	0.74	7.40
Standard Deviation	0.7435	1.001		

The effect of increasing the purge time was found to be similar to that of increasing the purge pressure. That is, as the purge time is increased, the perceived results get coarser. However, the change of purge time had the smallest overall effect on the reported results.

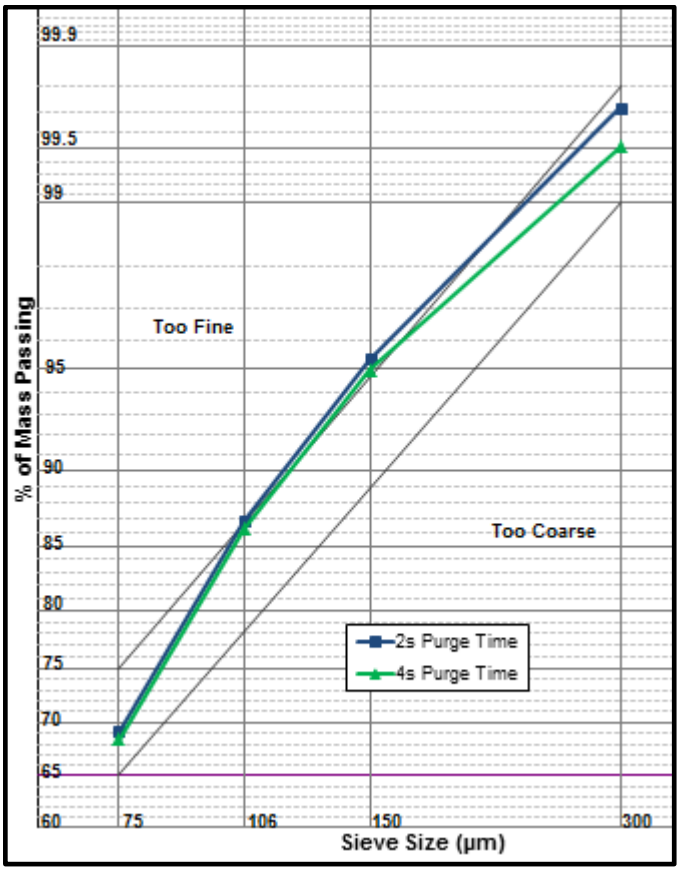

Figure 5.19: Rosin Rammler graph for varying purge time

Finer particles were most influenced by increasing the purge time, with the highest percentage point decrease of 0.74%. The influence of purging time on the reported particle fineness was consistent amongst repeatability tests. However the standard deviations did overlap due to the small magnitude of influence that this parameter has on the reported results (Figure 5.20).

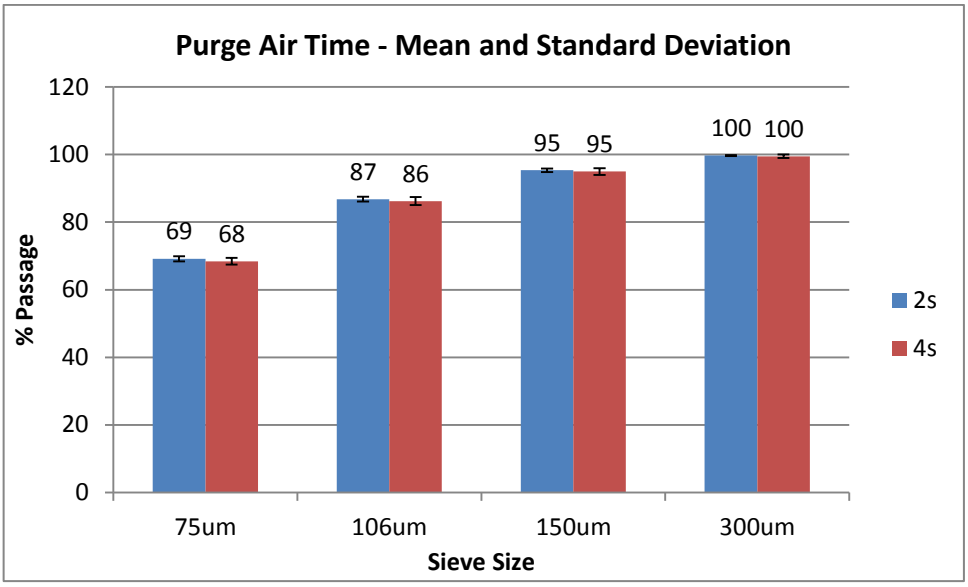

Figure 5.20: Purge air time results

All of the above findings show that the flow reacts to the pressure, flow rate, purge time as well as the angle of the probe. And different particle sizes react differently to these variations thus presenting a false (non-representative) flow to the laser eye for measurement.

5.4.4. Point Measurement Depth Effect

The ability of the measurement device to capture a representative sample of the actual flow may also be analysed on a larger scale than that of the flow dynamics around the measuring tip and laser eye. The iso-kinetic sampler, for example, will extract PF from a PF pipe by performing a traverse of nearly the entire cross section of the pipe. This is to ensure confidence that the sample extracted is representative of the entire flow.

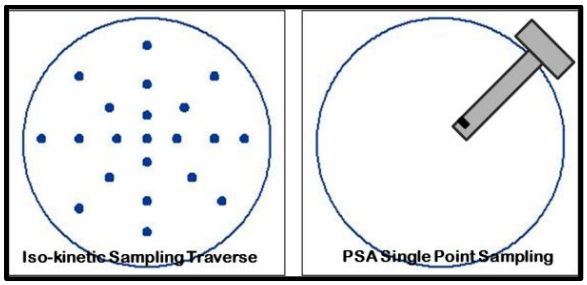

Figure 5.21: Multi-point traverse vs. single point measurement

PF is extracted from 32 points spread symmetrically over the cross section of the PF pipe, similarly depicted in Figure 5.21. The PSA probe is not designed to perform a traverse as the probe length does not permit it physically. The standard probe measures at a maximum PF pipe penetration of 125mm, of a 457mm internal diameter PF pipe. A longer PSA probe facilitated a traverse test up to a depth of 200mm into the PF pipe as in Figure 5.22.

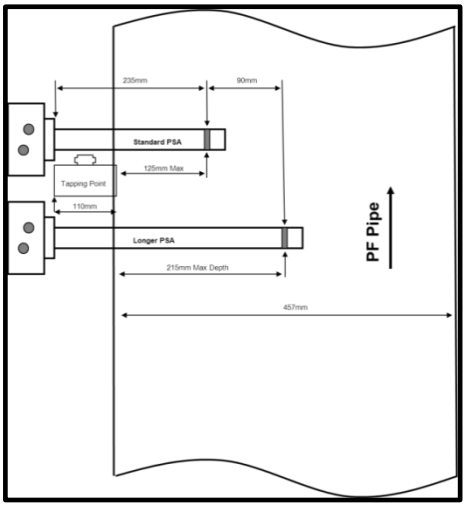

Figure 5.22: PSA dimensions with respect to the PF pipe

The results of the varying depth traverse test shown in Figure 5.22 reveal an interesting phenomenon about the nature of the flow inside a PF pipe. As the PSA probe penetrates deeper into the pipe the probe reports pulverised fuel that is coarser in nature. This indicates that there is a higher concentration of coarse particles that travel at the centre of the PF pipe while the bulk of the finer particles tend to travel closer to the pipe walls. The pipe itself is vertically oriented with an internal diameter of 457mm. The measurement point is located approximately 5m from the nearest bend upstream and the flow is vertically upward. The trend has also been consistent amongst the PF pipes of different mills and even on mills of two different power stations that were tested.

Table 5.7: Point measurement depth results

	50mm	100mm	150mm	200mm	Max % point diff	% of Window
%<300µm	99.92	99.89	99.90	99.86	0.06	7.50
Standard Deviation	0.0748	0.1135	0.0603	0.0881		
%<150µm	97.50	96.37	95.15	93.28	4.22	76.72
Standard Deviation	0.1341	0.2900	0.4979	0.4876		
%<106µm	88.75	85.77	82.87	78.42	10.33	98.38
Standard Deviation	0.5162	0.5797	0.7817	0.8494		
%<75µm	68.95	64.96	60.48	55.00	13.95	139.50
Standard Deviation	0.5315	0.7227	0.9212	1.0857		

The effect is largest at the smaller sieve sizes indicating a higher gradient of finer particles from the wall to the pipe centre. The change at the 300µm level is a mere 0.06 percentage points while at the 75µm particles size the change is 13.96 percentage points (139.5% of the window).

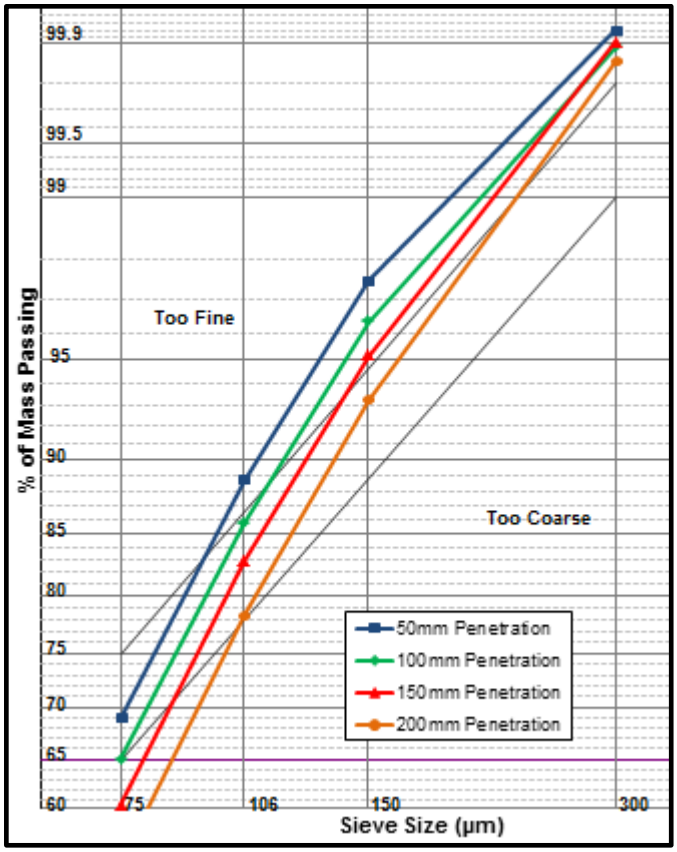

Figure 5.23: Rosin Rammler graph for varying PSA depth

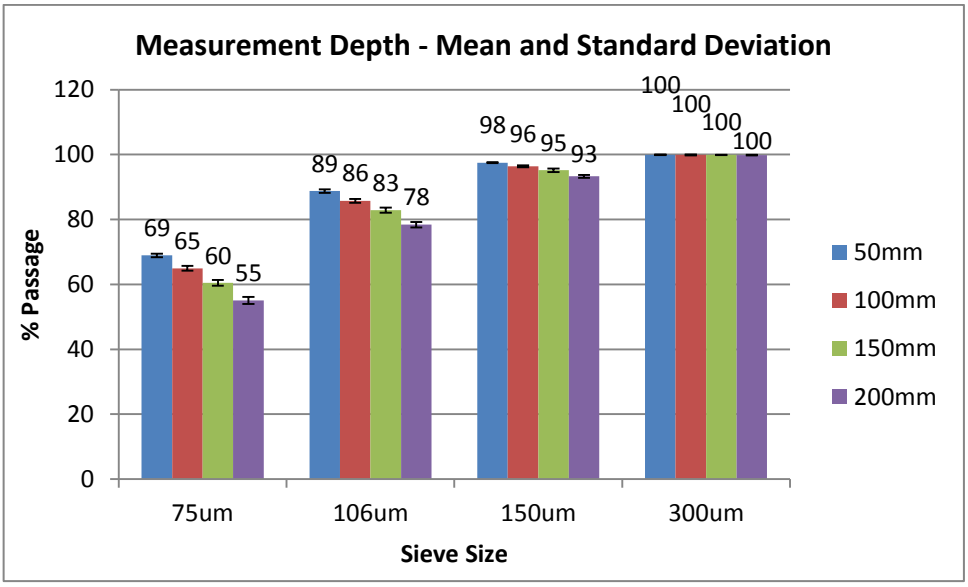

Figure 5.24: Measurement depth results

Figure 5.24 shows the consistent behaviour found by the PSA. The test also reveals that one may not assume a single point measurement to be representative of the entire flow. In order for this to be true one has to traverse the flow with the PSA probe and compare the results to the iso-kinetic sampling results. Only then can you determine that for a stable load and under those conditions, the closest matching results may pass as a single point measurement that is representative of the flow.

Multiple points of entry for the PSA into the PF pipe were not possible at Camden Power Station due to the physical layout of multiple pipes in close proximity to one another. Thus the PSA could not take measurements according to the BS 893 standard. Instead to confirm this phenomenon, the iso-kinetic sampler was used to extract PF from the same points in the PF pipe that the PSA was used to measure the particle size. Once separately sieved the results did in fact confirm the same relative difference in particle fineness across the cross section of the PF pipe.

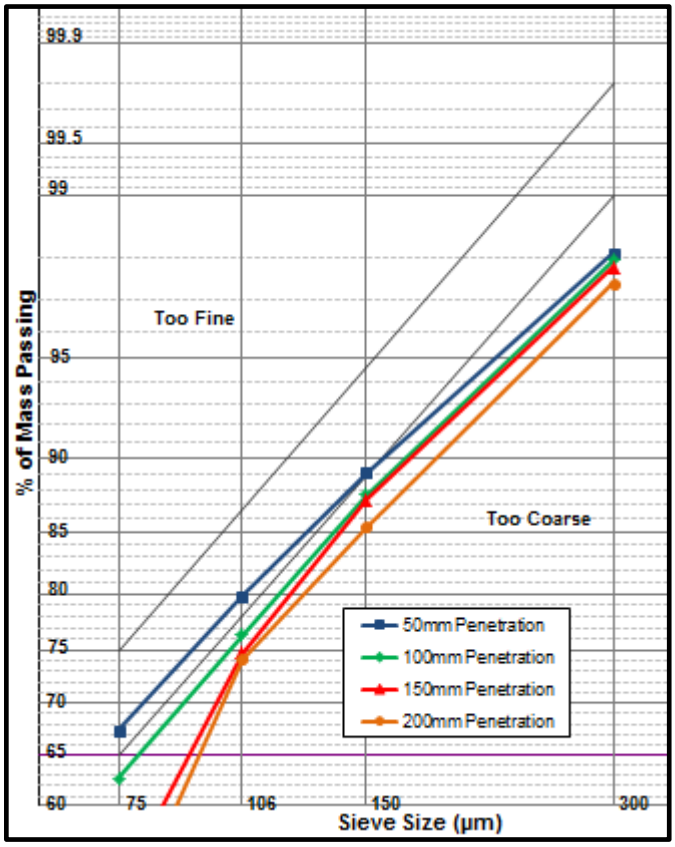

Figure 5.25: Rosin Rammler graph for varying Iso-kinetic depth

Mill 2C in this particular test was performing poorly and grinding too coarse according to the Rosin Rammler graph in Figure 5.25 above. The Particle fineness was particularly poor at the 75µm sieve size.

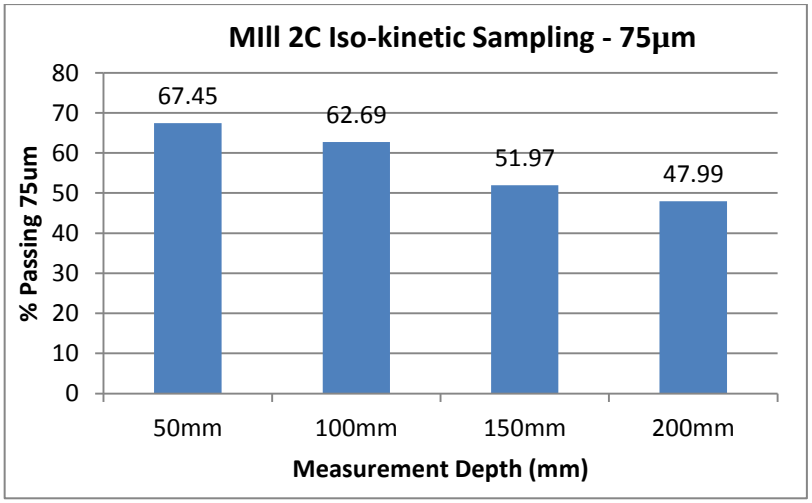

Figure 5.26: Iso-kinetic sampling results at 75µm

The results of the 75µm sieve size are shown in Figure 5.26 above. From this graph it is clear that the particle fineness decreases towards the centre of the PF pipe and the finer particles flow closer to the walls. It is also clear that the effect is much more noticeable at the 75µm sieve size than the coarser sieve sizes as was the case with the results of the PSA. Unfortunately, a final absolute result comparison was not possible, as the PSA instrument was not available at the time for further testing.

The results found in Figure 5.25 and Figure 5.26 relate to tests performed on mill 2C. For repeatability results of this test as well as similar findings on mill 2B refer to Appendix B: Iso-kinetic Sampling Results

Chapter 6: Monitoring Mill Recirculating Load

6.1. Introduction

The exercise of tracing a single coal particle on its path through the mill would result in multiple recirculating passes in the primary classification zone (see section 1.2.2) as well as multiple possible passes through the final classifier before exiting the mill. The nature of the flow in the primary recirculation zone and the mill body as a whole is that of a solid-gas dense phase flow where the coal particles are fluidised by the primary air. By the principles employed in circulating fluidised bed boilers to determine the mass of particles in suspension in the bed, one can determine the mass of particles in suspension in various levels of the mill body. Once this parameter can be measured continuously, any changes in the suspended mass of coal particles can be interpreted to provide vital information about the health of internal components of the mill.

The principle will be tested on a pilot scale mill at Eskom Research Testing and Development (R,T&D) department. The significant difference between the pilot scale mill and that of a full scale mill is that the final classification zone is not separated from the primary classification section by means of a classifier cone. Instead, the pilot scale mill has a rotating classifier which generates swirl in the mill body itself, but above the primary classification zone.

By measuring and comparing the suspended mass in the primary classification zone and the secondary classification zone, one can draw conclusions about the status of the internal components of the mill. An increase in primary recirculation coupled with a decrease in particle mass to the classifier is an indication that the PA velocity in the throat has reduced. This suggests that the throat area has increased as a result of high wear and is probably in need of repair.

An increase in primary recirculation load coupled with no change in mass flow to the classifier is indicative of high grinding element wear. An

increase in secondary classification mass flow coupled with a reduction in primary recirculation is indicative of having a throat velocity that is too high. This could be the result of a throat blockage or high coal rejects through the throat.

This is all vital information that can provide some currently unavailable information about the internal health of mill components provided that the parameter can be monitored in real time. The study herein aims to achieve the on-line monitoring of the mass of coal in suspension by means of differential pressure measurements at various heights of the mill body.

6.2. Investigation Findings

In the graphs to follow the mill throughput is quoted as the percentage of the maximum capable feeder speed of the mill and will also follow the short form of F10, F11 or F12 indicating a feeder speed of 10%, 11% or 12% respectively. The classifier speed is also quoted as a percentage of the maximum capable classifier motor speed and will follow the short form of CL10, CL12 or CL14 indicating classifier speeds of 10%, 12% or 14% respectively. Where a ratio is quoted, such as 4:1, it refers to an air/fuel ratio, i.e. 4 parts air to 1 part fuel.

6.2.1. Throat Differential Pressure

The throat differential pressure is expected to increase with mill load as the air mass flow and thus the throat velocity is increased accordingly. The increased coal mass flow should also act to increase the throat DP as the resistance to flow will increase. This relationship is evident in the results of Figure 6.1 below.

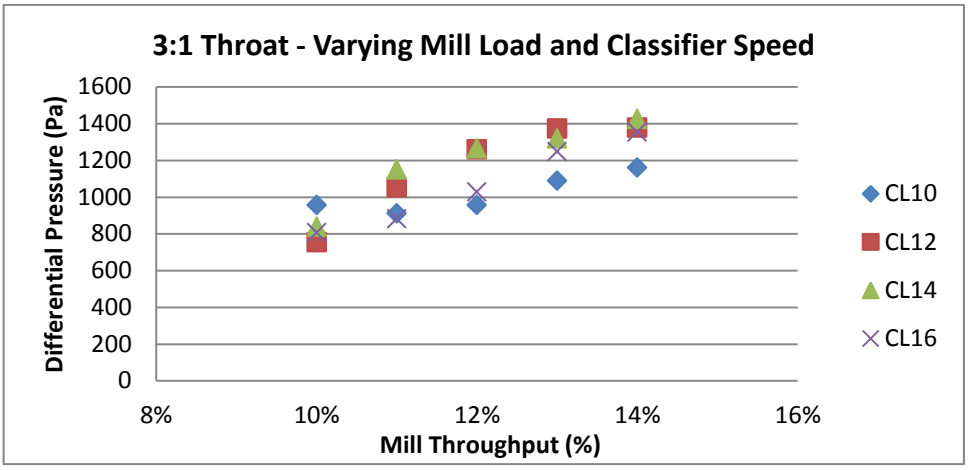

Figure 6.1: Air/fuel ratio 3:1 - varying mill load

It is difficult to establish a clear relationship between the differential pressure and the classifier speed from Figure 6.2. The DP tends to first increase then decrease with increasing classifier speed.

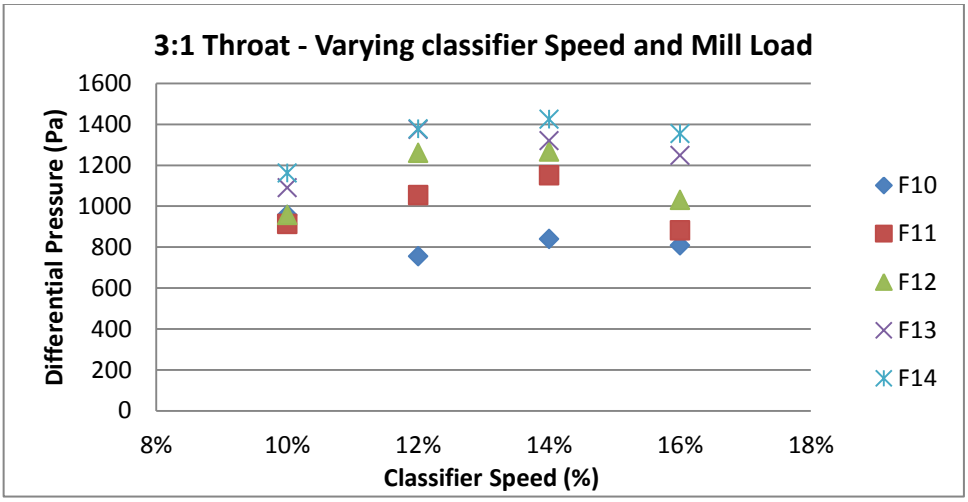

Figure 6.2: Air/fuel ratio 3:1 - varying classifier speed

Similar results were found for different air/fuel ratios of 4:1, 5:1 and 6:1 (Appendix C: Mill Recirculating Load). Increasing the mill load increases the air and coal mass flow, while increasing the classifier speed only increases the coal flow that the throat will. It does so by increasing the coal recirculation inside the mill. This implies that the throat DP is largely dependent on the air mass flow and to a lesser extent on the coal mass flow. This is expected as the flow that passes through the throat consists

primarily of air. Figure 6.3 and Figure 6.4 below show that for high air/fuel ratios the relationship begins to form between the differential pressure and the classifier speed.

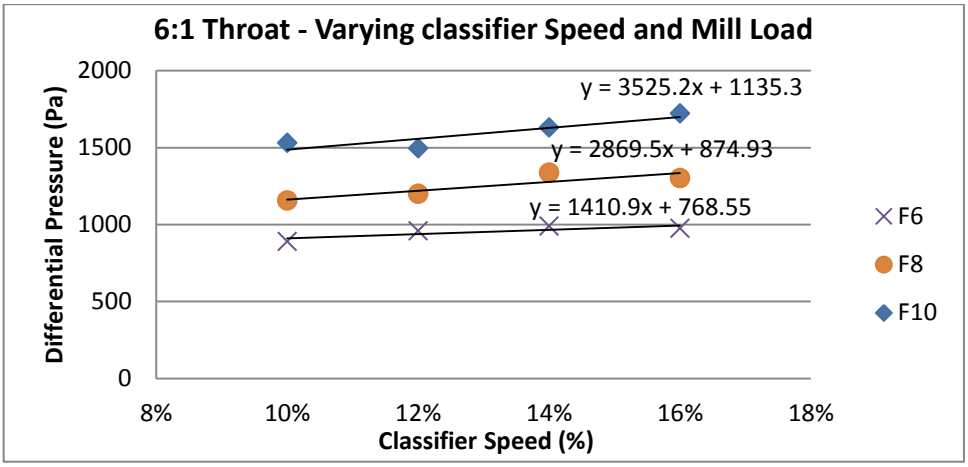

Figure 6.3: Air/fuel ratio 6:1 - varying classifier speed

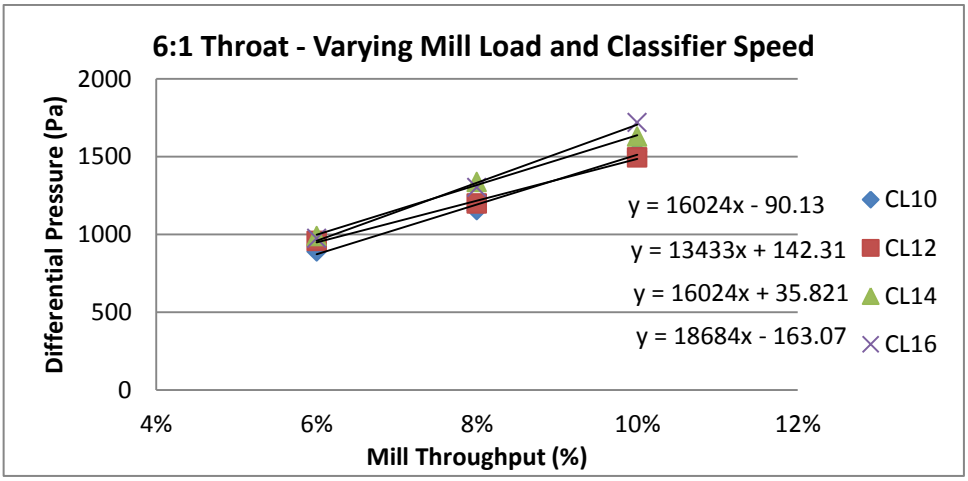

Figure 6.4: Air fuel ratio 6:1 - varying mill load

6.2.2. Tyre Differential Pressure

Measuring the tyre differential pressure is the key to determining the recirculating load of the mill. This parameter is measured across the main particle fluidisation area located in the area above the throat and below the classifier. One would expect to see increased tyre DP with increasing

classifier speed as the classifier recirculates more coal back to the table for regrinding.

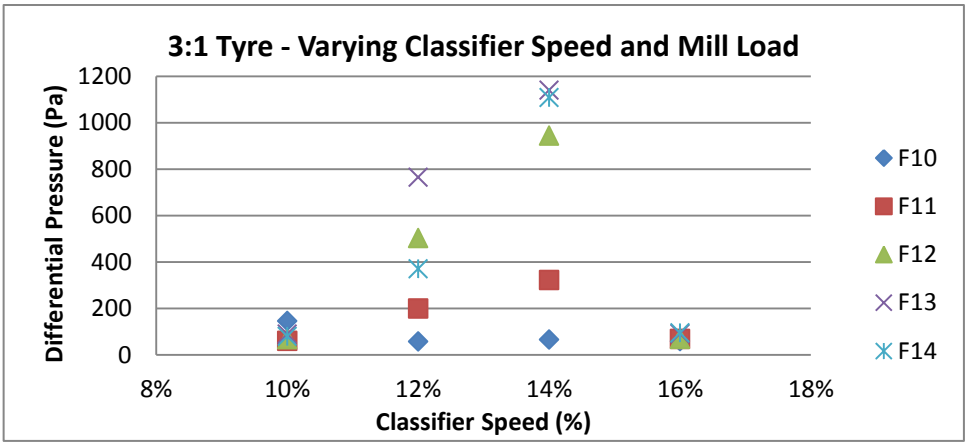

Figure 6.5: Air/fuel ratio 3:1 - varying classifier speed

Figure 6.5 shows erratic results as the differential pressure increases to a peak at 14% classifier speed and then decreases again for all loads. In Figure 6.6 the DP is almost identical for high and low classifier speeds of 16% and 10% respectively, while for classifier speeds of 12% and 14% the DP rises to a peak at 13% mill load and falls again.

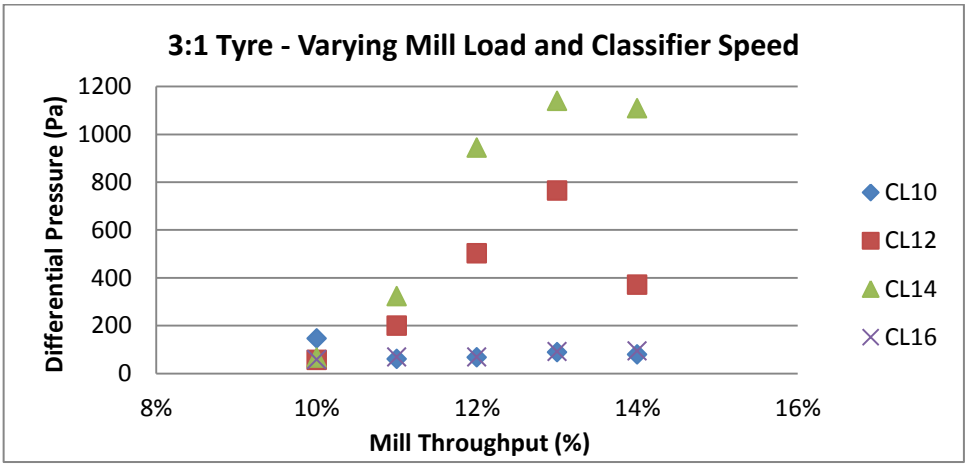

Figure 6.6: Air/fuel ratio 3:1 - varying mill load

A linear relationship was found between the mill throughput and tyre DP at an air/fuel ratio of 6:1 (Appendix C: Mill Recirculating Load), however this operational scenario is not sustainable as the mill does not reach stable operation. This is due to the high air flow causing the mill to run itself

empty over time. The point results displayed in the figures above are recorded as an average over a period of approximately five to ten minutes under stable mill conditions.

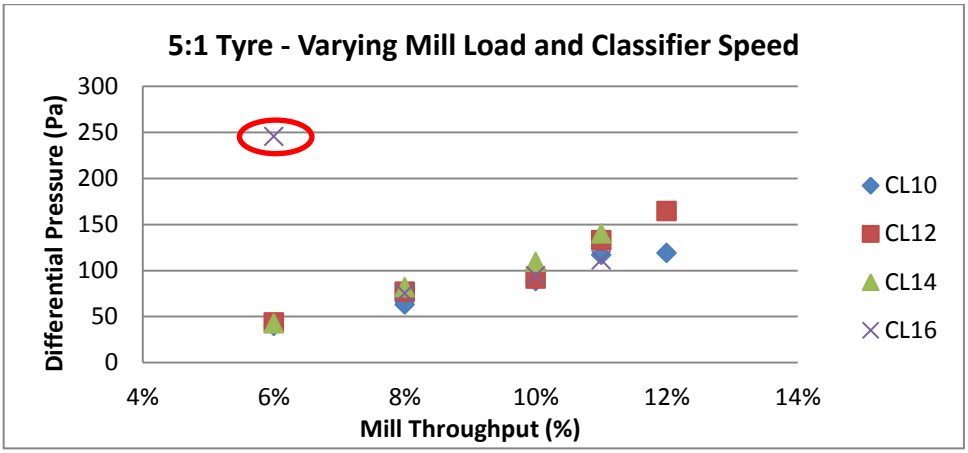

Figure 6.7: Air/fuel ratio 5:1 - varying mill load

Looking at the raw test data for Figure 6.7 above where such an outlying point exists, one can notice two things in Figure 6.8 below. The mill does not reach stabilisation as mentioned due to the high air flow. This will be discussed in more detail in Chapter 7.4.3. The second thing to notice is the large measurement fluctuation.

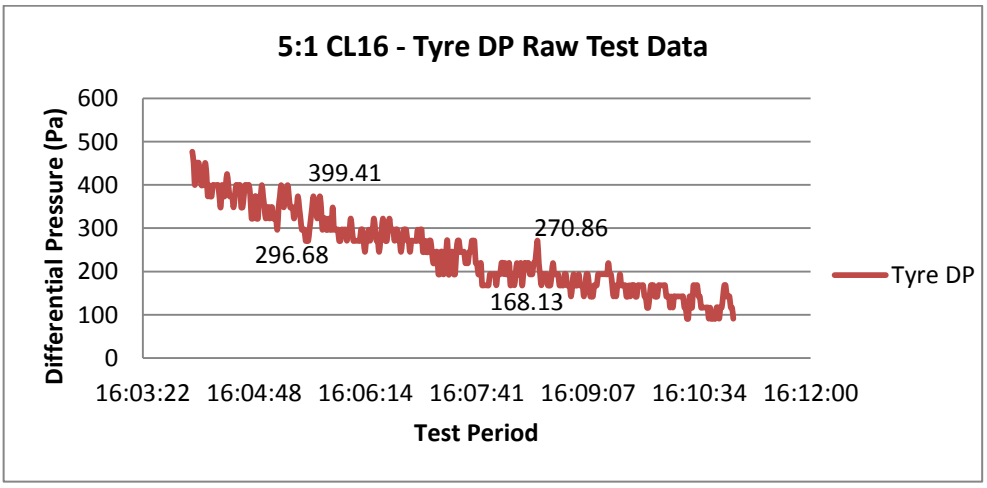

Figure 6.8: Raw test data for point highlighted in Figure 6.6

The two pairs of points highlighted are of values that fluctuate upward in both cases by just over 102Pa. That is a fluctuation of over 25% of the peak in the first case and over 33% of the peak in the second case.

Looking at a set of results that has reached stable operation, the fluctuation in pressure is approximately 257Pa for both cases in Figure 6.9. This equates to 20% and 19% of the peak values respectively.

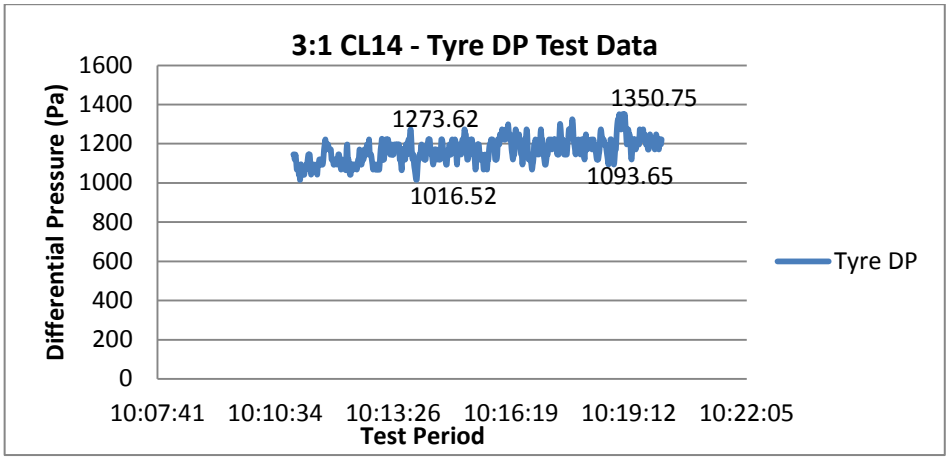

Figure 6.9: Raw test data for a stable test result

This large fluctuation in pressure is expected to be a cause of the mill and classifier design. In a full scale mill the classification area is separated from the tyre area by the classifier cone (Figure 6.10). This means that the classification swirl is induced only inside the classifier cone. The only swirling effect that exists in the lower mill is as a result of the throat vanes, but this is not as pronounced as the swirl induced by the classifier vanes (Figure 6.11).

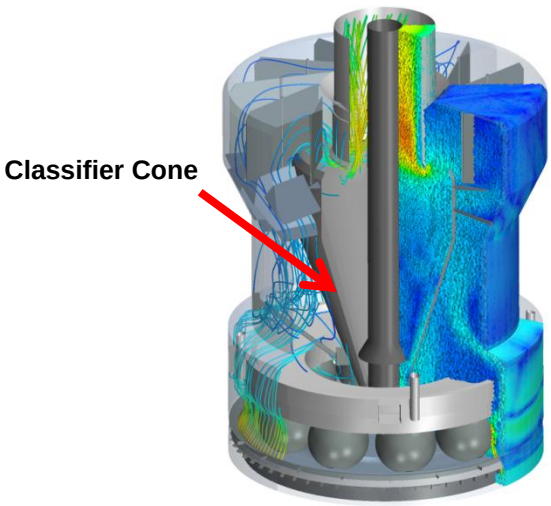

Figure 6.10: Flow inside a full scale mill (CMP 2012)

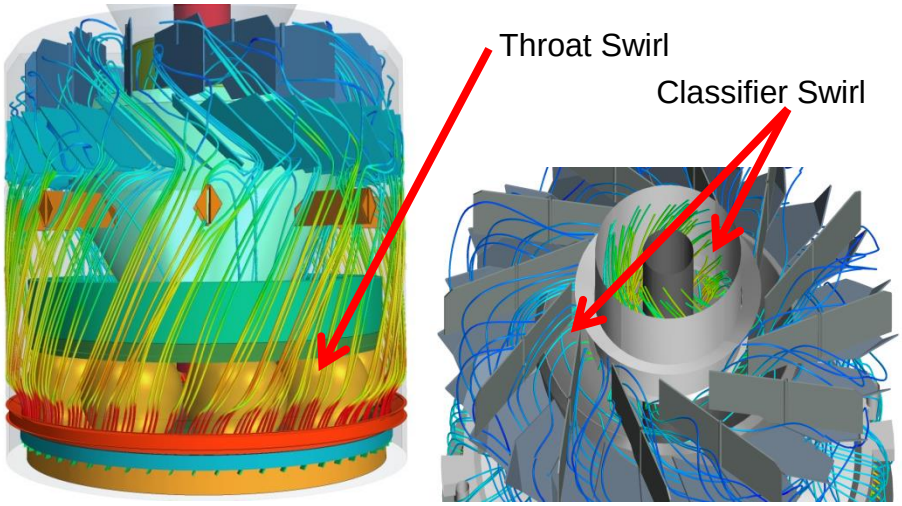

Figure 6.11: Throat induced swirl vs. classifier induced swirl (CMP 2012)

The pilot scale mill on the other hand has a rotating classifier that is designed to generate classification swirl in the mill body itself (Figure 6.12).

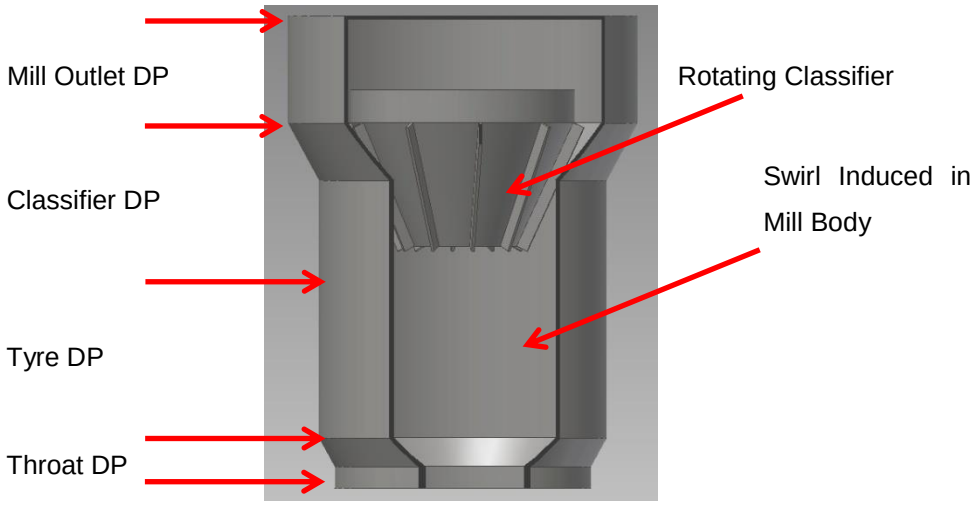

Figure 6.12: Pilot scale mill classifier

The swirl induced in the mill body may contribute a portion of dynamic pressure to what should ideally be a static differential pressure measurement.

6.2.3. Classifier Differential Pressure

The classifier differential pressure measurement results also showed fluctuating readings with respect to increasing classifier speed. In Figure 6.13, Figure 6.14 and Figure 6.15 below, there is no distinct relationship between the classifier speed and the differential pressure across the classifier. This means that the differential pressure measurements are not picking up the change in re-circulated mass introduced by changing the classifier speed. The cyclone effect of the classifier is at its strongest in this portion of the mill and thus a pure static measurement will be difficult to achieve unless the mill design is that of a static classifier such as the one depicted in Figure 6.11. The DP across the static classifier vane may be measured in order to get a more stable representative result.

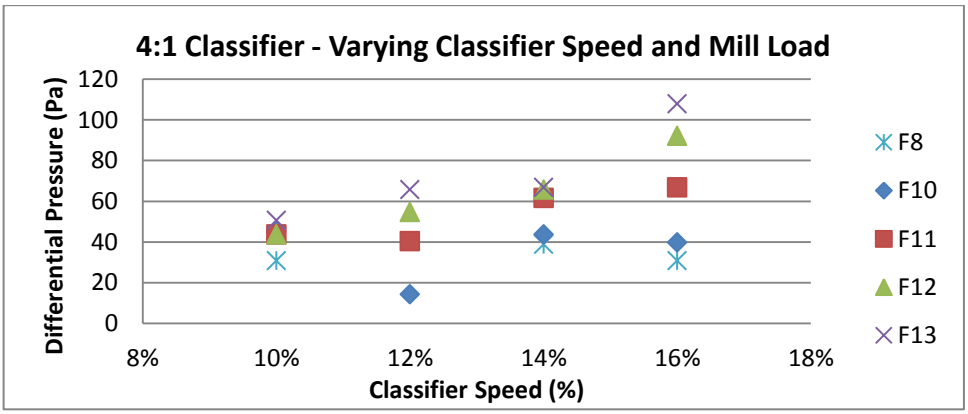

Figure 6.13: Air/fuel ratio 4:1 – varying classifier speed

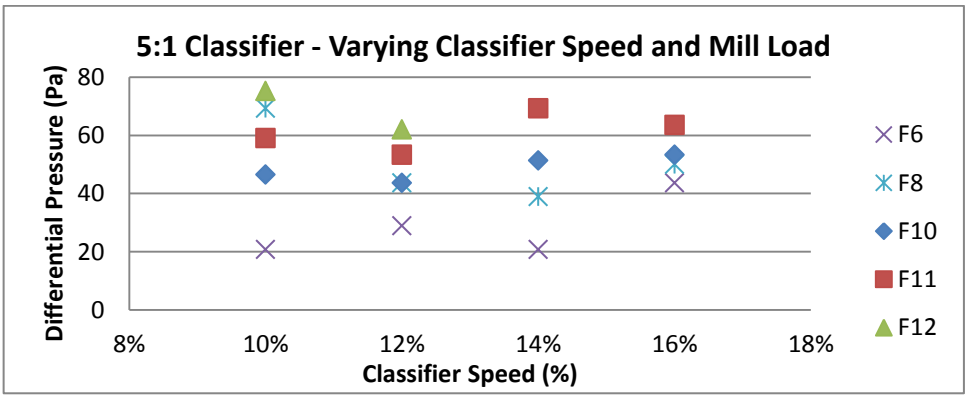

Figure 6.14: Air/fuel ratio 5:1 – varying classifier speed

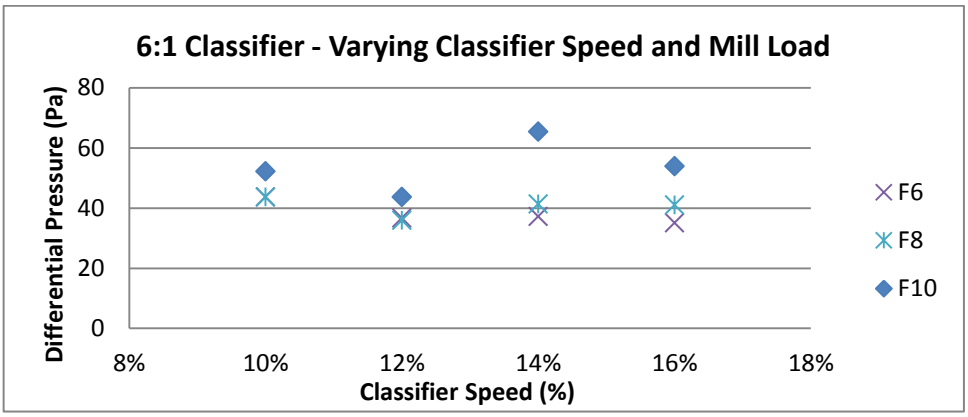

Figure 6.15: Air/fuel ratio 6:1 – varying classifier speed

The results suggest a relationship between the mill load and the differential pressure in the classifier region. However this is only evident under certain operating conditions such as the 12% and 16% classifier speed cases in Figure 6.16. In this figure the 10% and 14% classifier speeds show no reaction to certain changes in mill throughput.

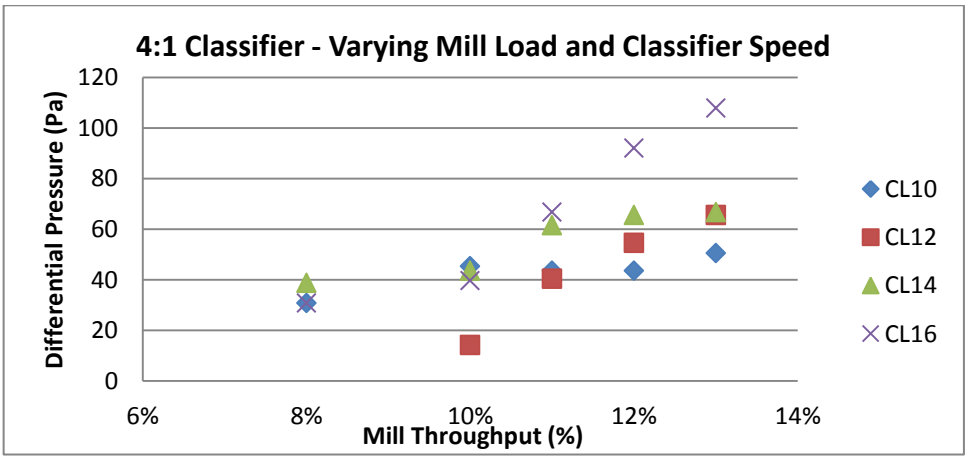

Figure 6.16: Air/fuel ratio 4:1 – varying mill load

In Figure 6.17 the relationship is much stronger for a higher air/fuel ratio, barring the low classifier speed case of 10%. Further results may be found in Appendix C: Mill Recirculating Load.

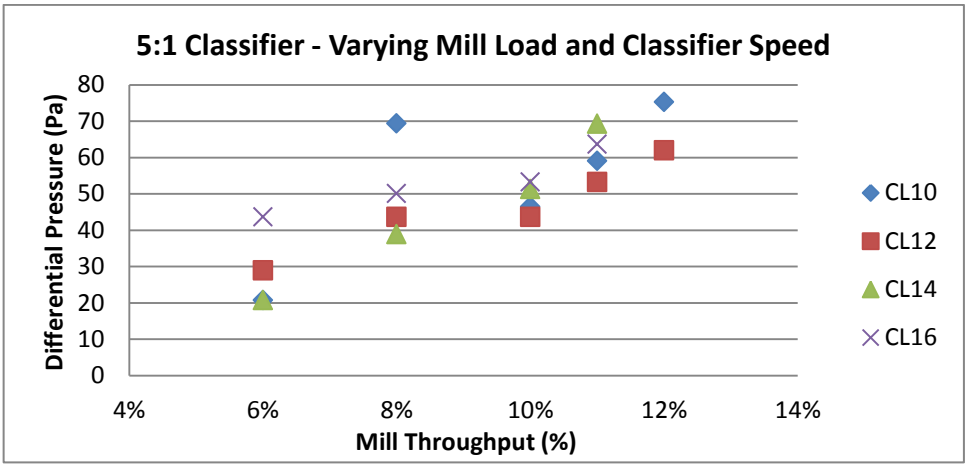

Figure 6.17: Air fuel ratio 5:1 – varying mill load

6.2.4. Mill Outlet Differential Pressure

The mill outlet differential pressure showed fairly convincing results. The differential pressure did not respond to changes in classifier speed as per Figure 6.18 below, and similar trends were found for other air/fuel ratios (Appendix C: Mill Recirculating Load).

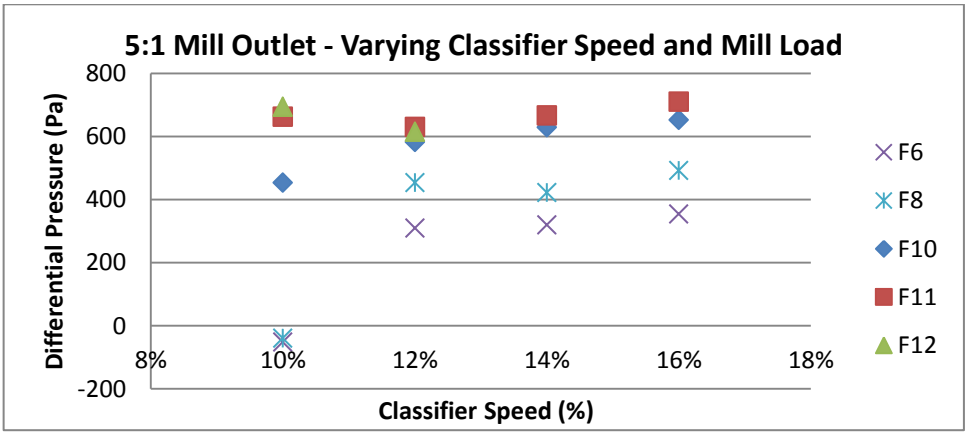

Figure 6.18: Air/fuel ratio 5:1 – varying classifier speed

However the relationship between the DP and the mill throughput at the mill outlet is fairly distinct, as it was at the throat. Although, as mentioned before, there is little to tell between the different classifier speeds tested.

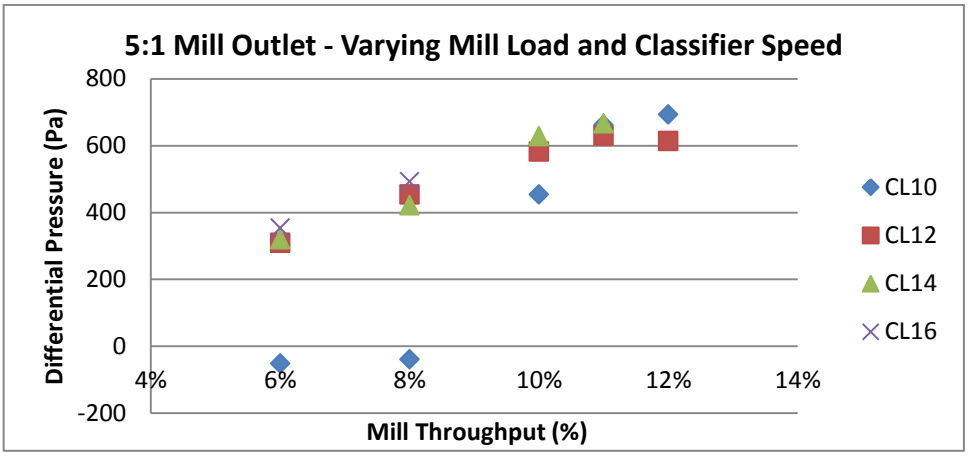

Figure 6.19: Air/fuel ratio 5:1 – varying mill load

One thing to note is that the DP tends to go negative at low classifier speeds and low air/fuel ratios, but not necessarily at low mill throughput as Figure 6.19 may suggest (Appendix C: Mill Recirculating Load).

Chapter 7: Pilot Scale Mill Testing

7.1. Introduction

In order to set up a mill for operation, two main parameters are required to be optimised. The particle fineness produced by the mill must be of the correct specification, and the mill should be able to supply the required mass flow of coal to the boiler without sacrificing the particle fineness. As outlined in the global introduction the coal fired power stations in South Africa are being forced to burn coal of lower calorific value, meaning that the mills are required to run at a higher average load/mass flow. Two problems currently exist as a result. Firstly, due to the high average age of these coal fired power stations, mills are not able to sustain the higher mass flow of coal. And secondly, an increase in mass flow through a mill has an influence on the other parameters of the mill such as particle fineness and differential pressure.

In order to improve the state of current mills one must first understand the relationships that govern the operation of a vertical spindle mill. Once these relationships are well understood, they can be used to optimise the operation of a mill in order to increase its throughput without sacrificing particle fineness.

Tests were performed on a pilot scale test mill that could be pushed to the limits of its operating ranges without causing disruption to any subsequent processes. The aim of this was to document the relationships that govern the operation of a mill while varying the mill load, classifier speed and air/fuel ratio through the ranges determined in the preliminary testing.

7.2. Description

The Eskom Research, Testing and Development (R,T&D) department operates a $1MW_{th}$ pilot scale unit that consists of a single downward firing burner used for the testing and evaluation of various coals. In order to

prepare the coal for firing, a pilot scale vertical spindle mill is used. This milling plant consists of a single vertical spindle mill that operates completely independent of the firing system and furnace plant. Coal is fed into the mill via a crusher and screw feeder and once ground; the pulverised fuel is stored in silos to be fed to the furnace and fired at a later stage. This is different from a coal fired power station which fires coal directly from the milling plant via the PF pipes and through to the burners. The advantage of having an isolated milling process is that the experiments performed on the mill do not have an impact on any subsequent systems. Producing a coarse or fine product while testing the limits of this milling system will result in merely discarding the silos of stored pulverised fuel.

However, due to the fact that the mill operates as an isolated process, there are differences in its operation that one must overcome in order to be able to relate the results to those of a mill in operation on a power station. A full scale mill would usually be controlled to operate according to a mill load line, which maintains a relationship between the air and fuel mass flow. There are a few reasons for this form of control:

1. To ensure that at mill start up and low load (throughput) operation, there is sufficient air flow to maintain the minimum required velocity to prevent particle settling in the PF pipes.
2. To ensure that as the fuel flow is increased the air flow is increased accordingly so as to prevent mill choking by evacuating the PF from the mill.

However since the pilot scale mill is an isolated system, this particular mill is normally operated without concern for PF pipe transportation or PF mass flow rate, and therefore does not operate according to an air/fuel ratio. Instead the air and fuel mass flows are set individually along with other settings such as classifier speed, according to the required product fineness for a specific experiment. In other words this pilot scale mill is operated in manual mode where most of the important control parameters are controlled by the operator. Operating the mill on manual is usually

performed on a power station by an operator under special instruction, usually while some test or measurement is being performed where the fluctuations and changes imposed by the automatic control system are undesired. In order to mimic the operation of a full scale mill the load line would have to be developed for the pilot scale mill.

In addition, the pilot scale mill is controlled in terms of coal flow as a percentage of the screw feeder's maximum speed in revolutions per minute. The same applies to the air flow where the air flow is controlled as a percentage of the maximum damper position of the fan. The coal and air mass flows are unknown parameters which have not been required under normal operation of this particular plant due to the fact that the coal milling process is isolated from the combustion process. Coal is milled according to the required particle fineness and stored for combustion later. Therefore the rate of throughput of coal through the mill itself has until now been irrelevant. However for the purpose of the current research, these parameters would have to first be characterised.

The pilot scale mill itself consists of a grinding table and two tyre elements. Coal is fed into the mill from a coal bunker via a screw feeder. The coal falls directly onto the rotating table and by the centrifugal action it is directed between the tyre and table grinding elements before reaching the outer part of the table where it meets the throat. The primary air fan is situated at the end of the air circuit and operates the mill under suction. Air at atmospheric temperature is drawn through an electric air heater at the mill inlet. The air heater temperature (T_{AH}) controls the inlet air temperature (T_i) so as to maintain the mill outlet temperature (T_o) at 100˚C (Full scale mills are normally controlled at an outlet temperature of 90˚C). The hot air enters the windbox where it is accelerated through the small area of the throat. At the throat it meets with the coal and begins to dry and fluidise the crushed coal particles.

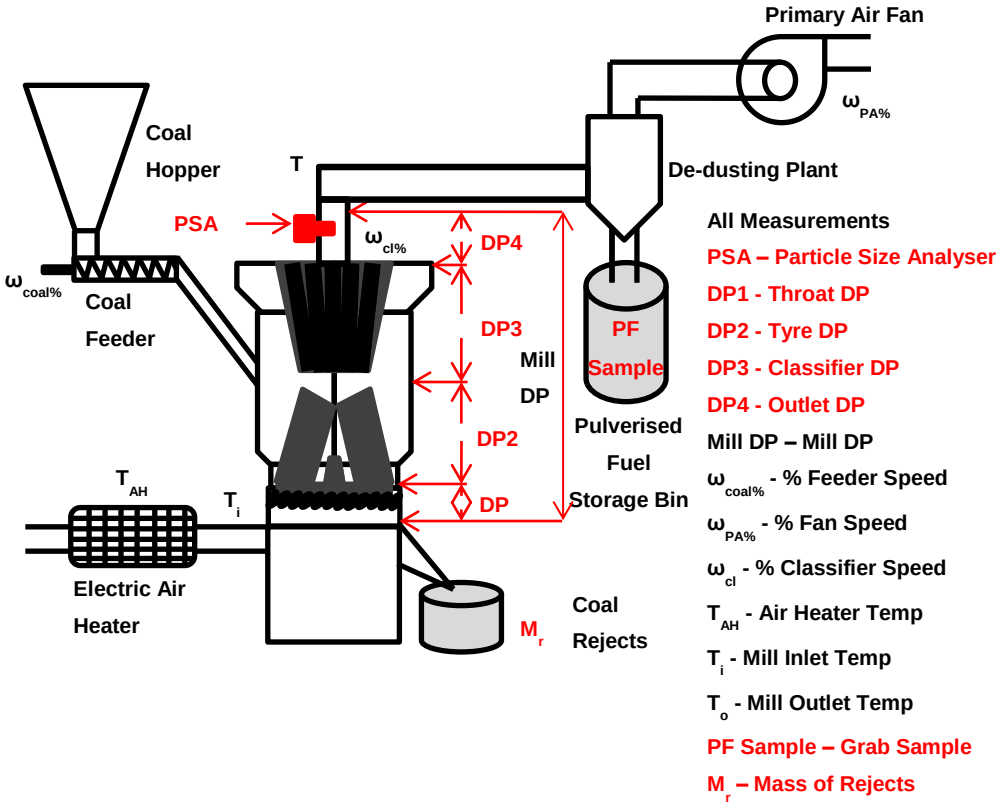

Figure 7.1: Pilot scale milling plant layout

Finer particles are carried up to the classifier and coarser particles immediately fall back to the table to be reground. Mill rejects such as stone and tramp iron fall through the throat and back into the windbox from which they are rejected. As the crushed coal is carried up in the mill it enters the classifier region. Swirl is generated by rotating vanes. By centrifugal force the coarse particles are separated and fall back to the grinding region while the finer particles are allowed to leave the mill. The classifier speed (ω_{CL}) determines what size of particle is allowed to leave and how much of crushed coal is re-circulated. Once the pulverised fuel leaves the mill it is transported via a PF pipe to the de-dusting plant. This consists of a cyclone separator which acts to separate the PF from the air. The PF falls to the storage silos and the clean air is drawn through the primary air fan and exhausted to the atmosphere.

7.3. Preliminary testing

7.3.1. Pilot Scale Mill Characterization

Load Line Development

Load lines for the operation of the pilot scale mill currently do not exist as the isolated nature of the plant meant there has been no need for maintaining a mass flow of fuel for combustion. This means that load lines would have to be developed in order to perform the required tests. Furthermore, the coal and air mass flows are not measured quantities and the equipment that control these flows would first have to be characterised.

Coal Feeder

The feeder consists of a bunker and screw feeder set up in which the rotational speed of the screw can be controlled as a percentage of its maximum speed. The challenge is to relate the speed of the screw feeder to the mass flow rate of the coal that passes through it. This was achieved by running the feeder at various speeds into a collection vessel and recording the time for each speed. At each feeder speed the collection vessel was filled for approximately two minutes and weighed thereafter. One can expect an uncertainty of half a second to start collecting and another half a second when removing the sample collection vessel. This leaves a total timing uncertainty of 1 second in 120 seconds which is approximately 0.83%. This process was repeated and the average of two mass flows was provided for each feeder speed setting from 6% to 20% of the feeder speed. The feeder is grossly oversized for this plant and cannot operate above 20% due to the restrictions of the small mill. The results are depicted in Table 7.1 and the full test results can be found in Appendix D: Preliminary Testing.

Table 7.1: Feeder characterisation data

Feeder %	kg/s Average	kg/h Average
6	0.06	217.87
8	0.07	268.89
10	0.09	345.12
12	0.12	443.34
14	0.15	551.92
16	0.18	659.30
18	0.20	742.78
20	0.22	803.96

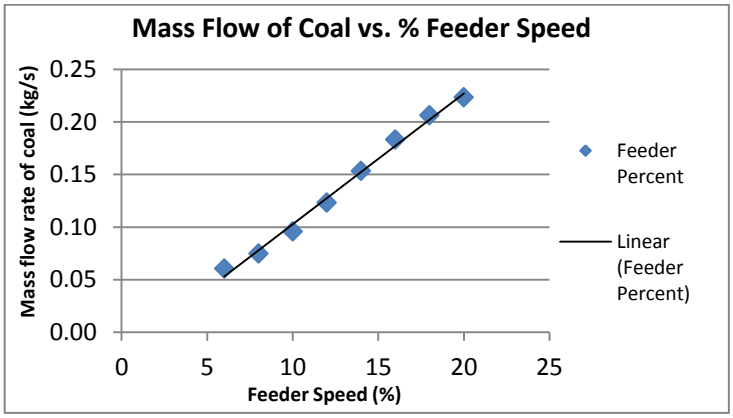

Figure 7.2: Feeder characterisation graph

The above feeder mass flow is true for a coal bulk density of 1100kg/m^3. This was measured by lab weighing a five litre measuring vessel filled with sampled coal. The results of which can be found in Appendix D: Preliminary Testing.

Primary Air Fan

The primary air fan is situated at the end of the air circuit and acts to draw air through the mill. The entire air system throughout the mill is therefore under suction. The air flow through the mill is controlled by a damper at the fan inlet and is operated as a percentage of the maximum open damper position (% primary air). The resistance of the air circuit is also affected by the speed of the rotating classifier. Therefore the mass flow of air changes accordingly. In order to characterise the primary air flow

through the mill, three classifier speeds were chosen and the air flow was measured at the mill outlet for various damper positions of the primary air fan. The classifier speeds were initially chosen under advice from the plant operator that the minimum and maximum allowable speeds are 8% and 34% respectively. The primary air fan was thus characterised on clean air according to these maximum and minimum values. It was later found (Table 7.4: Upper operating ranges) that operating at classifier speeds higher than 16% while grinding coal raises the DP too much and thus only low mill throughput is achievable. The mass flow of air was measured using a Pitot tube and electronic manometer along with a type K thermocouple. Full details of the test results and calculations are available in Appendix D: Preliminary Testing.

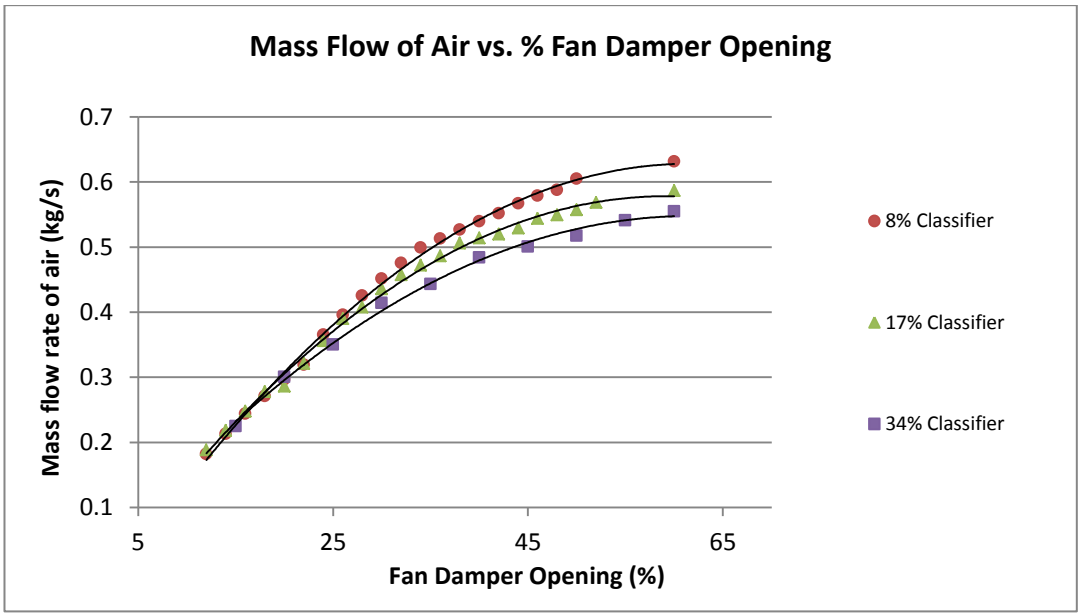

Figure 7.3: Primary air characteristic curves

Figure 7.3 above shows that the increasing mass flow rate with increasing fan damper position. The shapes of the curves are as expected for a typical fan curve and the decrease in mass flow with increasing classifier speed is also as expected.

Load Lines

A load line defines an air/fuel ratio for the mill to follow during operation. The primary air is automatically controlled to follow the fuel flow according to the load line. It is usually made up of two parts. The first part forms a horizontal line depicting a constant minimum air flow for low load operation. This is to ensure that there is sufficient air flow to maintain a certain transportation velocity in the PF pipes even before coal is introduced at mill start-up. The second part of the load line is a linear increase in air flow with increasing coal flow. This is to prevent the mill from choking and also to ensure that no particle settling occurs in the PF pipes under the increased mass loading of coal. Since this mill will only be operated above the minimum PF pipe velocity of 17m/s the load line will only consist of the linearly increasing portion.

In order to study the effect of changing air/fuel ratios and classifier speeds, multiple load lines were developed in order to satisfy the requirements for the various tests planned. The need for multiple load lines is due to the effects that the A/F ratio and classifier speed has on the fuel mass flow and air mass flow respectively, as indicated in the graphs above. Load lines for air/fuel ratios of 3:1, 4:1, 5:1 and 6:1 were created for 8%, 10%, 12% and 16% classifier speeds as per Table 7.5. The air and fuel flow is controlled in the DCS (Distributed Control System) to the nearest whole percent. The closest matching feeder speed had to then be chosen in order to meet the required fuel flow for, as an example, one third of the air flow.

In the pre-test, using a 17% classifier speed and an A/F ratio of 3:1, the following table of results were generated. The first column denotes the percentage opening of fan damper position, followed by the mass flow of air and PF pipe velocity relating to it. “Coal kg/s” indicates the mass flow of coal that is simply one third of the mass flow of air at a particular fan damper position. In effect, it is the required coal flow rate to meet a 3:1 air/fuel ratio. The last two columns are the feeder mass flow and

corresponding percentage of feeder speed, which have been placed in the rows that most closely matched the required coal mass flow of column 4.

Table 7.2: Relating %fan to %feeder for 3:1 A/F ratio, const. classifier speed at 17%

1	2	3	4	5	6	7
% Fan	Air kg/s	Air m/s	Coal kg/s	Feeder kg/s	% Feeder	True A/F Ratio
12	0.1884	10.593	0.0628	0.0605	6	3.11
14	0.2185	12.397	0.0728	0.0747	8	2.92
16	0.2477	14.385	0.0826			
18	0.2778	16.421	0.0926			
20	0.2861	16.938	0.0954	0.0959	10	2.98
22	0.3214	19.074	0.1071	0.1095	11	2.93
24	0.3562	21.21	0.1187	0.1232	12	2.89
26	0.3902	23.382	0.1301			
28	0.4078	24.466	0.1359	0.1382	13	2.95
30	0.4358	26.169	0.1453			
32	0.4572	27.439	0.1524	0.1533	14	2.98
34	0.4722	28.378	0.1574			
36	0.4866	29.297	0.1622			
38	0.5059	30.434	0.1686	0.1682	15	3.00
40	0.5139	30.789	0.1713			
42	0.5199	31.26	0.1733			
44	0.5294	31.774	0.1765			
46	0.5437	32.511	0.1812			
48	0.5491	32.968	0.183	0.1831	16	2.99
50	0.5573	33.51	0.1858			
60	0.5864	35.246	0.1955	0.1947	17	3.01

Furthermore, the FFFR (Fossil Fuel Firing Regulation) suggests that a “typically acceptable” minimum PF pipe velocity of 18m/s be maintained in order to prevent particle settling or flash back from the furnace. Since this facility is designed for experimentation purposes and it is isolated from combustion removing the risk of flashback, the minimum PF pipe velocity was chosen to be 16.94m/s corresponding to 20% fan damper position. The maximum air and coal flow is limited by the mill differential pressure trip set point of 3.5kPa. Extracting only the percentage fan damper and the percentage of feeder speed from similar tables to Table 7.2 (Appendix D:

Preliminary Testing), the following table can be derived for the operation of the mill corresponding to specific air/fuel ratios by mass flow.

Table 7.3: Load lines by % air flow and % coal flow

A/F Ratio	3:1		4:1		5:1		6:1	
CL 17%	Air	Coal	Air	Coal	Air	Coal	Air	Coal
%	20	10	20	8	20	6	24	6
%	22	11	26	10	24	8	31	8
%	24	12	30	11	34	10		
%	28	13	36	12	48	11		
%	32	14	50	13				
%	38	15						

Table 7.3 above shows the operational load lines in terms of the DCS input parameters. The graph below (Figure 7.4) shows the mass flows corresponding to the input parameters above. Slight deviations to the straight lines are due to the low resolution of the DCS control parameters as the fan damper position and the feeder speed can only be adjusted one percentage point at a time. Therefore the closest possible mass flow had to be chosen as was done in Table 7.2.

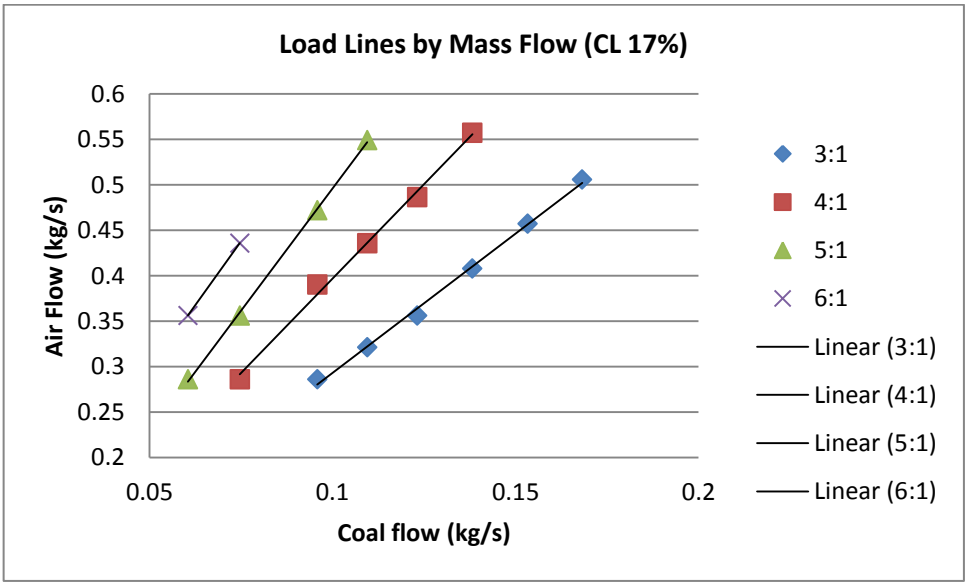

Figure 7.4: Load lines by mass flow

It must also be noted that due to there being only two load cases possible at an air/fuel ratio of 6:1, the linear relationship depicted above may not hold true. The balance of the load lines for other air/fuel ratios as well as the leading calculations may be found in Appendix D: Preliminary Testing.

7.3.2. Operating Ranges

The next preparatory task was to define the operating ranges of the mill for each test case. The minimum load was defined, when developing the load line, by the minimum velocity in the PF pipe of 17m/s. This equated to 20% of primary air flow and the corresponding coal flow according to each load line. The upper limit was defined by the maximum allowable mill differential pressure of 3.5kPa. Due to the fact that the mill diff pressure is affected by factors such as the classifier speed and air/fuel ratio, each load line was tested to determine the maximum stable coal throughput before reaching the trip point.

Table 7.4: Upper operating ranges

Load Line	Max Coal Flow (kg/s)	Mill Diff Press (kPa)
CL8 4:1 (Pre-Test)	13	2.12
CL10 3:1	14	2.21
CL10 4:1	13	2.87
CL10 5:1	12	3.06
CL10 6:1	10	2.90
CL12 3:1	14	2.48
CL12 4:1	13	2.82
CL12 5:1	12	2.66
CL12 6:1	10	2.83
CL14 3:1	14	3.16
CL14 4:1	13	2.41
CL14 5:1	11	2.59
CL14 6:1	10	2.73
CL16 3:1	15	2.89
CL16 4:1	13	2.95
CL16 5:1	11	2.56
CL16 6:1	10	2.75
CL17 4:1 (Pre-Test)	12	3.19
CL34 4:1 (Pre-Test)	8	1.94

The table above shows the maximum coal flow achieved for each load line scenario. Some of the mill differential pressures are some margin below the trip point. These have been selected as the maximum loads because the next load case caused a large jump in DP. The differential pressure approached the trip point and still did not reach stabilisation. Operating close to the trip point is ill advised as the fluctuations in mill differential pressure could cause the mill to trip at any moment. For example, the last test case in the table above (CL34 4:1) managed a coal flow of 8% with a DP of 1.94kPa. A DP of 1.94kPa seems reasonably safe from the trip value of 3.5kPa. However the next load case of 10% caused the mill to trip at 3.47kPa and was still in transient at the time. The mill differential pressure is the criteria to establish stable mill operation. After a load change or classifier change the mill DP would rise or fall slowly until it settles at a new pressure, at which point the mill is considered stable. It takes approximately 10 minutes for the mill to stabilise and then another 5 minutes of stable operation before a PF sample and measurements are taken.

7.3.3. Particle Size Analyser

The particle size analyser (PSA) was set up and used in the preliminary testing phase but the system was eventually dropped before the final phase of testing.

The problem had to do with the nature of the tests being performed on the pilot scale mill. The mill had to be operated at the extremes of its ability in order to evaluate effects on product fineness and throughput. This meant that at times the PF product would be extremely coarse and at other times extremely fine. The fine product would eventually block the laser eye and give erroneous results. This would build up until the PSA stops logging changes in data all together and produces a flat line. By this time it is impossible to tell how long ago the build-up had begun and the entire dataset would have to be discarded.

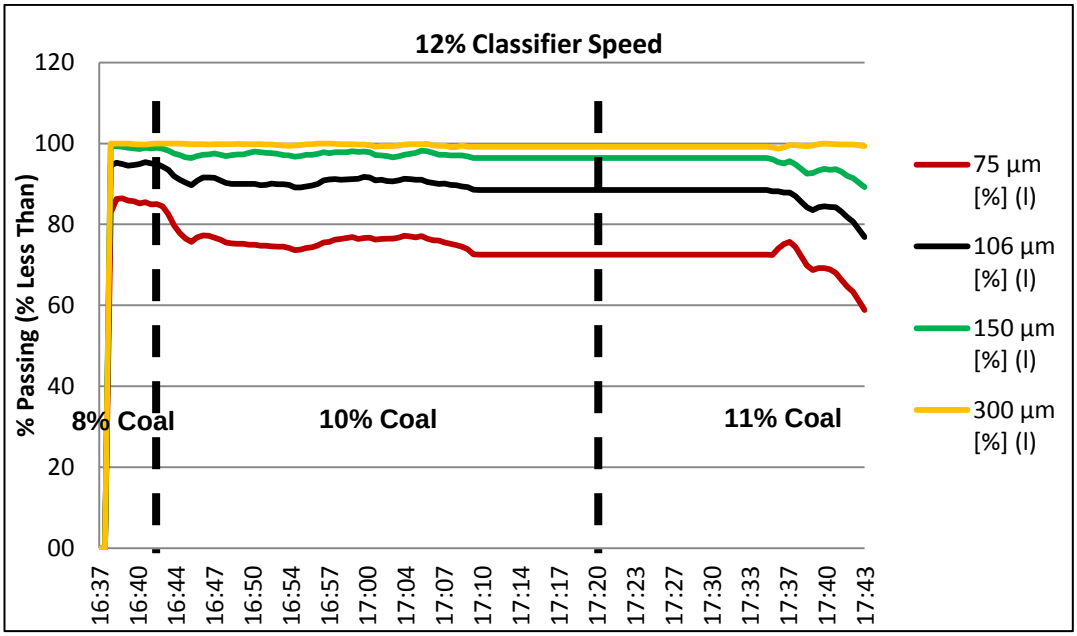

Figure 7.5: PSA Results - % Less than the four main sieve sizes

In Figure 7.5 above, the PSA probe stops updating data at 17:10, approximately 25 minutes through the 10% coal flow load case. This would occur even when the classifier speed and load case were not particularly expected to produce extremely fine PF, such as the case in point. However inspection of the laser eye revealed that a build-up of extremely fine PF, that the purging system is unable to remove, was indeed the cause of the problem.

It was decided to instead use the more reliable results of the PF sampling and lab sieve analysis in order to determine the product fineness for the period of the final testing.

7.3.4. Mastersizer

The Mastersizer is a lab based instrument that is used to measure the particle size distribution of fine powders in slurry. The Mastersizer uses the laser diffraction method for particle size determination. The number of virtual sieve sizes is much higher than those available as physical sieves and also provides size grading options much smaller than the smallest

available physical sieves. The Malvern can therefore produce a much higher resolution of measurement points. The Mastersizer was used on a random array of samples that were taken during the final testing phase. This was done in order to determine accurately the shape of the particle size distribution curve used for analysis of all the results. Figure 7.6 below shows the particle size distribution of one of the PF samples.

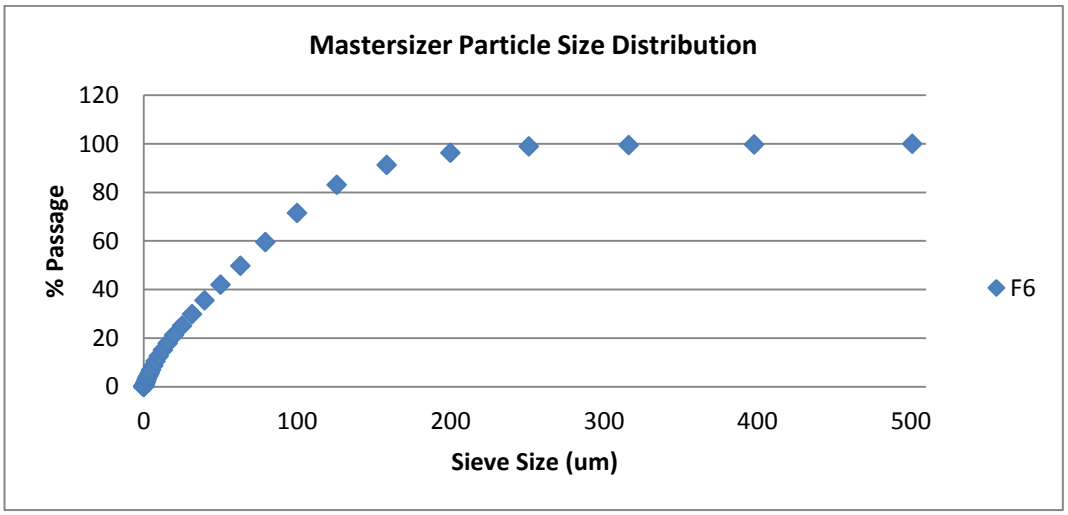

Figure 7.6: PF particle size distribution curve

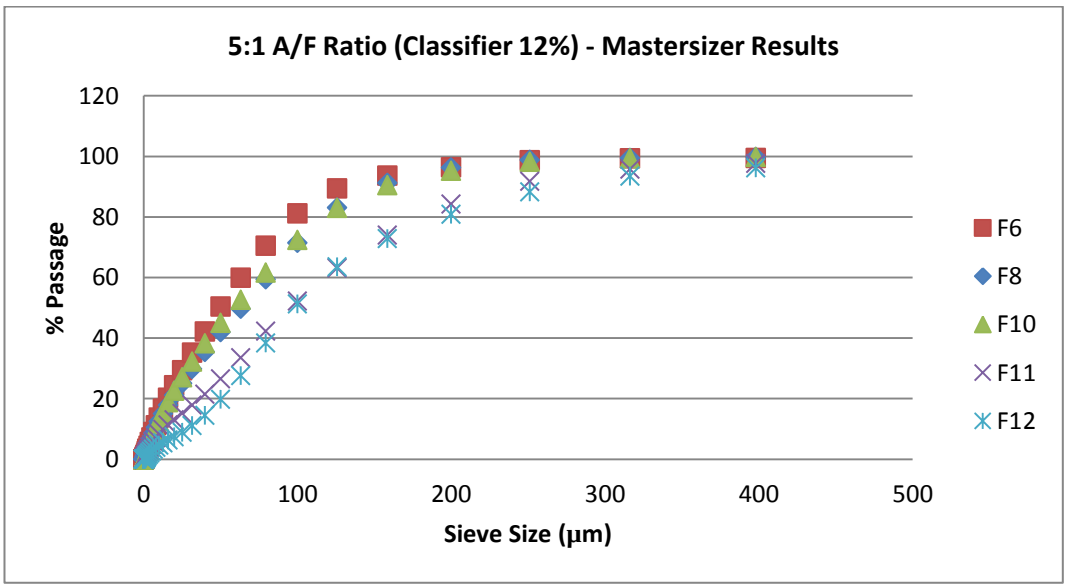

Figure 7.7: Mastersizer - PF particle size distribution

Figure 7.7 above shows the particle size distribution for a series of consecutive samples. The samples were taken from a test series where the classifier speed was set at 12% and the air/fuel ratio was 5:1. The different samples (F6 to F12) represent increasing the mill load from 6% to 12% of feeder speed. It can be noticed that by increasing the mill load the particle fineness drops. This is in line with the final testing results and will be discussed further in the following chapters.

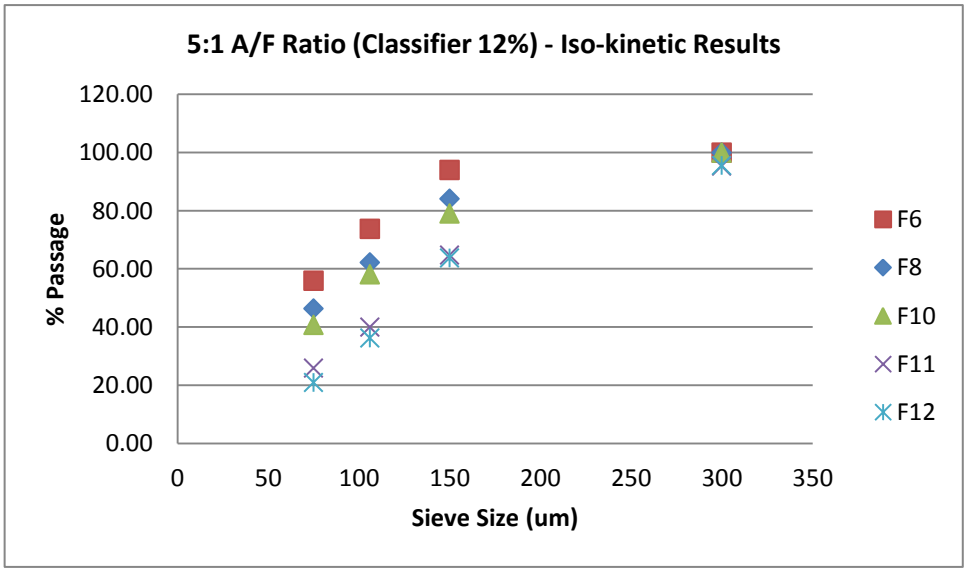

Figure 7.8: Physical sieving - PF particle size distribution

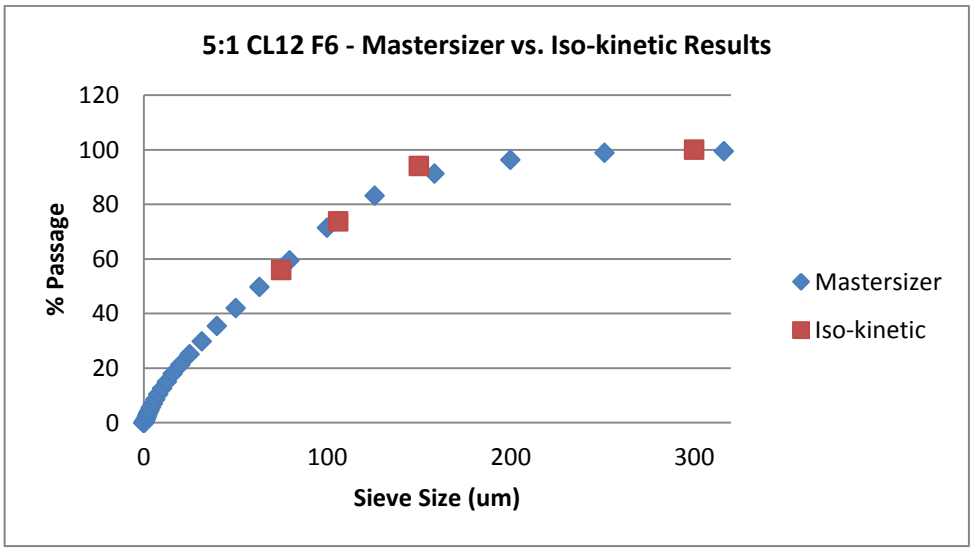

Figure 7.9: Mastersizer and iso kinetic result comparison for F6

By overlaying the Iso-kinetic result onto the Mastersizer result for a fuel load of F6 (Figure 7.9), it is noticeable how similar the results are both in shape as well as absolute value. For now it can be confirmed that the shape of the particle size distribution curve achieved from the manual sieving process (Figure 7.8) does indeed follow the shape of the curve provided by the Mastersizer (Figure 7.7). Further comparisons between the PF sieving results and Mastersizer results may be found in Appendix D: Preliminary Testing.

7.4. Investigation Findings

The final testing consisted of 16 different test scenarios of varying classifier speed and air/fuel ratios as shown in Table 7.5. The notation "CL10 3:1" indicates that the test scenario is at a classifier speed of 10% and an air/fuel ratio of 3:1. Each test scenario was also ramped up through the load of the mill from minimum to maximum allowable load. Notations such as "F11" and "F12" are indications of the fuel feed rate being 11% and 12% respectively. The air flow rate is assumed to follow the fuel flow according to the air/fuel ratio of the test scenario in question. For each load case, within a test scenario, a PF sample was taken and the particle size distribution was determined by lab sieving the sample.

Table 7.5: Test scenarios

	Air/Fuel Ratio			
% Classifier	**3:1**	**4:1**	**5:1**	**6:1**
10	CL10 3:1	CL10 4:1	CL10 5:1	CL10 6:1
12	CL12 3:1	CL12 4:1	CL12 5:1	CL12 6:1
14	CL14 3:1	CL14 4:1	CL14 5:1	CL14 6:1
16	CL16 3:1	CL16 4:1	CL16 5:1	CL16 6:1

Expanding each test scenario to look at the load cases provides us with Table 7.6 below which details the load lines that were followed as per the mill control system. As the classifier speed has an incremental effect on the PA mass flow, and the control system only allows whole percentage

point values, following the load line on a mass flow basis had to be performed to the closest possible percentage value in the control system. It can therefore be noticed that for classifier speeds of 10% and 12%, the load line values are similar. The same occurs for classifier speed of 14% and 16%.

Table 7.6: Load cases

A/F Ratio	**3:1**		**4:1**		**5:1**		**6:1**	
CL 10%	**Air**	**Coal**	**Air**	**Coal**	**Air**	**Coal**	**Air**	**Coal**
%	20	10	20	8	20	6	24	6
%	22	11	26	10	24	8	30	8
%	24	12	28	11	32	10	44	10
%	28	13	34	12	40	11		
%	30	14	42	13	50	12		
A/F Ratio	**3:1**		**4:1**		**5:1**		**6:1**	
CL 12%	**Air**	**Coal**	**Air**	**Coal**	**Air**	**Coal**	**Air**	**Coal**
%	20	10	20	8	20	6	24	6
%	22	11	26	10	24	8	30	8
%	24	12	28	11	32	10	44	10
%	28	13	34	12	40	11		
%	30	14	42	13	50	12		
A/F Ratio	**3:1**		**4:1**		**5:1**		**6:1**	
CL 14%	**Air**	**Coal**	**Air**	**Coal**	**Air**	**Coal**	**Air**	**Coal**
%	20	10	20	8	20	6	24	6
%	22	11	26	10	24	8	31	8
%	24	12	30	11	34	10		
%	28	13	36	12	48	11		
%	32	14	50	13				
%	38	15						
A/F Ratio	**3:1**		**4:1**		**5:1**		**6:1**	
CL 16%	**Air**	**Coal**	**Air**	**Coal**	**Air**	**Coal**	**Air**	**Coal**
%	20	10	20	8	20	6	24	6
%	22	11	26	10	24	8	31	8
%	24	12	30	11	34	10		
%	28	13	36	12	48	11		
%	32	14	50	13				
%	38	15						

7.4.1. Varying Classifier Speed

By varying the classifier speed for a fixed air/fuel ratio of 4:1, it was found that the particle fineness increased with increasing classifier speed. This was consistent for mill loads of 8%, 10% and 11%.

The figures below show the graphs of percentage passage at the 4 main sieve size levels, vs. classifier speed for the three loads in case.

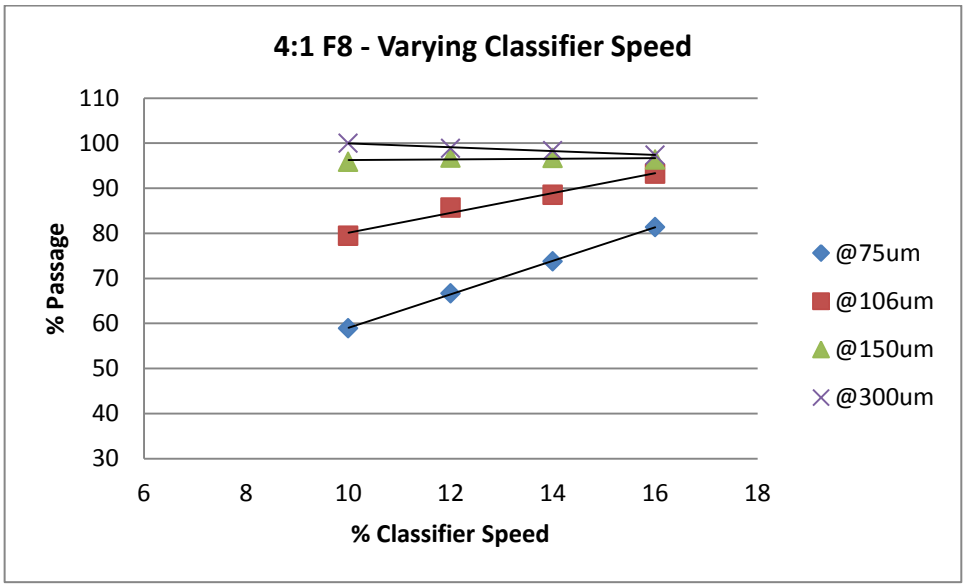

Figure 7.10: %Passage vs. classifier speed for 8% mill load

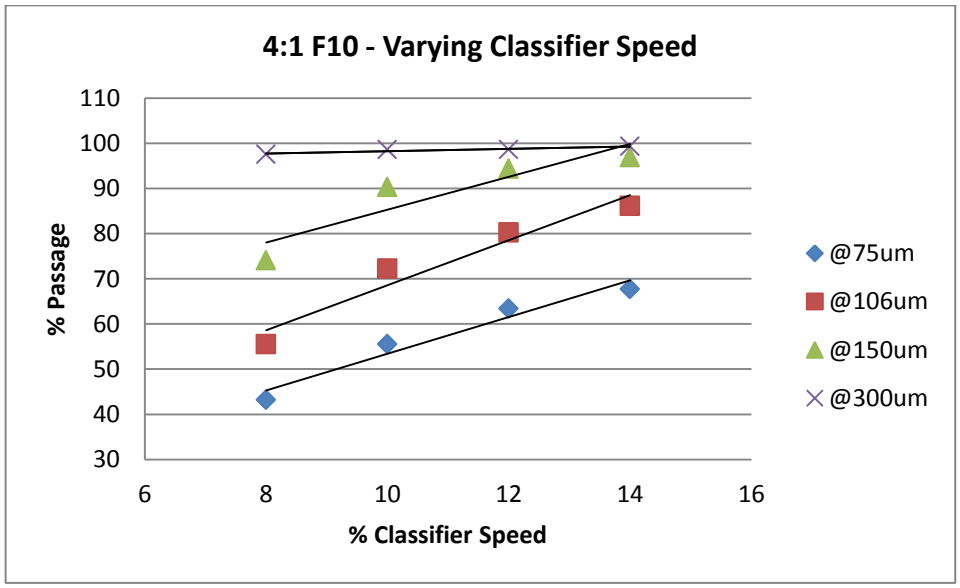

Figure 7.11: %Passage vs. classifier speed for 10% mill load

The graphs consistently show increasing particle fineness for increasing classifier speed at the major sieve size grading levels.

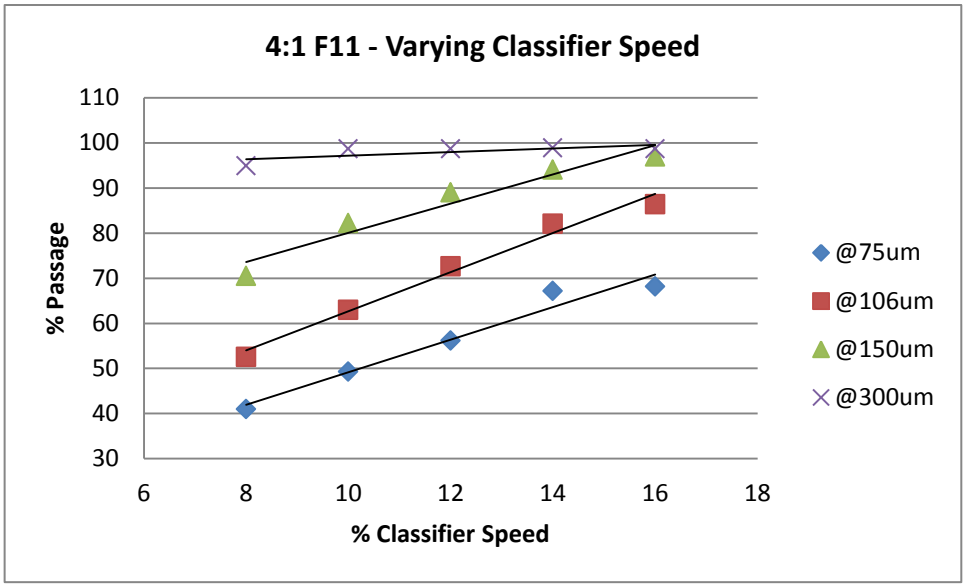

Figure 7.12: %Passage vs. classifier speed for 11% mill load

Looking at the above three graphs in a slightly different way by focussing on the % passage through the 75µm sieve size only. See Figure 7.13. Here it can be seen that a fairly consistent and linear ratio of increasing particle fineness as compared to increasing classifier speed is evident. The results of this test showed an average ratio of 3.8 percentage point increase in particle fineness per increment in classifier speed (Appendix E: Final Testing).

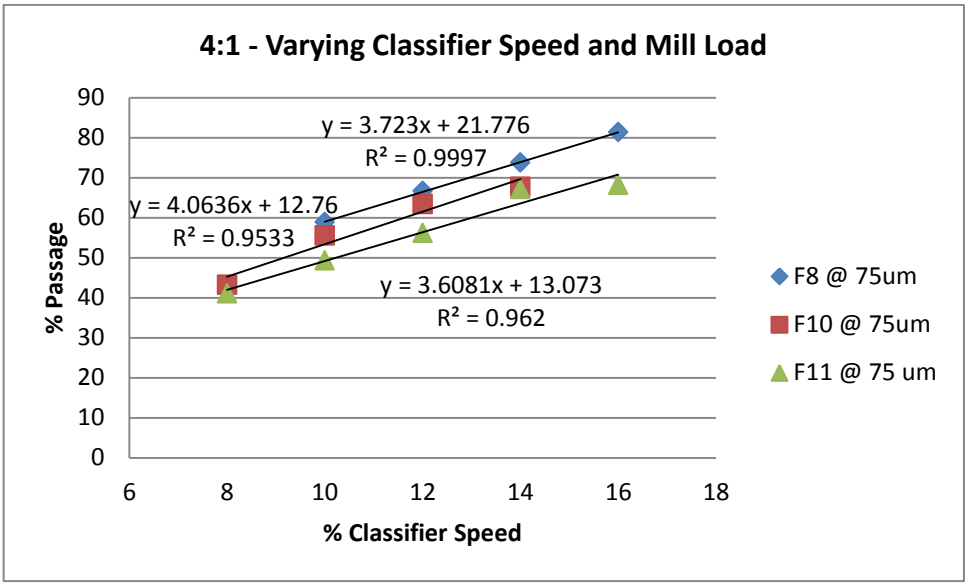

Figure 7.13: %Passage vs. classifier speed for 3 mill loads

It can also be noticed that by increasing the load the particle fineness decreases. This will be discussed further in the following section.

The relationship between the particle fineness and classifier speed is not unexpected. However it is important to quantify this relationship in order to be able to correctly set up the mill and optimise it during operation.

These results were consistent through the same test performed at different A/F ratios (Figure 7.14 and Figure 7.15). However it was noticed that at high A/F ratios and high feeder speeds the mill differential pressure would slowly drop indicating that the mill is emptying out the coal. A/F ratios of 6:1 acted to negate the effects of the classifier, especially at high loads, and even produce PF that is much coarser than that of lower classifier speeds. This can be seen in Figure 7.14.

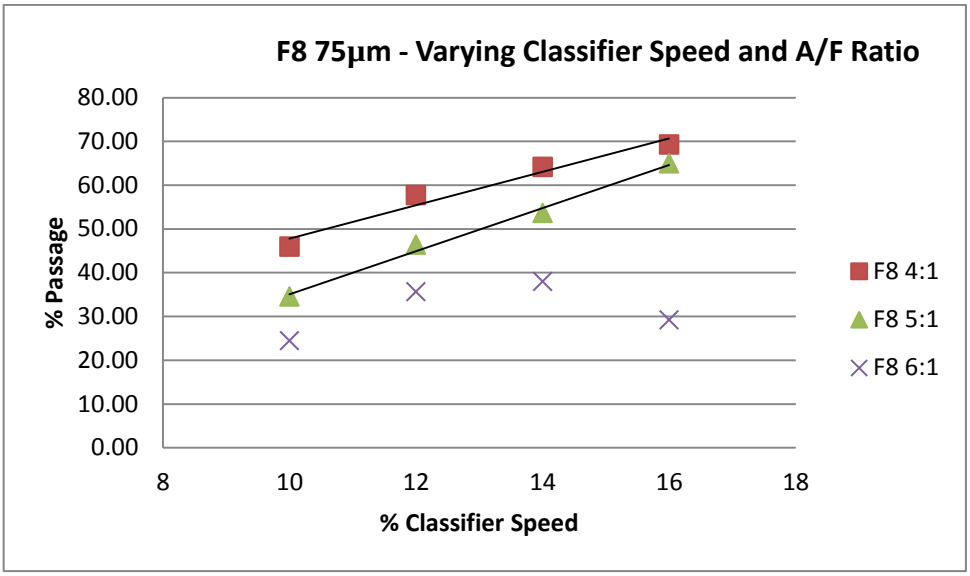

Figure 7.14: %Passage vs. classifier speed for various A/F ratios

In Figure 7.14 above it is noted that at A/F ratios of 4:1 and 5:1 the particle fineness is linearly increasing with increasing classifier speed. At an A/F ratio of 6:1 the same behaviour is observed until the classifier speed of 14%. At the classifier speed of 16% however the particle fineness drops rapidly indicating that classification is no longer taking place. This was first noticed for a fairly low load of 8% coal feeder speed.

In Figure 7.15 the same analysis is performed for a higher load of 10% feeder speed. The same effect on the particle fineness was noticed this time at a lower A/F ratio of 5:1, i.e. at higher loads the effect begins to show at a lower A/F ratio.

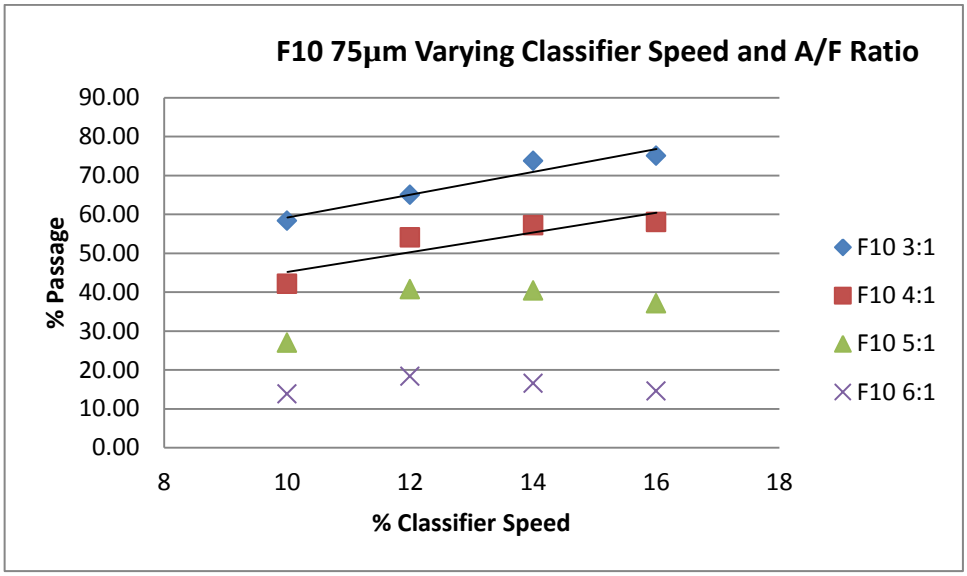

Figure 7.15: %Passage vs. classifier speed for various A/F ratios

The effects of operating the mill at high A/F ratios (6:1) can be noted by the following figures.

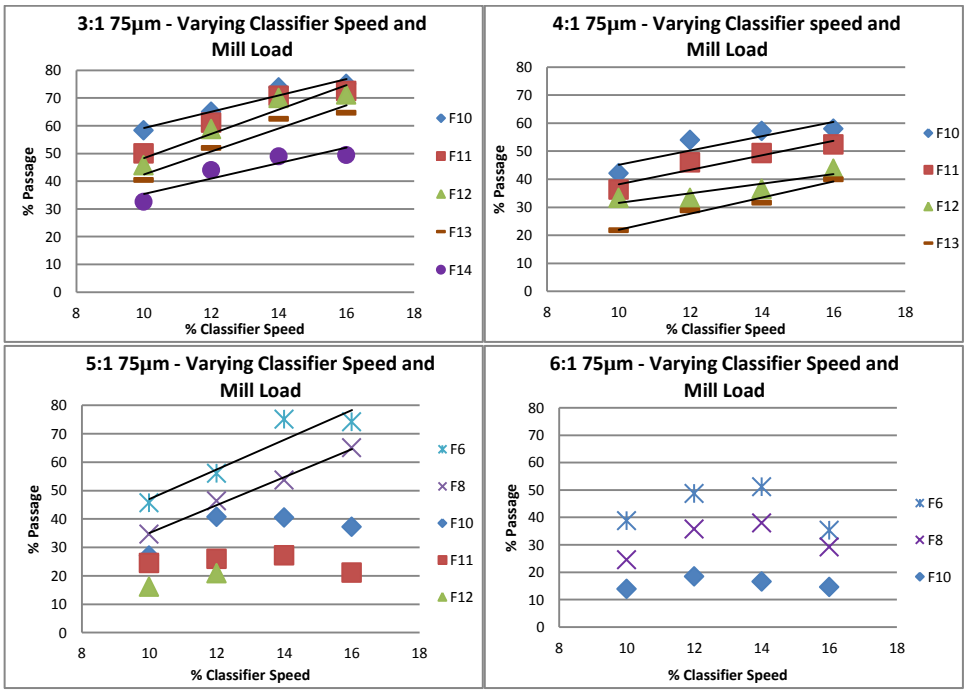

Figure 7.16: %Passage vs. classifier speed for various A/F ratios and mill loads

In Figure 7.16 above, by looking at the effect of increasing the A/F ratio from 3:1 to 6:1 it can be noticed that at low A/F ratios (3:1 and 4:1) a linear relationship can be established. However as the A/F ratio increases to 5:1,

the higher load cases (F10 and F11) begin to show coarser particles for classifiers speeds at 16%. Furthermore, at an A/F ratio of 6:1 even low loads show coarser particles at 16% classifier speeds.

The second major observation is noted in Figure 7.17 below. On each of the graphs in Figure 7.17 the 6:1 A/F ratio dataset shows that the particle fineness drops at 16% classifier speed. And as the load is increased beyond 10% feeder speed (F10 and F11) the effect begins to show on the 5:1 A/F ratio dataset as well. High mill loads act to amplify the effect of reduced classifier efficiency at high classifier speeds. This will be shown more clearly in chapter 7.4.2 to follow.

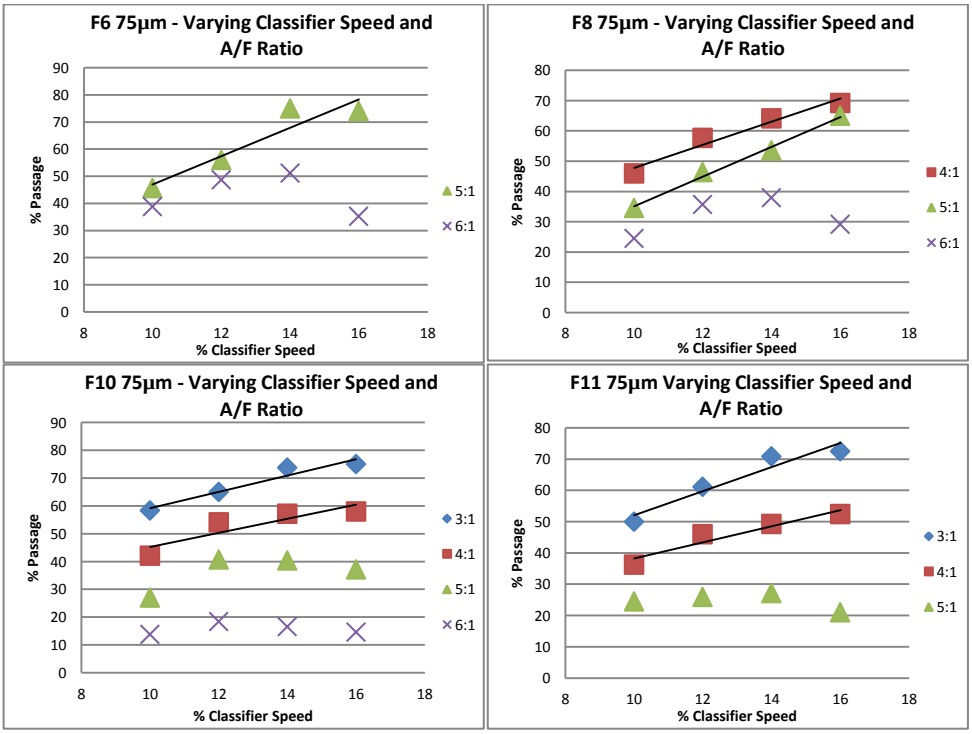

Figure 7.17: % Passage vs. classifier speed for various mill loads and A/F ratios

The above two observations show that, at high A/F ratios above 6:1, the effect of increasing the classifier speed has no positive effect on the particle fineness. In fact the combination of high classifier speed, high A/F ratio and high mill load actually decreases the classification efficiency and drastically decreases the particle fineness overall.

7.4.2. Varying Mill Load

By varying the mill load at fixed classifier speed and A/F ratio conditions it was found that an inverse relationship existed between the particle fineness and coal throughput, i.e. as throughput increases the particle fineness decreases. This is an unfortunate consequence as mills are currently required to operate a higher average throughput due to coal quality deterioration.

In the figures that follow, the results of varying the mill load for different classifier speeds are shown. It can be seen here that, apart from the increasing load causing a decrease in particle fineness, increasing the A/F ratio also causes the relationship to shift towards a lower grinding performance.

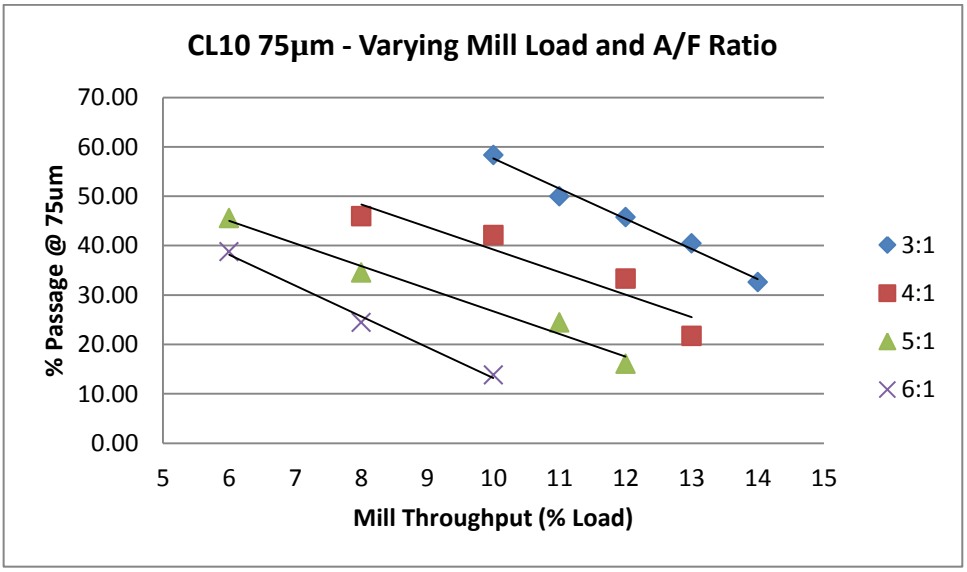

Figure 7.18: %Passage vs. mill load for various A/F ratios

This is consistent across the different classifier speeds as shown in the following figures for classifier speeds of 12%, 14% and 16%.

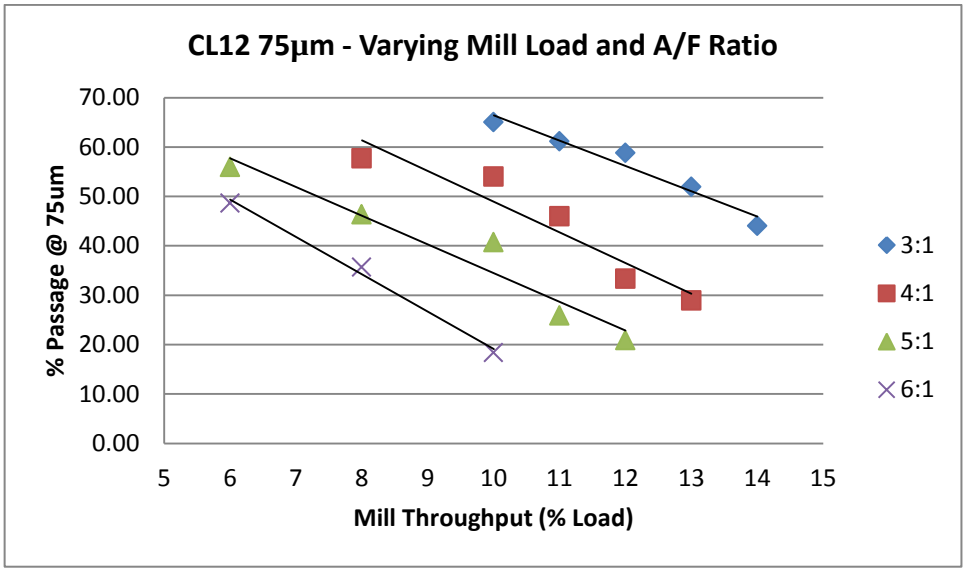

Figure 7.19: %Passage vs. mill load for various A/F ratios

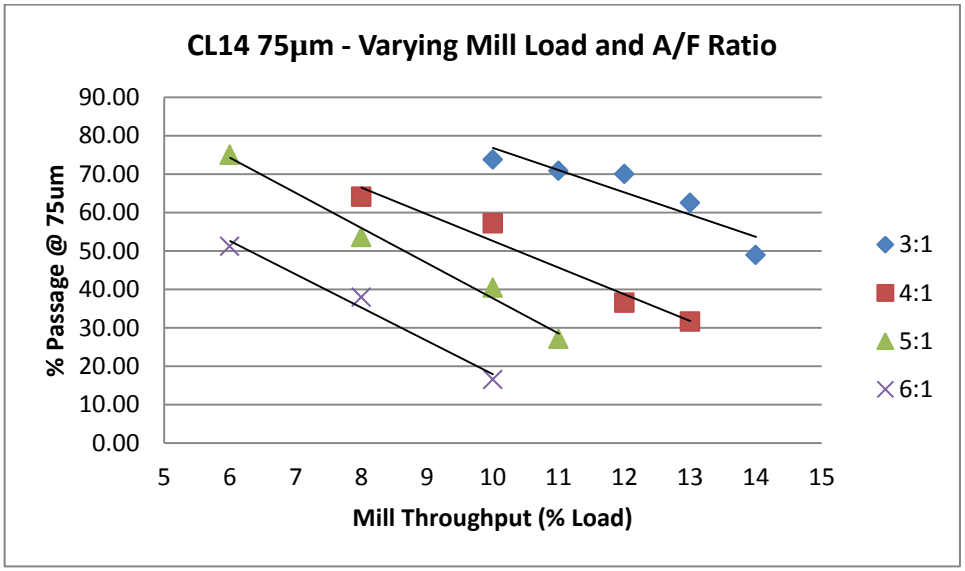

Figure 7.20: %Passage vs. mill load for various A/F ratios

In Figure 7.21 , the combination of extremely high mill load (15% feeder speed is only achievable due to the low A/F ratio of 3:1) and high classifier speed once again resulted in a poor grinding performance even at a low A/F ratio. The data point encircled in red is the outlier in question.

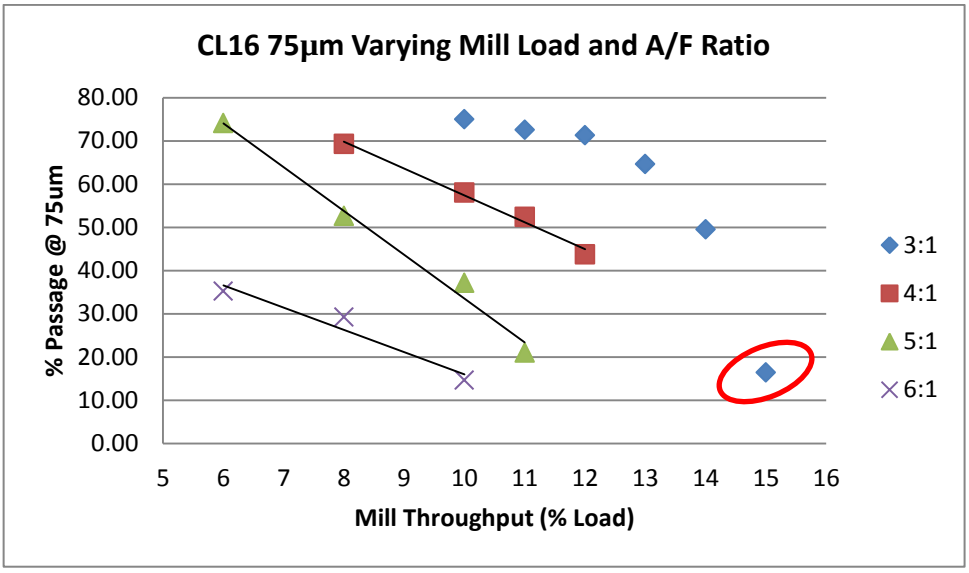

Figure 7.21: %Passage vs. mill load for various A/F ratios

Now looking at the same data from the point of fixed A/F ratio and different classifier speeds we have the following figures. The effect of increasing classifier speed is evident in that higher classifier speeds act to shift the relationship between particle fineness and mill load thereby increasing particle fineness.

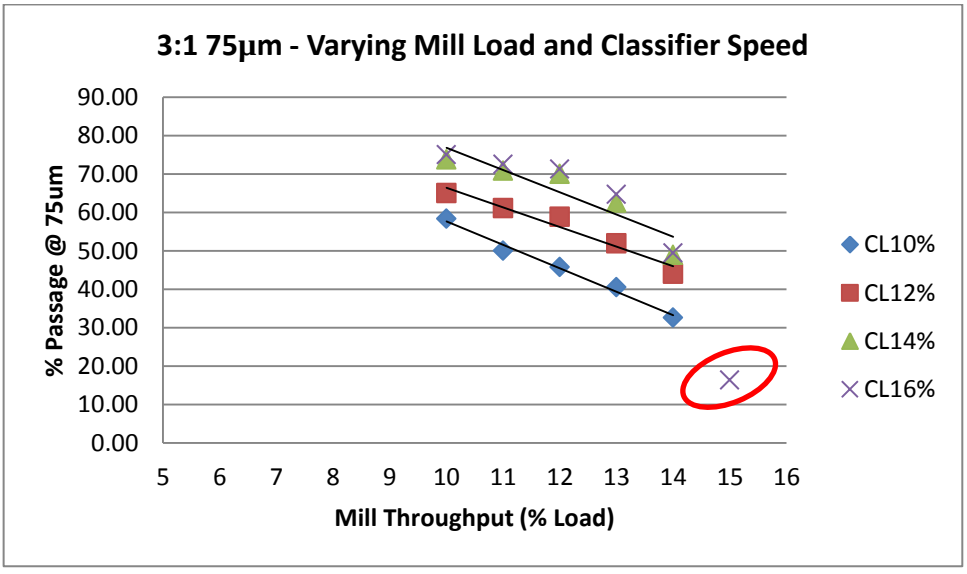

Figure 7.22: %Passage vs. mill load for various classifier speeds

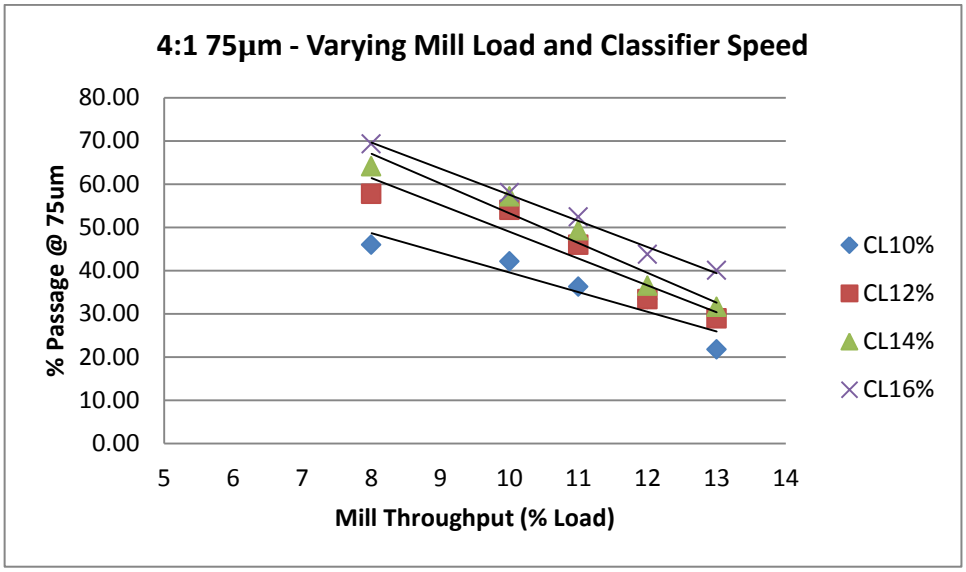

Figure 7.23: %Passage vs. mill load for various classifier speeds

This is consistent through the 3:1 and 4:1 A/F ratios. However at an A/F ratio of 5:1 the gradients cause intersections at certain points. At 16% classifier speed we know the particle fineness starts to drop rapidly for higher loads as classification fails. But the same begins to occur at the 14% classifier speed only at high loads (F11), where the particle fineness is similar to that of the lower 12% classifier speed at similar load (F11).

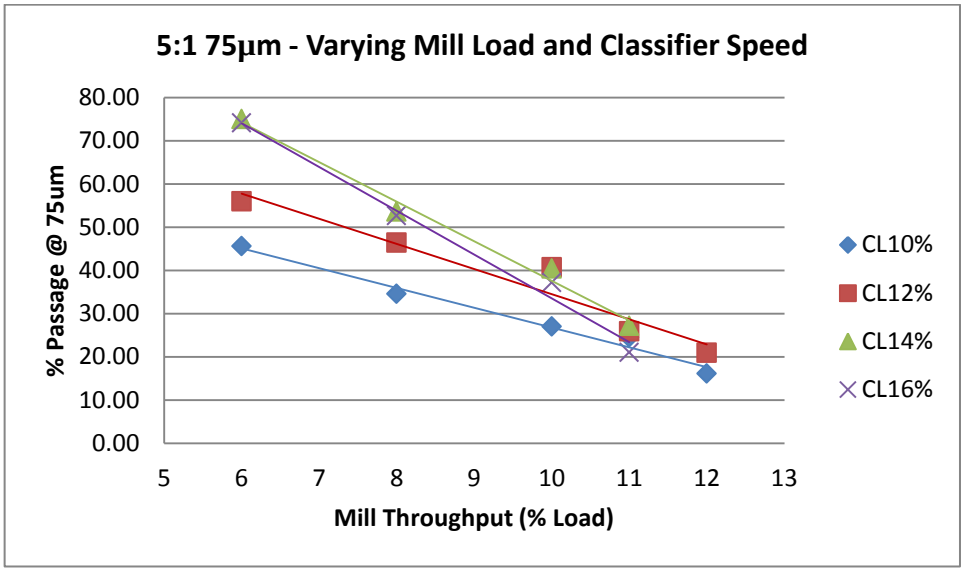

Figure 7.24: %Passage vs. mill load for various classifier speeds

At an A/F ratio of 6:1 (Figure 7.25 below) it was found that the results were unpredictable at best. If the 16% classifier case is ignored then the shift of the relationship holds true for the low feeder speed case (6% feeder speed). Increasing the classifier speed causes an increase in particle fineness. However for loads of 8% and 10% the high A/F ratio causes inconsistent shifts in particle fineness.

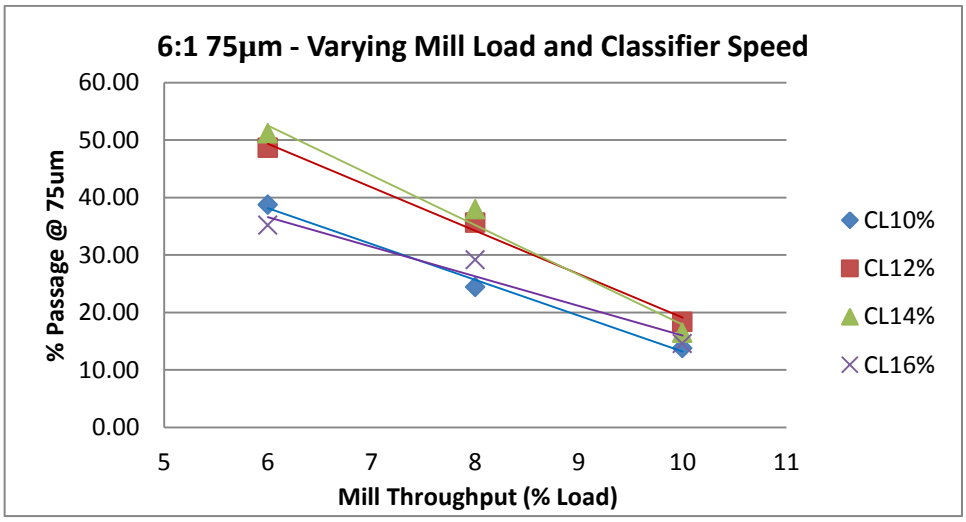

Figure 7.25: %Passage vs. mill load for various classifier speeds

The relationship between the particle fineness and mill throughput has a linearly inverse nature. As the mill load is increased, the particle fineness is then reduced. This is done so at a rate of between 4.5 and 10 times an increment in throughput, depending on the classifier speed and A/F ratio combination.

7.4.3. Varying Air/Fuel Ratio

The relationship between the particle fineness and the A/F ratio is such that an increase in A/F ratio causes a reduction in particle fineness. This is evident for different mill loads and across the different classifier speeds. Figure 7.26 below shows the decline in particle fineness with increasing A/F ratio.

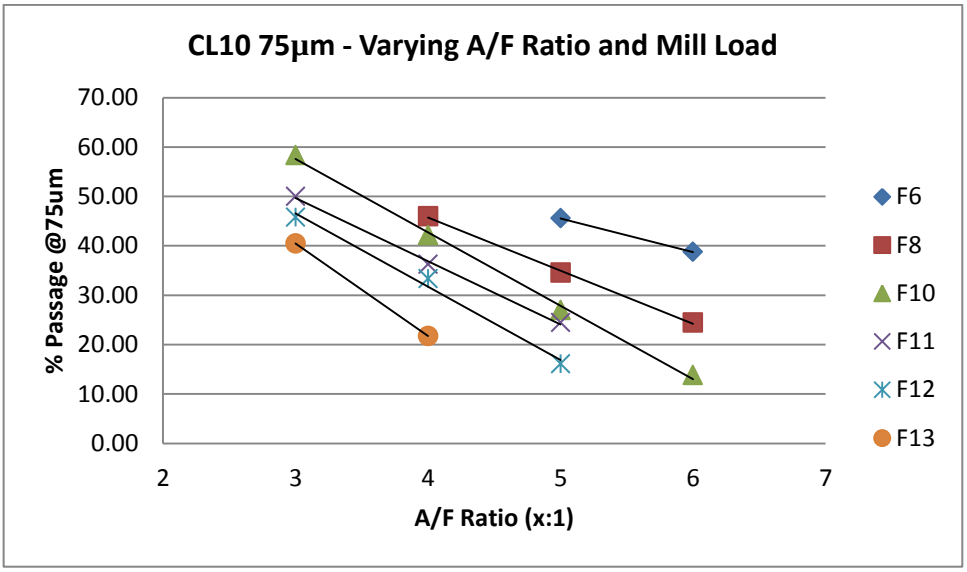

Figure 7.26: %Passage vs. A/F ratio for various mill loads

It is also evident from these curves that an increase in mill load acts to shift the curve towards a coarser particle size. An interesting note to make in Figure 7.27 below is that an increasing mill load also increases the rate at which the particle fineness declines for increasing A/F ratio. This effect is vaguely present in other data sets but the ideal example is found in the results in Figure 7.27 below.

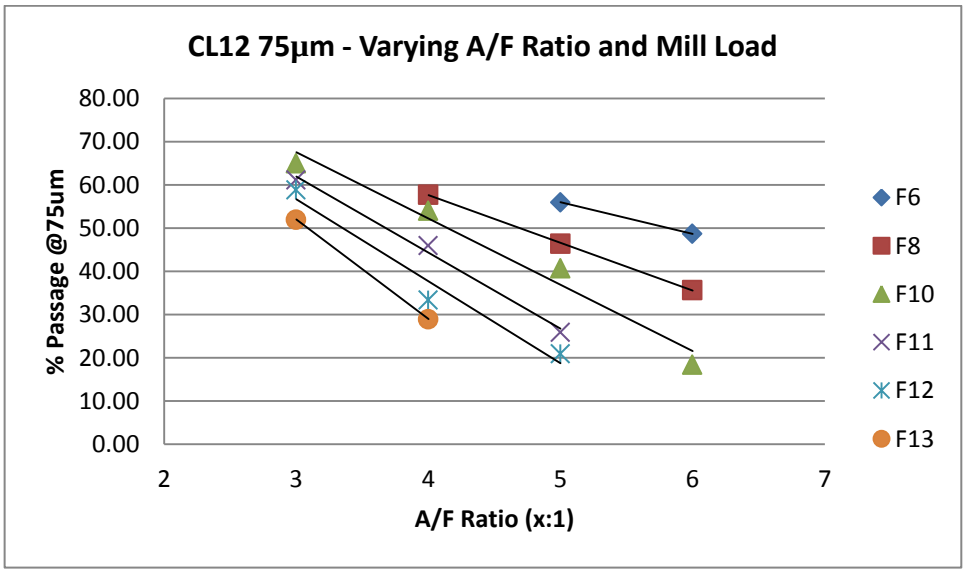

Figure 7.27: %Passage vs. A/F ratio for various mill loads

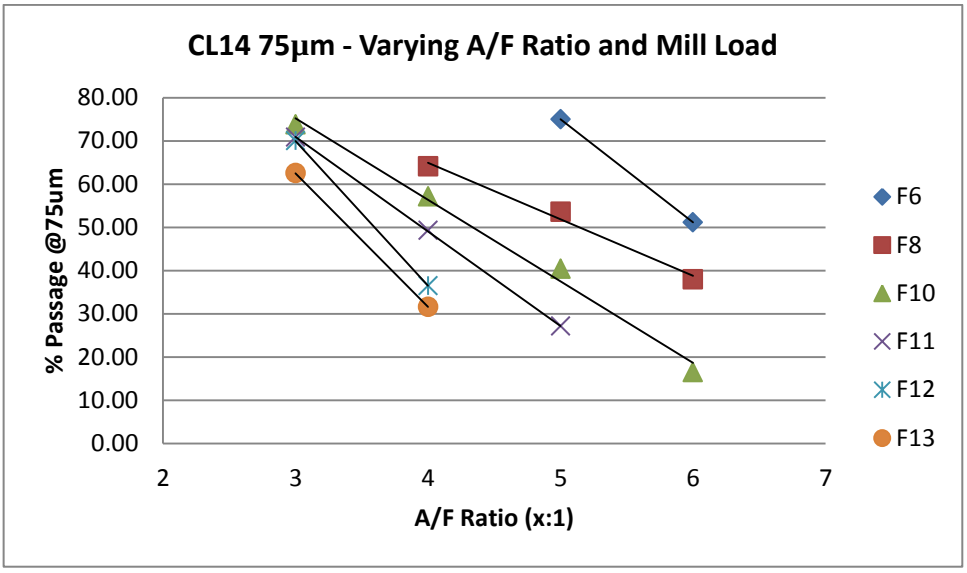

Figure 7.28: %Passage vs. A/F ratio for various mill loads

For classifier speeds of 14% and 16% a low load of F6 was only achievable at high A/F ratios of 5:1 and 6:1. This is due to the minimum PF pipe velocity requirement of 18m/s at the mill outlet. Similarly the high loads of F12 and F13 were only achievable at low A/F ratios of 3:1 and 4:1, due to the maximum allowable mill differential pressure set point of 3.5kPa.

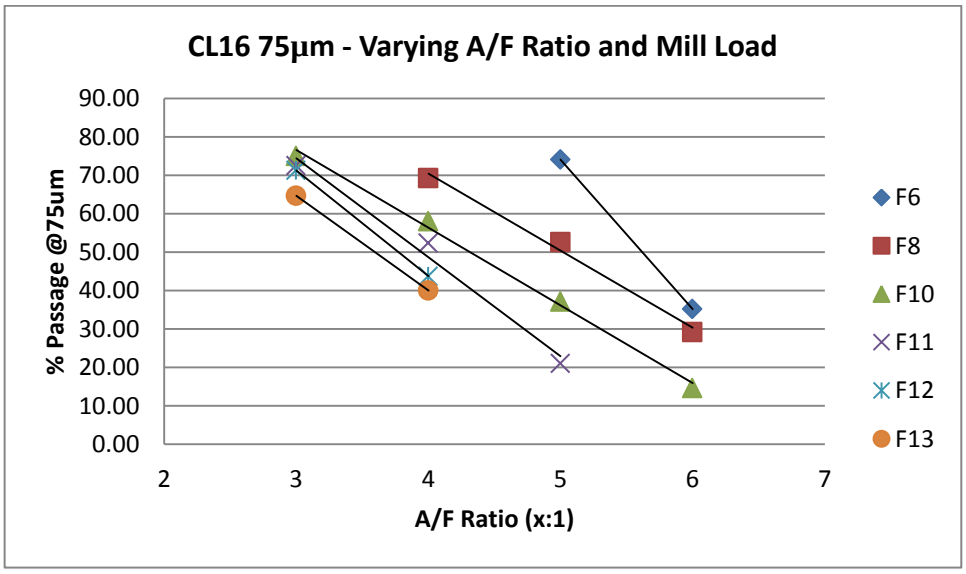

Figure 7.29: %Passage vs. A/F ratio for various mill loads

Looking at the effect of the A/F ratio on particle fineness for fixed loads and different classifier speeds, the following graphs are presented. Figure

7.30 shows the results at a feeder speed of 6%. Once again this low feeder speed was only achievable at high A/F ratios of 5:1 and 6:1.

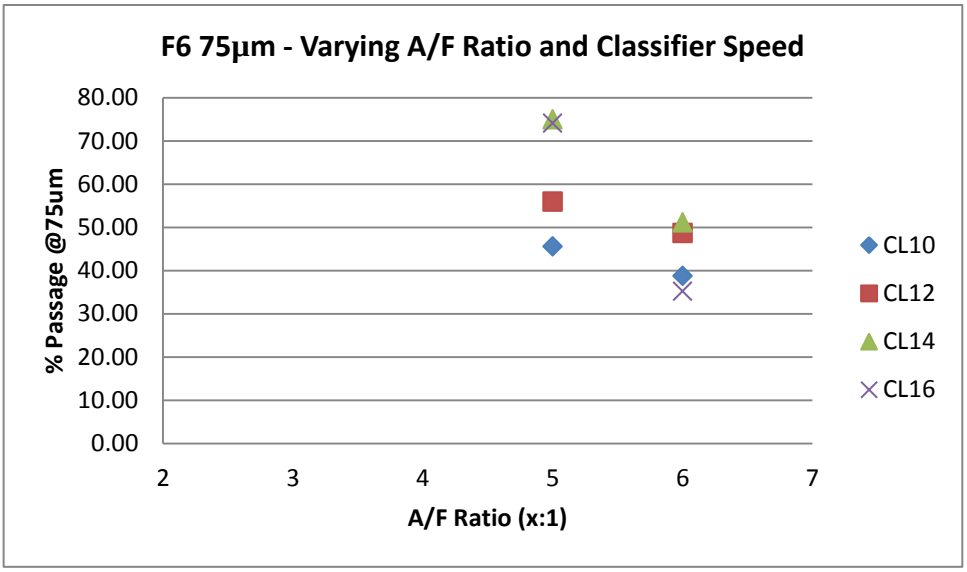

Figure 7.30: %Passage vs. A/F ratio for various classifier speeds

That being said, the trend is still evident where increasing A/F ratio causes decreasing particle fineness. In Figure 7.31, Figure 7.32, Figure 7.33 and Figure 7.34 to follow, the effect of high classifier speed and high A/F ratio once again shows a drastic drop in particle fineness, such that the particle fineness even drops below those of lower classifier speeds.

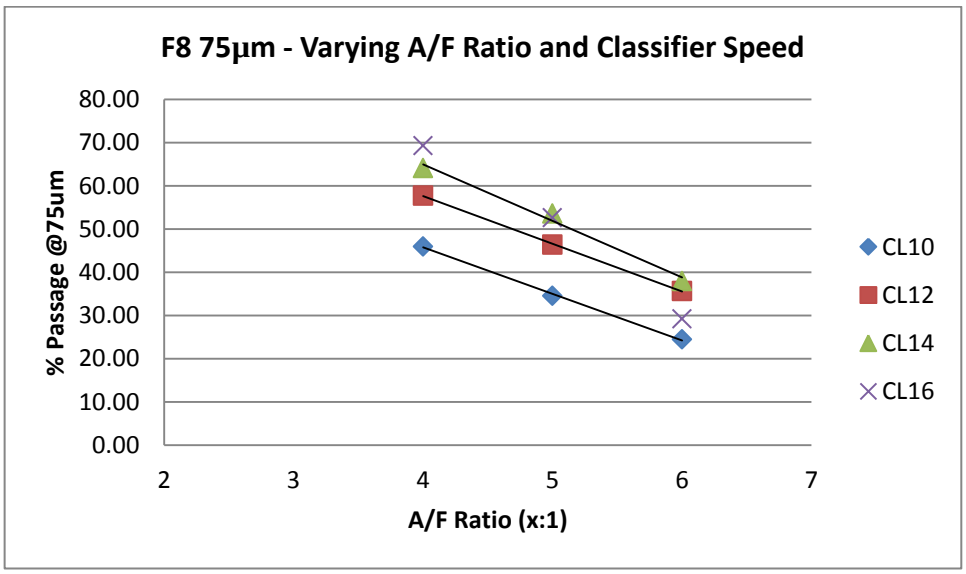

Figure 7.31: %Passage vs. A/F ratio for various classifier speeds

With the exception of the high classifier speed + high A/F ratio (CL16 + 6:1) case, the results show a consistent decline in particle fineness for increasing A/F ratio. It can also be seen that an increase in classifier speed acts to shift the curve towards a finer particle size. This is in line with the conclusions of the previous chapter.

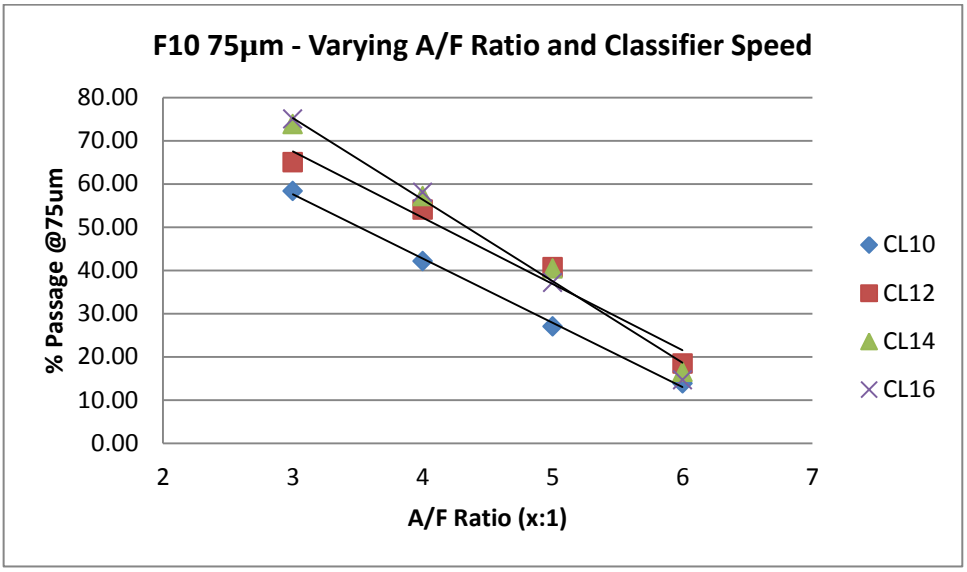

Figure 7.32: %Passage vs. A/F ratio for various classifier speeds

As we look at the higher loads of F10, F11 and F12 it is also noticed that the effect on particle fineness between classifier speeds is greater at lower A/F ratios and drops to almost no difference at higher A/F ratios. This is indicative that the combination of high A/F ratio and high load has a negating effect on the function of the classifier.

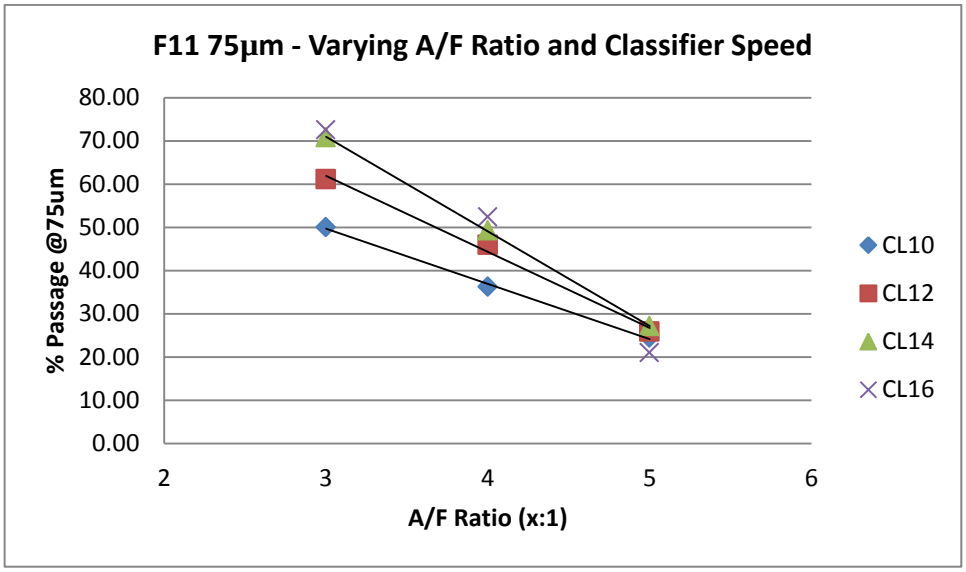

Figure 7.33: %Passage vs. A/F ratio for various classifier speeds

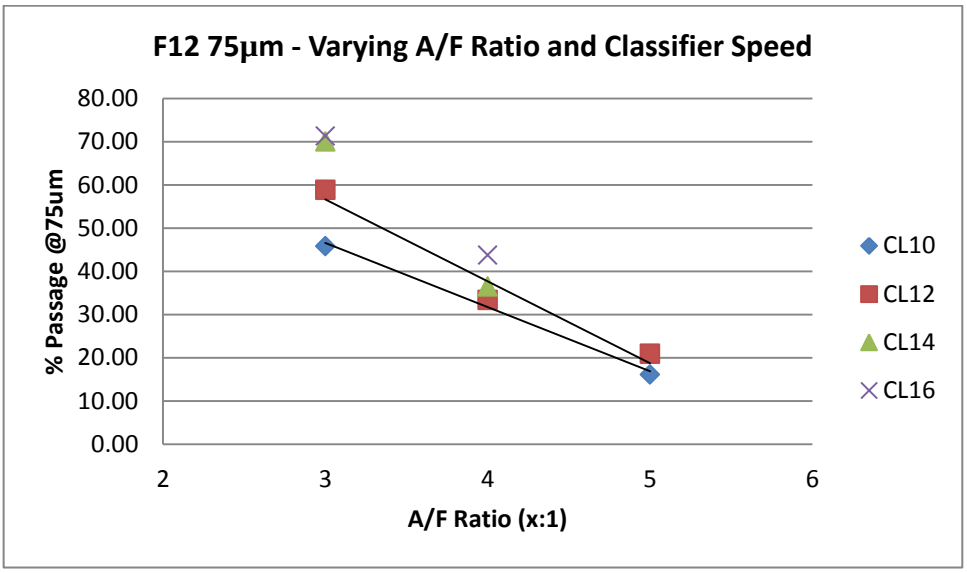

Figure 7.34: %Passage vs. A/F ratio for various classifier speeds

In Figure 7.34, a mill load of 12% feeder speed could not be achieved at high classifier speeds (14% and 16%) and high A/F ratios (5:1 and 6:1). This was due to the limitation of the mill trip set point for high mill differential pressure, mainly caused by the high classifier speed.

These results have shown that a directly inverse relationship exists between the particle fineness and the A/F ratio i.e. as the A/F ratio is

increased towards a leaner mixture, the Particle fineness is reduced. It was also observed that the increase in mill load increases the rate at which an increase in A/F ratio affects the particle fineness. This is in line with data from chapter 7.4.2. It is also confirmed that the classifier speed directly influences the particle fineness as was seen in the previous chapter 7.4.1.

7.5. Mill Performance Optimisation

To summarise the above findings, it can be noted that:

- An increase in classifier speed caused an increase in product fineness.
- An increase in mill load causes a decrease in product fineness.
- An increase in air/fuel ratio causes a decrease in particle fineness.

With these three relationships established and quantified, there were other interesting outcomes from the results. The combination of high mill load, high A/F ratio and high classifier speed actually caused a drastic drop in particle fineness as the classification completely fails under these conditions.

Increasing the A/F ratio decreases the particle fineness at a certain rate depending on the mill load conditions and classifier speed. However it was found that increasing mill load increases the rate at which A/F ratio decreases the particle fineness.

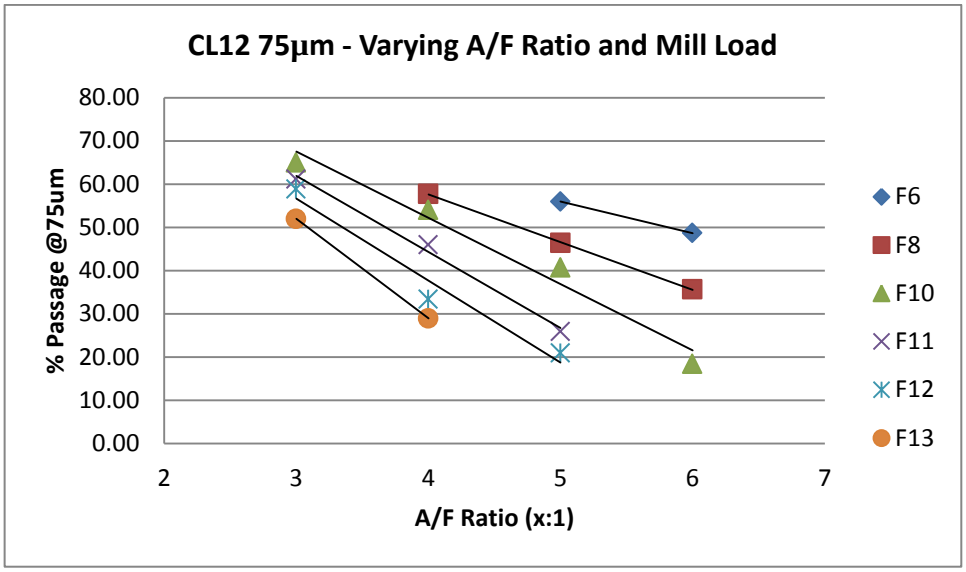

Figure 7.35: %Passage vs. A/F ratio for various mill loads

With these findings the operation of this mill can be optimised by building a load line that satisfies the particle fineness requirements at all load conditions. Furthermore the effect of the A/F ratio on particle fineness is new to the set of tools available for mill optimisation. And this is the key to improving on the maximum allowable throughput of the mill. The combination of the classifier influence and the A/F ratio influence will also be used to add flexibility to the mill by allowing variations in mill load while maintaining particle fineness.

As the mill is currently, the mill load operates at a fixed rate of 8% feeder speed. Other conditions are also fixed at 4:1 A/F ratio and 14% classifier speed. This produces a particle fineness at the lower range of the required 65% to 75% under 75µm specification. If the coal quality (low HGI for instance) affects the crushing performance then the classifier speed is increased by the operator, but no other parameter is changed. The operating point is shown in Figure 7.36 below.

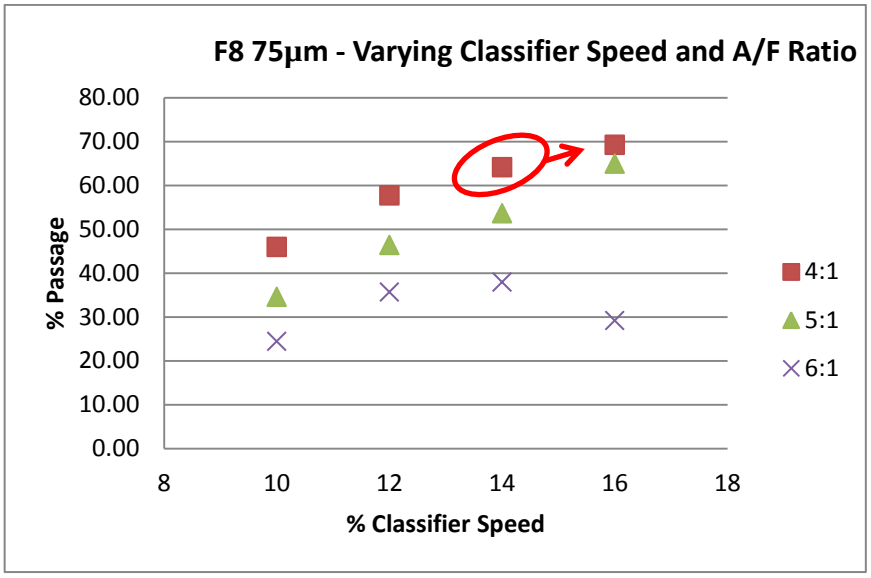

Figure 7.36: %Passage vs. classifier speed for various A/F ratios

The current load line for this mill would look like that of Figure 7.37 below.

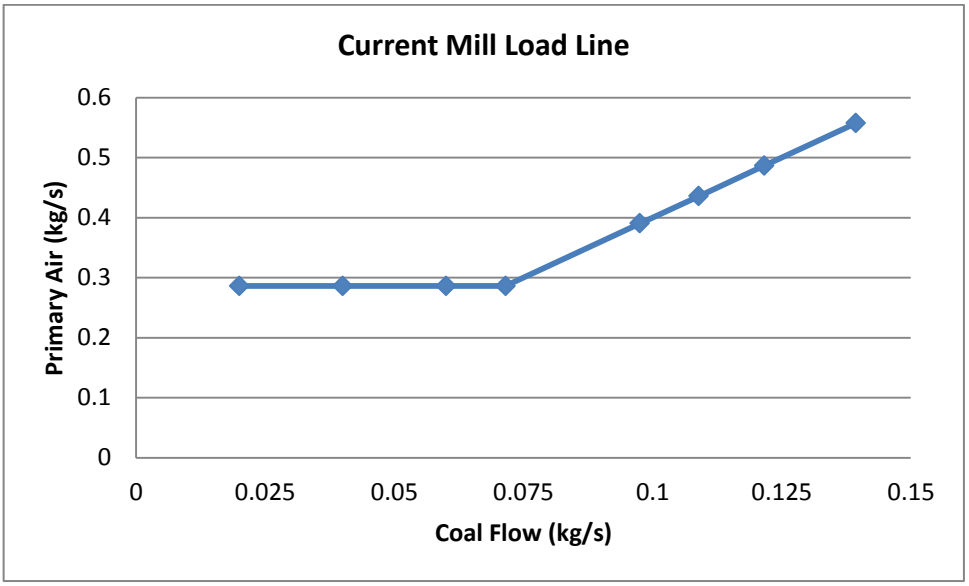

Figure 7.37: Current mill load line – mass flow basis

It is made up of two parts. The horizontal section is there to ensure that a minimum air velocity is maintained in the PF pipe even when the mill is under very low load, like start-up and shut-down conditions. The linearly increasing part increases the air flow of the mill linearly as the coal flow is increased. This is done so according to a defined A/F ratio when the load line is established. In this case the A/F ratio has been fixed at 4:1. Keep in mind that this is presented on a mass flow basis and not on a percentage

air and coal flow basis. If Figure 7.37 above were presented as it would be operated in the control room then the graph would look like Figure 7.38 below.

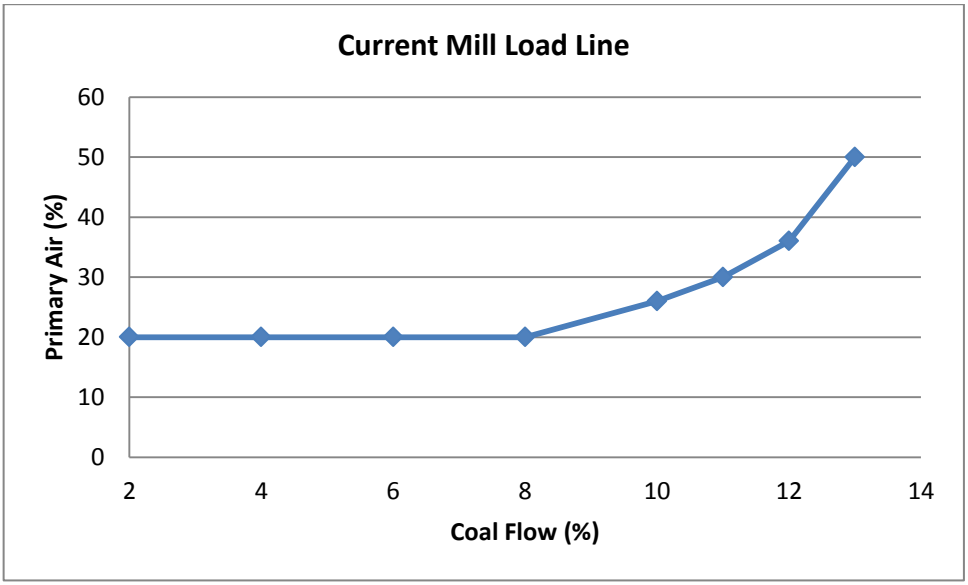

Figure 7.38: Current mill load line – % flow basis

The curve in the line is due to the non-linear relationship between the primary air fan damper position and the primary mass flow as was discussed in the mill characterisation chapter above. Figure 7.38 is difficult to understand because the mass flows appear to be arbitrary values in the discussion thus far. As the coal flow has a linear relationship of feeder speed to coal mass flow it would make more sense to depict the coal flow as a percentage and keep the air flow as a mass flow for further discussion.

We then have the current mill load line in Figure 7.39. Slight kinks in this line are due to the low control resolution that only allows the feeder speed to be adjusted whole percentage points at a time.

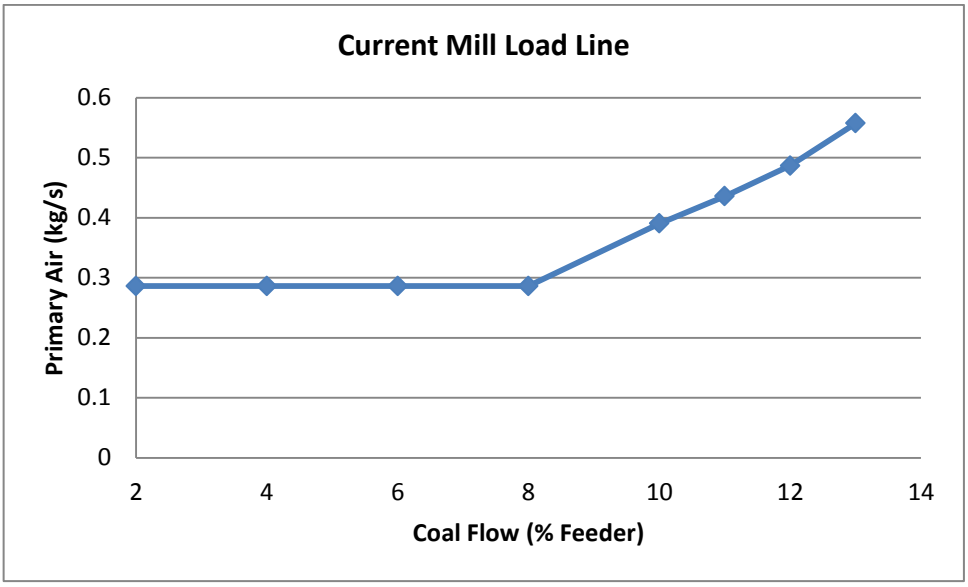

Figure 7.39: Current mill load line

As discussed previously, this mill is a stand-alone system and does not need to follow any mill load conditions according to the boiler energy requirements as is the case on a power station. So this mill is not operated at increased loads as it is unnecessary to do so. However the above graph represents exactly how the mill is currently set up to run if were operated under changing load conditions and this set up is not uncommon at the full scale power station level.

Under current set up conditions, if the mill were to ramp up load from F8 to F10 then the change in grinding performance would drop from 66.43% to 52.54% passing 75µm according to the linear approximation derived from testing at these conditions (see Appendix F: Mill Optimisation). This immediately falls out of the required specification for grinding performance as the particle fineness is below 65% passing 75µm. Increasing the load further to 11% feeder speed we find the particle fineness drops to 45.59% and so the trend continues.

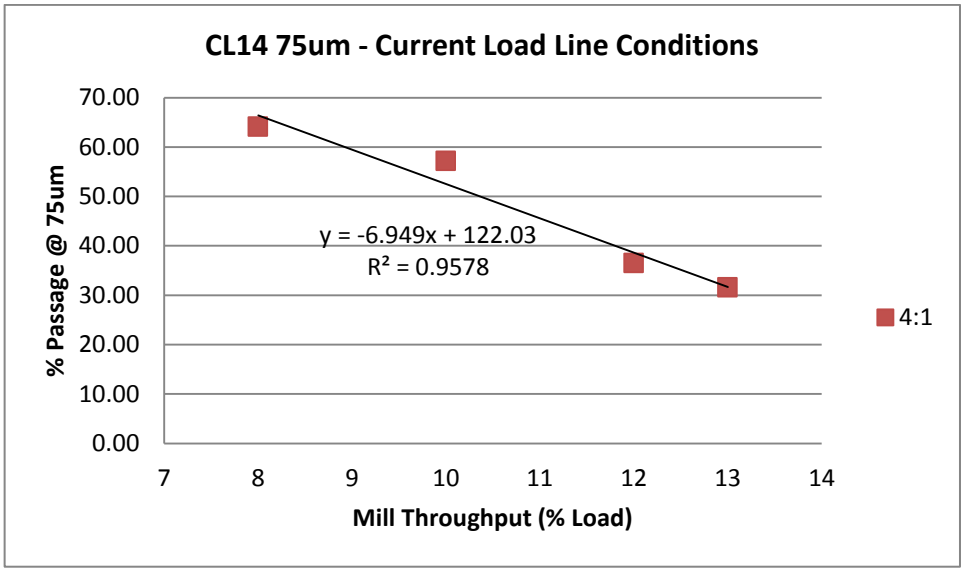

Figure 7.40: Performance at current mill load line conditions

By changing the operation of the mill to run at a lower A/F ratio of 3:1, one may improve on the maximum allowable mill throughput while maintaining the correct particle size as an output.

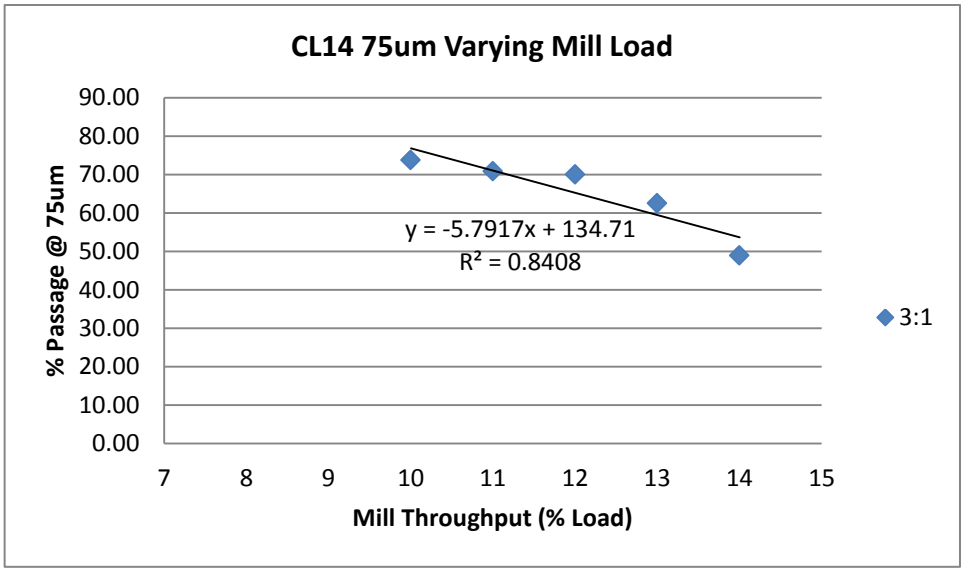

Figure 7.41: Performance at reduced A/F ratio conditions

By changing only the A/F ratio of the load line from 4:1 to 3:1, the mill would operate according to the grinding performance graph in Figure 7.41 above. Now it can be seen that the mill can operate at a fuel feeder speed of 10% while producing a particle fineness of 76.79% passing 75µm. This

is in fact slightly above the upper limit of the optimal grinding window indicating that the mill is over grinding even though the coal throughput has been increased. Increasing the coal throughput further to F11 produces 70.99% passing 75µm, and even further to F12 we have a particle fineness of 65.21% passing 75µm (Appendix F: Mill Optimisation). This drastic improvement in mill throughput was achieved by reducing the A/F ratio after the relationship between the A/F ratio and particle fineness was established during the pilot scale mill tests of Chapter 7.4: Investigation Findings.

It can also be noted that this was achieved without changing the classifier speed, which can introduce additional flexibility to the operation of the milling plant.

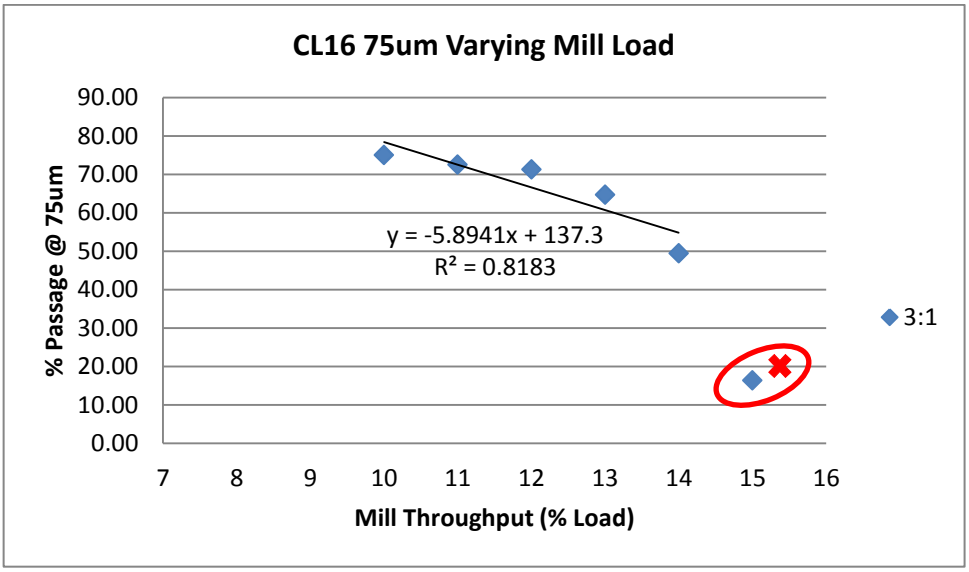

Figure 7.42: Performance at reduced A/F ratio and increased classifier speed conditions

From Figure 7.42 above, the extreme high load scenario (F15) is ignored due to the negative effect that such operation has on the classification process. The relationship up to the mill load of 14% shows that the particle fineness at F13 is 60.67% passing 75µm. This is below the 65% minimum at 75µm and thus this load is unsustainable. However at F12 the particle fineness is 65.57%, which is slightly higher than that of the 14%

classifier speed (Figure 7.41: CL14 F12 = 65.21% passing 75µm) and closer to the ideal value of 70%. The values are higher throughout the load range, where F11 is 72.46% and F10 is 78.36% passing 75µm. F10 is outside the upper limit of 75% and F11 is further away from the ideal of 70% than the 14% classifier speed was (CL14:F11 = 70.99) so it is not advisable to select this classifier speed for these loads. The only load that had improved in particle fineness as a result of the increase in classifiers speed was the highest load at F12.

Looking at the lower case of 12% classifier speed, it is expected then that the lower load cases can be optimised to run closer to the ideal 70% passing 75µm.

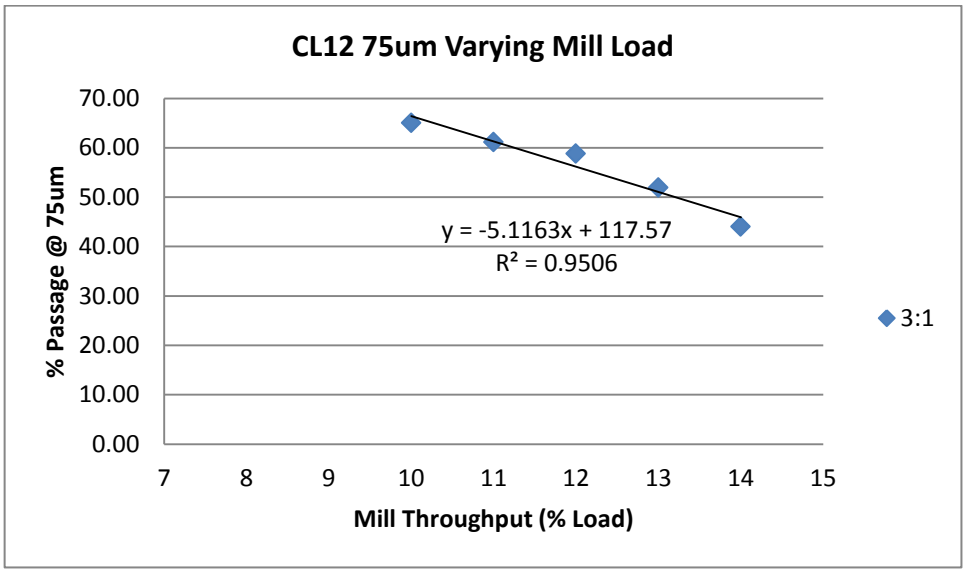

Figure 7.43: Performance at reduced A/F ratio and decreased classifier speed conditions

In Figure 7.41 the particle fineness of the CL14:3:1 case at a mill load of 10% was slightly above the optimal range at 76.79% passing 75µm. By reducing the classifier speed at lower loads (in this case F10) the particle fineness drops to 66.41% passing 75µm (Appendix E: Final Testing) thus optimising the mill grinding performance to within the required specification range.

Putting the above information together one may develop a load line, for the operation and control of the mill that allows for increased average mill throughput, as well as increased flexibility to change load while maintaining fairly consistent product fineness. Such a load line is depicted in Figure 7.44 below.

Table 7.7: Optimised mill load line data

Feeder Speed (%)	A/F Ratio	Classifier Speed (%)	Air Flow (%)	Air Flow (kg/s)
8	3:1	12	20	0.296399
9	3:1	12	20	0.296399
10	3:1	12	20	0.296399
11	3:1	14	22	0.321367
12	3:1	16	24	0.356211

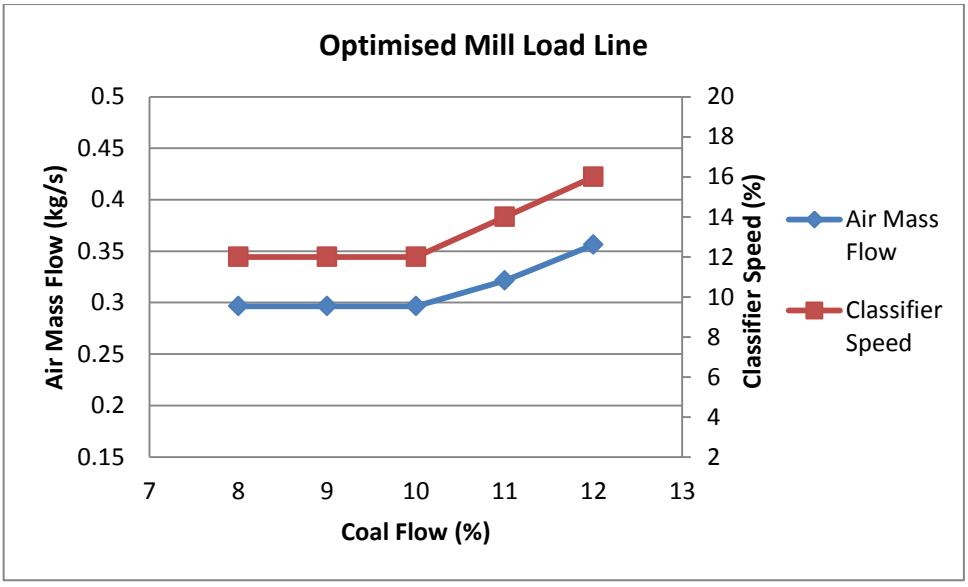

Figure 7.44: Optimised mill load line

The optimised load line in Figure 7.44 above, has a lower A/F ratio of 3:1 throughout, and changing classifier speed for changing load in order to maintain the particle fineness within the optimal range for combustion.

Chapter 8: Discussion

In order to have a condition monitoring system for the milling plant one must first be able to monitor the key parameters of a mill in an on-line manner, and furthermore one must understand the fundamental relationships that govern mill operation. In order to achieve this, four key topics were investigated. An on-line mill energy balance was developed in order predict the coal mass flow through the mill in real time. The Particle Size Analyser instrument was evaluated for use in measuring the pulverised fuel particle fineness at the mill outlet. An attempt was made to monitor the mill internal recirculation load by means of differential pressure measurements. And finally an extensive pilot scale mill investigation was conducted in order to relate the control parameters to the performance evaluation parameters of a mill. Once these relationships were quantified, the mill was optimised using the relationships developed during testing.

The mill energy balance tool successfully predicts the coal mass flow with fair accuracy. The equation developed accounts for the evaporation of moisture in coal and has been developed to operate on-line with the aim of predicting the coal mass flow. The MEB predicts the coal flow within an average of 2.33% of a calibrated feeder. It must be noted however that the MEB consistently over predicts the coal flow which indicates that the equation may not be accounting for all of the energies associated with the system. One possible contributor to this over prediction could be the assumption that all of the moisture in the coal is evaporated by the time the PF reaches the mill exit. Future efforts can be directed at optimising the model further by incorporating lookup steam tables into model. This will allow the real time calculation of the quality of vapour at the mill exit and will allow more accurate calculation of the energy used to evaporate the moisture in coal.

The model does have other shortcomings in the context of an on-line mass flow monitoring tool. All input parameters are measured on-line and

information is passed directly into the calculation from the DCS, apart from the coal moisture. The coal moisture is determined by taking a sample from the coal feeder and lab drying it to determine the change in mass and thus the moisture content. This value is then fixed in the calculation until the next daily coal moisture results become available. While the primary air inlet temperature, mill outlet temperature and primary air mass flow show the greatest effect on the sensitivity of the calculation (Figure 4.4), these are well measured parameters with uncertainties of 1˚C and 1% respectively. The only other significant contributor to changes in the coal flow by way of sensitivity is the coal moisture content. This is also the parameter with the second highest uncertainty in measurement (second to the raw coal temperature). As a result any changes in coal moisture between sampling and analysing the moisture content would result in large errors in coal flow prediction. The implementation of an on-line x-ray coal moisture analyser would provide the necessary input data to reduce the effect of this error in the calculation.

The alternative solution is to repurpose the MEB to calculate the coal moisture using a means of coal mass flow measurement as an input to the model. The sensitivity analysis showed that the model is more sensitive to changes in the coal moisture than it is to changes in the coal mass flow as input parameters (Figure 4.5). This suggests that in order to take advantage of the natural sensitivity of the calculation to improve the accuracy of the result, it is beneficial to measure the coal moisture as an input to the model. This is in line with the findings of Odgaard et al. (2007) who described the prediction of coal moisture by means of an energy balance as a “noisy measurement”.

The use of an on-line mill energy balance is vital for power stations which have screw type volumetric feeders. Volumetric screw feeders are simple mechanical devices with no form of coal mass flow measurement or feedback control, yet they are tasked with the important role of controlling the energy input to the boiler. Coal hang ups, raw coal density changes

and coal moisture changes all have an effect on the mass flow which the feeder is unable to detect. Such an energy balance could be used to verify the coal flow through the mill, detect feeder calibration drift, coal hang ups and, with a reliable on-line coal moisture measurement, can also be used for control of the mill load.

The particle size analyser has shown itself in repeatability tests to be a very precise instrument with very low standard deviation of measurement under normal circumstances. However many practical variables have been identified that do have adverse effects on the accuracy of the instrument. This makes it difficult to achieve a correct result (both high in precision and accuracy) as an off the shelf purchase. One needs to understand what parameters will affect the results, and develop an operating and test procedure to alleviate any gross inaccuracies as well as accommodate for power station specific requirements such as correct PF pipe penetration.

From the above investigation it can be seen that the correct set up of the purge air can be instrumental in achieving high accuracy. Gross error may be easily made if the angle of the measurement groove with respect to the PF flow has not been paid careful attention to. Finally the correct measurement depth should be determined during a commissioning phase and tests conducted in order to ensure that the area of measurement is a representative one.

Once the PSA has been commissioned and all measurement parameters have been determined for the highest accuracy, the system may be used to determine and evaluate the quality of product being produced by the mill. Any gradual or drastic deviation from a given norm may then be attributed to various mill conditions such as grinding element wear and remaining life. The PSA may then be used in the determination of blocked classifiers, worn classifier blades, poor grinding performance, classifier blade angle adjustments, and historical tracking of milling performance, to name a few applications.

The above applications are made possible due to the nature of the PSA being an on-line measurement. Not only do you achieve a much higher measurement frequency than is possible with iso-kinetic sampling, but you also have real time results. The instrument can therefore be used for condition monitoring as well as performance tuning and optimisation of the milling plant.

By applying the principles developed above, i.e., using the on-line mill energy balance to monitor the mass flow of coal through the mill, and applying the particle size analyser to monitor the particle fineness of the PF, one may accomplish a level of mill monitoring rarely achieved on a power station. That is to monitor accurately and reliably, in an on-line and real-time manner, the two key performance parameters of the milling plant. This is the key step towards enabling condition monitoring and finally paves the way for the implementation condition based maintenance of the milling plant.

Furthermore, steps were taken towards supplementing such a condition monitoring system with a method of monitoring aspects of the internal condition of the mill. In theory the nature of the flow in the mill body is similar to that of a fluidised bed. By applying the principles of monitoring the suspended mass of particles in different heights of the mill body by means of differential static pressure measurements, it was expected that the recirculation load could be measured and monitored.

Overall the differential pressure measurements taken during testing on a pilot scale mill showed a fair relationship to the mill coal throughput at all heights of the mill body. It is however expected that this has more to do with the increased air velocity than it has to do with the increased coal flow. The relationship between the differential pressure and the classifier speed did not show a clear relationship. The differential pressure in the tyre section and the classifier section did not respond directly to changes in the classifier speed and thus changes in the coal recirculation. Furthermore, the measurement fluctuations in these areas are expected to

be a result of the rotating classifier design on this particular mill. Performing these tests on a full scale mill with a static classifier where the classification swirl is separate from the mill body may produce more consistent results. The full scale mill is also considerably larger but the difference in pressure is expected to be similar per mill area. The difference in height of the pressure taps at the tyre level of the pilot scale mill is only 200mm whereas a full scale mill will be approximately 1.5m. This means that for similar pressure drop the pressure taps will be measuring considerably more suspended coal, both due to the increased height difference as well as the increased diameter of a full scale mill. It is also proposed to perform a CFD analysis for different recirculating loads of the mill in operation. This will confirm the theory employed on circulating fluidised bed combustion boilers for use in a mill internal environment.

The ability to monitor the mill internal recirculation load in an on-line manner has not been implemented before, mainly due to the harsh and abrasive environment inside the mill. The application of such a measurement in a mill condition monitoring system would be beneficial in many ways. By measuring and comparing the mill recirculation load in the tyre section, expansion area above and the classifier, one may infer the condition of certain internal components of the mill. An increase in primary circulation with no change in classifier recirculation is indicative of a worn throat. An increase in classifier recirculation with a decrease in primary recirculation is indicative of a possible blocked throat. In this way the mill recirculation load, as a supplement to the MEB and PSA measurements, may be used to detect common mill problems such a raw coal chute holes, blocked classifiers, grinding element failure, throat wear and even grinding element remaining life.

In order to successfully integrate these three measurement systems into a condition monitoring system one needs to implement them on a full scale mill and begin to track them over a long term and through multiple maintenance cycles along with all other parameters of the mill. Once a

large dataset is achieved then correlations between the measured and calculated dataset and the physical condition of mill parts may be made. The condition monitoring system should continuously be updated when mill failures are found so that they may be detected and flagged earlier when such failures are likely to occur again. Parameter drift needs to be monitored as well and compared to normal wear and tear of the mill as and when measured during inspections.

Understanding the principles that govern mill operation and quantifying the relationships between the mill operational parameters, mill control system and key performance parameters are vital to the implementation of a condition monitoring system. Such an exercise was performed on a pilot scale mill in order to gain this knowledge for application when implementing such a system on the milling plant.

The relationships between the mill load, classifier speed and the air/fuel ratio, and the effects of changing each of these operational parameters from their lower to upper extremes, were defined with respect to particle fineness.

Linear relationships were found when relating the classifier speed to particle fineness for various mill loads i.e. an increase in classifier speed led to an increase in particle fineness. It should be noted that changing the mill load caused this linear relationship to shift, where increasing the load has the effect of decreasing the particle fineness as can be seen in Figure 7.13. This effect was confirmed by the tests relating mill load to particle fineness. An example of which can be seen in Figure 7.18 where increasing the mill load caused a linear decrease in particle fineness. The relationship between classifier speed, mill load and particle fineness is an age old problem for milling plant engineers as increasing the classifier speed also causes an increase in mill differential pressure (due to increased recirculation in the mill) which in turn results in a lower sustainable maximum mill load. The problem is exacerbated in the South African context as deteriorating coal quality necessitates a higher average

mill load to be sustained, while new clean coal technologies such as low NOx burners require increased particle fineness from the mill. A key output from this exercise was to quantify the relationship between the air/fuel ratio and the particle fineness. It was found that lower air/fuel ratios naturally produced a finer PF product from the mill. This is true because the increased air flow will lead to higher velocity through the throat which will reduce primary classification carrying coarser particles up to the classifier and out of the mill. Such an effect could be confirmed and monitored if the monitoring and comparison of primary to secondary recirculation can be achieved. The result was consistent for varying mill loads and classifier speeds. It can be noted as well from Figure 7.27 that the rate of change of particle fineness with respect to the air/fuel ratio was found to be higher for increased mill loads. Reducing the air/fuel ratio at higher mill loads will have a greater impact on increasing the particle fineness, than it will at lower mill loads.

The relationships that were developed and quantified in Chapter 7.4 were then applied to demonstrate how a mill can be optimised for increased throughput while still achieving the optimal grinding performance and particle fineness. Milling plant throughput restrictions are a large contributor to load losses. Many of these losses can be reduced by optimisation of the operation of the mill. The pilot scale mill was being operated at a fixed feeder speed of 8% with an air/fuel ratio of 4:1 and a classifier speed of 14%. During testing this produced a particle fineness at the lower range of the required 65% to 75% under 75µm specification. Under these operational conditions an increase in the mill load from 8% to 10% would cause the particle fineness to decrease from 66.43% to 52.54% passing 75µm. This is too coarse to be considered for sustained operation.

By reducing the air/fuel ratio to 3:1 the mill could operate at 10% feeder speed to produce 76.79% passing 75µm and could be increased in load up to 12% feeder speed to produce 65.21% passing 75µm. Further

optimisation was made by developing a load line with variable classifier speeds in order to optimise the particle fineness as close as possible to the ideal 70% passing 75µm. By reducing the classifier speed to 12% at lower loads, the particle fineness decreased to 66.41% passing 75µm. And by increasing the classifier speed to 16% at higher load the particle fineness was increased to 71.25% passing 75µm.

Table 8.1: New mill operating parameters

Feeder Speed (%)	A/F Ratio	Classifier Speed (%)	<75µm
10	3:1	12	66.41%
11	3:1	14	70.99%
12	3:1	16	71.25%

Such an optimisation was made possible by the relationships defined during the pilot scale mill testing. The same relationships should be defined and quantified on a full scale plant for future use in both condition monitoring and performance optimisation of the milling plant.

Chapter 9: Conclusions and Recommendations

The vision to implement a mill health monitoring system was to be able to optimise the operation and maintenance of the milling plant by introducing condition monitoring alongside model based predictions and experience based detection of commonly occurring problems. Two key performance parameters of the mill were found to be inadequately measured for the purposes of condition monitoring. These were the mill throughput and the particle fineness. As an additional condition monitoring tool, the health of the internal components of the mill was to be monitored by online measurement of the mill internal recirculating load. And finally, a method of optimising the mill operational parameters in order to increase the mill throughput without reducing the particle fineness had to be determined.

These four tasks were executed in the four individual studies with the common aim to be integrated and incorporated in to a mill condition monitoring system. Monitoring of the mass flow through the mill was established by means of an on-line mill energy balance. Monitoring of the product fineness was achieved by evaluating the on-line particle size analyser as an instrument suited for use in pulverised fuel particle size measurement. The method of differential pressure measurements across different heights of the mill was used to determine the suspended mass, as is commonly used in fluidised bed boilers. And finally the improvement of the mill throughput was achieved by testing a pilot scale mill in order to characterise the relationships between the control parameters and the key performance indicators of a mill under different operating scenarios.

The mill energy balance tool was developed based on a simplified mill layout and takes into account the evaporation of moisture in coal as well as convective heat loss through the walls. The MEB tended to over predict the coal flow by an average of 2.33% as verified against plant measurement data and comparing with the coal flow reported by newly calibrated feeders. The MEB can be used to calculate and monitor the

feeder mass flow rate as well as cross check the feed factor, feeder calibration and even detect coal hang ups. The MEB can be further improved by installing an on-line coal moisture measurement device as the coal moisture is currently input once a day as per the daily proximate analysis of coal. The sensitivity analysis also showed that the coal moisture has a large influence on the result of the calculation. Although MEB is already fairly accurate, further work can be done to reduce the consistent over prediction of the coal flow. The possibility exists that not all of the moisture in the coal is realistically evaporated in the mill, and this could be a contributing factor to the over prediction.

The ability to measure the product fineness of the milling plant in real time has for many years been long overdue. The particle size analyser, as a solution to such measurement, is a leap forward for milling plant engineers. On-line measurement and real time result reporting while setting up the mill is something that has not been possible with iso-kinetic sampling.

The limitation with iso-kinetic sampling, as performed currently, is that there is a long delay between the time of a test being performed and usable results being produced. There also exist aspects of the iso-kinetic process where human error can have an influence on the results, such as under-sampling/over-sampling. The PSA on the other hand, almost completely removes human error while providing an instantaneous on-line and real-time result. This means it makes an ideal candidate for condition based monitoring and maintenance of the milling plant.

However, in order to rely on such measurement it was found that the instrument has to be calibrated to the plant specific layout and test conditions.

The findings of this investigation showed that:

- The angle of the probe as inserted into the PF pipe has a drastic influence on the results

- An increase in purge air pressure caused a drop in the reported particle fineness
- An increase in the mass flow of purge air caused an increase in the reported particle fineness
- An increase in the time of purge caused a decrease in the reported particle fineness
- As the measurement penetration depth is increased, the reported particle fineness decreases

With the above relationships established one may address the accuracy of the instrument by correct commissioning of equipment and the establishment of proper test procedures for each power station. Once high precision and accuracy of results have been achieved the particle size analyser may be used in a condition monitoring role, as mill performance may be tracked for relative deterioration over extended periods. Overall the PSA has shown great potential in its ability to handle applications of condition based monitoring and maintenance of the milling plant.

The monitoring of differential pressures at different heights of the mill body did not yield clear and convincing results. There was no clear relationship between the differential pressure and the classifier speed, which is expected to influence the recirculating load. Furthermore, large fluctuations in differential pressure were found in the lower part of the mill as well as the classifier area. These were attributed to the swirling effect generated by the classifier in the mill body itself. It is recommended to further pursue this concept on a full scale mill where:

- The height of the differential pressure taps will be an order of magnitude larger
- The classifier swirl is generated inside the classifier cone which is separate from the mill body

Improving the mill throughput was approached by first understanding the dynamics of the milling plant as a system. The control parameters were related to the key performance indices by means of extensive mill testing performed on a pilot scale mill. It was found that by increasing the classifier speed the particle fineness was increased, also by increasing the mill load the particle fineness was reduced. While these results were not unexpected, it is important that the extent to which these effects occur is quantified, as they are vital in setting up and operating a mill. An interesting outcome of the pilot scale testing was the extent to which the air/fuel ratio influenced the particle fineness produced. It was finally concluded that by reducing the air/fuel ratio, higher throughputs can be achieved by the mill while maintain the required specification of particle size distribution.

The pilot scale testing reported herein included a vast range of operating conditions and resulted in both extremely coarse and extremely fine particles at times. As a result, the full gamut of testing will not be possible on a full scale mill due to the effects this may have on subsequent systems. However it is recommended that a select few operating changes be tested on a full scale mill in order to establish the scalability of these findings and evaluate the feasibility of implementing such operating changes on a power station.

The implementation of the on-line energy balance model and particle size analyser will be a step forward in reaching the goal of condition monitoring and maintenance of the milling plant. While the knowledge gained during the optimisation of the pilot scale mill will be invaluable in improving the performance and reliability of full scale mills thereby alleviating a portion of the load losses currently experienced by older power stations. Understanding of these relationships will in turn contribute substantially to the development of a mill condition monitoring system. This study provides a step towards the condition monitoring of the milling plant by providing on-line methods of measuring the two vital performance evaluation

parameters of the mill. Those are the quantity (mass flow) and quality (particle fineness) of the product of the milling plant.

References

Eskom, n.d., *Company Information*, viewed 1 November 2013, from http://www.eskom.co.za/OurCompany/CompanyInformation/Pages/Company_Information.aspx

Kohler, M., 2013, Differential electricity pricing and energy efficiency in South Africa

Muller, M. A., Mthembu, M. K., Mathe, Z. T. 2014, Milling Plant and Coal Burners Generation Plant Engineering Strategic Report

Alstom, n.d., *Mills for Coal Fired Power Plants*, viewed 13 February 2014, from http://www.alstom.com/power/coal-oil/mills-pulverisers/

Powermag, 2011, *Pulverizers 101: Part 1*, viewed 7 February 2014, from http://www.powermag.com/pulverizers-101-part-i/?printmode=1

Kitto, J.B., Stultz, S.C., 2005, *Steam It's Generation and Use*, 41st Ed. McDermott

Williams, A., Pourkashanian, M., Jones, J. M. 2000, *"The Combustion of Coal and Some Other Solid Fuels"*, Proceedings of the Combustion Institute, Vol. 28, pp. 2141–2162.

CMP, 2010, Camden Power Station Milling Plant Operating and Maintenance Manual, Coal Milling Projects (Pty) Ltd

Van Wyk, C. 2003, "Eskom generation combustion manual – Mathimba power station"

Van Alphen, C. 2010, Ash/Calorific Value Variations, Technical Memorandum, Sustainability and Innovation.

R. Sonntag, C. Borgnakke and G. J. Wylen, 1998, Fundamentals of classical thermodynamics, 5th Ed. John Wiley & Sons.

Incropera, F. P., Dewitt, D. P., Bergman, T. L. and Lavine, A. S., 2007, Fundamentals of heat and mass transfer, 6th Ed. John Wiley & Sons.

CMP, 2012, Classifiers and Rotating Throats, Coal Milling Projects (Pty) Ltd

Fan, G.Q. & Rees, N.W. 1997, "An intelligent expert system (KBOSS) for power plant coal mill supervision and control", *Control Engineering Practice,* vol. 5, no. 1, pp. 101-108.

Makokha, A.B., Moys, M.H., Couvas, C. & Muumbo, A.M. 2009, "Steady state inferential modeling of temperature and pressure in an air-swept coal pulverizing ball mill", *Powder Technology,* vol. 192, no. 3, pp. 260-267.

Niemczyk, P., Dimon Bendtsen, J., Peter Ravn, A., Andersen, P. & Søndergaard Pedersen, T. 2012, "Derivation and validation of a coal mill model for control", *Control Engineering Practice,* vol. 20, no. 5, pp. 519-530.

Rees, N.W. & Fan, G.Q. 2003, Thermal power plant simulation and control. In: D. Flynn (Ed), *Thermal power plant simulation and control: Chapter 3. Modelling and control of pulverized fuel coal mills* (pp. 63-99). Institution of Electrical Engineers.

Yang, W.C., 2003, Handbook of Fluidization and Fluid-Particle Systems, In: W.C. Yang (Ed), Handbook of Fluidization and Fluid-Particle Systems: Chapter 3. Bubbling Fluidized Beds

Odgaard, P.F. & Mataji, B. 2007, "- Fault Detection in Coal Mills Used in Power Plants" in *Power Plants and Power Systems Control 2006*, ed. Dr. David Westwick, Elsevier Science Ltd, Oxford, pp. 177-182.

Wei, J.L., Wang, J., Wu, Q.U. 2007, "Development of a multisegmented coal mill model using an evolutionary computation technique", IEEE transactions on energy conversion, vol. 22, no. 3, pp. 718-727.

Parsum 2011a, In Line Particle Probe Hardware Manual

Bhambare, K.S., Ma, Z. & Lu, P. 2010, "CFD modeling of MPS coal mill with moisture evaporation", *Fuel Processing Technology,* vol. 91, no. 5, pp. 566-571.

Clark, N. N., McKenzie, E. A. Jr., Gautam, M. 1991, “Differential Pressure Measurements in a Slugging Fluidised Bed”, *Powder Technology*, vol. 67, pp. 187-199.

Saxena, S. C., Rao, N. S. 1990, “Pressure Fluctuations in a Gas Fluidized Bed and Fluidization Quality”, *Energy*, vol. 15, no. 6, pp 489-497.

Van der Merwe, J.C., Roohani, H., Jestin, L., Simonin, O., van Wyk, C., Archary, H. 2012, "Mastering pulverized fuel distribution to low-NOx burners for safety and environmental protection", POWER-GEN AFRICA CONFERENCE, 6-8 November 2012, Johannesburg, South Africa

Parham, J.J. & Easson, W.J. 2003, "Flow visualisation and velocity measurements in a vertical spindle coal mill static classifier☆", *Fuel,* vol. 82, no. 15–17, pp. 2115-2123.

Shah, K.V., Vuthaluru, R. & Vuthaluru, H.B. 2009, "CFD based investigations into optimization of coal pulveriser performance: Effect of classifier vane settings", *Fuel Processing Technology,* vol. 90, no. 9, pp. 1135-1141.

Vuthaluru, H.B., Pareek, V.K. & Vuthaluru, R. 2005, "Multiphase flow simulation of a simplified coal pulveriser", *Fuel Processing Technology,* vol. 86, no. 11, pp. 1195-1205.

Bhasker, C. 2002, "Numerical simulation of turbulent flow in complex geometries used in power plants", *Advances in Engineering Software,* vol. 33, no. 2, pp. 71-83.

Carter, R.M. & Yan, Y. 2005, "An instrumentation system using combined sensing strategies for online mass flow rate measurement and particle

sizing", *IEEE Transactions on Instrumentation and Measurement,* vol. 54, no. 4, pp. 1433-1437.

Carter, R. & Yan, Y. 2007, "On-line non-intrusive particle size measurement of pulverised fuel through digital imaging", Yi Qi Yi Biao Xue Bao/Chinese Journal of Scientific Instrument, vol. 28, no. 11, pp. 1942-1946.

Chinnayya, A., Chtab, A., Shao, J.Q., Carter, R.M., Yan, Y. & Caillat, S. 2009, "Characterization of pneumatic transportation of pulverised coal in a horizontal pipeline through measurement and computational modelling", Fuel, vol. 88, no. 12, pp. 2348-2356.

Coulthard, J., Cheng, R., Kane, P., Osborne, J.T. & Keech, R.P. 1997, "Online pulverised-fuel monitoring at Methil power station", Power Engineering Journal, vol. 11, no. 1, pp. 27-30.

Gao, L., Yan, Y., Lu, G. & Carter, R.M. 2012, "On-line measurement of particle size and shape distributions of pneumatically conveyed particles through multi-wavelength based digital imaging", Flow Measurement and Instrumentation, vol. 27, pp. 20-28.

Hancke, G.P. & Malan, R. 1996, "On-line particle size distribution analysis of pulverised coal", Part 1 (of 2), June 17, 1996 - June 20Warsaw, Poland, 1996, pp. 1066.

Shao, J., Yan, Y. & Lv, Z. 2011, "On-line non-intrusive measurements of the velocity and particle size distribution of pulverised fuel on a full scale power plant", 2011 IEEE International Instrumentation and Measurement Technology Conference, I2MTC 2011, May 10, 2011 - May 12Institute of Electrical and Electronics Engineers Inc, Binjiang, Hangzhou, China, 2011, pp. 1508.

Pieri, L., Bittelli, M. & Pisa, P.R. 2006, "Laser diffraction, transmission electron microscopy and image analysis to evaluate a bimodal Gaussian

model for particle size distribution in soils", *Geoderma,* vol. 135, pp. 118-132.

Abbas, T., Costa, M., Costen, P., Godoy, S., Lockwood, F.C., Ou, J.J., Romo-Millares, C. & Zhou, J. 1994, "NOx formation and reduction mechanisms in pulverized coal flames", *Fuel,* vol. 73, no. 9, pp. 1423-1436.

Van der Merwe, J.C., Jestin, L., Roohani, H. 2012, “Mastering Pulverised Fuel Distribution to Low-NO_x Burners for Safety and Environmental Protection”, Power-Gen Africa Conference 2012.

Dodds, J., Rasteiro, G., Scarlett, B., Weichert, R. & Williams, R. 2004, "From Particle Size Analysis (PSA 1970) to Particulate Systems Analysis (PSA 2003)", *Chemical Engineering Research and Design,* vol. 82, no. 12, pp. 1533-1540.

Wanogho, S., Gettinby, G. & Caddy, B. 1987, "Particle size distribution analysis of soils using laser diffraction", *Forensic science international,* vol. 33, no. 2, pp. 117-128.

Petrak, D. 2002, "Simultaneous measurement of particle size and particle velocity by the spatial filtering technique", *Particle and Particle Systems Characterization,* vol. 19, no. 6, pp. 391-400.

Aizu, Y. & Asakura, T. 1987, "PRINCIPLES AND DEVELOPMENT OF SPATIAL FILTERING VELOCIMETRY", *Applied physics.B, Photophysics and laser chemistry,* vol. B43, no. 4, pp. 209-224.

Petrak, D., Dietrich, S., Eckardt, G. & Köhler, M. 2011, "In-line particle sizing for real-time process control by fibre-optical spatial filtering technique (SFT)", *Advanced Powder Technology,* vol. 22, no. 2, pp. 203-208.

Langston, P.A., Burbidge, A.S., Jones, T.F. & Simmons, M.J.H. 2001, "Particle and droplet size analysis from chord measurements using Bayes' theorem", *Powder Technology,* vol. 116, no. 1, pp. 33-42.

JCGM 200:2012, International vocabulary of metrology – Basic and general concepts and associated terms, (VIM) 3rd edition, http://www.bipm.org/utils/common/documents/jcgm/JCGM_200_2012.pdf

Hayden, K.S., Park, K. & Curtis, J.S. 2003, "Effect of particle characteristics on particle pickup velocity", *Powder Technology,* vol. 131, no. 1, pp. 7-14.

Peta, S., Jestin, L., Roohani, H. 2012, “Burner flow controls for safe, reliable, complete and clean combustion”, Power-Gen Africa Conference 2012.

Appendix A: MEB Verification Results

MEB verification results

Unit 2 – Mill A	**Unit**	**Mill A**	**Mill B**	**Mill C**	**Mill D**	**Mill E**
Input Parameters						
Coal temp.	˚C	15	15	15	15	15
Coal moisture	%	7	8.9	9.2	8.7	8.8
PA moisture	%	0.5	0.5	0.5	0.5	0.5
PA mass flow	kg/s	11.205	11.21	11.87	11.18	11.63
PA temp. in	˚C	231.859	220.52	240.3	233.94	257.12
PA/PF temp. out	˚C	92.91	91.53	84.855	89.35	92.28
Seal air moisture	%	0.5	0.5	0.5	0.5	0.5
Seal air flow	kg/s	1.25	1.25	1.25	1.25	1.25
Seal air temp.	˚C	20	20	20	20	20
Mill motor power	kW	205	205	205	205	205
Convective heat loss	kW	5.932	5.932	5.932	5.932	5.932
Calculated Parameters						
Enthalpy – Seal air	kJ/kg	-73.49	-72.10	-65.37	-69.90	-72.86
Enthalpy – Seal air H_2O	kJ/kg	-145.31	-142.56	-129.26	-138.21	-144.05
Enthalpy – Primary air	kJ/kg	140.06	130.02	156.69	145.75	166.16
Enthalpy – PA H_2O	kJ/kg	276.93	257.08	309.80	288.17	328.53
Enthalpy – Coal H_2O	kJ/kg	327.77	321.96	293.88	312.79	325.12
Output Parameter						
MEB Coal mass flow	kg/s	6.24	4.99	6.34	5.69	6.53
Feeder Coal mass flow	kg/s	6.11	4.82	6.2329	5.58	6.36
% Difference	%	2.13	3.33	1.71	1.94	2.53
Ave. % Difference	%	2.33				

Appendix B: Iso-kinetic Sampling Results

Mill 2C results – Test 1

	75µm	106µm	150µm	300µm
50mm	67.4486	79.77658	89.08996	98.10627
100mm	62.6878	76.34826	87.64508	97.95151
150mm	51.96511	74.69062	87.31884	97.80787
200mm	47.9912	74.16166	85.32888	97.41723

Mill 2C results – Test 2

	75µm	106µm	150µm	300µm
50mm	53.79378	75.78664	89.02401	97.98797
100mm	63.37174	77.94836	88.31949	98.00313
150mm	53.75452	73.22467	86.87926	97.73778
200mm	60.93651	76.96636	87.51054	97.71741

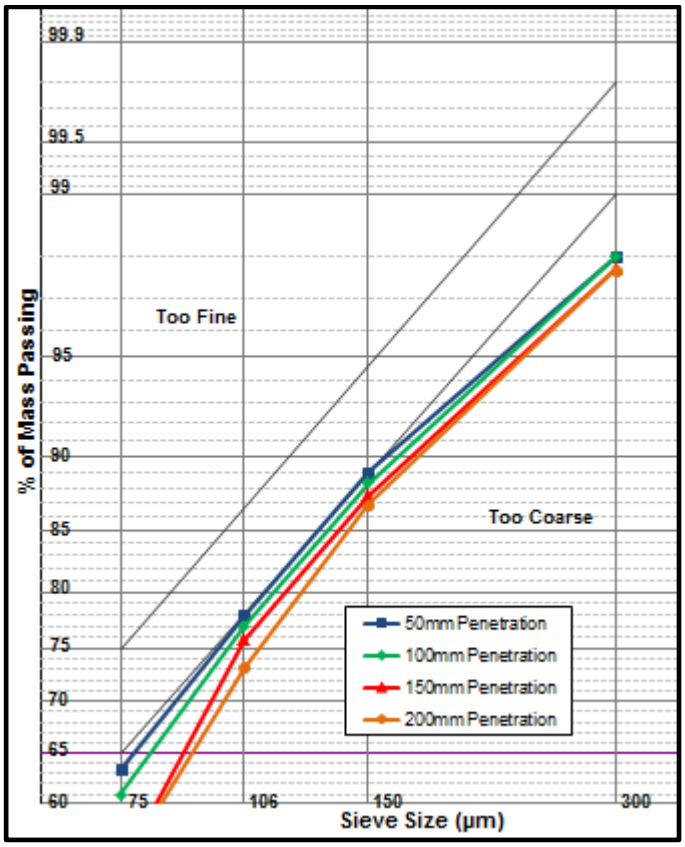

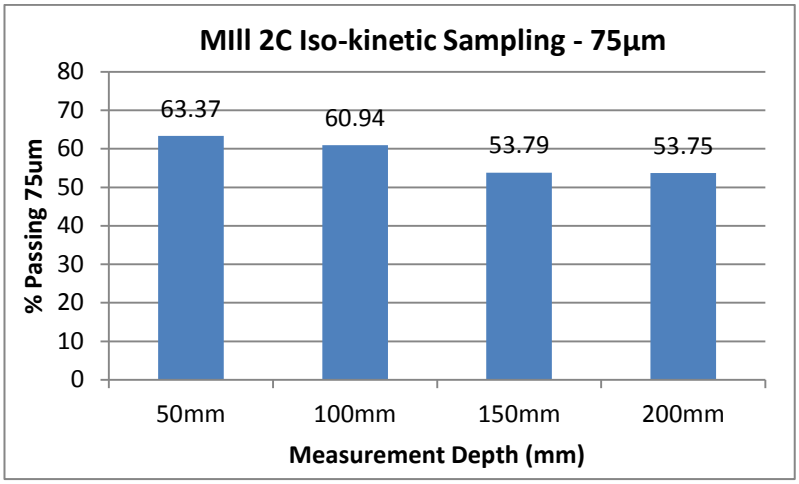

Mill 2B results

	75µm	106µm	150µm	300µm
50mm	74.66649	83.23108	91.45946	98.94865
100mm	72.35172	82.48434	91.09633	98.61093
150mm	67.03191	81.44818	90.46517	98.10533
200mm	53.42176	80.61341	89.28027	97.81073

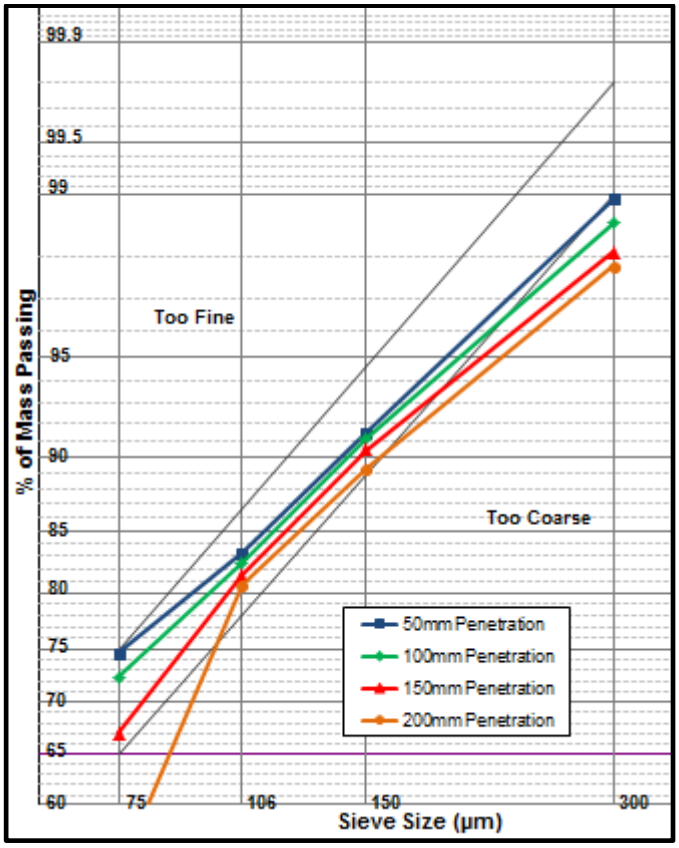

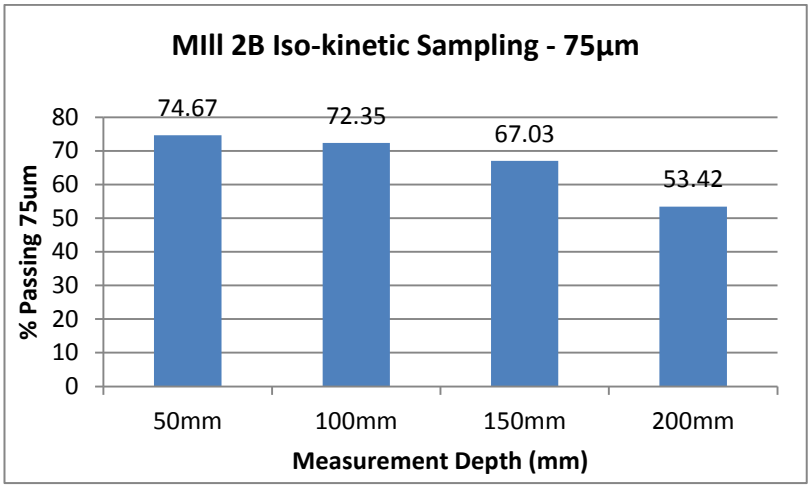
MIll 2B Iso-kinetic Sampling - 75µm
% Passing 75um
80
70
60
50
40
30
20
10
0
74.67
72.35
67.03
53.42
50mm
100mm
150mm
200mm
Measurement Depth (mm)

Appendix C: Mill Recirculating Load

Throat Differential Pressure:

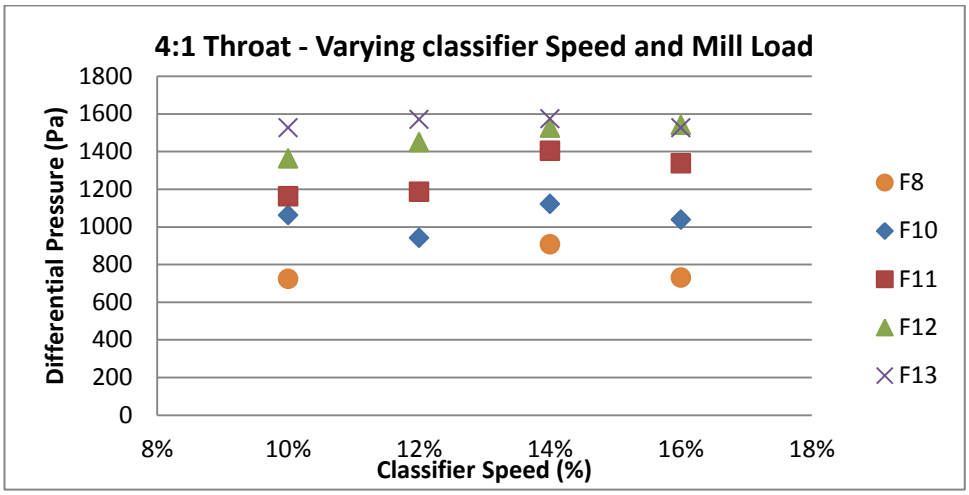

Air/fuel ratio 4:1 - varying classifier speed

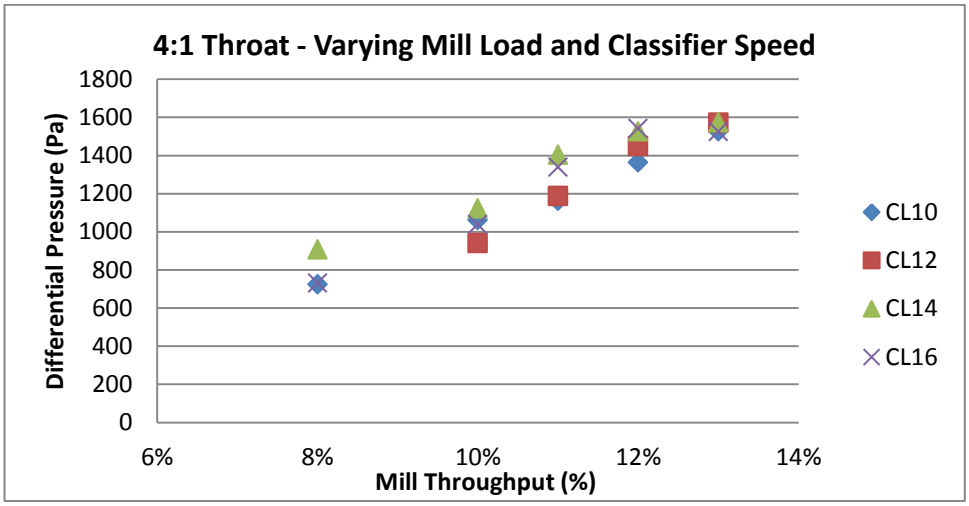

Air/fuel ratio 4:1 - varying mill load

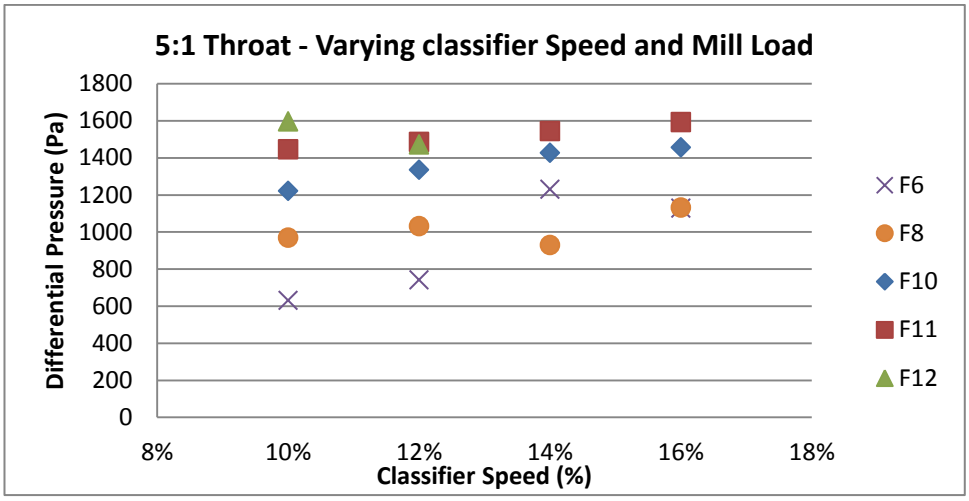

Air/fuel ratio 5:1 - varying classifier speed

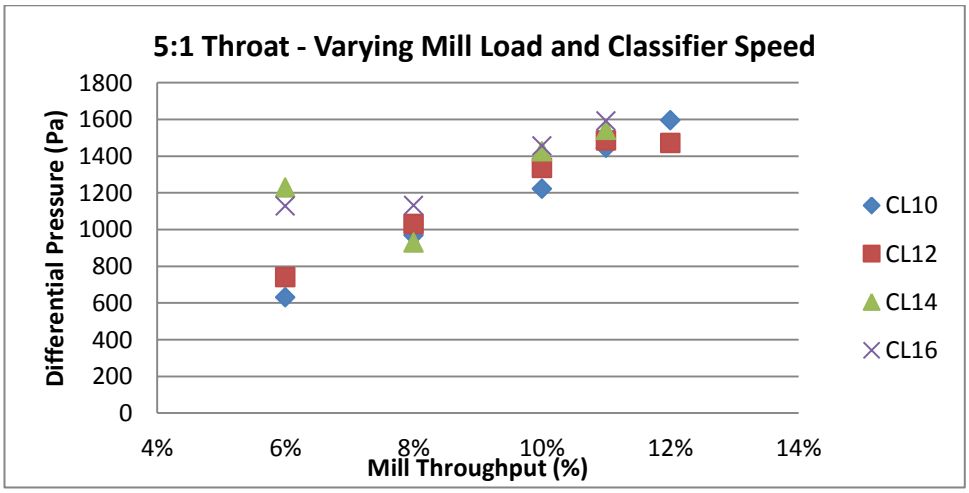

Air/fuel ratio 5:1 - varying mill load

Figure 6.4: Equations

CL10: $y = 16024x - 90.13$

CL12: $y = 13433x + 142.31$

CL14: $y = 16024x + 35.821$

CL16: $y = 18684x - 163.07$

$$Average\ gradient = \frac{16024 + 13433 + 16024 + 18684}{4} = 16041.25$$

Throat Differential Pressure Varying A/F Ratio:

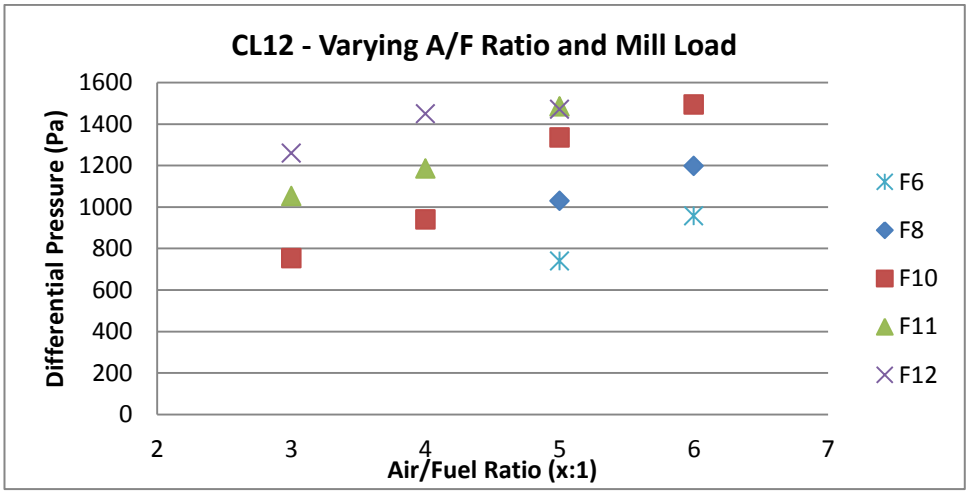

Classifier 12% - varying air/fuel ratio

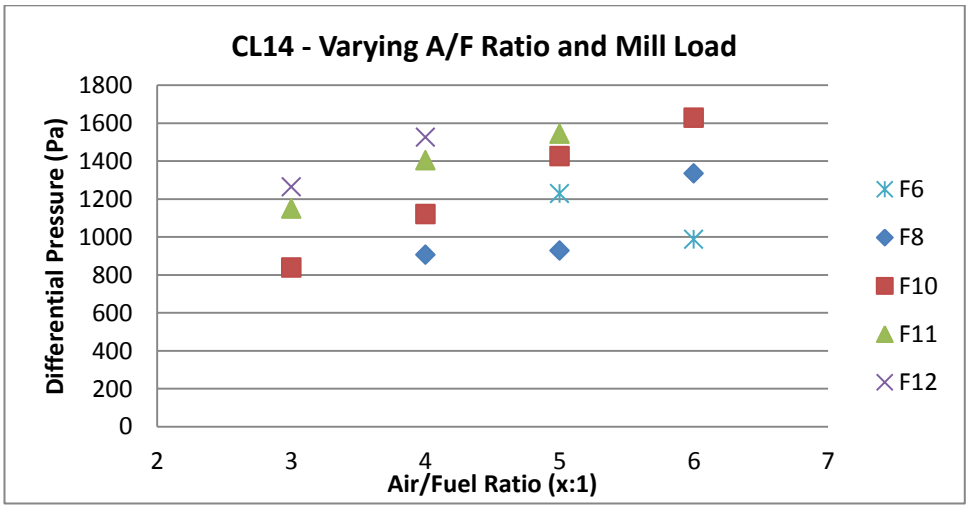

Classifier 14% - varying air/fuel ratio

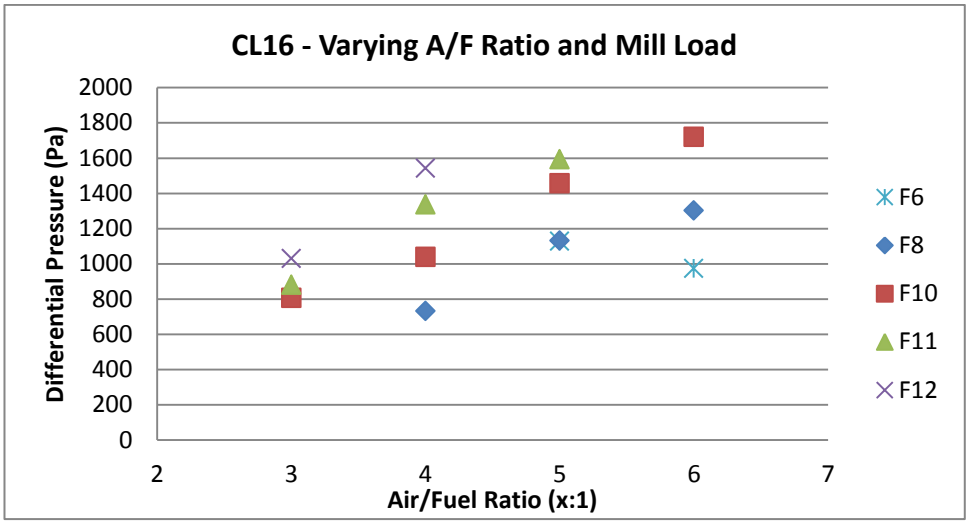

Classifier 16% - varying air/fuel ratio

Tyre Differential Pressure:

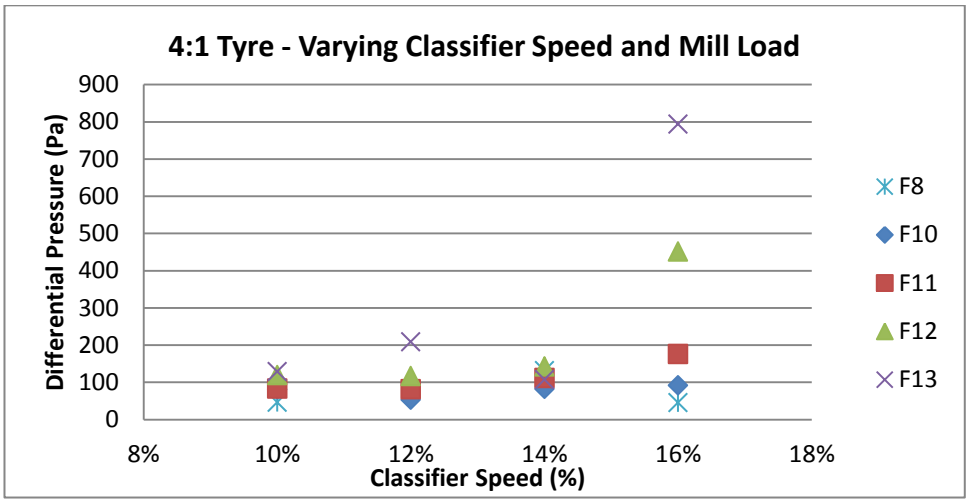

Air/fuel ratio 4:1 - varying classifier speed

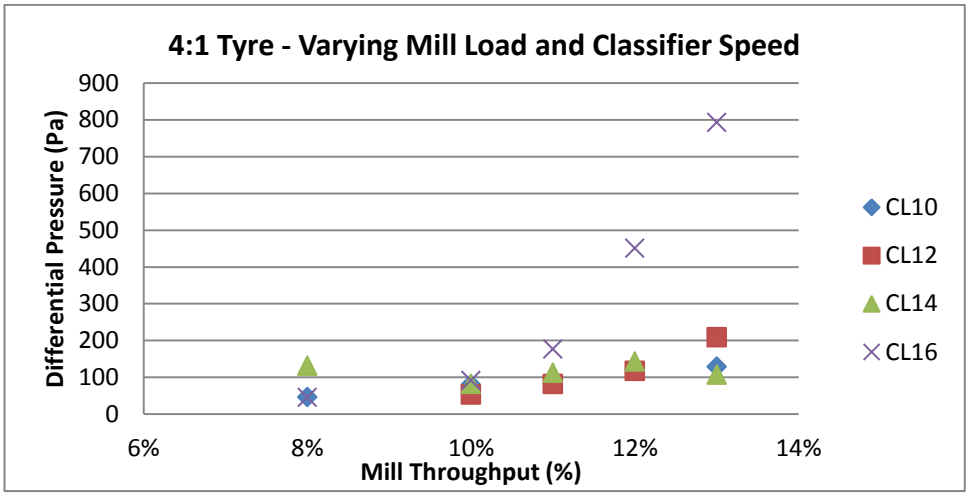

Air/fuel ratio 4:1 - varying mill load

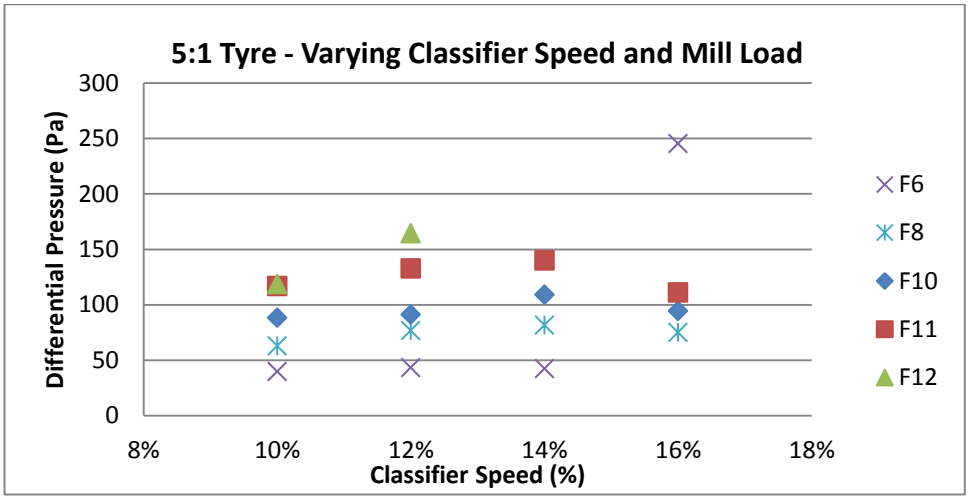

Air/fuel ratio 5:1 - varying classifier speed

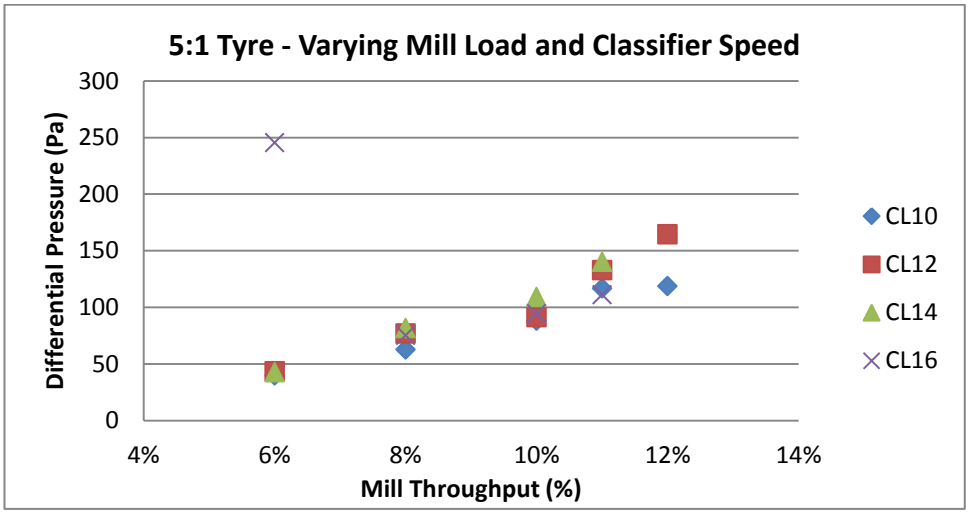

Air/fuel ratio 5:1 - varying mill load

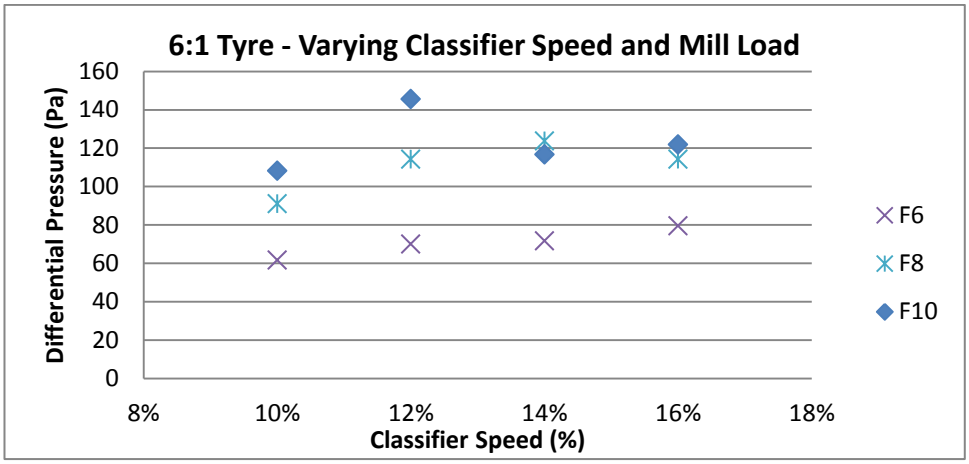

Air/fuel ratio 6:1 - varying classifier speed

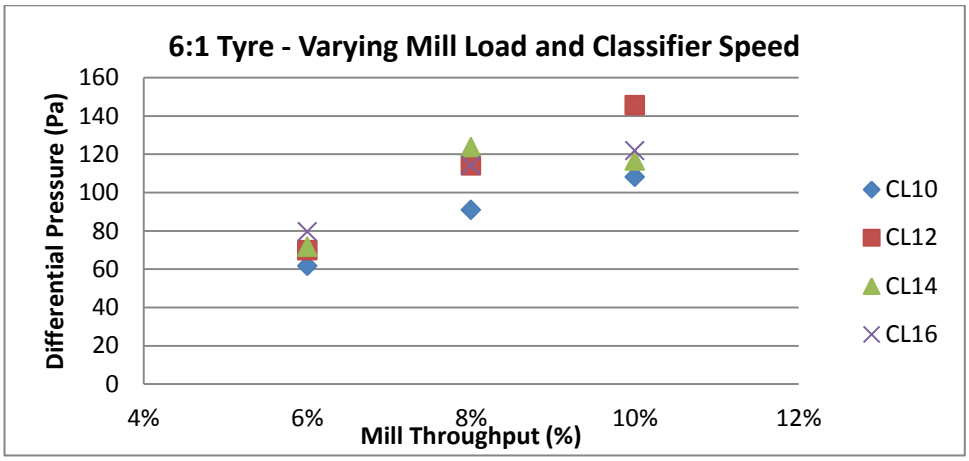

Air/fuel ratio 6:1 - varying mill load

Mill Outlet Differential Pressure:

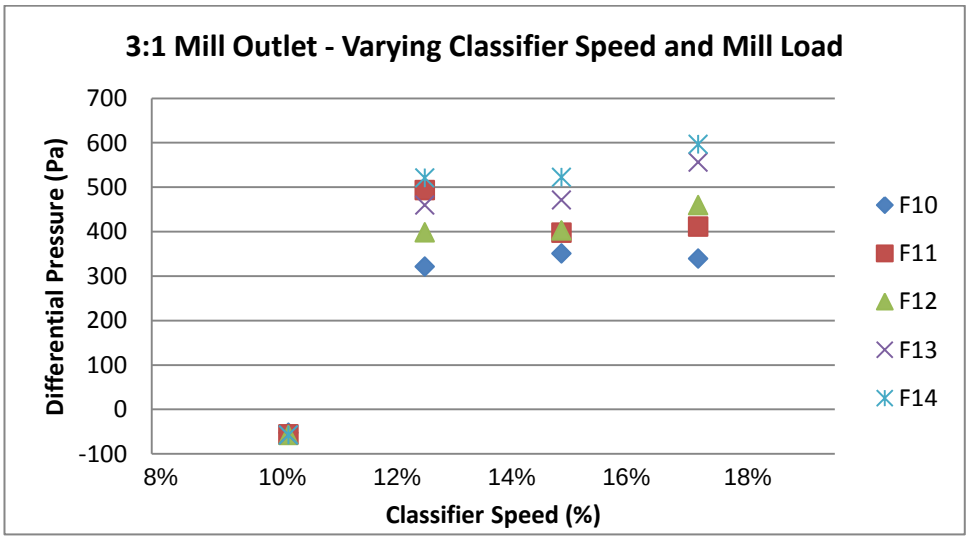

Air/fuel ratio 3:1 - varying classifier speed

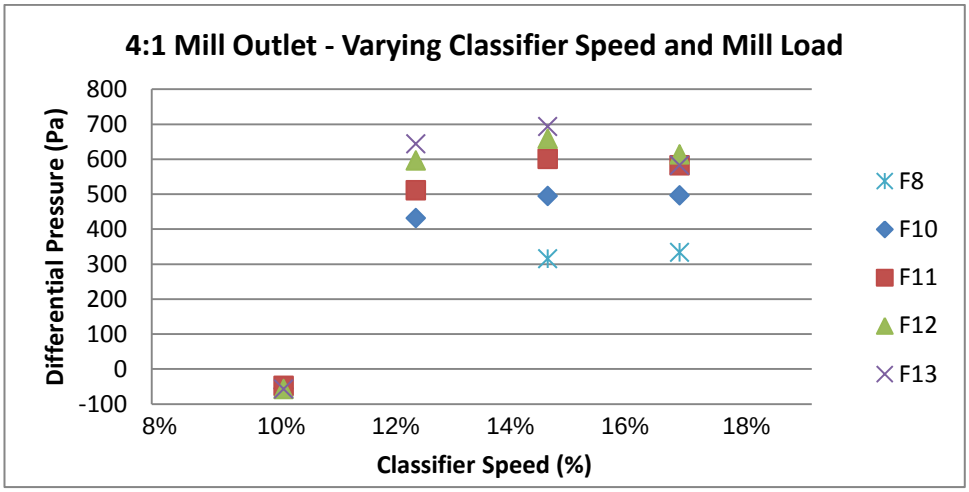

Air/fuel ratio 4:1 - varying classifier speed

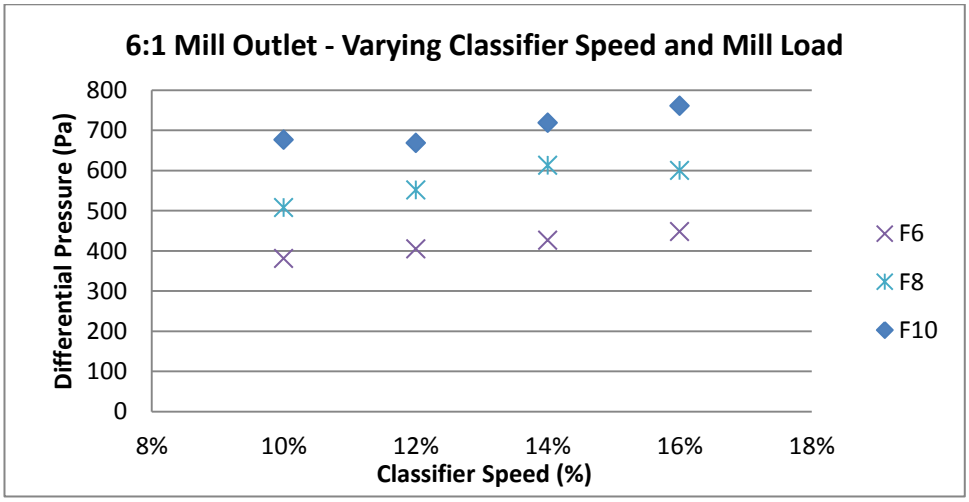

Air/fuel ratio 6:1 - varying classifier speed

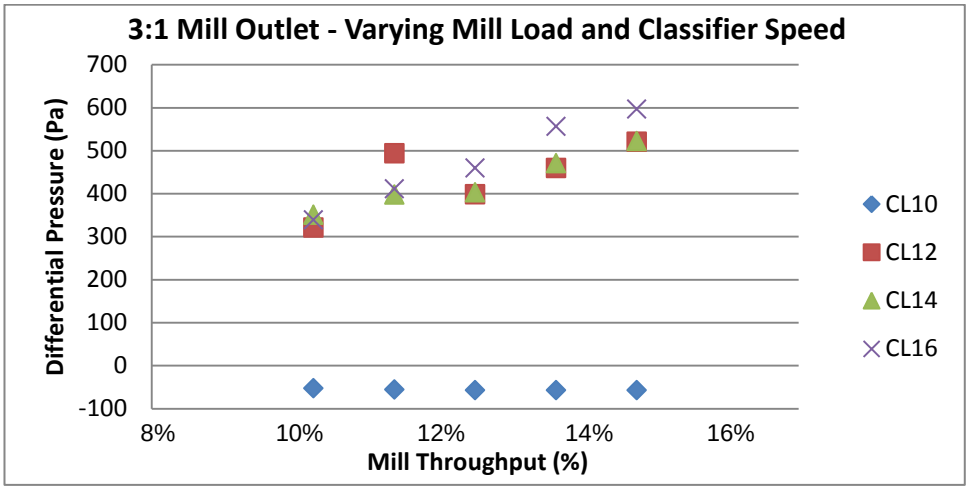

Air/fuel ratio 3:1 - varying mill load

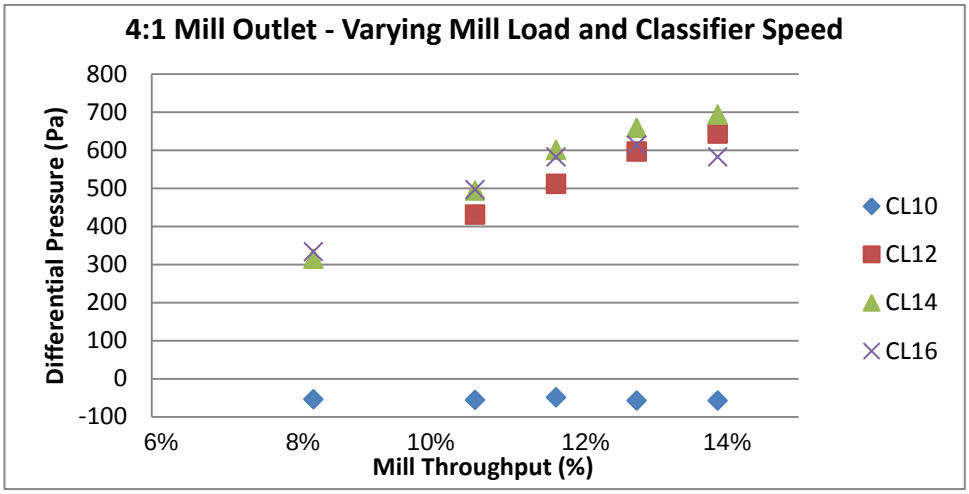

Air/fuel ratio 4:1 - varying mill load

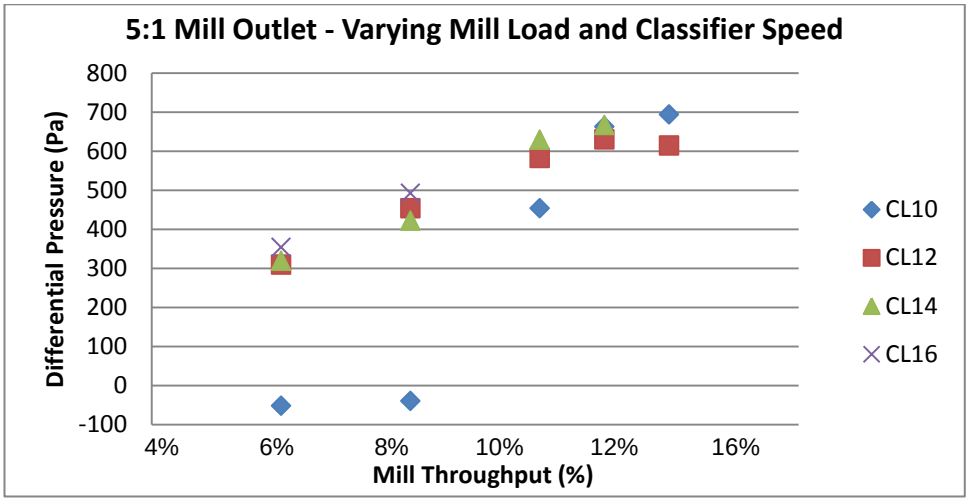

Air/fuel ratio 5:1 - varying mill load

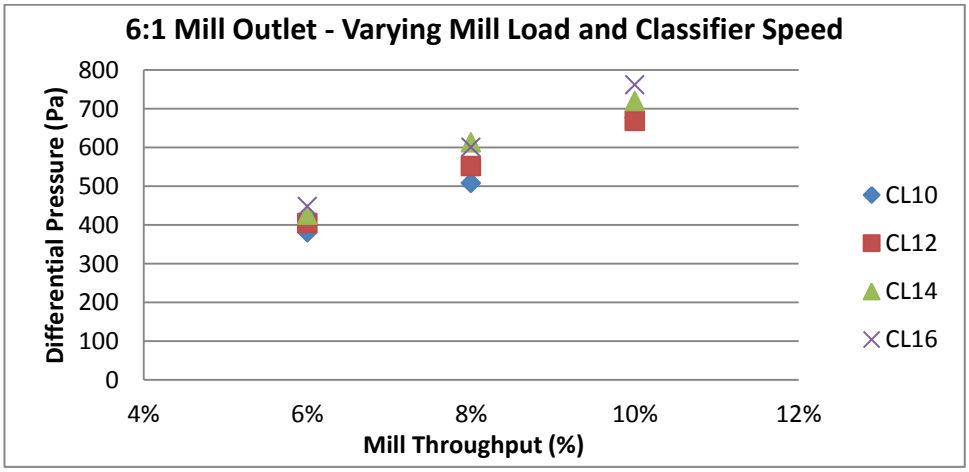

Air/fuel ratio 6:1 - varying mill load

Appendix D: Preliminary Testing

Screw Feeder Characterisation Results

Calculation example:

Feeder = 6 %

$$Mass\ Flow\ 1 = \frac{(Mass\ 1 + Bag) - (Bag)}{Time\ 1}$$

$$Mass\ Flow\ 1 = \frac{(7.43) - (0.14)}{120.86}$$

$$Mass\ Flow\ 1 = 0.06\ kg/s$$

Mass Flow Rate of Coal @ Bulk Density of 1100kg/m3										
Feeder %	Time 1	Mass + Bag	Mass 1	Kg/s 1	Time 2	Mass + Bag	Mass 2	Kg/s 2	Kg/s Average	Kg/h Average
6	120.86	7.43	7.29	0.060318	120.87	7.48	7.34	0.060726	0.060522062	217.8794219
8	120.23	9.32	9.18	0.076354	121.45	9.01	8.87	0.073034	0.074693913	268.8980867
10	121.99	11.72	11.58	0.094926	121.99	11.95	11.81	0.096811	0.095868514	345.1266497
12	121.63	14.39	14.25	0.117159	120.64	15.72	15.58	0.129145	0.123151579	443.3456845
14	121.32	18.47	18.33	0.151088	121	18.96	18.82	0.155537	0.153312611	551.9253991
16	125.45	23.38	23.24	0.185253	122.8	22.37	22.23	0.181026	0.183139574	659.3024655
18	121.23	24.52	24.38	0.201105	121.72	25.89	25.75	0.211551	0.206328219	742.7815881
20	120.58	27.17	27.03	0.224167	120.19	26.88	26.74	0.222481	0.2233238	803.9656801

Coal Bulk Density

Calculation:

$$Relative\ Bulk\ Density = \frac{(Container + Coal) - (Container)}{Container\ Volume}$$

$$Relative\ Bulk\ Density = \frac{8.98 - 3.48}{0.005}$$

$$Relative\ Bulk\ Density = 1100\ kg/m^3$$

Bulk Density		
Container Empty Mass	3.48	kg
Container + Coal Mass	8.98	kg
Container Volume	0.005	m3
Coal Bulk Density	1100	kg/m3

Primary Air Fan Characterisation Results

Calculation:

$$DP\ Ave = \frac{DP1 + DP2 + DP3}{3}$$

$$Air\ Density = \frac{84300}{\left(287.05 \times (273 + Air\ Temperature)\right)}$$

$$Air\ Velocity = \sqrt{\left(\frac{2 \times DP\ Ave}{Air\ Density}\right)}$$

$$Pipe\ Area = \frac{\pi \times (Pipe\ Diameter)^2}{4}$$

$$Mass\ Flow = Air\ Density \times Air\ Velocity \times Pipe\ Area$$

Air Mass Flow – 8% Classifier Speed

Fan Mass Flow Rate Calculation @ 8% Classifier										
% Fan Speed	**DP 1**	**DP 2**	**DP 3**	**DP Ave (Pa)**	**Air Temperature**	**Air Density**	**Air Velocity**	**Pipe Diameter**	**Pipe Area**	**Mass Flow (kg/s)**
12	40	50	50	46.67	104.8	0.78	10.96	0.165	0.021	0.1821
14	50	70	70	63.33	102.6	0.78	12.73	0.165	0.021	0.2128
16	70	90	90	83.33	102.5	0.78	14.60	0.165	0.021	0.2441
18	90	110	110	103.33	104.6	0.78	16.30	0.165	0.021	0.2711
20	100	130	140	123.33	104	0.78	17.79	0.165	0.021	0.2964
22	120	150	160	143.33	104.4	0.78	19.19	0.165	0.021	0.3194
24	160	200	200	186.67	102.9	0.78	21.86	0.165	0.021	0.3652
26	200	230	230	220.00	104	0.78	23.77	0.165	0.021	0.3959
28	230	260	270	253.33	102.8	0.78	25.46	0.165	0.021	0.4255
30	250	300	310	286.67	105.1	0.78	27.17	0.165	0.021	0.4512
32	290	330	330	316.67	103.2	0.78	28.48	0.165	0.021	0.4754
34	330	360	360	350.00	104.6	0.78	30.00	0.165	0.021	0.4989
36	340	380	390	370.00	104.9	0.78	30.86	0.165	0.021	0.5128

38	350	410	410	390.00	104.3	0.78	31.66	0.165	0.021	0.5269
40	370	430	430	410.00	105.3	0.78	32.50	0.165	0.021	0.5395
42	390	440	450	426.67	103.1	0.78	33.06	0.165	0.021	0.5520
44	420	460	470	450.00	103.6	0.78	33.95	0.165	0.021	0.5668
46	450	480	480	470.00	105.5	0.78	34.72	0.165	0.021	0.5789
48	460	500	500	486.67	103.9	0.78	35.42	0.165	0.021	0.5876
50	480	530	530	513.33	104.4	0.78	36.30	0.165	0.021	0.6048
60	530	570	580	560.00	104.7	0.78	37.94	0.165	0.021	0.6312

Air Mass Flow – 17% Classifier Speed

Fan Mass Flow Rate Calculation @ 17% Classifier										
% Fan Speed	**DP 1**	**DP 2**	**DP 3**	**DP Ave (Pa)**	**Air Temperature**	**Air Density**	**Air Velocity**	**Pipe Diameter**	**Pipe Area**	**Mass Flow (kg/s)**
12	40	50	50	46.67	80.1	0.83	10.59	0.165	0.021	0.1884
14	50	70	70	63.33	83.3	0.82	12.40	0.165	0.021	0.2185
16	70	90	90	83.33	91.6	0.81	14.38	0.165	0.021	0.2477
18	100	110	110	106.67	98.2	0.79	16.42	0.165	0.021	0.2778
20	100	120	120	113.33	98.7	0.79	16.94	0.165	0.021	0.2861
22	130	150	150	143.33	99.7	0.79	19.07	0.165	0.021	0.3214
24	150	190	190	176.67	100.9	0.79	21.21	0.165	0.021	0.3562
26	200	220	220	213.33	103.3	0.78	23.38	0.165	0.021	0.3902
28	220	240	240	233.33	103.7	0.78	24.47	0.165	0.021	0.4078
30	240	280	280	266.67	104.1	0.78	26.17	0.165	0.021	0.4358
32	280	300	300	293.33	103.9	0.78	27.44	0.165	0.021	0.4572
34	280	330	330	313.33	104.4	0.78	28.38	0.165	0.021	0.4722
36	300	350	350	333.33	105.1	0.78	29.30	0.165	0.021	0.4866
38	320	380	380	360.00	104.8	0.78	30.43	0.165	0.021	0.5059
40	330	390	390	370.00	103.2	0.78	30.79	0.165	0.021	0.5139
42	340	400	400	380.00	104.6	0.78	31.26	0.165	0.021	0.5199
44	350	410	420	393.33	103.9	0.78	31.77	0.165	0.021	0.5294
46	370	430	440	413.33	102.5	0.78	32.51	0.165	0.021	0.5437
48	390	440	440	423.33	104	0.78	32.97	0.165	0.021	0.5491
50	400	450	460	436.67	104.6	0.78	33.51	0.165	0.021	0.5573
52	420	470	470	453.33	103.8	0.78	34.11	0.165	0.021	0.5684
60	430	510	510	483.33	104.4	0.78	35.25	0.165	0.021	0.5864

Air Mass Flow – 34% Classifier Speed

Fan Mass Flow Rate Calculation @ 34% Classifier										
% Fan Spee	**DP 1**	**DP 2**	**DP 3**	**DP Ave (Pa)**	**Air Temperature**	**Air Density**	**Air Velocity**	**Pipe Diameter**	**Pipe Area**	**Mass Flow (kg/s)**

d										
10	50	60	60	56.67	100.5	0.79	12.01	0.165	0.021	0.2018
15	50	80	80	70.00	98.5	0.79	13.31	0.165	0.021	0.2249
20	100	140	140	126.67	103.2	0.78	18.01	0.165	0.021	0.3007
25	120	190	200	170.00	99.7	0.79	20.77	0.165	0.021	0.3500
30	170	270	280	240.00	102.5	0.78	24.77	0.165	0.021	0.4143
35	190	300	330	273.33	100.8	0.79	26.38	0.165	0.021	0.4431
40	250	360	370	326.67	101.9	0.78	28.88	0.165	0.021	0.4837
45	270	380	400	350.00	102.2	0.78	29.91	0.165	0.021	0.5005
50	300	400	430	376.67	105	0.78	31.14	0.165	0.021	0.5173
55	330	440	460	410.00	103	0.78	32.40	0.165	0.021	0.5411
60	360	460	480	433.33	105	0.78	33.40	0.165	0.021	0.5548

Load lines

Air/Fuel Ratio = 3:1

% Fan	Air kg/s	Air m/s	Coal kg/s	Feeder kg/s	% Feeder	A/F Ratio	3:1	
12	0.1884	10.593	0.0628	0.0605	6	CL 17%	Air	Coal
14	0.2185	12.397	0.0728	0.0747	8	%	20	10
16	0.2477	14.385	0.0826			%	22	11
18	0.2778	16.421	0.0926			%	24	12
20	0.2861	16.938	0.0954	0.0959	10	%	28	13
22	0.3214	19.074	0.1071	0.1095	11	%	32	14
24	0.3562	21.21	0.1187	0.1232	12	%	38	15
26	0.3902	23.382	0.1301					
28	0.4078	24.466	0.1359	0.1382	13			
30	0.4358	26.169	0.1453					
32	0.4572	27.439	0.1524	0.1533	14			
34	0.4722	28.378	0.1574					
36	0.4866	29.297	0.1622					
38	0.5059	30.434	0.1686	0.1682	15			
40	0.5139	30.789	0.1713					
42	0.5199	31.26	0.1733					
44	0.5294	31.774	0.1765					
46	0.5437	32.511	0.1812					
48	0.5491	32.968	0.183	0.1831	16			
50	0.5573	33.51	0.1858					
60	0.5864	35.246	0.1955	0.1947	17			

Air/Fuel Ratio = 4:1

% Fan	Air kg/s	Air m/s	Coal kg/s	Feeder kg/s	% Feeder	A/F Ratio	4:1	
12	0.188	10.59	0.047			CL 17%	Air	Coal
14	0.218	12.40	0.055			%	20	8
16	0.248	14.38	0.062	0.061	6	%	26	10
18	0.278	16.42	0.069			%	30	11
20	0.286	16.94	0.072	0.075	8	%	36	12
22	0.321	19.07	0.080			%	50	13
24	0.356	21.21	0.089					
26	0.390	23.38	0.098	0.096	10			
28	0.408	24.47	0.102					
30	0.436	26.17	0.109	0.110	11			
32	0.457	27.44	0.114					
34	0.472	28.38	0.118					
36	0.487	29.30	0.122	0.123	12			
38	0.506	30.43	0.126					
40	0.514	30.79	0.128					
42	0.520	31.26	0.130					
44	0.529	31.77	0.132					
46	0.544	32.51	0.136					
48	0.549	32.97	0.137					
50	0.557	33.51	0.139	0.138	13			
60	0.586	35.25	0.147	0.153	14			

Air/Fuel Ratio = 5:1

% Fan	Air kg/s	Air m/s	Coal kg/s	Feeder kg/s	% Feeder	A/F Ratio	5:1	
12	0.188	10.59	0.038			CL 17%	Air	Coal
14	0.218	12.40	0.044			%	20	6
16	0.248	14.38	0.050			%	24	8
18	0.278	16.42	0.056			%	34	10
20	0.286	16.94	0.057	0.061	6	%	48	11
22	0.321	19.07	0.064					
24	0.356	21.21	0.071	0.075	8			
26	0.390	23.38	0.078					
28	0.408	24.47	0.082					
30	0.436	26.17	0.087					
32	0.457	27.44	0.091					
34	0.472	28.38	0.094	0.096	10			
36	0.487	29.30	0.097					

38	0.506	30.43	0.101		
40	0.514	30.79	0.103		
42	0.520	31.26	0.104		
44	0.529	31.77	0.106		
46	0.544	32.51	0.109		
48	0.549	32.97	0.110	0.110	11
50	0.557	33.51	0.111	0.123	12
60	0.586	35.25	0.117	0.138	13

Air/Fuel Ratio = 6:1

% Fan	Air kg/s	Air m/s	Coal kg/s	Feeder kg/s	% Feeder	A/F Ratio	6:1	
12	0.188	10.59	0.031			CL 17%	Air	Coal
14	0.218	12.40	0.036			%	24	6
16	0.248	14.38	0.041			%	31	8
18	0.278	16.42	0.046					
20	0.286	16.94	0.048		2			
22	0.321	19.07	0.054		4			
24	0.356	21.21	0.059	0.061	6			
26	0.390	23.38	0.065					
28	0.408	24.47	0.068					
30	0.436	26.17	0.073	0.075	8			
32	0.457	27.44	0.076					
34	0.472	28.38	0.079					
36	0.487	29.30	0.081					
38	0.506	30.43	0.084					
40	0.514	30.79	0.086					
42	0.520	31.26	0.087					
44	0.529	31.77	0.088					
46	0.544	32.51	0.091					
48	0.549	32.97	0.092					
50	0.557	33.51	0.093					
60	0.586	35.25	0.098	0.096	10			

Comparison of Mastersizer and Lab Sieving Results

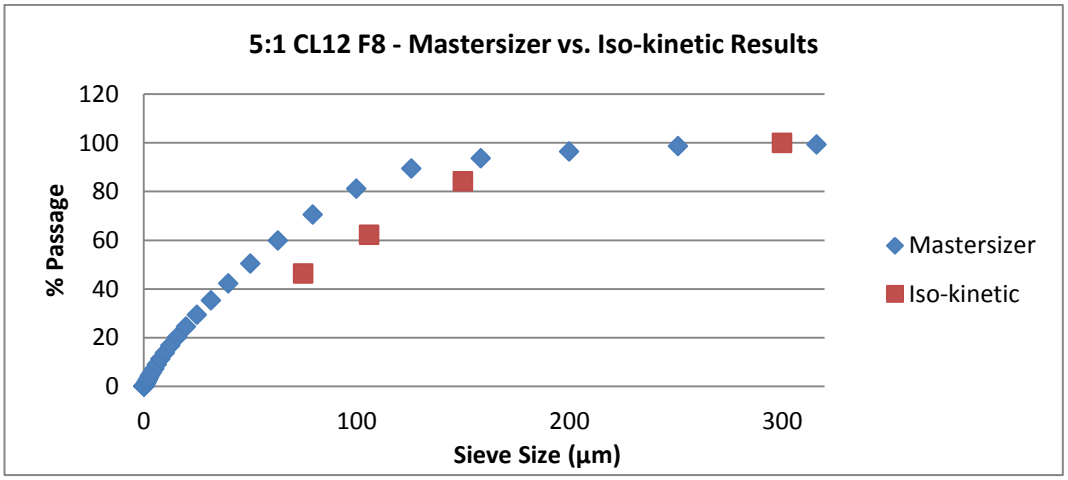

F8 5:1 – Mastersizer vs. physical sieve analysis

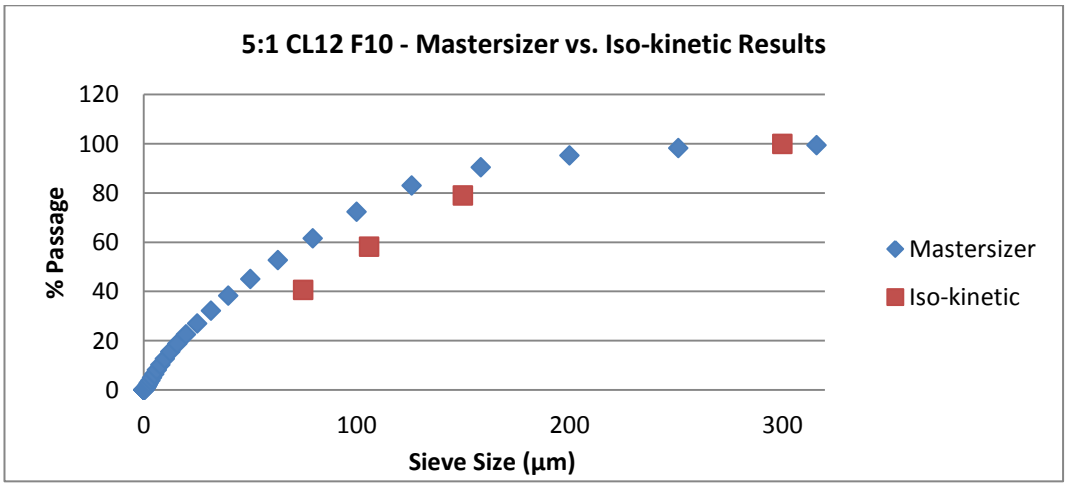

F10 5:1 – Mastersizer vs. physical sieve analysis

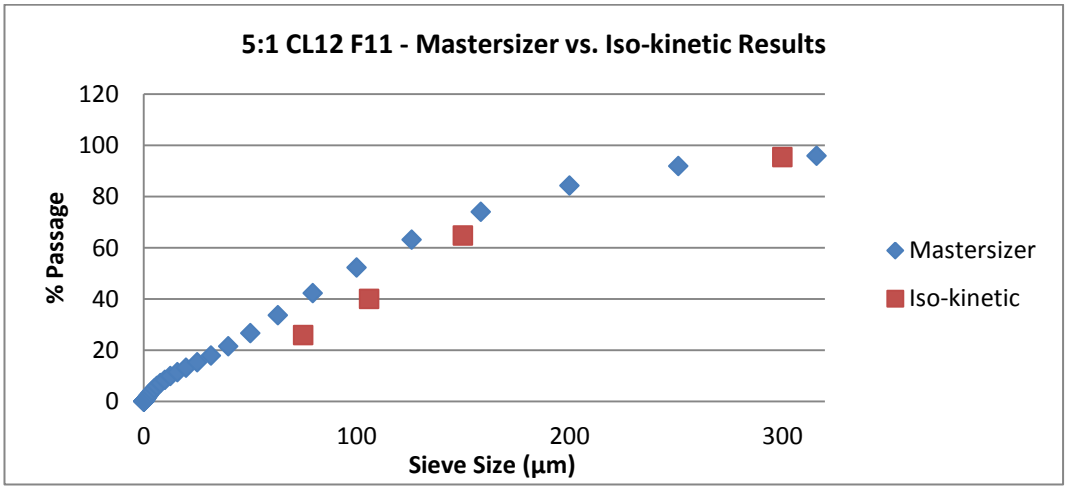

F11 5:1 – Mastersizer vs. physical sieve analysis

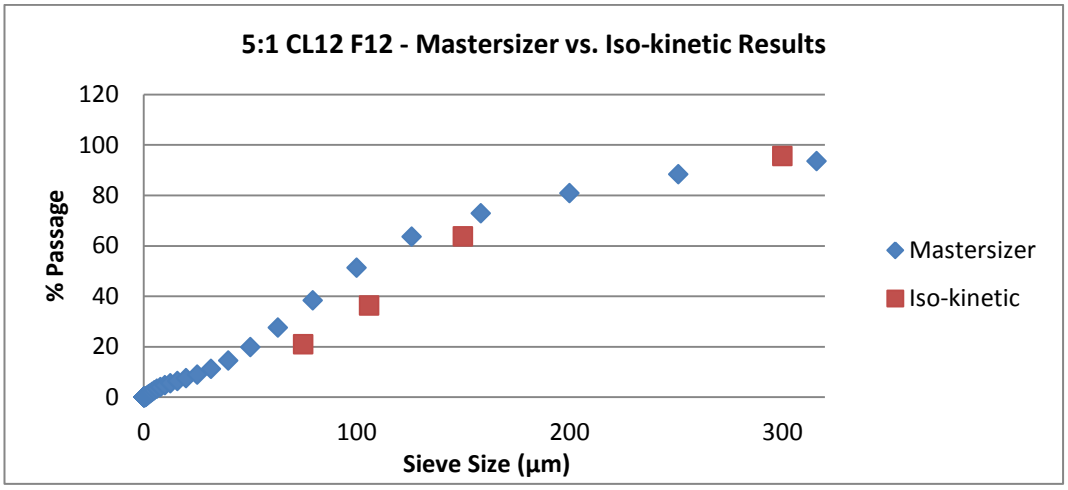

F12 5:1 – Mastersizer vs. physical sieve analysis

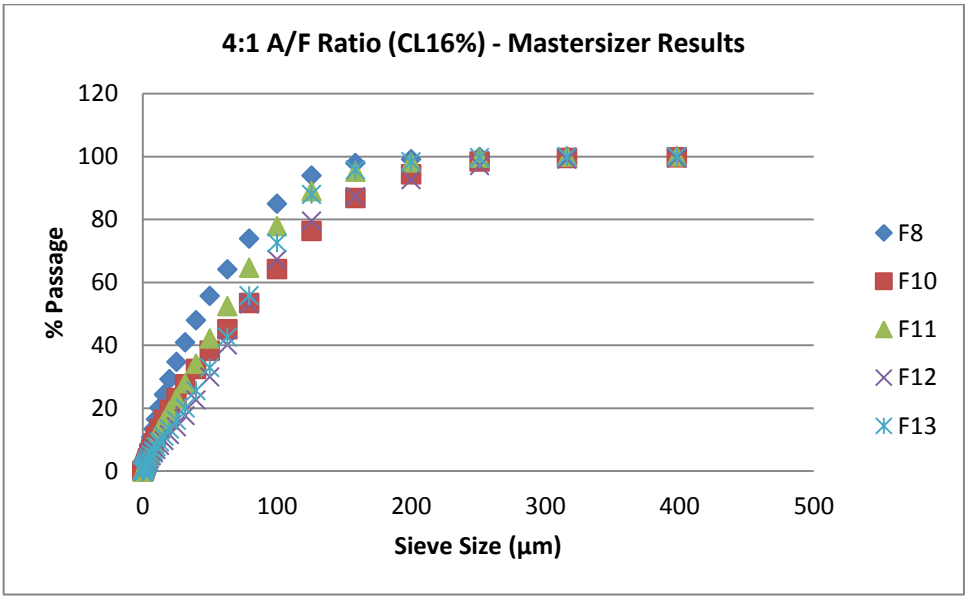

Mastersizer - PF particle size distribution

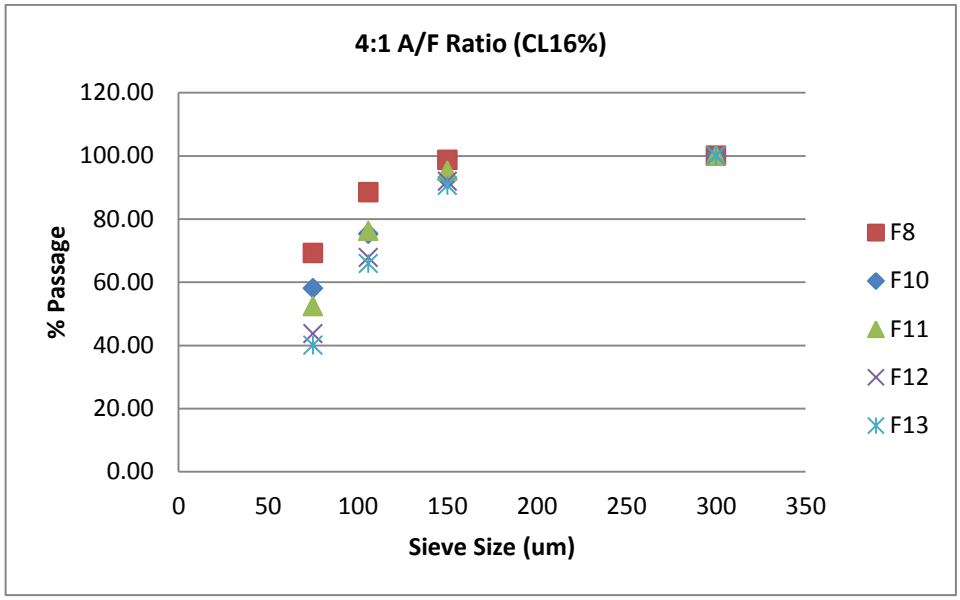

Physical Sieving - PF particle size distribution

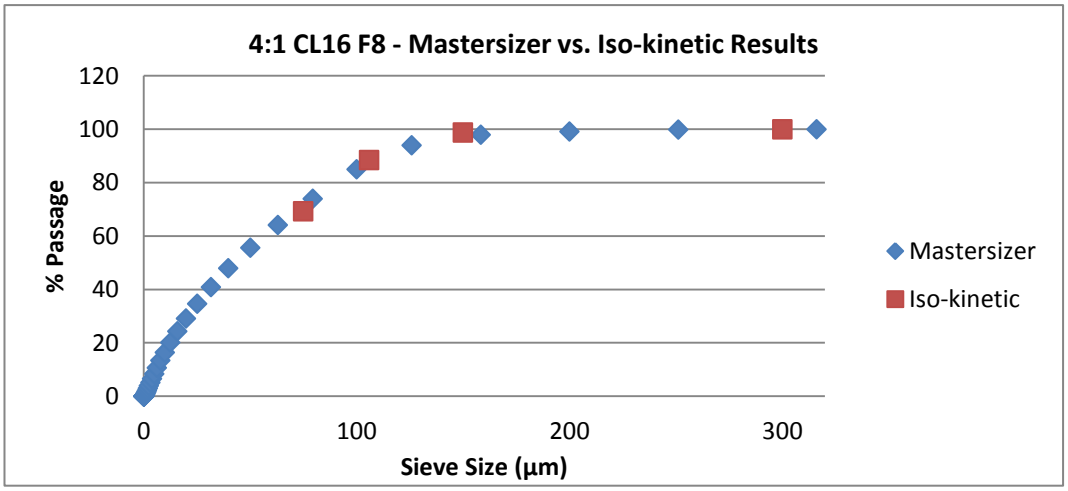

F8 4:1 – Mastersizer vs. physical sieve analysis

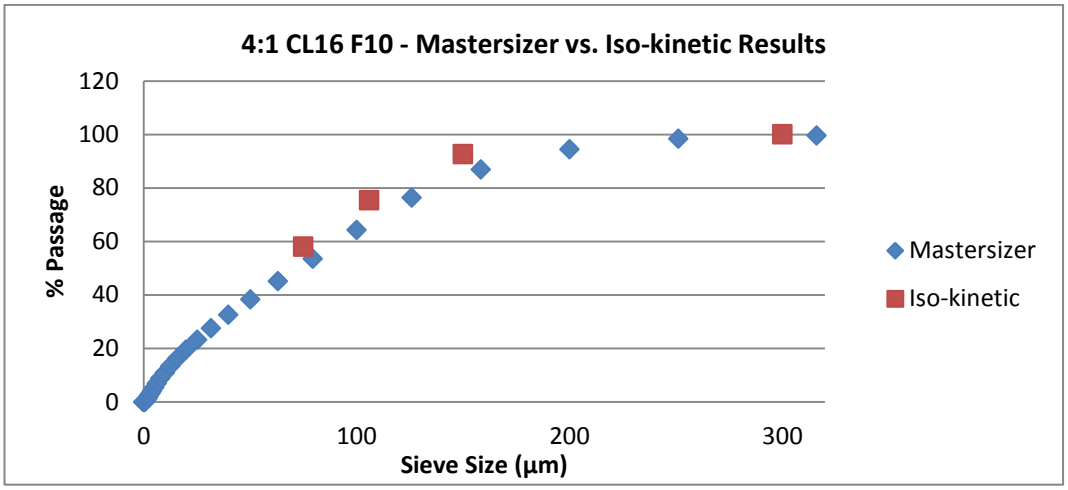

F10 4:1 – Mastersizer vs. physical sieve analysis

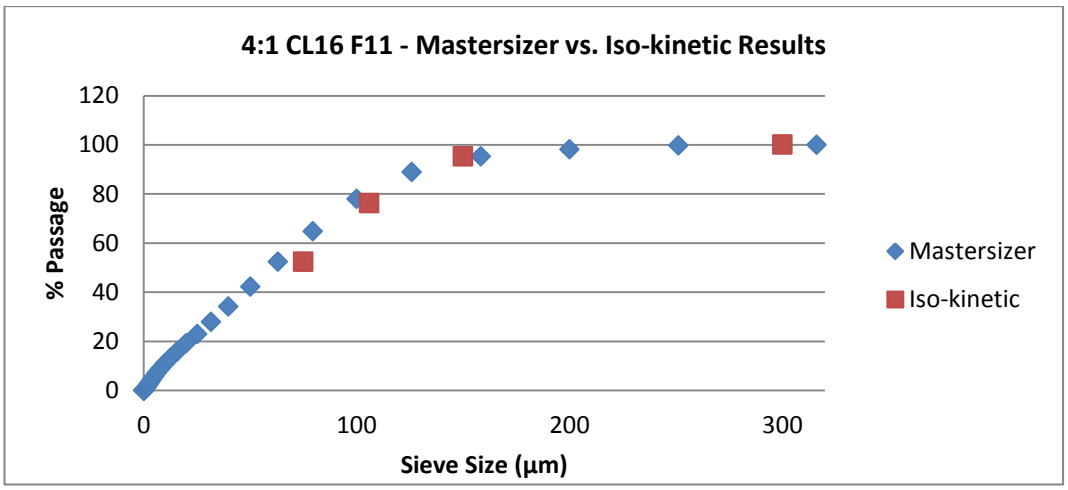

F11 4:1 – Mastersizer vs. physical sieve analysis

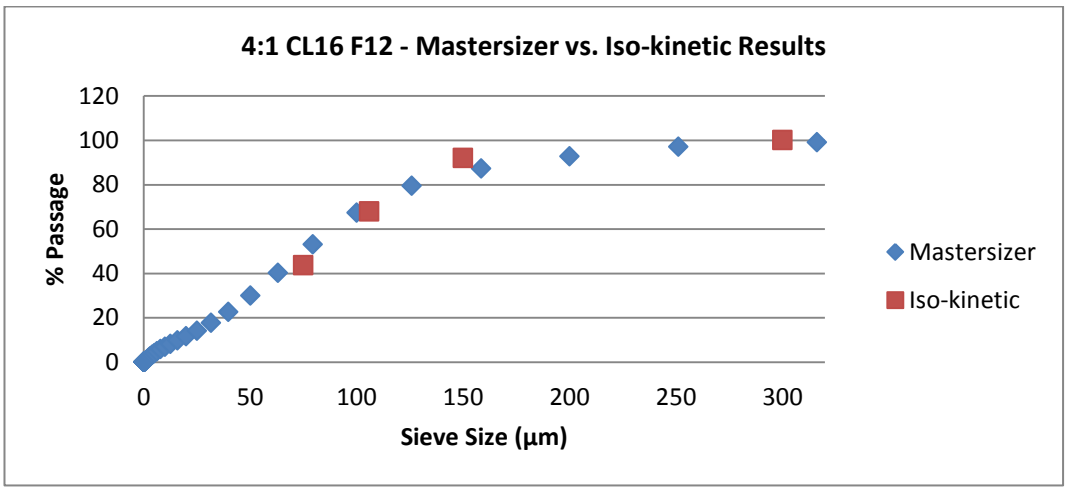

F12 4:1 – Mastersizer vs. physical sieve analysis

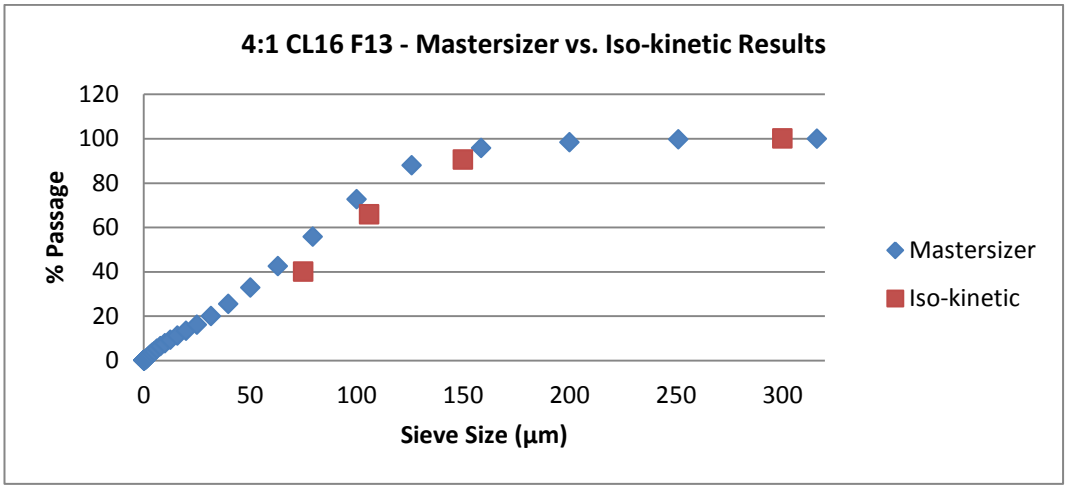

F13 4:1 – Mastersizer vs. physical sieve analysis

Appendix E: Final Testing

Varying Classifier Speed:

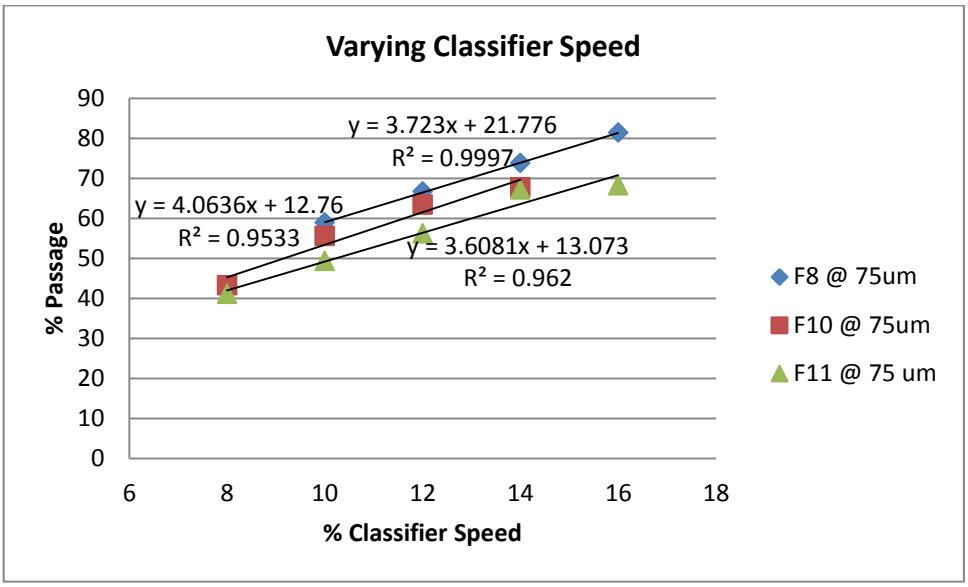

F8:

$$y = 3.723x + 21.776$$

F10:

$$y = 4.0636x + 12.76$$

F11:

$$y = 3.6081x + 13.073$$

$$\text{Average gradient} = \frac{3.732 + 4.0636 + 3.6081}{3} = 3.8$$

Appendix F: Mill Optimisation

Performance for current mill load line and operating conditions:

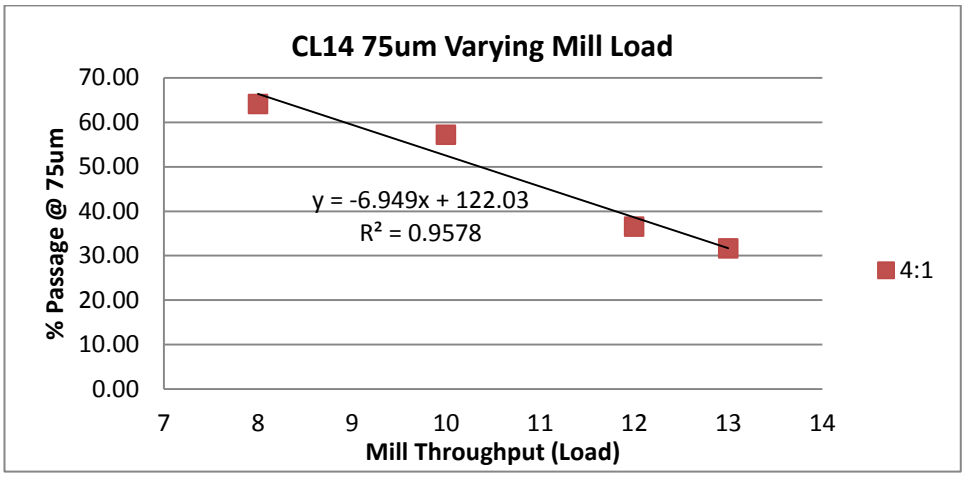

Performance at current mill load conditions

F8:

$$Particle\ Fineness = -6.949(Load) + 122.03$$

$$= -6.949(8) + 122.03$$

$$= 66.43\%\ @\ 75\mu m$$

F10:

$$Particle\ Fineness = -6.949(Load) + 122.03$$

$$= -6.949(10) + 122.03$$

$$= 52.54\%\ @\ 75\mu m$$

F11:

$$Particle\ Fineness = -6.949(Load) + 122.03$$

$$= -6.949(11) + 122.03$$

$$= 45.59\%\ @\ 75\mu m$$

Performance for 'reduced A/F ratio' mill load line:

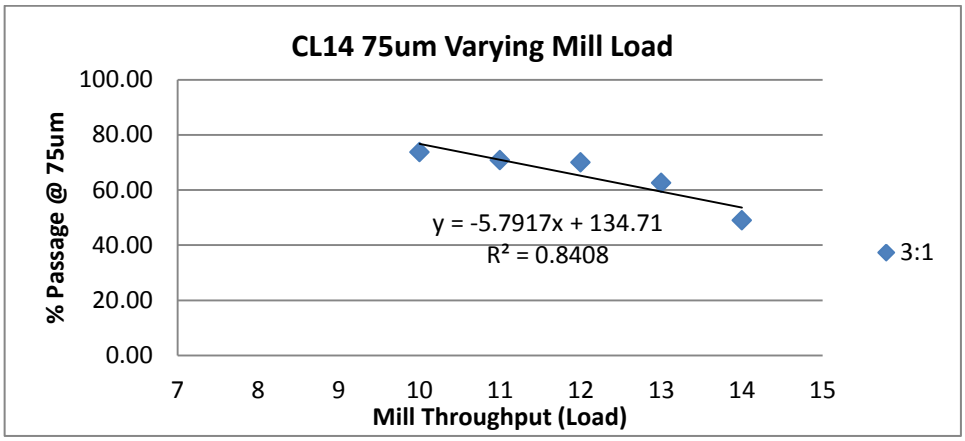

Performance at Reduced A/F Ratio conditions

F10:

$$Particle\ Fineness = -5.7917(Load) + 134.71$$

$$= -5.7917(10) + 134.71$$

$$= 76.79\% @ 75\mu m$$

F11:

$$Particle\ Fineness = -5.7917(Load) + 134.71$$

$$= -5.7917(11) + 134.71$$

$$= 70.99\% @ 75\mu m$$

F12:

$$Particle\ Fineness = -5.7917(Load) + 134.71$$

$$= -5.7917(12) + 134.71$$

$$= 65.21\% @ 75\mu m$$

Performance for 'reduced A/F ratio' and 'increased classifier speed' mill load line:

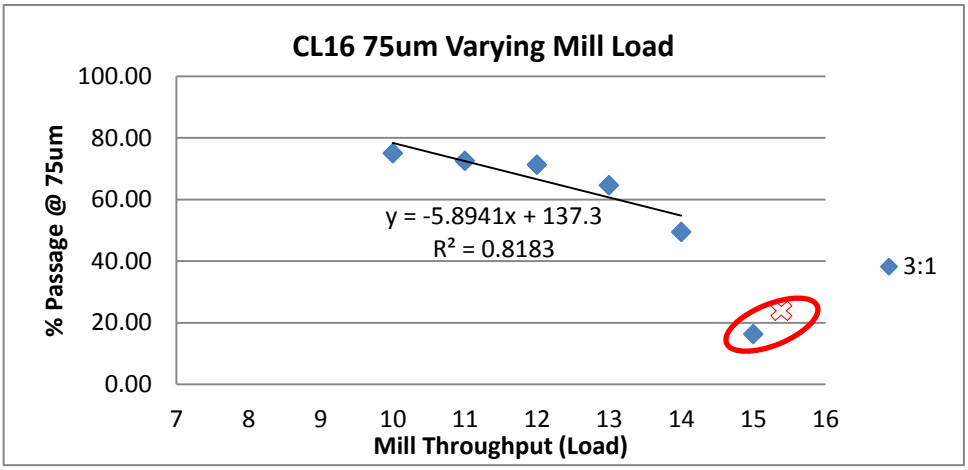

Performance at Reduced A/F Ratio and Increased Classifier Speed Conditions

F13:

$$Particle\ Fineness = -5.8941(Load) + 137.3$$

$$= -5.8941(13) + 137.3$$

$$= 60.67\%\ @\ 75\mu m$$

F12:

$$Particle\ Fineness = -5.8941(Load) + 137.3$$

$$= -5.8941(12) + 137.3$$

$$= 66.57\%\ @\ 75\mu m$$

F11:

$$Particle\ Fineness = -5.8941(Load) + 137.3$$

$$= -5.8941(11) + 137.3$$

$$= 72.46\%\ @\ 75\mu m$$

F10:

$$Particle\ Fineness = -5.8941(Load) + 137.3$$

$$= -5.8941(10) + 137.3$$

$$= 78.36\% @ 75\mu m$$

Performance for 'reduced A/F ratio' and 'decreased classifier speed' mill load line:

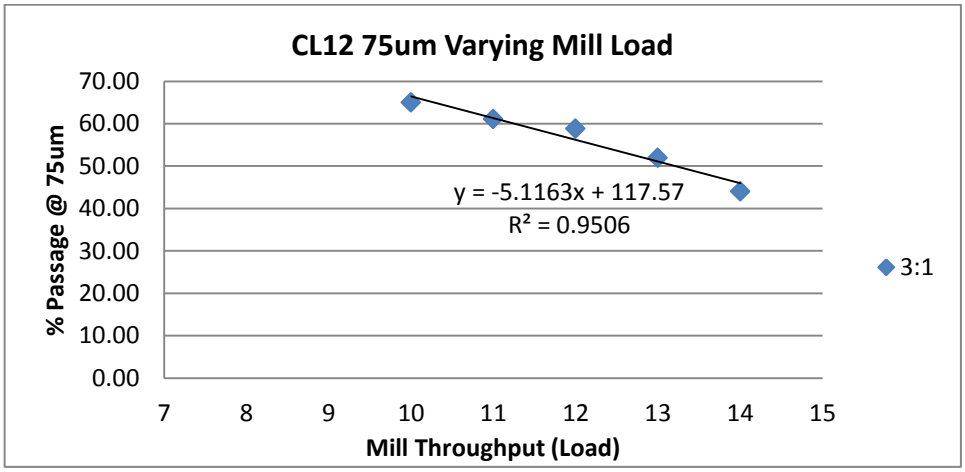

Performance at Reduced A/F Ratio and Decreased Classifier Speed Conditions

F10:

$$Particle\ Fineness = -5.1163(Load) + 117.57$$

$$= -5.1163(10) + 117.57$$

$$= 66.41\% @ 75\mu m$$

Appendix G: Instrument Specification and Calibration Certificates

Particle Size Analyser - Data Sheet

Technical data of the measurement system IPP70

(This general technical data applies to the special types IPP 70-S, IPP 70-Se, IPP 70-SL, IPP 70-SLe)

Particle-size measurement range :	50 µm to 6000 µm
Velocity measurement range :	0,01 m/s to 50 m/s
Particle concentration:	200 .... 120 000 ppm volume content (dependent on particle size and velocity)
Data rate:	up to ca. 20.000 particles/sec (depending on process)
Data output:	Distributions and characteristic particle properties as ASCII file (text file, Excel-compatible)
Optional interfaces:	Current interface 4...20 mA TCP/IP-interface, OPC-Server
Temperature range:	-20°C to 100°C at the probe's sensing volume in continuous operation; -20 °C to 60 °C on probe housing
Pressure range:	4 bar (at the probes sensing volume)
Degree of protection:	IP 65 (probe and electronics housing)
Operating voltage: Probe current:	12V, DC, ⎓ typ. 150 mA (max. 210mA)
Materials:	
media-contacting parts:	stainless steel 316L (probe head, probe tube) (DIN 1.4404; 1.4435) crystalline sapphire (optical windows) epoxy resin (contact point steel-sapphire)
Housing material IPP 70-S, IPP 70-Se:	pressure-cast aluminium, powder-coated
Housing material IPP 70-SL, IPP 70-SLe:	stainless steel 316L (DIN 1.4404; 1.4435)

parsum® - Gesellschaft für Partikel-, Strömungs- und Umweltmeßtechnik mbH
Reichenhainer Straße 34 – 36, 09126 Chemnitz, Germany
Tel. +49(0)371/26758690, Fax +49(0)371/26758699, Email: info@parsum.de, Internet: www.parsum.de

Siemens Pressure Transducer – Data Sheet

Technical data of the measurement system IPP70

(This general technical data applies to the special types IPP 70-S, IPP 70-Se, IPP 70-SL, IPP 70-SLe)

Particle-size measurement range :	50 µm to 6000 µm
Velocity measurement range :	0,01 m/s to 50 m/s
Particle concentration:	200 .... 120 000 ppm volume content (dependent on particle size and velocity)
Data rate:	up to ca. 20.000 particles/sec (depending on process)
Data output:	Distributions and characteristic particle properties as ASCII file (text file, Excel-compatible)
Optional interfaces:	Current interface 4...20 mA TCP/IP-interface, OPC-Server
Temperature range:	-20°C to 100°C at the probe's sensing volume in continuous operation; -20 °C to 60 °C on probe housing
Pressure range:	4 bar (at the probes sensing volume)
Degree of protection:	IP 65 (probe and electronics housing)
Operating voltage: Probe current:	12V, DC, ⎓ typ. 150 mA (max. 210mA)
Materials:	
media-contacting parts:	stainless steel 316L (probe head, probe tube) (DIN 1.4404; 1.4435) crystalline sapphire (optical windows) epoxy resin (contact point steel-sapphire)
Housing material IPP 70-S, IPP 70-Se:	pressure-cast aluminium, powder-coated
Housing material IPP 70-SL, IPP 70-SLe:	stainless steel 316L (DIN 1.4404; 1.4435)

parsum® - Gesellschaft für Partikel-, Strömungs- und Umweltmeßtechnik mbH
Reichenhainer Straße 34 – 36, 09126 Chemnitz, Germany
Tel. +49(0)371/26758690, Fax +49(0)371/26758699, Email: info@parsum.de, Internet: www.parsum.de

Influence of static pressure	
• on the zero point	≤ (0.15* r) % per 100 bar (1450 psi)
- 20 mbar (0.29 psi)-measuring cell	≤ (0.15 % r)% per 32 bar (464 psi)
• on the span	≤ 0.2% je 100 bar (1450 psi)
- 20 mbar (0.29 psi)-measuring cell	≤ 0.2% je 32 bar (464 psi)
Rated operating conditions	
Degree of protection (to EN 60529)	IP65
Process temperature	
• Measuring cell, silicon oil filling	-40 to +100°C (-40 to +212°F)
• Measuring cell, inert filling liquid	-20 to +100°C (-4 to +212°F)
• In conjunction with dust explosion protection	-20 to +60°C (-4 to +140°F)
Ambient conditions	
• Ambient temperature, digital indicators	-30 to +85°C (-22 to +185°F)
• Storage temperature	-50 to +85°C (-58 to +185°F)
• Climatic class, condensation	Permissible
• Electromagnet compatibility	To EN 61326 and NAMUR NE 21
Design	
Weight, approximate, without options	4.5 kg (9.9 lb)
Housing material	Low copper die-cast aluminum, GD-AlSi 12 or stainless steel precision casing, mat. No. 1.4408
Wetted parts materials	
• Seal diaphragm	Stainless steel, mat. No. 1.4404/316L or Hastelloy C276, mat. No. 2.4819, Monel, mat. No. 2.4360, tantalum or gold
Measuring cell filling	Silicone oil or inert filling liquid; max. 160 bar g (2320 psi g) with oxygen measurement
Process connection	Female thread 1/4-18 NPT and flange connection with mounting thread M10 to DIN 19213 or 7/16-20 UNF to EN 61518
Power Supply U_H	
Terminal voltage at transmitter	10.5 to 45 Vdc 10.5 to 30 Vdc in intrinsically-safe mode
Certificate and approvals	See Table 9-20
HART communication	
HART communication	230 to 1100 Ω
Protocol	HART Version 5.x
Software for computer	SIMATIC PDM

75µm Sieve – Certificate of Examination

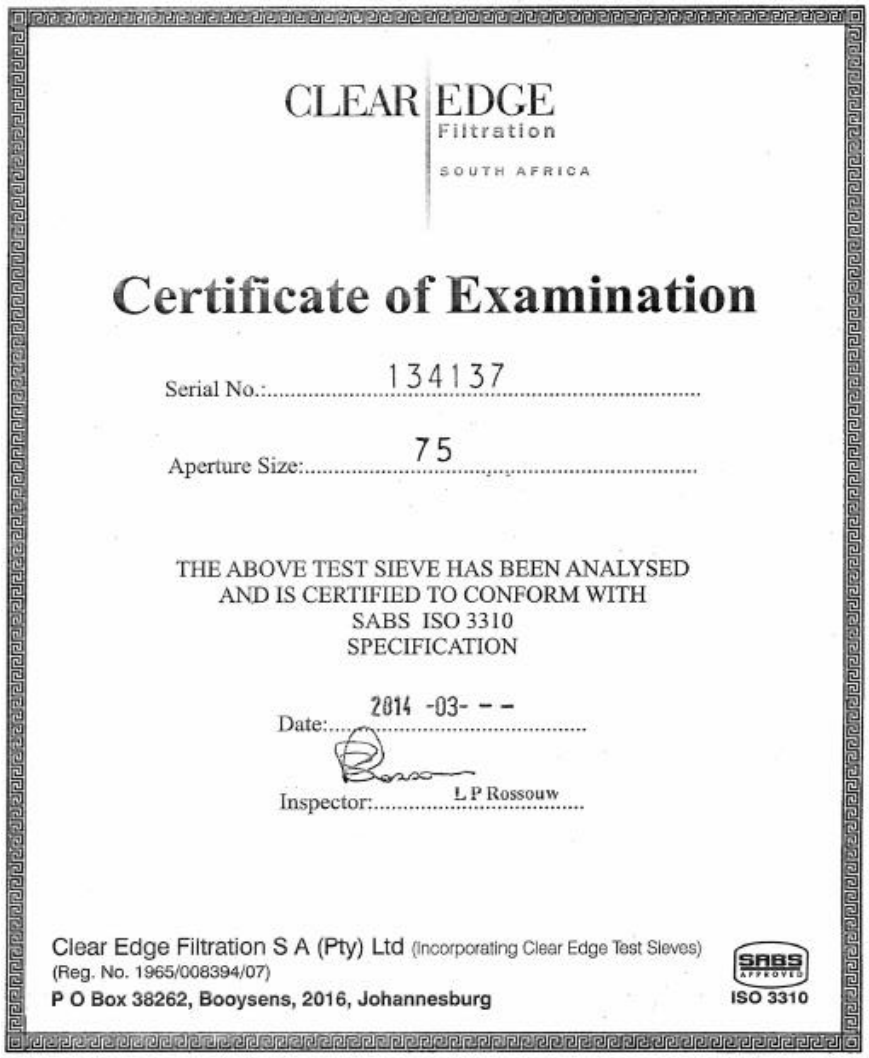

CLEAR EDGE
Filtration
SOUTH AFRICA

Certificate of Examination

Serial No.: 134137

Aperture Size: 75

THE ABOVE TEST SIEVE HAS BEEN ANALYSED
AND IS CERTIFIED TO CONFORM WITH
SABS ISO 3310
SPECIFICATION

Date: 2014 -03- - -

Inspector: L P Rossouw

Clear Edge Filtration S A (Pty) Ltd (Incorporating Clear Edge Test Sieves)
(Reg. No. 1965/008394/07)
P O Box 38262, Booysens, 2016, Johannesburg

SABS APPROVED
ISO 3310

106µm Sieve – Certificate of Examination

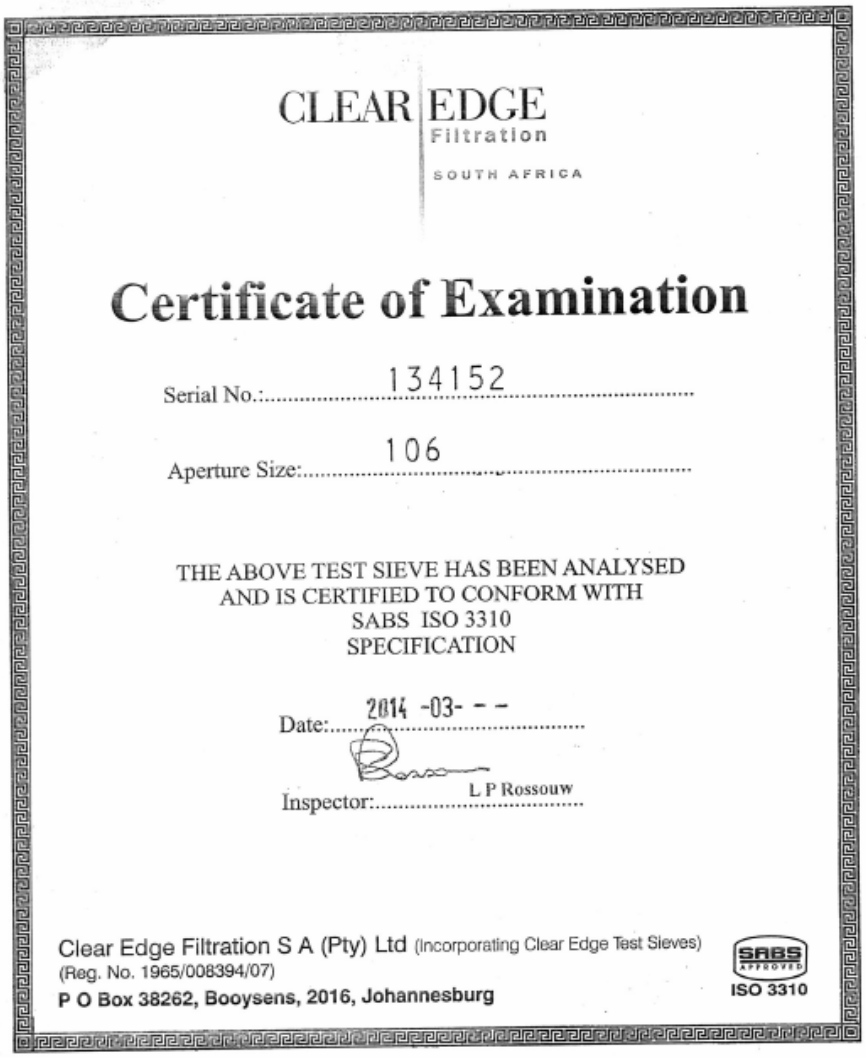

CLEAR EDGE
Filtration
SOUTH AFRICA

Certificate of Examination

Serial No.: 134152

Aperture Size: 106

THE ABOVE TEST SIEVE HAS BEEN ANALYSED
AND IS CERTIFIED TO CONFORM WITH
SABS ISO 3310
SPECIFICATION

Date: 2014 -03- - -

Inspector: L P Rossouw

Clear Edge Filtration S A (Pty) Ltd (Incorporating Clear Edge Test Sieves)
(Reg. No. 1965/008394/07)
P O Box 38262, Booysens, 2016, Johannesburg

SABS APPROVED
ISO 3310

150µm Sieve – Certificate of Examination

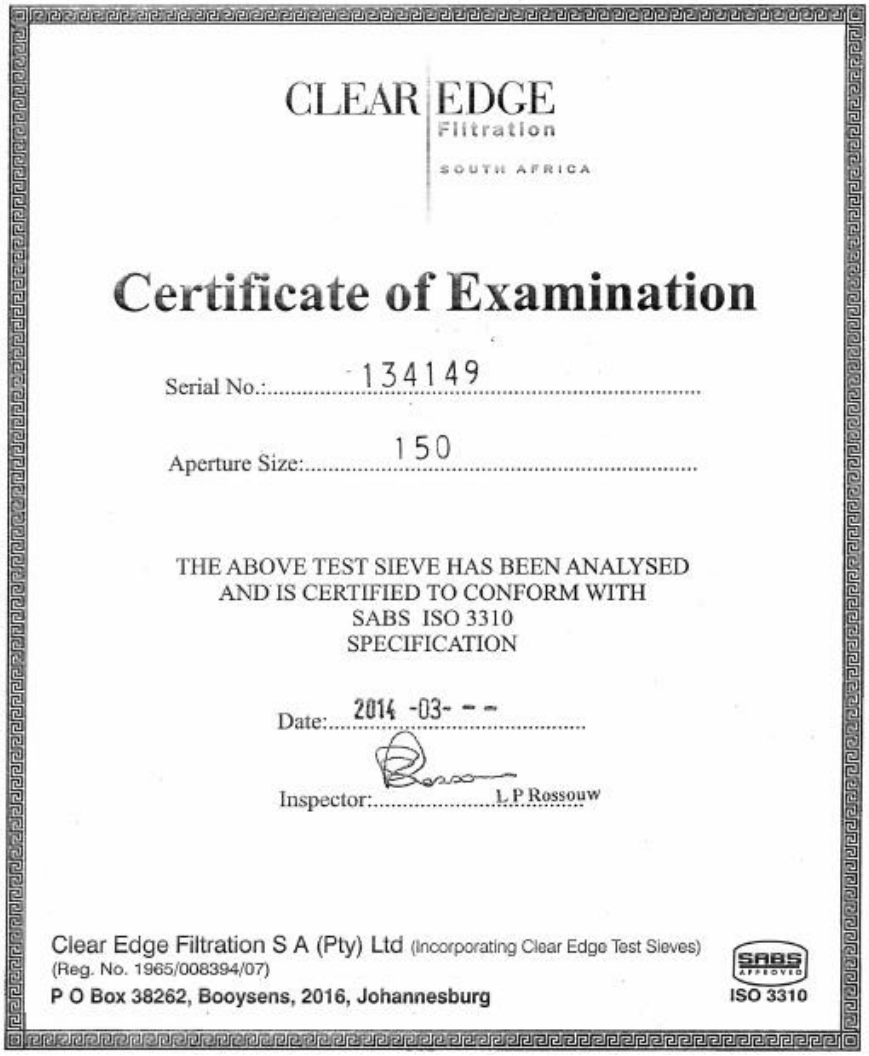

CLEAR EDGE
Filtration
SOUTH AFRICA

Certificate of Examination

Serial No.: 134149

Aperture Size: 150

THE ABOVE TEST SIEVE HAS BEEN ANALYSED
AND IS CERTIFIED TO CONFORM WITH
SABS ISO 3310
SPECIFICATION

Date: 2014 -03- - -

Inspector: L P Rossouw

Clear Edge Filtration S A (Pty) Ltd (Incorporating Clear Edge Test Sieves)
(Reg. No. 1965/008394/07)
P O Box 38262, Booysens, 2016, Johannesburg

SABS APPROVED
ISO 3310

300µm Sieve – Certificate of Examination

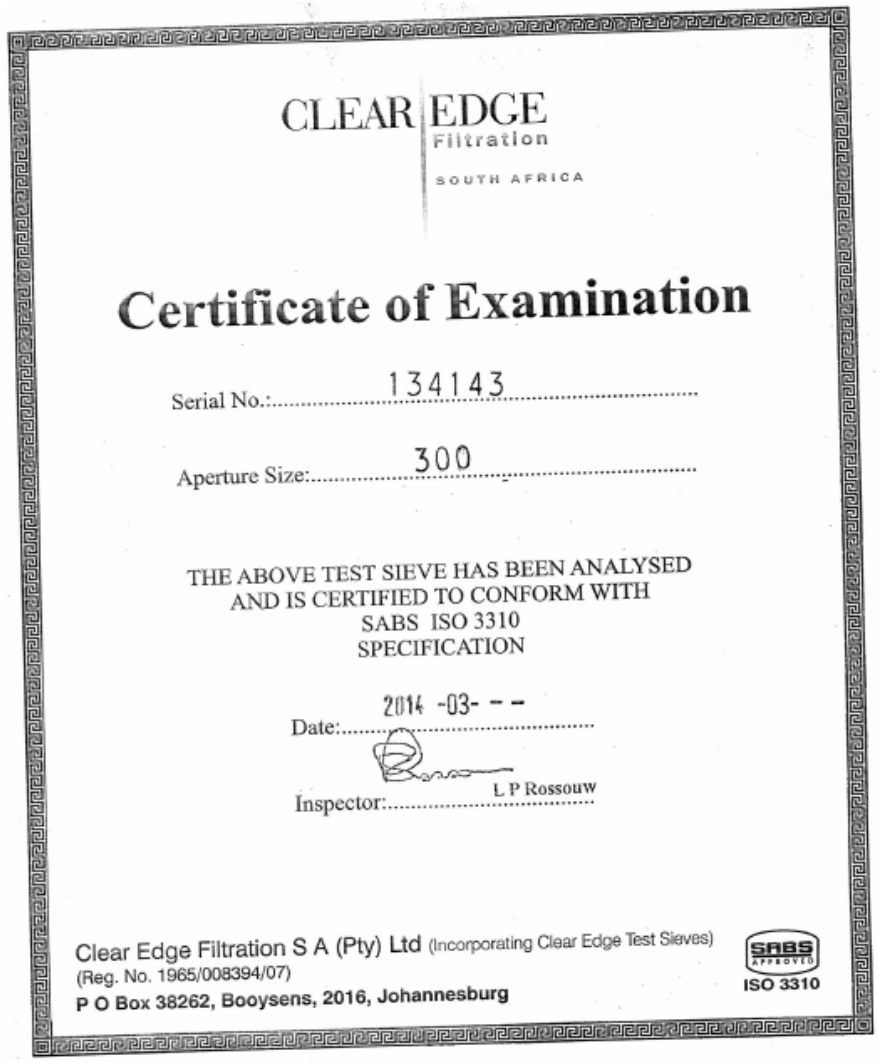

CLEAR EDGE
Filtration
SOUTH AFRICA

Certificate of Examination

Serial No.: 134143

Aperture Size: 300

THE ABOVE TEST SIEVE HAS BEEN ANALYSED
AND IS CERTIFIED TO CONFORM WITH
SABS ISO 3310
SPECIFICATION

Date: 2014 -03- - -

Inspector: L P Rossouw

Clear Edge Filtration S A (Pty) Ltd (Incorporating Clear Edge Test Sieves)
(Reg. No. 1965/008394/07)
P O Box 38262, Booysens, 2016, Johannesburg

SABS APPROVED
ISO 3310

Balance – Calibration Certificates

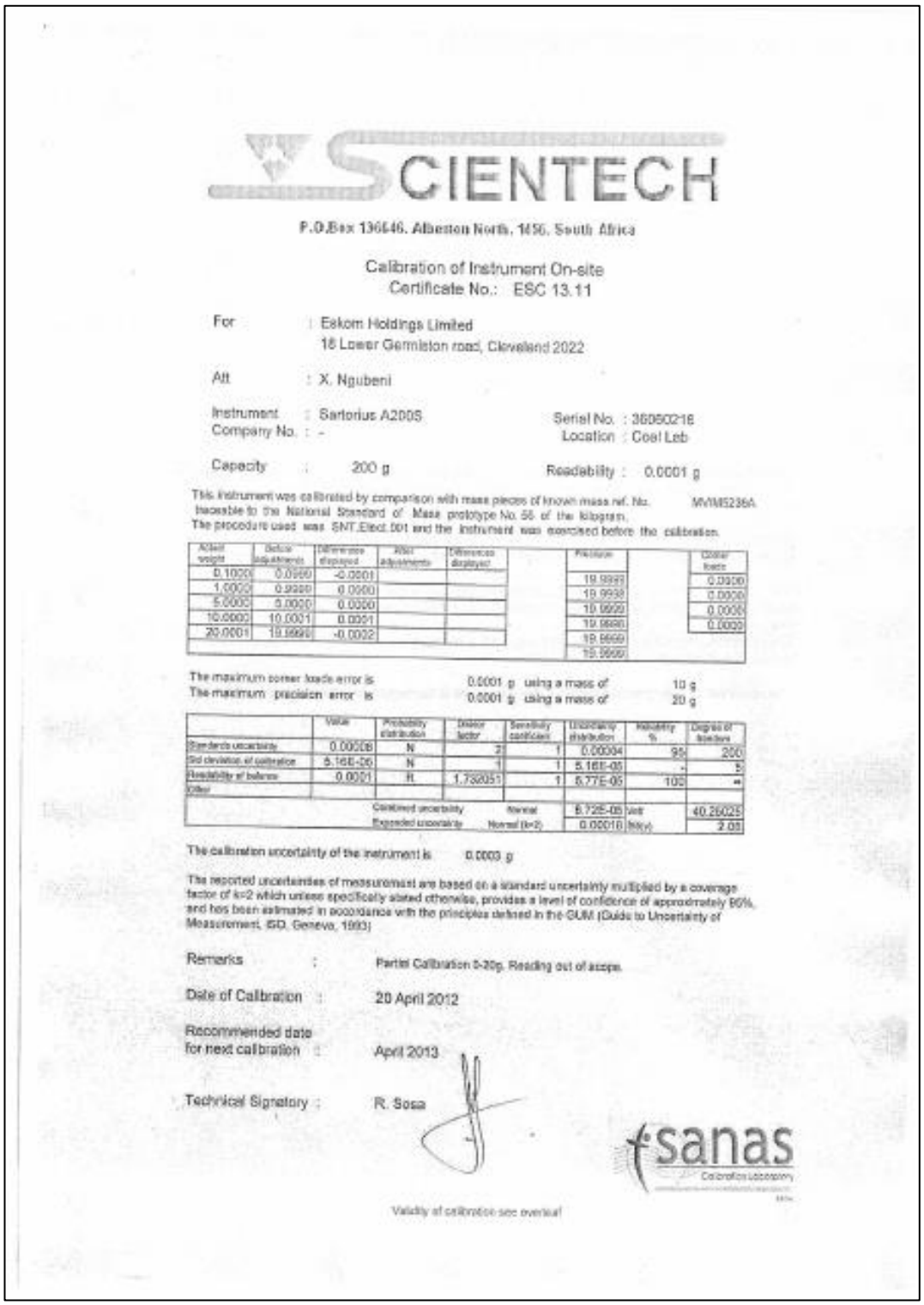

SCIENTECH

P.O.Box 136646, Alberton North, 1456, South Africa

Calibration of Instrument On-site
Certificate No.: ESC 13.11

For : Eskom Holdings Limited
16 Lower Germiston road, Cleveland 2022

Att : X. Ngubeni

Instrument : Sartorius A200S
Company No. : -
Serial No. : 36060216
Location : Coal Lab

Capacity : 200 g
Readability : 0.0001 g

This instrument was calibrated by comparison with mass pieces of known mass ref. No. MVM5236A traceable to the National Standard of Mass prototype No. 56 of the kilogram.
The procedure used was SNT.Elect.001 and the instrument was operated before the calibration.

Actual weight	Before adjustment	Difference displayed	After adjustment	Difference displayed	Precision	Corner loads
0.1000	0.0999	-0.0001			19.9999	0.0000
1.0000	0.9999	0.0000			19.9999	0.0000
5.0000	5.0000	0.0000			19.9999	0.0000
10.0000	10.0001	0.0001			19.9999	0.0000
20.0001	19.9999	-0.0002			19.9999	
					19.9999	

The maximum corner loads error is 0.0001 g using a mass of 10 g
The maximum precision error is 0.0001 g using a mass of 20 g

	Value	Probability distribution	Divisor factor	Sensitivity coefficient	Uncertainty distribution	Reliability %	Degrees of freedom
Standards uncertainty	0.00008	N	2	1	0.00004	95	200
Std deviation of calibration	5.16E-05	N	1	1	5.16E-05	-	5
Readability of balance	0.0001	R	1.732051	1	5.77E-05	100	∞
Other							
		Combined uncertainty		Normal	8.72E-05	Veff	40.26025
		Expanded uncertainty		Normal (k=2)	0.00018	Ni(y)	2.05

The calibration uncertainty of the instrument is 0.0003 g

The reported uncertainties of measurement are based on a standard uncertainty multiplied by a coverage factor of k=2 which unless specifically stated otherwise, provides a level of confidence of approximately 95%, and has been estimated in accordance with the principles defined in the GUM (Guide to Uncertainty of Measurement, ISO, Geneva, 1993)

Remarks : Partial Calibration 0-20g. Reading out of scope.

Date of Calibration : 20 April 2012

Recommended date for next calibration : April 2013

Technical Signatory : R. Sosa

sanas Calibration Laboratory

Validity of calibration see overleaf

SCIENTECH

P.O.Box 136646, Alberton North, 1456, South Africa

Calibration of Instrument On-site
Certificate No.: ESC 13.11

For : Eskom Holdings Limited
18 Lower Germiston road, Cleveland 2022

Att : X. Ngubeni

Instrument : Sartorius A200S
Company No. : -

Serial No. : 39060216
Location : Coal Lab

Capacity : 200 g

Readability : 0.0001 g

This instrument was calibrated by comparison with mass pieces of known mass set No. MWM5535 traceable to the National Standard of Mass prototype No. 56 of the kilogram.
The procedure used was SNT Elect 001 and the instrument was exercised before the calibration.

Actual weight	Before adjustment	Difference displayed	After adjustment	Difference displayed	Precision	Linear Both
0.1000	0.0990	-0.0001			19.9999	0.0000
1.0005	0.9990	-0.0005			19.9999	0.0000
5.0000	4.9997	-0.0003			19.9999	0.0000
9.9990	9.9985	-0.0001			19.9999	0.0000
19.9990	19.9990	0.0000			19.9999	
					19.9999	

The maximum corner loads error is 0.0001 g using a mass of 10 g
The maximum precision error is 0.0001 g using a mass of 20 g

	Value	Probability distribution	Divisor factor	Sensitivity coefficient	Uncertainty distribution	Reliability %	Degree of freedom
Standards uncertainty	0.00006	N	2	1	0.00003	95	200
Std deviation of calibration	0	N	1	1	0	-	5
Readability of balance	0.0001	R	1.732051	1	5.77E-05	100	∞
Other							
		Combined uncertainty		Normal	7.02E-05	Ref	1901.389
		Expanded uncertainty		Normal (k=2)	0.00014	Ref	2

The calibration uncertainty of the instrument is 0.0003 g

The reported uncertainties of measurement are based on a standard uncertainty multiplied by a coverage factor of k=2 which unless specifically stated otherwise, provides a level of confidence of approximately 95%, and has been estimated in accordance with the principles defined in the GUM (Guide to Uncertainty of Measurement, ISO, Geneva, 1993)

Remarks : Partial Calibration 0-20g. Reading out of scope.

Date of Calibration : 17 April 2013

Recommended date for next calibration : April 2014

Technical Signatory : R. Sosa

sanas

Validity of calibration see overleaf

SCIENTECH

P.O.Box 136646. Alberton North. 1456. South Africa

Calibration of Instrument On-site
Certificate No.: ESC 13.13

For : Eskom Holdings Limited
16 Lower Germiston road, Cleveland 2022

Att : X. Nguberi

Instrument : Sartorius A200S Serial No. : 39060216
Company No. : - Location : Coal Lab

Capacity : 200 g Readability : 0.0001 g

This instrument was calibrated by comparison with mass pieces of known mass ref. No. MVM49035 traceable to the National Standard of Mass prototype No.56 of the kilogram.
The procedure used was SNT.Elect.001 and the instrument was exercised before the calibration.

Actual weight	Before adjustment	Difference displayed	After adjustment	Difference displayed		Precision		Corner loads
1.0001	1.0000	-0.0001				50.0001		0.0000
9.9995	9.9999	0.0000				50.0001		0.0000
29.9997	29.9999	0.0002				50.0000		0.0000
39.9998	39.9998	0.0000				50.0001		0.0000
49.9995	50.0001	0.0003				50.0001		
						50.0000		

The maximum corner loads error is 0.0001 g using a mass of 20 g
The maximum precision error is 0.0001 g using a mass of 50 g

	Value	Probability distribution	Divisor factor	Sensitivity coefficient	Uncertainty distribution	Reliability %	Degrees of freedom
Standards uncertainty	0.0001	N	2	1	0.00005	95	200
Std deviation at calibration	5.16E-05	N	1	1	5.16E-05	-	5
Readability of balance	0.0001	R	1.732051	1	5.77E-05	100	∞
Other							
		Combined uncertainty		Normal	9.22E-05	v.eff	49.70555
		Expended uncertainty		Normal (k=2)	0.00019	limit(v)	2.06

The calibration uncertainty of the instrument is 0.0003 g

The reported uncertainties of measurement are based on a standard uncertainty multiplied by a coverage factor of k=2 which unless specifically stated otherwise, provides a level of confidence of approximately 95%, and has been estimated in accordance with the principles defined in the GUM (Guide to Uncertainty of Measurement, ISO, Geneva, 1993)

Remarks : Partial Calibration 0-50g. Reading out of scope.

Date of Calibration : 17 January 2014

Recommended date for next calibration : January 2015

Technical Signatory : R. Sosa

ISO 17025

Mastersizer – Calibration Cetificates

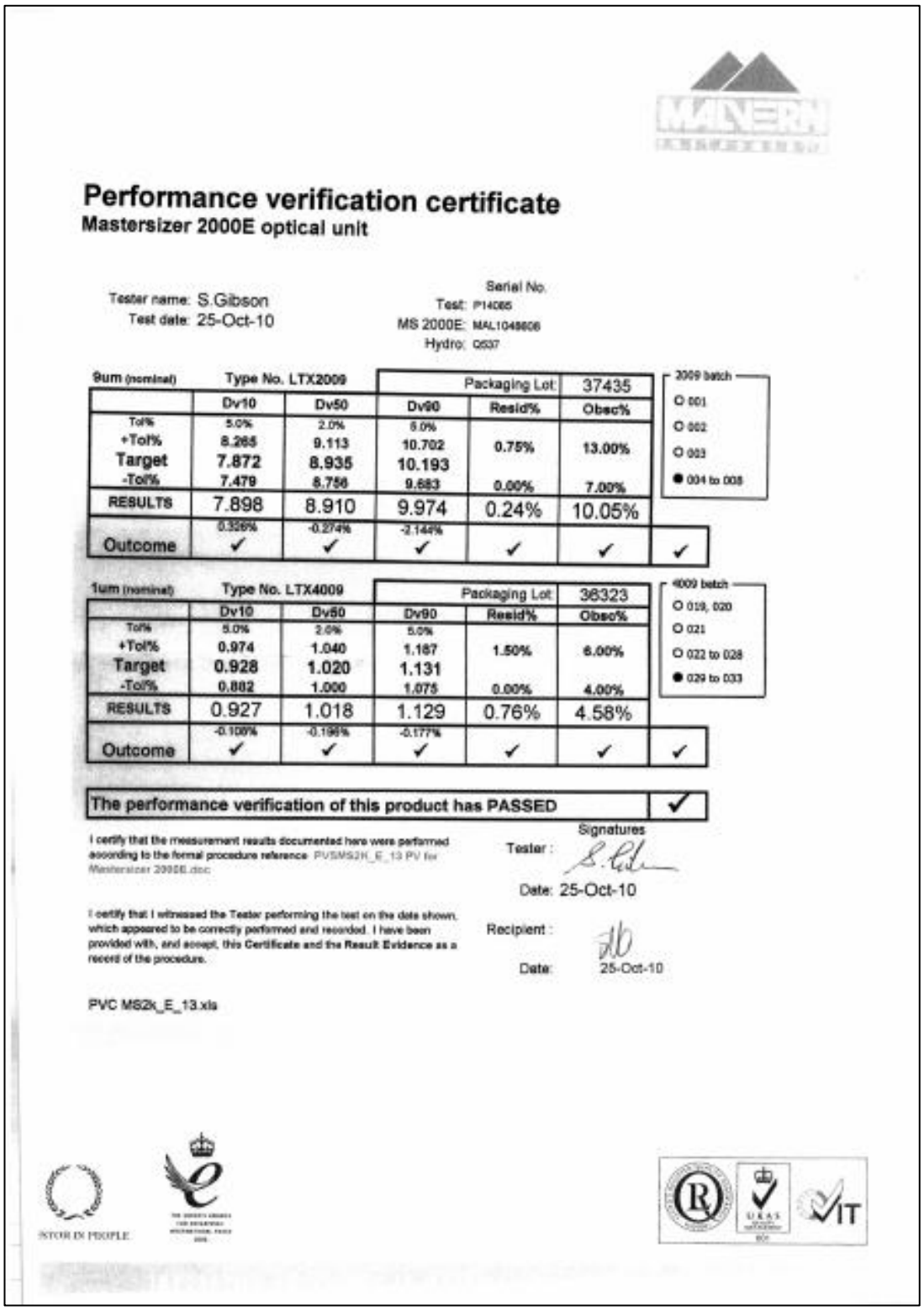

Performance verification certificate

Mastersizer 2000E optical unit

Tester name: S.Gibson
Test date: 25-Oct-10

Serial No.
Test: P14065
MS 2000E: MAL1048606
Hydro: G537

9um (nominal)	Type No. LTX2009			Packaging Lot:	37435	2009 batch
	Dv10	Dv50	Dv90	Resid%	Obsc%	○ 001
Tol%	5.0%	2.0%	5.0%			○ 002
+Tol%	8.265	9.113	10.702	0.75%	13.00%	○ 003
Target	7.872	8.935	10.193			● 004 to 008
-Tol%	7.479	8.756	9.683	0.00%	7.00%	
RESULTS	7.898	8.910	9.974	0.24%	10.05%	
Outcome	0.326% ✓	-0.274% ✓	-2.144% ✓	✓	✓	✓

1um (nominal)	Type No. LTX4009			Packaging Lot:	36323	4009 batch
	Dv10	Dv50	Dv90	Resid%	Obsc%	○ 019, 020
Tol%	5.0%	2.0%	5.0%			○ 021
+Tol%	0.974	1.040	1.187	1.50%	6.00%	○ 022 to 028
Target	0.928	1.020	1.131			● 029 to 033
-Tol%	0.882	1.000	1.075	0.00%	4.00%	
RESULTS	0.927	1.018	1.129	0.76%	4.58%	
Outcome	-0.109% ✓	-0.196% ✓	-0.177% ✓	✓	✓	✓

The performance verification of this product has PASSED ✓

I certify that the measurement results documented here were performed according to the formal procedure reference PVSMS2K_E_13 PV for Mastersizer 2000E.doc

Signatures

Tester: S. Gibson

Date: 25-Oct-10

I certify that I witnessed the Tester performing the test on the date shown, which appeared to be correctly performed and recorded. I have been provided with, and accept, this Certificate and the Result Evidence as a record of the procedure.

Recipient: JD

Date: 25-Oct-10

PVC MS2k_E_13.xls

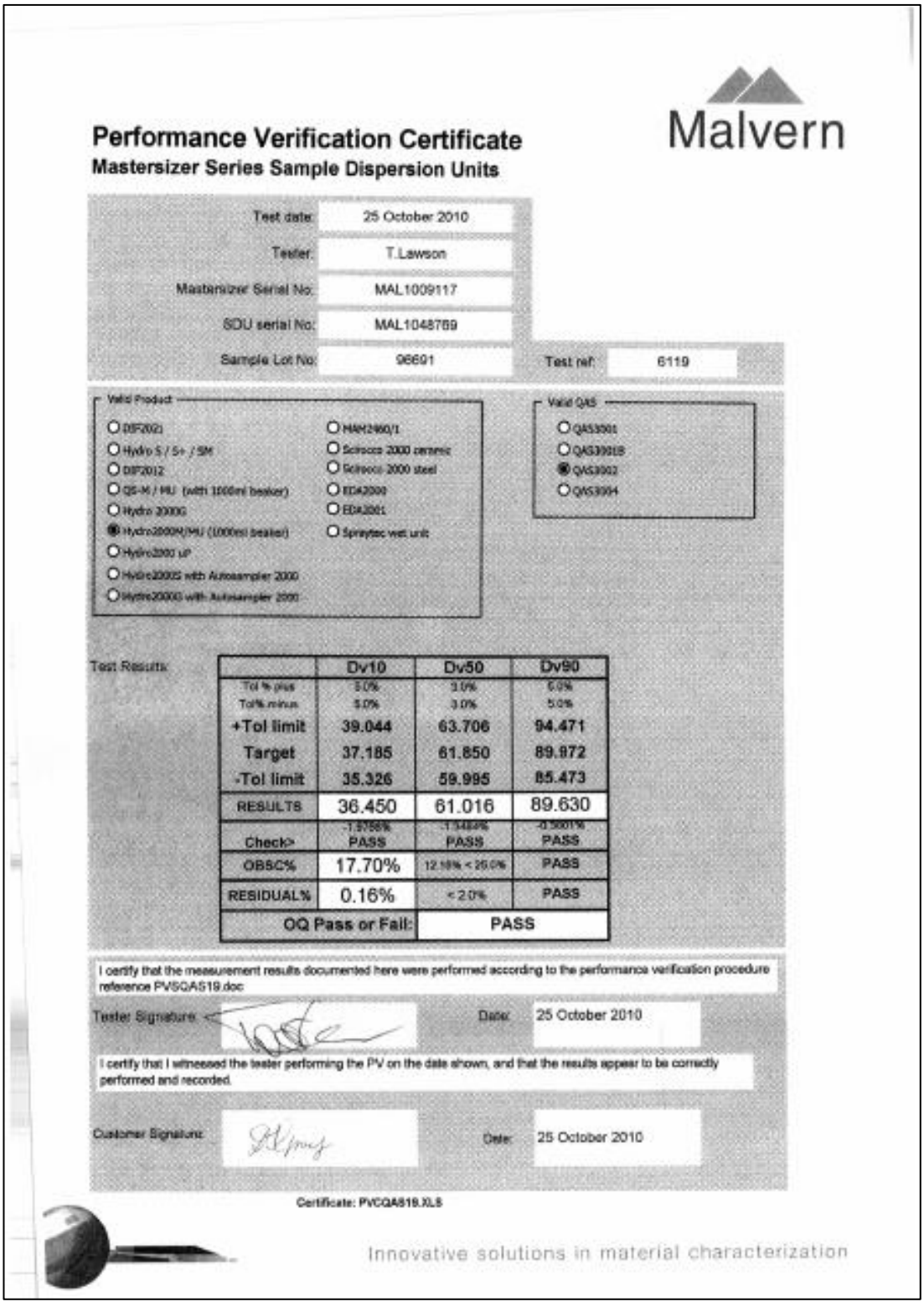

Malvern

Performance Verification Certificate

Mastersizer Series Sample Dispersion Units

Test date:	25 October 2010
Tester:	T.Lawson
Mastersizer Serial No:	MAL1009117
SDU serial No:	MAL1048789
Sample Lot No:	96691
Test ref:	6119

Valid Product

- ○ DIF2021
- ○ Hydro S / S+ / SM
- ○ DIF2012
- ○ QS-M / MU (with 1000ml beaker)
- ○ Hydro 2000G
- ◉ Hydro2000M/MU (1000ml beaker)
- ○ Hydro2000 uP
- ○ Hydro2000S with Autosampler 2000
- ○ Hydro2000G with Autosampler 2000
- ○ MAM1960/1
- ○ Scirocco 2000 ceramic
- ○ Scirocco 2000 steel
- ○ EDA2000
- ○ EDA2001
- ○ Spraytec wet unit

Valid QAS

- ○ QAS3001
- ○ QAS3001B
- ◉ QAS3002
- ○ QAS3004

Test Results:

	Dv10	Dv50	Dv90
Tol % plus	5.0%	3.0%	5.0%
Tol% minus	5.0%	3.0%	5.0%
+Tol limit	39.044	63.706	94.471
Target	37.185	61.850	89.972
-Tol limit	35.326	59.995	85.473
RESULTS	36.450	61.016	89.630
Check>	-1.975% PASS	-1.348% PASS	-0.501% PASS
OBSC%	17.70%	12.18% < 20.0%	PASS
RESIDUAL%	0.16%	< 2.0%	PASS
OQ Pass or Fail:		PASS	

I certify that the measurement results documented here were performed according to the performance verification procedure reference PVSQA519.doc

Tester Signature: Date: 25 October 2010

I certify that I witnessed the tester performing the PV on the date shown, and that the results appear to be correctly performed and recorded.

Customer Signature: Date: 25 October 2010

Certificate: PVCQA519.XLS

Innovative solutions in material characterization

Production Test Certificate

Malvern

Instrument : AWM2000
Serial Number : MAL1048769
Certificate No : 006119

TESTING RESULTS:

CHECKS CARRIED OUT	PASS/FAIL /NA
Drain Valve Check	N/A
Mechanical Checks	Passed
Electrical Integrity Checks	N/A
Cell ID	N/A
Kernel & Firmware	N/A
Flow Regulator Set Up	N/A
Wet Cell Configuration	Passed
Ultrasonic Performance Check	Passed
Temperature Sensor Calibration	N/A

OTHER CHECKS CARRIED OUT			
Pump/Stirrer Calibration			
Pump Speed		Stirrer Speed	
Tolerance(rpm)	Actual(rpm)	Tolerance(rpm)	Actual(V)
4000 (+/-20)	4004	N/A	
Level Sensor Calibration			
Empty Tank		Full Tank	
Tolerance(V)	Actual(V)	Tolerance(V)	Actual(V)
N/A		N/A	

I hereby declare that this instrument was calibrated and performed according to the specifications set out in the test schedule (AWM2000STS03). *Signed for and on the behalf of Malvern Instruments.*

Name: Trevor Lawson	Date: 25/10/2010	Signature :